5-2015

DEVELOPMENT, VALIDATION, AND APPLICATION OF ANALYTICAL METHODS FOR CHARACTERIZING ADSORBED PROTEIN ORIENTATION, CONFORMATION, AND BIOACTIVITY

Aby Thyparambil
Clemson University, athypar@g.clemson.edu

DEVELOPMENT, VALIDATION, AND APPLICATION OF ANALYTICAL METHODS FOR CHARACTERIZING ADSORBED PROTEIN ORIENTATION, CONFORMATION, AND BIOACTIVITY

A Dissertation
Presented to
the Graduate School of
Clemson University

In Partial Fulfillment
of the Requirements for the Degree
Doctor of Philosophy
Bioengineering

---

by
Aby Abraham Thyparambil
May 2015

Accepted by:
Dr. Robert A. Latour, Committee Chair
Dr. Alexey Vertegel
Dr. Delphine Dean
Dr. Frank Alexis

ABSTRACT

The structure and bioactivity of adsorbed proteins are tightly interrelated and play a key role in their interaction with the surrounding environment. These factors are of critical importance in many biotechnological applications. However, because the bioactive state of an adsorbed protein is a function of the orientation, conformation, and accessibility of its bioactive site(s), the isolated determination of just one or two of these factors will typically not be sufficient to understand the structure-function relationships of the adsorbed layer. Rather a combination of methods is needed to address each of these factors in a synergistic manner to provide a complementary dataset to characterize and understand the bioactive state of adsorbed protein. In this research, I describe and demonstrate the potential of a set of complementary methods: (a) circular dichroism spectropolarimetry to determine adsorption-induced changes in protein secondary structure, (b) amino-acid labeling/mass spectrometry to assess adsorbed protein orientation and tertiary structure by monitoring adsorption-induced changes in a residue's solvent accessibility, and (c) bioactivity assays to assess adsorption-induced changes in a protein's bioactivity. Subsequently, the developed techniques were applied to characterize: (a) the role of protein-protein interactions (PPI) in influencing the structure and activity of a protein during its layer formation, and (b) the influence of chemical excipients on the stability and potency of an adsorbed layer of protein. While the effect of PPI on the initial adsorbed configuration and bioactivity of a protein layer varied with the type of adsorbent surface and protein composition, the effects of chemical excipients on the stability and potency of an adsorbed protein layer primarily depended on its initial

adsorbed configuration. From an evaluation of the structure-function relationship within these adsorbed layers, their bioactivity was found to reduce in direct proportion to the disruption in protein structure in majority of the systems studied. Although, the presented techniques do have the limitation of being low in resolution, the techniques developed in this study do provide insights into the molecular processes influencing the structure-function relationships of adsorbed protein that were previously unknown.

DEDICATION

To my '*Rô'eh*', and one of the finest teacher I know.

ACKNOWLEDGMENTS

First and foremost I offer my sincerest gratitude to my advisor, Dr. Robert Latour, who has supported me throughout my PhD studies with his patience and knowledge whilst allowing me the room to work in most of my own way. In this equal note, I would also like to express my sincere gratitude to Dr. Yang Wei as well, for his mentoring throughout this doctoral work. I do owe a lot of my academic accomplishments to the sincere efforts from both of them.

Sincere thanks are due to my committee members, Dr. Alexey Vertegel, Dr. Delphine Dean, and Dr. Frank Alexis for their accommodative nature. I would also like to thank the past and present members of Biomolecular Interactions and Biomolecular Modeling laboratories, Dr. Yonnie Wu, (Auburn University) and Dr. Guzeliya Korneva, for their support. Likewise, I sincerely thank other faculty and support staff at the Department of Bioengineering, for all the assistances provided throughout my time at Clemson. Moreover, I sincerely thank and acknowledge the facility and funding supports from DTRA (Grant no. HDTRA1-10-1-0028), NIH NIBIB (grant # EB002027) and NIH Grants (5P20RR021949-04 and 8P20GM103444-04).

On a closing note, I additionally acknowledge the immense scientific help provided by the blogs of Dr. Martin Chaplin (London South Bank University) and Philip Ball. Special thanks to my friends and their families, for making the time in Clemson so memorable and eventful. Lastly, I am sincerely and most grateful to my parents, brothers, and my dear wife for their patience, prayer, support, encouragement and inspiration provided throughout my doctoral years.

TABLE OF CONTENTS

Table of Contents (Continued)

Page

Table of Contents (Continued)

Page

LIST OF TABLES

List of Tables (Continued)

List of Tables (Continued)

List of Tables (Continued)

Table Page

LIST OF FIGURES

List of Figures (Continued)

Figure Page

List of Figures (Continued)

Figure Page

List of Figures (Continued)

Figure Page

CHAPTER ONE

INTRODUCTION

The biological activity of adsorbed/immobilized proteins like toxins on solid surfaces is of critical importance in biodefense, biotechnological, and medical applications. Although toxins are inherently lethal and could be potentially used as a bio-warfare agent, the application of these biologics as a therapeutic alternative for chronic diseases like cancer is of exceptional interest to pharmaceutical industry. In these scenarios, the development of strategies to control the bioactive state of adsorbed/immobilized protein systems on material surfaces is important because, if unchecked, these systems are capable of triggering adverse responses like altered biological activity, immunogenicity, and product adulteration. One direct strategy for controlling the biological responses of adsorbed/immobilized protein systems is to modulate the adsorbed structure of a protein. But, the specific mechanism by which this can be achieved is intricately complex, and not yet well understood. Therefore, the overall aim of this research was to gain a molecular-scale understanding of the factors influencing the structure of an adsorbed protein that would facilitate the development of strategies to control their biological responses by modulating the adsorbed structure of the protein. To a considerable extent, many of the underlying mechanisms and strategies developed for adsorbed systems are also applicable to an immobilized protein system as well.

The structure and bioactivity of a protein on a material surface are affected by different types of interactions. It has proven to be extremely difficult to quantitatively

understand and control these types of interactions because of the complexities involved. Additionally, existing methods that have been developed and used to characterize the interactions of a protein on a material surface have proven to be largely inadequate to provide the level of detail necessary to achieve this type of understanding. An extensive review of the challenges involved in characterizing adsorbed/immobilized protein systems are provided in Chapter Two, the background section of this dissertation. Through this review process, this author has identified three specific challenges currently posed by adsorption/immobilized protein systems, the addressing of which would highly benefit the furthering the objective of this dissertation. These three specific challenges are identified as the three specific aims listed in Chapter Three of this dissertation.

Since the bioactivity of a native protein results from its hierarchical structural arrangement, the first main challenge impeding the development of strategies to control the biological response of adsorbed/immobilized protein systems, is the lack of a single technique that can comprehensively characterize the influence of structural changes on the bioactivity of adsorbed/immobilized protein. Structural shifts in an adsorbed protein can result from the interplay of interactions between the proteins, surface, and solvent, and other extrinsic factors like solution constituents, flow, temperature, and pressure. To effectively probe the influence of each of these interactions on the structure of an adsorption system, multiple techniques need to be synergistically combined and methodologies need to be fine-tuned. Towards this purpose, the strategy adopted in my studies was to develop and expand the existing capabilities of monitoring the shifts in

secondary structure (via circular dichroism spectropolarimeter), solvent exposure of residues (via amino acid labeling combined with mass spectrometry), and bioactivity assays (via turbidimetric assay) so as to systematically understand the factors influencing the structure of adsorbed proteins and how the adsorbed protein influences protein bioactivity. An overview of the experimental techniques and methodologies used in the current study to achieve the objective of this dissertation are provided in Chapter Four, with the detailed description of the methodologies and scope of application provided in the subsequent chapters.

The subsequent aim of this research work was to characterize how protein interactions with a surface affects protein structure and bioactivity. Though the effects of protein interactions with a surface on the adsorbed configuration of a protein have been investigated by many other groups, these previous studies have typically not separated out the influences of protein-protein interactions and a protein's inherent stability within these interactions. Chapters Five, Six, and Seven provide a detailed description on the role of these individual interactions on the secondary and tertiary structure of an adsorbed protein. The adsorption model system used in these studies include two types of protein (hen egg white lysozyme and bovine pancreatic ribonuclease) on three different surfaces (fused silica glass, high density polyethylene, and poly(methyl methacrylate) under a constant solution environment (10 mM potassium phosphate buffer, pH 7.4). All adsorption experiments were carried out at room temperature and pressure, under static (or non-flow) conditions.

The final aim of this study was to further expand these adsorption system in order to understand the molecular mechanisms involved in the interaction of solution constituents like chemical excipients on the adsorbed structure of a protein. The types and solution concentrations of the chemical excipients were restricted to those that are commonly used for stabilizing or destabilizing the native structure of protein in solution. A major challenge in determining the influence of these chemical excipients on the solution or adsorbed structure of proteins by any spectroscopic technique, is the strong interference that such additives have on the peak specific to the structure of a protein. Chapter Eight provides a detailed description of the technique that we developed to overcome this problem and determine the helix content of proteins in a solution environment containing strongly absorbing solution constituents. Chapter Nine apply and expand the above methods for further use with adsorbed proteins. In this set of studies, the molecular mechanisms involved in the interactions by each of these individual chemical excipients on the adsorbed protein were identified by examining the structures of both the desorbed and the residual fractions of protein on the surface. The model chemical excipients used in the current study were three types of surfactants (sodium dodecyl sulphate, octyl glucoside, and 3-[(3-Cholamidopropyl) dimethylammonio]-1-propane sulfonate) and two types of salts (guanidium hydrochloride, and urea).

A summary of the refinements and developments to the analytical techniques used in this research work, scope of its synergistic applications, and a brief overview of the limitations and future directions for development are provided in Chapter Ten.

CHAPTER TWO

BACKGROUND

2.1 INTRODUCTION

Protein toxins represents a specialized class of proteins that have garnered attention not only because of its inherent destructive potential and thus their use as a biological weapon, but also due to their ever-increasing role as therapeutics in anti-proliferative, antitumor, immunomodulatory, antiviral, antifungal or anti-insect applications.[1-6] Such toxins have been identified in many plant, microbial, and predatory (e.g., insects) sources, and can be isolated and purified into their natural form with relative ease.[2] The potency of these natural defensive molecules relies on three main components—a targeting moiety, a biodegradable linker molecules, and a cytotoxic moiety (usually by enzymatically inhibiting the ribosomes from synthesizing proteins)—quite analogous to the modern-day approach in targeted drug-delivery applications.[2, 7] The precision involved in a toxin's targeting, also reduces the volume requirement for such systems. However, as these types of proteins are quickly cleared from the circulatory system in the host, proteins used for pharmaceutical applications are often altered from their natural state or bound to a drug delivery platform to prolong their distribution and elimination phases, thereby, increasing the duration of therapeutic effects.[8] Additionally, these type of alterations may also be used to reduce the toxicity and immunogenicity by these specialized protein molecules.[3, 9-12] In recent applications, naturally occurring toxins have been linked with poly(ethylene-glycol), nanoparticles, and/or antibodies to slow clearance and provide targeting for therapeutic applications.[5-6, 8, 13-22]

Depending on the type of engineered system, two types of interactions are possible—the interaction of proteins with an adsorbent surface that is much larger than itself, or protein interactions with a smaller or similar sized material surfaces. Although there are some differences in the interaction of the proteins in each of these systems, the therapeutic effects of the proteins adsorbed/immobilized in both these systems are influenced by conformation and accessibility of the toxin's bioactive site.[20-21, 23-29] In addition to the influence of processing steps on the bioactive state of the protein, the organic and inorganic excipients within the biological environment can also influence the operational stability of these engineered systems.[1, 30] In many ways, the problems faced by a toxin-based engineered system is not unique, and is faced in other types of protein-based drug delivery systems involving antibodies, enzymes, and recombinant proteins.[15, 20-21, 23-29] Even outside the realms of the molecular processes influencing the design of drug-delivery systems, retention of the biological activity and operational stability of protein-based biologics is a concern during the storage, packaging and handling stage of these biologics, especially when the route of drug administration is via parenteral.[10-11, 31]

Most biologics are formulated as aqueous solutions, and packaged in glass or polymeric vials, which makes these molecules vulnerable to physical adsorption.[10-11] Adsorption of biologics has been known to affect the dosage levels (with over 50% loss in the amount of expensive proteins) and weaken the biological integrity of the product.[10-11, 32] Even if the adsorption-induced loss in the amounts of protein can be mitigated by increasing the dosage or by filling the vials with more concentrated solutions, a graver concern of protein adsorption to vial surfaces is with regard to the biological safety of the

tainted product as a therapeutic. Experience has shown that these adsorption events can interfere with the normal functions of an autogenic protein and result in the break-down of immune-tolerance towards these biologics.[10-11, 32-33] A classic example in this regard, is the occurrence of erythroblastopenia in erythropoietin medicated patients.[31] In the cited example, as well as in many other studies which examined the cause of unexpected immunogenic responses to the biologics stored in glass or polymeric vials, interactions with container surfaces have been linked to structural and bioactivity changes of the packaged therapeutic proteins.[10-11, 32-33] Although, strategies like the addition of organic and inorganic excipients to the formulation (like amino acids, carbohydrates, organic solvent, polyols, salts, and surfactants in the formulation) have been pursued along with surface modification (via protein-resistant surface coatings, or pre-adsorption with proteins), these approaches are based on trial-and-error methods and are hardly optimized. The effectiveness of these approaches are often extremely limited in their ability to stabilize the bioactive state of the target protein against adsorption-induced conformational changes.[10-11, 32-33]

While, strategies to stabilize a protein's bioactivity is a general concern in the pharmaceutical industry, the strategies to deactivate the bioactive state of adsorbed proteins are of more important concern to the medical reprocessing industry as well as the biodefense community.[34-36] A review of the existing practices that are used to decontaminate surfaces that are contaminated with adsorbed protein has indicated that these methods have been proven to be either ineffective or limited in their applicability.[34-36] Among these practices, the most common decontamination techniques include the use

of ultra-violet light, oxidizing agents (e.g., ethylene oxide, chlorine dioxide), and heat.[34-36] While these techniques have proven very effective and are often considered to be the gold standards for decontamination, they represent harsh conditions that may also lead to substantial damage to the underlying material surfaces that are being treated.[34-36] The handling of strongly oxidizing agents also raises environmental and toxicity concerns of their own. The resulting damage to environmental surfaces and the subsequent disposal issues associated with the use of these treatments call for the development of less harsh and more viable approaches for surface decontamination. In this context, water-based formulated wash solutions would be a more attractive option especially since most proteins are water-soluble.[2] Even by this approach, a formulated wash solution by a mere trial-and-error approach of using known organic and inorganic excipients may not be effective, as the interactions underlying different types of protein-surface interactions can be both protein- and surface-dependent. Custom designed wash solutions may therefore be needed for surface decontamination as a function of both the type of bio-agent and environmental surface involved. A fundamental understanding of the underlying molecular mechanisms mediating protein-surface interactions is essential to support this type of approach for effective and efficient decontamination agent design. Also, because proteins are presented by the outer surface of many types of bacteria, fungi, and viruses and mediate their adhesion to surfaces, this understanding has application for decontamination strategies against these types of biological entities as well.

In addition to the importance of protein-surface interactions for pharmaceutical and decontamination applications, the biotechnological and biomaterials fields are

interested in the incorporation of proteins in the form of enzymes, growth factors, and various other signaling macromolecules for the design of biosensors and substrates for tissue engineering and regenerative medicine.[37-42] A fundamental understanding of the influence of the supporting substrate on the structure and bioactivity of the peptides and proteins incorporated into these systems is critically important as well.

In this regard, the purpose of this chapter was to provide a comprehensive review of three principal aspects: (a) the scope and limitations of current experimental techniques for characterizing the molecular processes influencing the bioactive state of adsorbed proteins, (b) factors influencing the bioactive state of adsorbed proteins, and (c) the general applicability of the strategies using chemical agents to desorb and deactivate adsorbed proteins on different surface chemistries.

2.2 METHODS TO CHARACTERIZE THE MOLECULAR PROCESSES INFLUENCING THE BIOACTVITY OF ADSORBED PROTEIN

The biological function of a native protein is imparted by the binding strength as well as the correct alignment and orientation of the ligand to the proteins's active site, which results from its folded structure that is arranged in four hierarchical levels.[37, 43] The primary structure of a protein is comprised of the specific amino acid sequence along its polypeptide chain. This set of amino acids is typically composed of the 20 naturally occurring L-amino acids, which are classified by their side-group as being non-polar, polar, or charged amino acids.[37] The polypeptide chain formed by the primary sequence is then organized into three basic types of secondary structure: helices (α, 3_{10}, and π), β-sheets, and loops (connects helix and sheet elements), which are then organized together

to form tertiary protein structure. Finally, more than one polypeptide chain can be organized together to form quaternary structures, with each of the individual polypeptide chain having a separate beginning (N-terminus) and ending (C-terminus).

When proteins adsorbs on a larger material surface, the native state of the protein often no longer represents the low free energy state of the combined protein-surface-solution system.[43] This situation can lead to substantial shifts in the protein away from its native-state structure. If these structural shifts influence the structure of the bioactive site in the protein such that its intended ligand or receptor can no longer bind to that site, bioactivity will be lost. Likewise, if the protein adsorbs or is tethered to a surface such that accessibility to the binding site is stearically blocked, bioactivity can be lost as well.[37-42] These events are illustrated in Fig. 2.1.

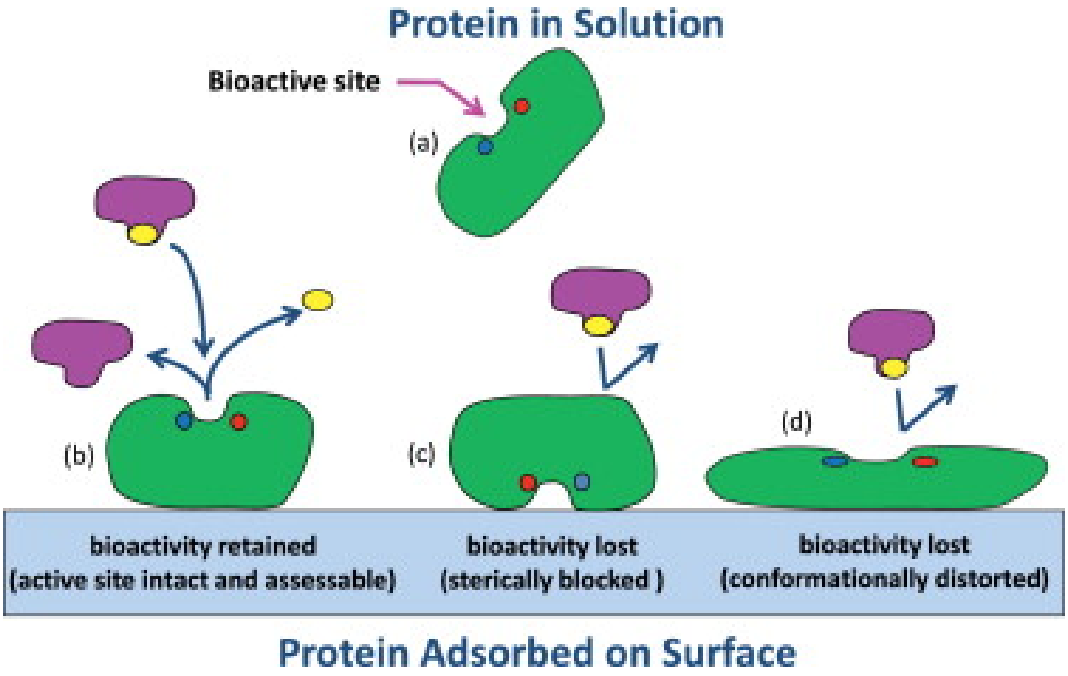

Figure 2.1: Illustration of the influence of adsorption on the bioactive state of a protein.[43] (a) The protein in its native-state structure in solution, and (b) when adsorbed with its bioactive site accessible and conformationally intact, thus providing native-state-

like bioactivity. (c) Protein adsorbed with its bioactive site stearically blocked by the surface, thus inhibiting substrate binding with subsequent loss in bioactivity due to adsorbed orientation. (d) Protein adsorbed with its bioactive site accessible but conformationally distorted with subsequent loss in bioactivity due to structural changes of the bioactive site. Reproduced with permission from Ref. 43. Copyright 2014 Elsevier B.V.

2.2.1 Techniques to Characterize the Bioactivity of Adsorbed Proteins

As illustrated in Fig. 2.1, the adsorption of a protein to a surface can result in a loss in its bioactivity. Adsorption-induced loss in bioactivity can be assessed by relative comparison of the interaction of a ligand or its byproduct with the adsorbed state of a protein relative to its native state. In most of the spectrophotometric methods (e.g., turbidometric and colorimetric assays) the bioactivity of adsorbed enzymes like lysozyme and trypsin were assessed by monitoring the decrease in absorbance of ligand or increase in absorbance of the byproduct at a specific wavelength.[44] Other variants of spectrophotometric assays involve coupled assays (e.g., lactose dehydrogenase assay to measure cytotoxicity of cells, and enzyme-linked immunosorbent assays (ELISA)) have also been used for measuring the platelet/cellular attachment to adsorbed plasma proteins.[45-48] But in case of adsorbed oxido-reductive proteins like glucose oxidase, lactose dehydrogenase, and cytochrome-C, electrochemical techniques like voltammetry or chornoamperometry or impedance spectroscopy have been used to measure the adsorbed state bioactivity.[49-53] Similarly, properties like chemiluminescence (e.g. luciferase) and fluorescence (e.g., β-galactosidase) have also been used for characterizing the bioactivity of adsorbed proteins.[39, 54-55]

Once a suitable technique have been identified, the bioactivity of an adsorbed protein can be expressed in the units of specific activity, turnover number, or the catalytic center

activity, which can be subsequently compared with that of the protein in its native state. Additionally, with electrochemically active proteins, kinetic parameters like Michaelis constant (K_m) have also been used to express the bioactive state of the adsorbed proteins. However one of the most significant limitation in all biological assays lies in their inability to distinguish the source of bioactivity loss, which in addition to the structure, as described in Fig 2.1 could also be influenced by the dynamics of the protein-ligand system, thus making it difficult to determine how a given system should be redesigned to correct the problem the can also influence the bioactivity.[40, 56-58] To address this limitation, experimental methods are needed to characterize how adsorption influences both the orientation and structure of protein on a surface. With these combined data sets, assessment can be made regarding the actual factor(s) that are responsible for a loss in bioactivity, if it occurs.

2.2.2. Techniques to Characterize the Orientation and Structure of Proteins

Current spectroscopic techniques rely on one or more of the following properties—absorption, chirality, fluorescence, mass, nuclear magnetic resonance, reflection, scattering, or vibrational motion—in order to characterize the adsorbed configuration of a protein.[39, 59] While some of these techniques could be used to monitor the structural shifts of adsorbed proteins online (i.e., in the presence of protein containing solutions), other types of techniques require the removal of protein containing solution. Similarly, while some of the techniques provide information on the global shift in the structure of proteins, other types of techniques provide only localized information on the shift in protein structure. Additionally, there are limitations in the type of adsorbent surface to which a given type of technique can be applied. Currently, among all the available techniques, those relying on X-ray and nuclear magnetic

resonance (NMR) are the only two techniques capable of providing detailed structural information on the adsorbed proteins. All of the other techniques provide only limited information on the hierarchical structure of the protein. In the following sub-sections, the scope and limitations of some of the most commonly applied techniques in characterizing the adsorbed protein structures are discussed.

2.2.2.1 Quantifying the Structural Shift in Proteins

The structural shifts in adsorbed proteins can involve shifts in secondary, tertiary or quaternary structure, and can be monitored either at a structural level (global) and/or at a residue level (local) with varying degree of molecular detail. Most of these spectroscopic techniques rely on either the shifts in electro-magnetic properties or mass shifts for protein structural determination.

2.2.2.1.a. Techniques for Monitoring the Global Shift in Protein Structure

Two of the most commonly applied techniques for globally monitoring the structural shifts in adsorbed proteins rely on the optical activity and vibrational motion of the bond groups within the protein's structural elements. Among these techniques, circular dichroism (CD) spectroscopy is the only known technique to utilize the chiral property of the structural elements to monitor the adsorption-induced shifts in protein structure. However, the characteristic vibrational motion of the bonded chemical groups within a protein have been exploited by techniques like infrared spectroscopy (FTIR), surface-enhanced Raman spectroscopy (SERS), and sum-frequency-generation (SFG) spectroscopy to quantify the secondary structural elements in adsorbed proteins. All of these techniques generate low resolution spectra that require deconvolution to quantify the individual structural elements.

2.2.2.1.a.1. Circular dichroism (CD) spectroscopy

A distinct advantage of the CD technique over vibrational techniques lies in its amenability of directly probing the structure of adsorbed molecules while immersed in aqueous solution. CD has been extensively used to spectroscopically study the adsorbed and native structure of protein due to its characteristics of being non-destructive, relative easy to operate, requirement of small sample volume, and providing fast, reliable data analyses.[60-62] In particular, CD provides a very convenient experimental method for quantifying the secondary structure and environmentally induced structural changes in proteins since the different forms of the main secondary structural elements found in proteins (e.g., α-helix, β-sheet, and random loop) exhibit distinctly different CD spectra.[62-63] More detailed insights into the polarity or dipole moment of the protein conformation can be obtained by combining CD with vibrational spectroscopy, as demonstrated by vibrational circular dichroism spectropolarimetry.

To quantify the relative proportion of each associated secondary structure contained in a protein sample, the CD spectrum acquired between wavelengths of 190 to 240 nm is typically empirically interpreted as a sum of fractional multiples of reference spectra for each type of secondary structure.[63] This process is conducted using a variety of mathematical tools[64] along with reference datasets of highly resolved protein structures (i.e., protein structures from X-ray crystallography and NMR spectroscopy).[65] Although quantification of protein structure with CD has been usually reported for proteins in solution or adsorbed to colloidal particles suspended in solution, its use has also been extended to characterize adsorbed protein secondary structure on flat transparent material

surfaces. Initial reports of this application were reported as early as 1974 by McMillin and Walton.[66] Unlike then, the modern versions of CD spectropolarimeters are equipped with photo-elastic modulators instead of Pockel's cells, which have much improved signal-to-noise ratio, thus placing less stringent requirement on the minimal amount of protein that is required for analysis.[48, 65, 67] The method to acquire high quality spectra and the considerations in data analysis have been extensively reviewed. The key requirement for using CD to quantify adsorbed protein structure is that the signal to noise ratio (S/N) from the adsorbed protein should be sufficiently high (typically > 4:1) from the rest of the system (adsorbent surface, surrounding solution, and cuvette) to obtain a discernible spectrum.[63] Additionally, these techniques cannot be used for online monitoring of the structural shifts in adsorbed proteins due to the inability to separate the signal from the adsorbed protein from that of the protein in the surrounding solution. This later condition means that the structural determination of adsorbed protein can only be achieved for proteins that are effectively irreversibly adsorbed so that they can be immersed in a surrounding protein-free buffer solution and not desorb from the surface while the CD spectrum is obtained.

In addition to the use of CD for determining the secondary structure of protein, this technique has also been used in determining the tertiary structure of protein, like the '*molten globule*' states, by monitoring the shape and magnitude of near-UV (260–320 nm) fingerprints in the CD spectra.[60, 62, 65, 68] However, such spectral features are influenced by the type of protein and thus, as a result, strategies to quantify the tertiary structural shifts using CD techniques are lacking. Similarly, in proteins containing co-

factors as an important functional part of the bioactive site, such as metal ions, shifts in the spectral features in visible light related to the cofactor's position have also been used as indicators of the integrity of the binding site.[69]

2.2.2.1.a.2. Vibrational spectroscopy

The most attractive feature of vibrational spectroscopic like infra-red spectroscopy (FTIR) and surface-enhanced Raman scattering (SERS) is its broader applicability with a wider range of adsorbent surfaces as opposed to CD.[70] While FTIR spectroscopy is used with molecularly smooth adsorbent surfaces, SERS is used with roughened metallic adsorbent surfaces which promotes scattering.[71-73] In both these techniques, the secondary structures in the proteins are quantified using the same approach as it was used for CD, but over the wavelength range of 1500 cm^{-1} – 1700 cm^{-1} using multivariate statistical techniques on a reference database of proteins with resolved structures.[73] But the accuracy of such quantification, relies on the intensities, position and shape of the spectra, and is affected by the background interference from the aqueous solution and adsorbent surfaces.[73] Therefore, background correction represents an important step in both these types of technique. Another concern with these techniques is with regard to the signal dampening by the limited vibrational motion of the side-chain groups within the amino acids within the protein that are directly in contact with the adsorbent surface.[74]

Recent, technological advancements have addressed the limitations in FTIR by multiplexing with SFG spectroscopy, to provide surface-sensitivity (i.e., these techniques are sensitive to only proteins on the adsorbent surfaces, even if the proteins are present in

solution).[75-79] This type of multiplexing also permits online monitoring of the structural shifts in the proteins on the adsorbent surfaces. But, with larger proteins, the spectral intensities from number of functional groups within the protein that are adsorbed in varied configurations tend to overlap, thereby broadening the spectral peak position and weakening the spectral signal intensities, which raises concerns on the accuracy of secondary structures quantified using these techniques.

Similar to CD techniques, vibrational spectroscopy has also been used to qualitatively determine the tertiary structural shift in adsorbed protein by monitoring the extent of deuterium exchange that occurs when exposing these proteins to deuterated water.[39, 73-74] Higher deuterium exchange in adsorbed protein is often associated with higher extent of unfolding. However, the exposure duration to deuterated water and the moisture content in the atmosphere are potential concerns, as rapid exchange of hydrogen-deuterium within the adsorbed molecules decreases the accuracy of the results.

2.2.2.1.b Techniques for Monitoring the Local Shift in Protein Structure

Optical techniques like total internal reflection fluorescence, dual-focus fluorescence correlation spectroscopy and Forster resonance energy transfer have been used extensively to qualitatively interpret changes in the overall conformation of proteins that are conjugated to nano-particles or tethered to other chemical moieties.[80-90] All these techniques rely on fluorescence and these effects can be either intrinsic in origin (like from tryptophan or tyrosine), or emanating from extrinsic fluorophores (like thioflavin-T(4-(3,6-dimethylbenzothiazol-2-yl)-N,N-dimethyl-aniline, ThT), and 1-anilinonaphtha-lene-8-sulfonic acid (ANS)).[54, 91] The quantum yield of these labels generally increase

several fold upon contact with hydrophobic domains within the protein, which are only accessible upon undergoing denaturation. However, photo bleaching is a major concerns in these systems, and much care must be taken to avoid the influence of these effects in qualitative analysis.

In addition to the techniques that rely on absorption, other physical properties such as mass shift, nuclear magnetic resonance (NMR), and scattering can be exploited for providing residue-level information on the changes in protein structure. However, some of these techniques require high vacuum conditions, which limits their application for monitoring the structural shifts in proteins in biologically relevant environments. One strategy commonly used to overcome this limitation is via external labeling of the protein either by deuterated water to study hydrogen-deuterium (H/D) exchange or covalent modification of the side chains in amino acids. Alternatively, chemical excipients such as carbohydrates have been used as protective agents to preserve the adsorbed configuration of the protein before being introduced in the vacuum conditions for direct analysis.

2.2.2.1.b.1 Mass spectrometry

Mass spectrometry (MS) has been widely employed in characterizing adsorbed proteins. A key step in this process involves ionization of the protein/peptide samples. While laser-desorption ionization and electrospray ionization are the most common techniques for molecular weight analysis, these techniques are not amenable to direct analysis of protein samples due to concerns of high vacuum conditions, ionization interference due to the adsorbent surfaces, and problems in mass spectral mapping.[92-93] To overcome this limitation, MS are often used with labeled proteins, as demonstrated

with amino acid labeling in tandem with mass spectrometry (AAL/MS) and H/D exchange with mass spectrometry (HD/MS), to provide residue-level information on the local structure of the adsorbed proteins.[68, 94-97] These labeled proteins can be directly ionized ('top-down approach'), or enzymatically digested to peptide fragments that are subsequently ionized, to be identified by peptide mass fingerprinting ('bottom-up approach'). The amino acid residues that are found to be labeled in solution but unlabeled following adsorption indicate regions of the protein that are sterically blocked by the surface (i.e., indicative of adsorbed orientation) or by neighboring proteins (i.e., indicative of protein-protein interactions). Alternatively, amino acids that were unlabeled in solution but become labeled following adsorption are indicative of the sites in protein that underwent adsorption-induced tertiary unfolding and solvent exposure of amino acids that are otherwise buried in the protein's native-state structure.

However, sufficient care must be taken while using AAL/MS and HD/MS to ensure that such labeling approaches do not introduce artifactual structural shifts in the adsorbed proteins. Also, the existing reagents for chemical labeling are limited to few amino acids (Table 2.1). More importantly, though the AAL/MS technique has been previously applied to the adsorbed protein by many groups, its use has been restricted to determining the labeling profile of just one type of amino acid [94-97] that is localized to a very small portion in the overall protein structure. Therefore, comprehensive information on a protein's adsorbed configuration would require sampling of the labeling profiles from multiple localized regions within a protein.

Table 2.1: Commonly used side-chain modification agents.[98-99]

Side chain/ group	Reagent/procedure	Optimum pH	Cross-reactivity
Amino (Lys + α-amino group)	Amidination (ethyl acetimidate)zy	pH 9	None, positive charge maintained
	Reductive alkylation HCHO + $NaBH_4$	pH 9	None, positive charge maintained
	Reductive alkylation HCHO + NaBH,CN	pH 7	None, positive charge maintained
	Acylation (acetic anhydride, succinic anhydride)	pH 8 and above	Tyr, His and Cys residues also modified, elimination of positive charge
	Tri nitrobenzene sulfonate	pH 8 and above	Tyr residues also modified , Eliminates positive charge and introduces large hydrophobic substituent,
Carboxyl (Asp + Glu)	Water-soluble carbodiimide + Nucleophile (EDC + glycine ethyl ester)	pH 4.5-5	Some side reactions with Tyr and thiol groups
Guanidino (Arg)	Dicarbonyls (2,3-butanedione, phenylglyoxal, and p-(hydroxyphenyl) glyoxal)	pH 7 or higher	None, reaction promoted by borate buffer, partially reversible upon dialysis, eliminates positive charge,
Imidazole (His)	Diethyl pyrocarbonate (ethoxyformic anhydride)	pH 4-5	Side reactions with Lys kept to minimum by low pH
Indole (Trp)	N-bromo succinimide	pH 4 or lower, slightly higher pH values can also be used	Thiol groups are rapidly oxidized;
	2-hydroxy-5- nitrobenzyl Bromide (DHNBS)	pH < 7.5	Tyr and His react more slow1y, slight reaction with thiols
Phenol (Tyr)	Iodination	pH 8 or higher	His also reacts , thiol groups are rapidly oxidized, both mono and diiodo derivatives are formed
	Tetra nitro methane	pH 8 or slightly higher	Thiol groups are also rapidly oxidized, some nitration of Trp

Thiol (Cys-SH)	Carboxymethylation (iodo- and bromo acetate/amide)	pH 7 or higher	Lys, His, Tyr and Met react slowly with excess reagent and long reaction times
	N-ethylmaleimide	pH 6 or higher	None
	5,5'-dithiobis(2-nitrobenzoic acid) (Ellman's reagent)	pH 7 or higher	None
Thioether (Met)	Oxidation (H,O,)	pH 2 and higher	Thiols react very rapidly

While the limitations of AAL/MS techniques are less applicable to H/D exchange, the rapid back-exchange (within 2-5 ms of exposure) with water molecules in the chamber environment of an ionization unit, are a serious concern for analysis of modified proteins or modified peptide fragments, and is a unique limitation to this technique. Nevertheless, recent developments in ionization units like the rapid evaporative ionization, desorption electrospray ionization, electrospray laser desorption ionization, and laser ablation electrospray ionizatio) promise more direct ionization of the intact protein, but have not yet been applied to study adsorbed proteins.[100]

Time-of-flight secondary-ion mass spectrometry (ToF-SIMS) is another variant of mass spectrometry that has been used for characterizing adsorbed protein layers.[77-79, 101-106] Since these techniques have a low sampling depth (10-15 Å), when compared to the usual thickness of an adsorbed protein layer, relative amino acid concentrations (based on the intensity of reference peaks for each amino acid) and their signature peaks have been used to determine the structure of adsorbed protein films on different surfaces For this purpose, the data analysis is usually done using an established multivariate-analysis technique known as principal-component analysis, which decomposes a large dataset into two cross-product matrices (scores and loadings) with the score plot indicating the

interrelationship between different samples and the variability within each sample.[105] Although, ToF-SIMS is one of the only known techniques capable of monitoring the conformational shifts within a mixture of adsorbed proteins, this technique is only semi-quantitative in nature.[105] Additionally, since ToF-SIMS must be performed under ultrahigh vacuum conditions (UHV) , one other concern with this technique is the adverse impact of the UHV condition on the structure of adsorbed proteins.[105] To overcome this limitation, two recent improvements have been made to ToF-SIMS—by multiplexing the ToF-SIMS with SFG-FTIR systems, or by coating the proteins with H-bondable groups like sugars or polyols, or by crosslinking to preserve the adsorption-induced structure of the protein.[76, 105] An obvious concern with these preserving methods, however, is their possible influence on the structure of the adsorbed protein as well.

2.2.2.1.b.2 Neutron Scattering

Conformational shifts in adsorbed proteins by small-angle neutron scattering is often determined post-exposure to deutrated water, based on the difference in scattering cross-sectional area for hydrogen (high cross-sectional area) and deuterium (low cross-sectional area) containing segments within the proteins.[107-116] As unfolded segments within the protein tend to be more solvent exposed than when the protein is in its native state, these segments are increasingly prone to deuterium exchange. The increased exchange results in overall reduction in the mean-square displacement and vibrational density of the unfolded proteins as opposed to the native protein, which can be qualitatively correlated to the loss in conformation. However, the same drawbacks that affect all the techniques that rely on H/D exchange affect the conformational analysis by

neutron scattering as well. Additionally, the infrastructure requirement for these types of techniques further affect their wider applicability.

2.2.2.1.b.3 Nuclear Magnetic Resonance (NMR)

X-ray diffraction and NMR spectroscopy are the only techniques that can provide detailed structural information about macromolecules at atomic resolution. However, the effect of photon flux and radiation-induced damage on the protein structure prevents X-rays from directly being applied on proteins for characterizing the adsorption-induced conformational shifts. Additionally, obtaining the crystal structure of adsorbed protein on surfaces is of considerable difficulty due to low surface area-to-volume of typical samples, which further inhibits the use of X-ray diffraction for adsorbed protein structure determination. In contrast, NMR can be directly applied on the protein to obtain a plot of intensity by isotopes like $^{1}H_{\alpha}$, ^{13}C and ^{15}N as a function of sequence or chemical shift index (CSI) for the difference amino acids within its structure.[73] Two types of NMR are currently in use—solution-state NMR and solid-state NMR (ssNMR).[68, 117] The strategy used for resolving the adsorbed protein structure using solution NMR was to initially deutrate the adsorbed protein, following which the proteins are desorbed, and refolded in detergents, and solution state NMR is then applied to elucidate the structure. The final structure of adsorbed protein is resolved by background correcting the spectra obtained for the native protein, which are subjected to the same treatment without the adsorption process. In contrast, ssNMR uses rare spin isotopes like ^{13}C and ^{15}N to determine the structure of protein via orientation constraints and/or distance and torsion-angle constraints by making use of chemical-shift anisotropies (CSAs) in the spin state of two

homologous isotopes.[117] Currently, the capability of ssNMR has been demonstrated with ceramic and more recently on hydrophobic surfaces.[117-118] Although these techniques are very powerful in resolving protein structure, NMR has not been applied to proteins that are > 30 kDa due to significant broadening of the narrow spectral signatures, which can seriously hamper the accuracy of the structural assignment.[73] Additionally, concerns of back exchange with H/D exchange technique also limits its application.

2.2.2.2 Techniques for Monitoring the Orientation of Proteins

Most techniques that probe the local shift in structure of the adsorbed protein are also capable of providing qualitative or semi-quantitative information on the orientation of adsorbed proteins. But, more quantitative and detailed insight into the orientation of adsorbed protein have been demonstrated by multiplexing several of these techniques. Many optical techniques, like SFG, dual-polarization interferometry, and whispering-gallery mode, are currently used for determining the orientation of protein on a surface.[76, 119-120] A common optical property exploited in all these techniques is the difference in polarization of the incident beam relative to the reflected beam, following its interaction with the adsorbed proteins.

Similarly, more detailed insight into the orientation of protein and individual structural elements can be obtained by techniques like near-edge X-ray-absorption fine structure (NEXAFS), which is very sensitive to molecular bonds. The ordering of protein backbone on the surface can be obtained using NEXAFS by varying the angle of incidence and orientation of the incident X-rays.[76, 78] But, the UHV conditions required for NEXAFS is again a major limitation with this type of technique. Alternatively,

multiplexing of techniques like SFG when combined ssNMR, and SFG combined with NEXAFS and ToF-SIMS have demonstrated their capability to provide information on the orientations of the peptide backbone, the individual side chains, and the dynamics and proximity of side chains in individual residues with respect to a surface. Other type of techniques like the atomic force microscopy (AFM), synchrotron based X-ray photoemission electron microscopy (X-PEEM), and scanning transmission X-ray microscopy (STXM) have also been used for characterizing protein topology and the organization of proteins on an adsorbent surface. These are very useful techniques for visualizing the dynamics occurring at the interfaces.[121] But their application for determining adsorbed protein configuration is less direct and is severely limited by low lateral resolution.

Based on my review of current applied techniques, there are considerable technical opportunities at a researcher's disposal to resolve the configuration of an adsorbed protein. But, given the limitations of each individual technique, a combination of methods applied in a synergistic manner may be necessary to provide more detailed insight into the adsorbed configuration of a protein than when these techniques are applied alone. Some combination of techniques that have been demonstrated to be particularly effective in characterizing the adsorbed configuration of a protein are AAL/MS-CD, SFG-FTIR-ToF SIMS, SFG-ssNMR, and SFG-NEXAFS.[44, 76, 94] But the capability of these multiplexed tools must be further fine-tuned in order to provide detailed insight into the role of the adsorbed configuration of a protein on its adsorbed-state bioactivity.

2.3 FACTORS INFLUENCING THE BIOACTIVE STATE OF ADSORBED/ IMMOBILIZED PROTEIN LAYERS

As discussed above, the bioactivity of a native protein is attributed to its folded structure. The folded structure of a protein depends on the amino acid composition, solvent environment (usually aqueous environment) and intra- and inter-polypeptide chain residue-residue interactions. As the native environment of a protein is generally aqueous, the interaction between amino acid side chains play a critical role in a protein's folded structure and can be visualized to be within a 3D mesh of hydrogen-bonding (H-bonding).[122-124] The side-chains of polar and charged amino acids are hydrophilic and can form strong bonds with each other and with water through electrostatic and dipole-dipole interactions, such as H-bonding. In contrast, the side chains of alkyl and aromatic amino side chains are non-polar and more hydrophobic than the polar counterparts and tend to be buried inside the protein structure to minimize their solvent-accessible surface area.[37, 125-126] For example, in a protein of 15 kDa molecular weight, it is estimated that solvation of these molecules would require 600-1000 water molecules, thereby, bringing the ratio of protein to hydration mass to approximately 1:1, and it is expected that this ratio is similar for larger proteins as well.[127] The resulting protein structure in aqueous solution is generally assumed to be at a global minimum Gibbs free energy[37, 127-129] and can be considered to be stabilized by two main thermodynamic contributions:

- Enthalpic contributions ($H_{protein}$), which account for the bonded contributions within the protein like van der Waals, hydrophobic, or electrostatic interactions, and

- Entropic contributions ($S_{protein}$), which account for the degree of structural order within the protein, like structural packing of amino acids in protein, cavity area, and solvation effects.

The hydration layers along the protein surface are ordered and extend 1-2 nm into bulk water.[130] The most innermost of these hydration shells are often considered to be made up of a highly dense and ordered water layers. The exchange of this layer with bulk water is controlled by the exposed functional groups on protein surface, which imparts the protein with its necessary conformational flexibility.[56, 131-133] Water molecules, which have gotten isolated and trapped inside a protein's core are also known to provide segments of the protein chain with the essential *'fluidity'* that is often necessary for the bioactivity of a protein.[134] It has also been suggested that water ordering may be responsible for keeping proteins in solution and providing *'visibility'* to ligands.[135]

However, in the event of protein adsorption onto a material surface, water structure reorganization is expected to occur on a time-scale that is concomitant with protein adsorption.[136] Generally, the water structuring in the interfacial phase exhibits a spatial orientation corresponding to the distribution of surface charge and H-bonding groups on the adsorbent surface. As a result, the structured water at the interface is more *'ice-like'* and ordered than the distorted tetrahedral molecular arrangement of the water in the bulk phase.[137] These ordered structure of water at an interface being relatively at a higher free energy state than the bulk water, the adsorption system tends to lower its overall free energy by displacing some of the outer layers of water from the adsorbent as well as the protein's surface to the surrounding bulk aqueous solution.[138-140] Such loss in

the hydration sheath results in proteins being adsorbed on the surface in preferred or random orientations followed by changes in its folded structure.[141-142] However, the extent of such shifts on protein conformation and adsorbed orientation depend on the combined effects of protein-surface interactions, protein-protein interactions, and the internal stability of the protein.[37, 39, 143] All of these factors additionally affect the bioactive state of adsorbed protein.

2.3.1 Role of Internal Stability of Protein

The native structure of a protein is influenced by its solvent environment (e.g., salt concentration and pH). The role of solvent and its constituents in maintaining the stability in the native structure of a protein is based on two main principles: (1) strengthening the forces that stabilize the protein's structure; and (2) destabilizing the denatured state relative to the native state.[144] Variations in solution conditions such as the composition and concentration of salts and pH are known to affect the adsorption behavior of the same protein differently even on the same adsorbent surface.[145-146] This is attributed to the interaction of proteins with the solution constituents.

2.3.1.1.Role of Solution Constituents and pH

Although a general idea on the role of buffer constituents on the adsorption response of a protein is lacking, their effects on the native structure of protein is well recognized. Both buffer species and their concentrations are known to affect the physical stability of a native protein.[144-145, 147] The effect of some of these buffer species like salts on the protein stability is complex, because of the intricate interactions occurring on both the protein surface and its interior. Salts may stabilize, destabilize, or have no effect on

the native structure of protein depending on their effect on (a) solvent properties, (b) the ionizable groups, and (c) electrostatic screening length (Debye-Huckel screening).[144] An excellent example in the regard is shown by the Hofmeister series, which represents the impact of ionic groups on the structural integrity of proteins (Fig 2.2).[148]

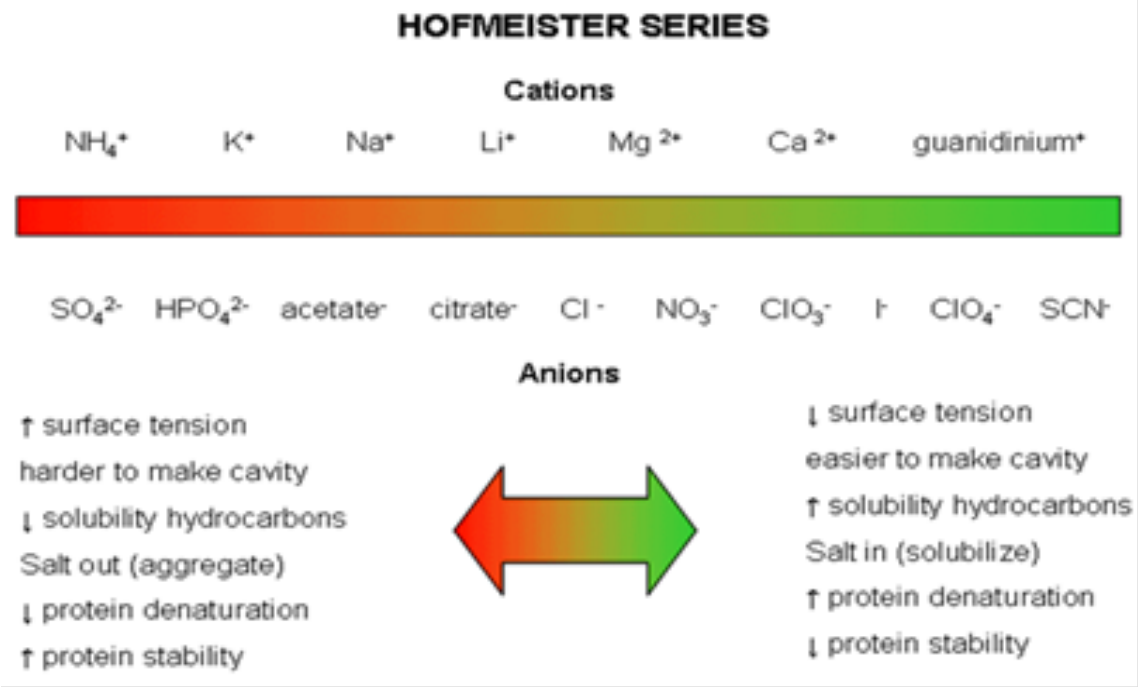

Figure 2.2 Hofmeister series.[149] Anions and cations to the left of Cl− are termed *'kosmotropes'* (red) while those to the right are termed *'chaotropes'* (green). Specific ion effects of each on water and proteins have also been indicated. Reproduced with permission from Ref.149. Copyright 2006 Elsevier B.V.

The Hofmeister series is based on the affinity of ions to water, and can be broadly classified based on their affinities towards water as either being kosmotropes (stronger affinity and hence strongly hydrated) or chaotropes (weaker affinity and thus weakly hydrated).[139, 141-142, 149-152] Kosmotropic ions are considered to stabilize the protein by preferential exclusion which involves enhancing hydrophobic interactions and

reducing the solubility of hydrophobic groups in proteins. In contrast, the chaotropic ions are considered to destabilize the protein by preferential solvation due to their higher ionic affinity to the polar groups, which results in the disruption of a protein's H-bond network, which can subsequently weaken the stability of the hydrophobic core within the protein.[144] Similarly, the concentrations of ionic salts play an important role in the solvation of the protein. At lower concentrations of kosmotropic salts, the solubility of the proteins is usually higher (salting in), but at higher concentrations, the proteins solubility decreases (salting out) due to the absence of a sufficient solvating molecules.

However, the effects of Hofmeister series are not universal on all proteins; for example these effects have been reported to be reversed at low concentrations for some positively charged proteins.[150-151] Similarly, it has also been reported that while high concentrations of kosmotropic salts are found to have a stabilizing influence on the proteins that are stabilized by non-electrostatic interactions, these same salts were found to have a destabilizing influence on the proteins that are stabilized by salt bridges or electrostatic interactions. In more recent studies, it has also been suggested that specific effect of ions on the protein structure could be arising due to the direct interaction of the ions with the protein.[139, 141-142, 149-152]

The pH of a solution is another factor that can influence the protein's stability and its adsorption response.[39, 145] The pH of the solution dictates the charged state of ionizable groups, and hence, the accurate control of solution pH is important for protein stability. At a bulk solution pH of 7.4, protein-protein repulsions are dominant

as the isoelectric points of many proteins are above or below this pH. As a general observation, proteins with a net charge are adsorbed more strongly on oppositely charged surfaces than similarly-charged surfaces. Also, electrostatic repulsion between adsorbed proteins also reduces tendencies for proteins to aggregate on a surface.[144] The importance of electrostatic interaction on the protein adsorption process is also evident by the maximal surface coverage observed at the isoelectric points of protein as opposed to when the proteins have a net charge.[39] But, the charge distribution and polarization of ionizable groups on a protein is not uniform and is quite complex, as the acidic dissociation constant (pKa) of even similar types of amino acid residues can vary drastically depending on their position with the protein.

2.3.1.2 Role of Protein Size

Large, high molecular weight proteins (i.e., > 67 kDa) are generally structured in a manner such that the majority of non-polar amino acids constituting the protein occupy the non-solvent-accessible interior, while the polar and charged amino acids constituting the protein occupy the solvent-accessible outer layer of the protein. In contrast, small, low molecular weight proteins, which are not large enough to be stabilized by a hydrophobic core, tend to rely more on covalent disulphide bonds between cysteine residues for structural stabilization, and generally have a more equal distribution of non-polar and polar amino-acids throughout their structure.[127] As a result, in the event of protein adsorption on a material surface from a solution containing a mixture of low molecular weight proteins and high molecular weight proteins, larger proteins are favored over smaller proteins on an adsorbent surface because of the enthalpic (electrostatic, H-

bonding, hydrophobic and van der Waals interactions) and entropic (i.e., redistribution of charged groups, hydration changes and structural perturbations) benefits provided by the size of a larger protein.[37, 39, 129, 143, 153] This favorable tendency occurs despite the smaller, low-molecular weight proteins being transported by diffusion to the surface much faster than the larger, heavier molecular weight proteins. Additionally, the smaller proteins that are stabilized by disulphide bonds usually tend to be more rigid, and more resistant to adsorption-induced confromational shifts than the larger proteins that are stabilized by non-covalent interactions.

However, there have been instances in which adsorption of low molecular weight proteins are favored over high molecular weight proteins, such as in the case of displacement of fibrinogen (340 kDa) by high molecular weight kininogen (88 kDa-120 kDa, depending on glycosylation) on a hydrophilic surface.[37] Also, the tendency of larger proteins to displace smaller proteins that are pre-adsorbed on a surface decreases with increasing residence time of the adsorbed protein. This behavior underlines the importance of understanding and quantifying the affinity of specific amino-acid groups and effect of protein structure to an adsorbent surface, so as to better understand the adsorption tendency of different proteins containing different primary sequences and exposing different functional groups on its surface.

2.3.2 Role of Protein-Surface Interactions

Protein adsorption to material surfaces can be quite complex, with proteins adsorbing in differing surface coverages, conformations, and orientations depending on the chemical and physical characteristics of the adsorbent surface.[39, 48, 143, 154-155] In the interpretation of

many adsorption experiments, it is often assumed that the surface structure of the material is stable, which is not always the case. For example, glasses are known to undergo surface dissolution at high alkaline solution conditions.[156] Similarly, polymers are known to undergo structural rearrangements or hydrolysis (if hydrolytically degradable).[42] Further difficulties in developing a theoretical understanding of the influence that materials have on protein adsorption behavior is exemplified by the variations in the structural make up of materials (e.g. polycrystalline materials) in which the crystalline orientation of the grains, their size, and structure of the grain boundaries creates surface heterogeneity. Considerations must also be given towards the conformational stability of material surfaces while developing a quantitative understanding of the peptide/protein adsorption behavior on material surfaces. For example, in AFM experiments performed by Wei and Latour on Nylon 6/6, the effective standard-state adsorption free energy (ΔG^{o}_{ads}) value deviated markedly from values obtained on a SAM-$NHCOCH_3$ model surface despite the surfaces having similar functional group chemistry.[157] The authors speculated that the swollen hydrogel-like behavior of Nylon surface could be the reason for the deviation in measured ΔG^{o}_{ads}, which would result in surface structure that was substantially different than that presented by a SAM surface. Such structural rearrangements of long chains in polymers are, however, not uncommon in the field of biomaterials and other areas of material science, and complicates the interpretation of the process of protein adsorption.[42]

2.3.2.1. Role of Material Properties

It has long been known that interfacial water is very different from bulk water.[139, 158-159] Studies have also indicated that the variations in functional groups on an adsorbent surface

can result in different types of H-bond networks that can vary in dynamics, ordering and strength, and can potentially affect the water ordering at the surface.[160-162] While in case of a hydrophilic surface, water structure may be not that different from bulk solution, in the case of a hydrophobic surface, there exists a *'hydrophobic gap'* immediately above the adsorbent surface that is otherwise adjacent to an ordered structure of water due to the inability of water to form H-bonds with the functional groups of the surface.[163-164] Furthermore, in the case of charged solid substrates, ordered water could extend for several layers over the surface depending on the charge density and variation in spacing between the functional groups on the interacting sites on the adsorbent surface.[165] Therefore, when compared to the structure of H-bonds in bulk water, the interactions of adsorbent surfaces with interfacial water via polar and H-bondable groups, can vary between very weak to very strong interactions depending on the distribution and type of functional groups on the adsorbent surface.[166]

Protein-surface interactions can result in an adsorbed protein monolayer undergoing conformational shifts or reorientations depending on the type of surface.[37, 46, 48, 94, 154, 167] Although a quantitative understanding on hydration as a function of surface properties as well as its effect on protein adsorption is not fully understood, a qualitative understanding on hydration as a function of surface properties is clearly emerging, at least on neutrally charged surfaces.[157, 168] Based on the interplay of synergistic and antagonistic short-range forces influencing protein-surface interactions, it has been generally proposed that:

(a) All proteins adsorb to hydrophobic surfaces,

(b) Adsorption of highly stabilized protein on hydrophilic surfaces is mediated by attractive electrostatic interactions, and

(c) Adsorption of weakly stabilized protein is primarily driven by conformational entropy that is large enough to cause adsorption even on a hydrophilic electrostatically repelling surface.

Given longer residence time, neutral hydrophilic surfaces tend to induce primarily orientational shifts in the protein structure while a neutral hydrophobic surface tends to cause conformational as well as orientation shifts.[110, 116, 169] Similarly, the adsorption response of protein on charged surfaces can vary depending on the charge density on the adsorbent and the protein surface, with weakly charged adsorbent surfaces inducing orientation shifts while strongly charged surfaces inducing conformation shifts or even repelling protein adsorption.

Another factor influencing the surface property of the adsorbent surface is surface roughness. Surface roughness is known to affect the wettability of surface and also lead to localized changes in surface chemistry.[24] These effects tend to increase the available surface area and therefore, generally promotes protein adsorption.[143] The amount of protein that is adsorbed on an adsorbent is limited by the available surface area and it has been established that protein adsorption is higher on adsorbent surfaces with convex and irregular geometries rather than on flat surfaces.[24, 27] For example, in a recent study that examined the influence of surface roughness on bovine serum albumin (BSA) and fibrinogen (Fg) adsorption on tantalum, it was observed that adsorbed BSA increased by 30%, while Fg adsorption increased by 88% when surface roughness of the adsorbent was increased by 15%.[170] Typical

topographical modifications of adsorbent surfaces such as random roughness, gratings or isolated bumps are therefore, expected to increase adsorbed protein densities and conformational shifts, and may also introduce different degrees of geometrical packing of proteins.[24, 27, 171]

Other physical factors that can also be attributed to promoting protein adsorption on a rough adsorbent surface are the dimensional matching between a material's topographic features,[172-174] electrical-electronic nature,[175] crystalline orientation,[176-177] and molecular architecture.[103] However, some groups have claimed that nano-metric scale roughness do not affect the amount or the conformation of adsorbed proteins.[178] Nevertheless, despite the general understanding on the influence of surface properties on protein adsorption, the role of surface chemistry on the adsorption process in unclear. For example, it has been shown that -CH_3 and -OCH_2CF_3 model SAM surfaces are strongly hydrophobic and have similar peptide adsorption properties.[168] On such surfaces, proteins have a higher thermodynamic driving force to unfold their hydrophobic core over the adsorbent surface to reduce their solvent accessible surface area.[46-48, 94, 154-155, 167, 179-181] Yet, the conformational shift of the same protein at similar adsorption conditions were significantly different on each of these surfaces.[48]

Similarly, solution conditions can also influence the material properties and thereby, protein-surface interactions. As previously mentioned, the pH of bulk solution affects the charged state of the protein. Similarly the surface dissociation constant (pK_d) and the bulk solution pH also affects the charge density of the adsorbent surface.[182] As the surface charge density of an adsorbent surface varies with the bulk pH, counter ions in solution are attracted

to the adsorbent surface while the co-ions are repelled. This results in localized charge accumulation at the adsorbent interface, which results in establishing a pH gradient between the adsorbent and bulk solution, which, in turn, affects the extent of ionization within the proteins. These effects can also influence the subsequent adsorption behavior of proteins.[182] In addition, it has also been observed that the charge density determined for the same substrate can vary for otherwise same conditions depending on the cationic and anionic constituents in the solution.[146, 183]

The ionic strength and the type of ions in solution are other common determinants of protein-surface interactions.[145-146] For example, on a hydrophilic surface, the entropic benefits associated with the release of ordered water is more favorable in the presence of kosmotropic than chaotropic ions, which favor higher amounts of protein being adsorbed on a hydrophilic surface.[146] Therefore, a detailed insight into the chemical, morphological, and structural properties of the material surfaces is essential prior to investigating the sub-molecular mechanisms that are involved in protein-surface interactions.

2.3.2.2. Role of Protein Properties

Following the initial adsorption of a protein on an adsorbent surface, the solvent and surface co-operatively tend to weaken the hydrophobic interaction within a protein while also strengthening its H-bond interaction with the aqueous solution. Earlier studies exploring the dynamic nature of proteins in solution have often linked the rapidity of H-bond making and breaking with rapid structural fluctuations within the protein.[184] As a result, on strongly interacting adsorbent surfaces, proteins are more likely to undergo both conformational and orientation shifts, while on weakly interacting surfaces, adsorbed proteins can be expected to

undergo orientation shifts without substantial conformational changes as a function of exposure time.[37, 39] Therefore, following the initial adsorption on a strongly interacting adsorbent surface, the longer exposure time of proteins on surfaces can lead to an increased probability that the proteins will be adsorbed in an effectively irreversible manner.[37, 39, 153] Some of the markers used for monitoring such structural transitions in the adsorbed protein involve conversion of α-helix to β-sheet, fluctuations in the exposure of buried tryptophan groups, and change in the cofactor position. Also, a molecular simulation study by Agashe at al.,[185] had suggested that the kinetics of protein reorientation on a surface following adsorption are faster than the kinetics of adsorption-induced unfolding, thus possibly providing an alternative mechanism to separately control adsorbed protein orientation from adsorbed conformation on a surface.

If a protein is structurally stable, proteins would tend to adsorb to surfaces in preferred orientations that would correspond to its free energy minima, provided the rotational freedom for the protein is available. This is primarily because a folded protein exhibits different adsorption affinity in different regions of its surface. Thus, it can be expected that on hydrophilic interfaces, proteins predominantly expose those patches toward the surface that are rich in hydrophilic residues and on hydrophobic surfaces proteins direct their hydrophobic patches to the adsorbent surface. Similarly, proteins adsorbing at positively or negatively charged surface tend to expose oppositely charged regions to the surface. Clearly, in such cases, it is necessary to understand the affinity of specific amino-acid groups with the functional groups on an adsorbent surface, so as to predict the adsorption tendency of different proteins containing different primary sequence and exposing different functional

groups. Furthermore, the adsorption characteristics of different peptides expressed by phage systems on gold surfaces,[186] have also demonstrated the need to quantitatively understand the adsorption characteristics of peptides on different adsorbent surfaces as a function of its surface property; more specifically as a function of its surface chemistry.

The general technique to characterize the thermodynamic parameters involved in peptide adsorption is based on the determination of static or dynamic adsorption isotherms of peptides on different adsorbent surfaces with controlled chemistries. In this context, of particular interest are the studies done by Latour and coworkers, in characterizing the standard-state Gibbs free energy of adsorption (ΔG^{o}_{ads}) involved with host-guest peptides (TGTG-X-GTGT, with T, G, and X representing threonine, glycine, and a variable guest amino acid) on alkanethiol SAM surfaces with different functional groups and on bulk material surfaces.[157, 168, 187-188] When compared to the conventional approach of determining the individual thermodynamic parameters such as enthalpy and entropy,[189-190] determination of ΔG^{o}_{ads} provides a direct assessment of the thermodynamic driving force responsible for peptide adsorption to the surface. Results from these studies indicated that the ΔG^{o}_{ads} correlates strongly with the static water contact angle for non-charged surfaces, with charged surfaces resulting in additional adsorption affinity beyond what is represented by the water contact angle alone.[157]

It is also relevant to discuss the applicability of the adsorption characteristics of linear non-structured peptides to the adsorptive behavior of structured proteins, especially since the peptide adsorption isotherms are based on a reversible process while protein adsorption on most material surfaces is effectively non-reversible. On a fundamental level, since all proteins

are made up of amino acids, the greater the number of amino acids constituting a peptide, the stronger should be the peptide-surface interaction due to an additive effect.[191] In fact, a linear relationship is observed between the ΔG^{o}_{ads} and the number of amino acid residues interacting with a material surface until about eight amino acid residues, above which this linear trend starts weakening and then completely disappears,[190, 192] possibly due to a transition from reversible to irreversible adsorption behavior. This response was specifically observed with leucine-lysine (LK) peptides with model α-helical ($LK\alpha_{14}$, ~ 2 kDa) and β-sheet ($LK\beta_{15}$, ~ 2 kDa) structures on hydrophobic and carboxylic-acid SAM surfaces.[101-102, 118] Such peptides were found to adsorb in preferred orientations with Leu facing the hydrophobic adsorbent surface, and Lys facing the carboxylic SAM surface. Similar responses were also observed when these peptides were adsorbed on fused silica and polystyrene surfaces.[79] More noticeably, in all these cases, the secondary structural content of the peptides were preserved. Even in the case of low molecular weight proteins like statherin (~5 kDa, unstructured near the N-terminus but contains 3_{10} helical structure near the *C*-terminus) and the B1-domain of G-protein (~6 kDa, containing mixed helical and β-sheet structures).[77-79, 117] These proteins were found to adsorb in either random or preferred orientations but no loss in the secondary structures were observed. This is clearly different from the usual trend observed with the adsorption of protein that tend to adsorb on the surface by significantly undergoing conformational shift.[48, 94, 193]

A possible reason for such contrasting observation could be due to the positive entropies involved with the loss in ordered water layer and reduced structural freedom associated with the protein ordering and secondary structural motifs. But in case of larger

proteins, the binding enthalpy could be compensated by structural transitions from helices to β-sheet structure. For example, inherently among all secondary structures, β-sheet structure, specifically the anti-parallel β-sheet structure, promotes the most stable intra-molecular interactions due to its tighter packing of the protein backbone and optimization of van der Waals interactions. This efficient packing also tends to minimize unfavorable hydrophobic interactions with water.[127, 194] On the other hand in helices, H-bond interactions within a protein's backbone chain is lessened compared to β-sheet structure. Additionally, by the virtue of its shape, the helical structure interacts with the solvent molecules more favorably than the β-sheets.[195] Thus, protein-surface interaction on an adsorbent surface can be expected to be higher for adsorbed proteins that promote β-sheet structure, as opposed to those retaining helices. This in turn, may also be indicative of the protein's stability at the interface, with strong protein-surface interactions promoting a more stable adsorbed protein layer, with weaker interactions indicating otherwise. These type of responses clearly indicate that the structural ordering of peptides influences the binding strength involved in their adsorption.[196] Thus the affinity of amino acid residues along with their structural ordering are responsible for the orientation and conformational shifts within a protein during the adsorption process.

2.3.3 Role of Protein-Protein Interactions (PPI)

Protein-protein or lateral interactions (PPI) are other significant contributors towards adsorption responses at a solid-liquid interface, and their influence on the adsorbed configuration of a protein is known to substantially increase at increasing surface coverage.[39] For example, the surface complementarity between the protein and an

irregular adsorbent surface promotes multiple short range interactions. But, these short-range interactions by the surface are easily overcome by PPI effects.[39] Therefore, in many studies attempting to identify the role of surface chemistry on the conformation and orientation shifts of a protein, significant lateral interactions may have inadvertently influenced these responses.[180] A possible methodology to determine the influence of PPI on the molecular events occurring at the solid-liquid interface is to monitor the adsorption response of protein layer as a function of the adsorbed mass of protein, protein solution concentration, and exposure time.[44, 47-48, 94, 154, 167, 179]

2.3.3.1. Role of PPI on Orientation

Irrespective of the composition of a given adsorption system, transport of protein from the solution to the solid phase is mediated by diffusion through a stagnant layer of solvent molecules immediately above the adsorbent surface.[37] On a uncharged adsorbent surface, the adsorption of individual protein molecules is considered to occur at different sites in random orientations, without interfering with the previously adsorbed protein molecules to maximize the favorable protein-surface interactions.[39] But, as the concentration of the protein in the stagnant layer depletes with the proteins adsorbing to the surface, the resulting concentration gradient drives further diffusion of proteins into the stagnant layer from the surrounding bulk solution and eventually saturates the non-charged adsorbent surface, provided the proteins adsorb irreversibly.

As the surface coverage increases, the entropic gain due to "*random*" adsorption is offset by a thermodynamic penalty due to PPI, which results in the tighter packing of proteins on the adsorbent surface. The resulting PPI effects may become increasingly

dominating and create a different free-energy-minimum state to which the adsorbed proteins adapt, possibly even involving different thermodynamic parameters. For example, at low coverage, statherin adsorbs onto HAP with a significant favorable free energy change that is driven by both entropy and enthalpy.[75, 117] But, at higher coverage, the adsorption of HAP becomes enthalpically neutral and is driven solely by the positive entropy change associated with the release of bound water molecules. Even at such saturated conditions when rotational diffusion is greatly hindered, proteins can still alter their orientation if the local surrounding conditions change. This is particularly observed when electrostatic interactions on both the adsorbent and protein surface are electrically altered, or the protein densities on the adsorbent surface are decreased upon rinsing. According to Lenhoff and Roth, each protein within this saturated layer of adsorbed protein molecules contributes a net charge (assuming the protein is not at its isoelectric point), which eventually leads to a considerable kinetic barrier that prevents further adsorption and the formation of multilayers.[197]

2.3.3.2. Role of PPI Effects on Conformation

On a highly adsorbing surface, higher concentrations of protein in the bulk solution will result in faster surface saturation, which provides less time for a protein to spread out on the surface (i.e., greater conformational shift from the protein's solution structure), before further spreading is blocked by neighboring adsorbed proteins. On a hydrophilic surface, proteins that adsorb from more concentrated solutions have a lower tendency to undergo spreading than those that are adsorbed from a low solution concentration. But, on a highly hydrophobic surface, the effects of PPI on the

conformational may be minimal or insignificant when compared to the stronger protein-surface interactions. However, the varying influence of these PPI effects on the conformation of different protein-surface systems have not been previously identified or quantified, and may explain the molecular mechanisms involved in aggregation, cooperative effects, kinetic overshoots, and multilayered adsorption.[39, 145]

2.3.4 Role of Other Extrinsic Factors

Other extrinsic system parameters such as flow, pressure, and temperature can also influence the adsorption behavior of protein at solid-liquid interfaces.[39] The flow rate of the adsorption system influences the exposure time of protein on the adsorbent surface and decreases the adsorption tendency of protein at higher flow rates.[198] However, at higher flow regimes, the stability of the native structure of protein may be affected, resulting in the adsorption and aggregation at material surface. In contrast to flow rate, high temperature and pressure both promote protein adsorption. While, temperature affects the equilibrium and kinetics of protein adsorption by influencing the diffusivity and entropic stability of the adsorption system,[111, 199] high solvent pressures promote denaturation on hydrophobic surfaces by inducing conformational shifts in a protein by promoting the solvation of its hydrophobic groups.[200]

2.3.5 Influence of Adsorption on the Bioactive State of Proteins

Although, many experimental and theoretical studies have elucidated the individual molecular-level events involved in the conformational shifts and orientational shifts of adsorbed protein, relatively few studies have been done to quantitatively connect the role of

these adsorption-induced configurational shifts on the bioactive state of a protein. In a recent study using a combination of different techniques including bioactivity assays, CD, AAL/MS, the role of conformation and orientation on the native state bioactivity have been clearly distinguished on SAM surfaces.[44, 94] Loss in the conformation of a protein is generally considered to be accompanied with loss in its bioactivity. Studies have also indicated that conformation-induced losses in bioactivity may be either related to loss in flexibility of the key residues/segments, or by the burial/exposure of the residues within the pocket containing the bioactive site.[44, 94, 201]

It is, however, worth noting from these studies that the decrease in bioactivity due to loss in secondary structure is not a generic response, but is system-specific. An adsorbed protein can lose its native-state bioactivity when its active site is sterically occluded by the adsorbent surface or neighboring adsorbed proteins. An excellent example of this behavior, is the loss in bioactivity of a charged protein on a charged surface. The orientation of the bioactive site of a protein is influenced by the charge on the adsorbent surface and the charge surrounding the bioactive site of the protein, especially at low surface coverages.[15, 79] But, at higher surface coverages, the access of the ligand to the active site will have higher tendency to be inhibited by physical blocking of neighboring proteins as well as the surface, or by inducing a conformational shift in the bioactive site of the adsorbed protein.

In addition to the role of adsorption-induced configuration, the loss in bioactvity of the protein can also result from the loss in water structuring or the loss in '*fluidity*' around the structure. But the influence of such loss in hydration on the bioactive state of a protein has not been widely studied, largely because current expoerimental techniques are generally not

sensitive enough to identify the role of hydration on the bioactvity of adsorbed proteins. Instead, a better alternative would be to quantify the influence of adsorption-induced changes in the protein configuration on its native-state bioactvity. Such structural changes in the adsorbed protein can be indirectly related to the loss in its hydration sheath. But as indicated in section 2.2, no single experimental technique is sufficient to provide comprehensive information on the adsorbed configuration of a protein. Instead, a synergistic combination of techniques like the CD, AAL/MS, and adsorbed state bioactivity assays, are considered to be more suitable for resolving the molecular processes causing adsorption-induced loss in native-state protein bioactivity. Additionally, in order to delineate the specific mechanisms involved in such adsorption processes, a systematic understanding of the adsorption system is essential, especially since these systems can be '*history dependent*'.[37]

2.4 MOLECULAR MECHANISMS INVOLVED IN THE INTERACTION OF EXCIPIENTS IN AQUEOUS SOLUTION WITH AN ADSORBED/ IMMOBILIZED PROTEIN LAYER

The bioactive state of an adsorbed/immobilized protein can have a wide-ranging impact in its scope of application and underscore the need to stabilize or deactivate the adsorbed protein, depending on the specific application. As illustrated in section 2.1, the inadvertent or intentional exposure of proteins to material surfaces can be associated with their prolonged persistence and potency.[202] Such effects have resulted in device failures, fouling, and in the case of protein toxins, have also led to costly quarantine procedures to mitigate public health concerns. But in many other applications, adsorbed/immobilized protein systems represent a cost-effective, design-austere, and technologically robust

alternative to using native proteins to perform a designed function such as drug delivery or bio-sensing. Therefore, strategies to control the bioactive state of adsorbed/immobilized proteins is of general interest.

In this context, aqueous-based formulated solutions are most often used to adsorb and otherwise manipulate proteins, as water is generally an essential medium for protein bioactivity. Additionally, aqueous solutions are generally less harsh on the underlying material surfaces to which proteins are tethered or adsorbed, and the strategies to stabilize or destabilize the native state structure of a protein in aqueous solution using chemical excipients are relatively well-understood.[144] Two of the central strategies by which aqueous based excipients are considered to stabilize or destabilize a protein's structure are by (a) inducing water re-structuring or (b) by directly interacting with proteins. But in contrast to its solution counterpart, the behavior of proteins that are immobilized on a material surface can be quite different than the proteins in their adsorbed or tethered states, and the extent to which such strategies can be applied and their resulting effects on the bioactive state of surface-immobilized proteins are not yet well understood. Therefore, the purpose of this section was to review the feasibility of extending some of the strategies utilized in stabilizing or destabilizing the native state structure of proteins in solution, to those that are adsorbed.

2.4.1 Indirect Interaction of Chemical Excipients with Protein Structure by Restructuring of Water

Proteins in solution are tightly coupled to a layer of solvent molecules, and the exchange of these water is dynamically controlled by the exposed functional groups, which provides it with the essential *'fluidity'* to the protein structure. These tightly

coupled water layers are considered to be essential for protein's bioactivity and is retained even in an anhydrous solvent. In fact, studies have indicated that though the proteins tend to lose its bioactivity in anhydrous solvents, more hydrophilic proteins tend to retain higher bioactivity in more hydrophobic solvents, due to the reduced tendency of these solvents to strip away essential water, and the self-interacting nature of the organic solutes to be partitioned near hydrophobic interfaces.[203] The addition of solvents that are less polar than water or tend to form linear H-bond with water, can lead to weakening of the internal interactions within the protein. But, the extent of such weakening often tend to increase as organic solvent-to-water ratio is increased, until a point in which further reduction in water content could no longer affect the protein structure.[204-206] Such structural transitions can result in altered conformations and limited co-operativity within these conformations when binding to a bioactive substrate. Such effects are however, reversible and a part of the protein's native flexibility can be restored by addition of water or water-mimicking organic solvents, such as glycerol or ethylene glycol, that are capable of forming multiple H-bonds.

Ionic and non-ionic solutes are another important constituents in solution that could perturb water structure surrounding functional groups on adsorbent surface as well as proteins.[138, 150] Dissolved salts are considered to affect the surface tension of water and the dissociated ionic species have been observed to follow a general trend in its effect on the protein, which is known as the *'Hofmeister series'*. However, these effects are not prominent if the 'bulk water' is in excess or insufficient.[150, 207] Traditionally, large single charged ions with low charge density exhibiting weaker interactions with water than

water with itself are termed *'chaotropes'* (disorder-maker) while multiply-charged ions with high charge density are called *'kosmotropes'* (order-maker). As a result, the chaotropes loose its hydration sheath much faster than the kosmotropes. Since much of the water reorganization around these ions are entropically compensated by the water in bulk, ionic kosmotropes are usually found hydrated and accumulate at the strongly hydrated interfaces preferring *'ice-like'* (high density water) structures, while ionic chaotropes prefer more *'water-like'* (low density water) structures. In other words, H-bonds between water molecules are more broken in the immediate vicinity of ionic kosmotropes than ionic chaotropes. Similarly, non-ionic kosmotropes (like polyhydroxy (e.g. sugars), zwitterioninc groups (e.g. amino acids)), are also excluded from interacting with proteins in solution. While the chaotropic groups tend to disrupt the intra- and inter-H-bond network of water and proteins resulting in alteration of the protein structure, the kosmotropic groups is considered to decrease the water diffusion around the protein and the exchange rates of protons, which in turn, renders proteins less flexible and inactive.[208] Since the first solvation layer is dynamically coupled to protein,[209] the presence of chaotropic or kosmotropic agents alone in the surrounding solution can decrease the protein activity. Therefore, it has generally been recommended that for the optimal activity of protein molecules in aqueous solution, aqueous solution should contain a mixture of kosmotropic groups and chaotropic groups.[210]

However, in contrast to the trends exhibited by ions in *'Hofmeister series'* on the native proteins, the ion-induced effects have been known to be reversed or completely absent with the adsorbed proteins.[148-152, 211-214] A part of this reason could be because of

the affinities of adsorbent surfaces to the ions in aqueous solution that would in turn affect the type of ions or solutes that are accumulated at the solid-liquid interfaces. For example, on hydrophobic solid surfaces, large anions (such as bromide or iodide) readily adsorb, while smaller anions like chloride are only weakly adsorbed, and cations are repelled.[215] The general ordering of ion adsorption on hydrophilic negatively charged and hydrophobic positive charge surfaces is $I^- > Cl^- > F^-$, but on hydrophobic negatively charged and hydrophilic positive charge surfaces this ordering is reversed to $F^- > Cl^- > I^-$. [212] Smaller anions that have lower surface charge densities interact strongly with the polar groups of adsorbent,[216] while larger ions that are singly charged, bind to adsorbent surfaces not only based on charge but also due to van der Waals forces.[214] Such specific affinities of the surface to ions have been associated with shifts in the bulk and interfacial pH, and the thermodynamic shift in the equilibrium of the water structure near to the interface and within the solution, that subsequently could lead to protein desorption off the support surfaces or inhibition of protein's adsorbed state bioactivity.[182, 217] Another potential reason for the reversal or complete absence of ion-induced effects with the proteins on support surfaces could be because of the partial or complete loss in hydration sheath encompassing the protein in its native state, which limits the extent of solute induced water restructuring surrounding the protein. Such estimates on the hydrated states of the adsorbed proteins has been used as indicators of its susceptibility to lose its adsorbed conformation as well as its tendency to desorb off the support systems in the presence of different chemical additives.

2.4.2 Direct Interaction of Chemical Excipients with Protein Structure via Side-chains or Protein Backbone

Earlier studies on protein denaturing with chemical additives like ionic, non-ionic, and organic solvents have accounted the destabilization mechanism to the creation of *'water cavities'* or the reduction in *'water activity'* around a protein.[218-220] But, in recent years, the notion of solute-induced re-ordering in water accompanied by the structural alteration of the protein has been challenged, with the observed trend in such shifts being considered to be due to the direct interaction of the excipient with the protein backbone or side-chain. [141, 149-150] To this end, molecular mechanisms by which ionic and non-ionic excipients like guanidium hydrochloride, guanidium thiocyanide,[221] sodium thiocyanide,[222] sodium chloride,[223] tetrapropylammonium chloride,[224] trimethylamine N-oxide[225], and urea [108, 220, 225-241], interact with the native structure of protein have been extensively investigated. These studies all led to the conclusion of the direct interaction of an excipient with a protein in its native state. But, as opposed to salts and non-ionic solutes, zwitterionic groups and amphiphillic molecules like detergents interact with proteins, at concentrations above their critical micelle concentration via micelles.[242]

The thermodynamic driving force for the interactions between proteins and weakly solvated solutes, such as certain ionic salts and non-ionic osmolytes, has been determined to primarily be enthalpic in origin via electrostatic or dispersive interactions.[221, 223-224] Such interactions, which can be specific to the amino acid side chains or localized to the peptide backbone, can cause proteins to swell, unfold, and be eventually re-stabilized by the restructuring of water around the unfolded segments.[223-224,

[243-244] The initial swelling in the protein results from weakening of the hydrophobic interactions within the protein's core, positional displacement of the residues within the hydrophobic core (positional exchange), and gradual unraveling of secondary structural elements.[211, 220, 224, 227] A characteristic intermediary stage of a protein's unfolding process involves the hydrophobic interior of the protein being shielded away from the aqueous solvent by these excipients (dry molten globule state).[245]

In contrast, the more solvated solutes, specifically kosmotropic excipients, have been found to have a non-denaturing or a stabilizing influence on the structure of a protein. One of the probable mechanisms by which most non-ionic solutes stabilize proteins is by preferential exclusion and their solvophobic effect on the peptide backbone.[225, 246-247] Similarly, low concentrations of highly hydrated ionic salts stabilize the proteins by a non-specific shielding of unfavorable electrostatic interaction(s) in the native-state of the protein.[248] Additional studies have indicated that specific mechanism with which the charged ionic molecules can have a stabilizing and destabilizing influence on the protein structure can be better understood by taking into account the molecular complementarity between the ion and protein moieties and between the ion and its counterions.[221, 224, 249]

In addition to using additives like salts and surfactants alone, studies have been also done on mixtures of additives like the "*artificial chaperone"* (a combination of solubilizing surfactant and hydrophobic cyclic sugars) which were found to prevent protein aggregation and reverse the unfolding effects due to certain additives.[150, 250-252] It has also been shown that the mixture of different additives like addition of ionic salts

such as Na_2SO_4 or NaCl to ionic surfactants can screen the electrostatic repulsion between the surfactants, thereby reducing the critical micelle concentration.[253] Similarly, based on the effect of alcohol and sugars on surfactants, an analogous behavior of non-ionic salts can be expected.[203, 254-255] However, at relatively lower concentrations (< 0.5 M), most of these solutes were not found to influence the native protein structure.

2.4.3 Current Understanding of the Molecular Mechanisms involved in the Interaction of Chemical Additives with Adsorbed Protein

Though much is known about the molecular mechanisms involved in the interaction of additives with the native structure of protein, much less is currently known on the influence of chemical additives on the structure of adsorbed proteins. One of the major limitation in directly probing the structure of adsorbed proteins in the presence of chemical additives is its strong interference on the peptide signals. Therefore, much of the current understanding is limited to an indirect method by probing the influence of chemical excipients, on the surface coverage of proteins on different surface chemistries that can be indirectly correlated to the structure of the adsorbed protein.

The elution efficiency of most chemical excipients is dependent on the surface chemistry, lateral interactions between the proteins on the surface, and the residence time of proteins on the surface.[28, 256-258] For example, the protein removal mechanisms by anionic detergents like SDS and non-ionic detergents like octyl gluoside has been widely investigated and known to be mediated by two processes: (a) affinity of the detergent to proteins and (b) affinity of detergent to the surfaces. But among these interactions, the dominant interaction varies with the type of detergent and type of surface chemistry.[257-260]

Therefore, while the stronger substrate affinity of SDS on more hydrophobic surfaces (contact angle > 60º) and stronger affinity of SDS to the protein on more hydrophilic surfaces (contact angle < 20º) drives the protein elution process on these surfaces. However, the lack of a dominating interaction in the intermediate surface chemistries limits its effectiveness for protein desorption.[261] In contrast, nonionic detergents rely only on their affinity to the adsorbent surface for protein elution, and are usually efficient on more hydrophobic surface chemistries.[262] In both cases, protein elutability has been found to increase with higher protein surface coverages and decrease with increasing residence time of adsorbed proteins.[28, 257-258, 260] In many such elutability experiments, higher elutability of the adsorbed proteins from a surface by an excipient was associated with lesser binding and lesser conformational unfolding. Also, it was assumed that the affinity or interaction of a chemical additive with an adsorbed proteins would be identical to that in solution.[28, 257-258, 260] However, this assumption may not be necessarily true.

When compared to the native proteins, adsorbed proteins tend to undergo structural refolding to a new minimum free energy state, which depends on the type of protein, type of surface, and type of solution environment. Most often these refolding events involve secondary structural transitions of helical structures into β-sheets or random coils. Such structural transitions are not unique to adsorption systems alone but are also observed in solvent environment as well. As opposed to β-sheets in the native proteins which are stabilized by long-range interactions (via intra-peptide and hydrophobic contacts), helices are majorly stabilized by local interactions (via intra-peptide interactions).[194, 263-265] Within these helical structures, all of the amino acids except for alanines, experience an

unfavorable change in entropy which can be compensated by electrostatic interactions, steric packing of the amino acid side-chains, van der Waal interactions and/or hydrophobic collapse of the amino acids.[266] But in the event of an increased conformational entropy resulting from neutralization of net charge or increased hydrophobicity, the amino acids within these helical segments of a protein could adopt β-sheets or unstructured conformations.[267-269] Although not yet proven, similar molecular processes can be expected with the helix to sheet or coil transitions in the protein on adsorbent surfaces.

Nevertheless, the structural alterations in protein could alter the interactions of an excipient with the secondary structural elements or the unfolded segments within a protein. For example, it has been shown that among all the secondary structural features, guanidium has increased preference to unwind helical protein secondary structures while urea prefers to unwind the sheet content within a protein.[220, 270-271] Similarly, zwitterionic and non-ionic surfactants which tend to weakly interact with the native structure of the proteins have shown increased affinity to the molten globule state of the proteins.[242] Because of such structural transitions in the adsorbed proteins and altered affinity of chemical excipients, it is difficult to predict the influence of chemical additives on an adsorbed protein based on its solution structure alone. As a result, a more direct methodology or technique is required to fully comprehend the influence of chemical excipients on the adsorbed structure and thereby the bioactivity of a protein.

2.5 CHAPTER SUMMARY AND CONCLUSION

The bioactive state of adsorbed/immobilized proteins is a key factor in most technological application. While in the pharmaceutical industry, strategies to improve the

bioactive state of proteins are preferred, most bio-defense and medical recycling industries prefer strategies to deactivate the bioactive state of protein. In many other biotechnological and biomaterial applications, an effective control on the bioactive state of material-supported proteins are preferred, for which an extensive understanding on both the strategies to stabilize and deactivate the bioactive state of the proteins are required. As demonstrated through this review, there are three fundamental challenges that are critical to the development of strategies to control the bioactive state of the adsorbed/immobilized proteins.

The first main issue relates to the selection of a suitable techniques that can be used to comprehensively characterize the influence of adsorbed protein configuration on protein bioactivity. Although many spectroscopic techniques have been used to determine the influence of individual processes on the bioactivity of a protein system, individual techniques typically do not provide sufficient information to relate adsorbed protein configuration and adsorption-induced changes in protein bioactivity. Instead, the synergistic application of techniques like CD-AAL/MS-adsorbed state bioactivity assays could provide complementary information on the adsorbed configuration of the protein and may provide more insights into the role of these adsorbed configuration on its bioactivity.[38-39]

Subsequently, the second main purpose of this review was to identify the factors influencing the adsorbed configuration of a protein on its bioactive state. While many previous studies have elucidated the adsorbed configuration of proteins on a surface, it should be recognized that these responses are caused by the combined effects of protein-surface interactions, PPI, and the inherent stability of a protein. The contribution of these individual interactions to the overall adsorbed protein structure is rarely addressed in the literature. Even

less is known about the generality of these interactions with different protein-surface systems. The inability to control or distinguish between these interactions may be the root cause for the often contrasting results that are reported by different groups for the same adsorption system.

The last part of my review focused on evaluating the general applicability of the strategies using chemical excipients to either stabilize or destabilize the structure of protein in its solution or adsorbed state in order to control the protein bioactivity. Except for some indirect studies based on the elutability of adsorbed proteins using surfactants, there is a scarcity of data on the influence of chemical excipients on the adsorbed-state structure of proteins. One major reason for the lack of direct structural data in this regard is the lack of spectroscopic techniques that can get around the typically occurring strong interference by the chemical excipients on the structural peaks corresponding to the protein. While several studies have been conducted to investigate the influence of excipient molecules on the structure and bioactivity of protein in solution, these same effects cannot necessarily be expected to occur with proteins in their adsorbed state due to the substantial differences in the molecular environment between a bulk aqueous solution and a solid-liquid interface.

In the subsequent chapters, I present the strategy that I adopted in my doctoral studies to address these challenges and the insights that I obtained on the molecular-level events involved in protein adsorption and its effects on protein bioactivity.

REFERENCES

1. Jallouk, A.; Palekar, R.; Schlesinger, P.; Pan, H.; Wickline, S. Protease-activated peptide toxins for selective nanoparticle therapeutics (1054.4). *The FASEB Journal* **2014,** *28* (1 Supplement), 1054.4.
2. Parker, M. W.; Feil, S. C. Pore-forming protein toxins: from structure to function. *Prog Biophys Mol Biol* **2005,** *88* (1), 91-142.
3. Holzman, D. C. Whatever happened to immunotoxins? Research, and hope, are still alive. *J Natl Cancer I* **2009,** *101* (9), 624-5.
4. Johannes, L.; Romer, W. Shiga toxins -- from cell biology to biomedical applications. *Nat Rev Micro* **2010,** *8* (2), 105-16.
5. Koh, C. Y.; Kini, R. M. From snake venom toxins to therapeutics–cardiovascular examples. *Toxicon* **2012,** *59* (4), 497-506.
6. Masuyer, G.; Chaddock, J. A.; Foster, K. A.; Acharya, K. R. Engineered botulinum neurotoxins as new therapeutics. *Annu Rev Pharmacool Toxicol* **2014,** *54*, 27-51.
7. Audi, J.; Belson, M.; Patel, M.; Schier, J.; Osterloh, J. Ricin poisoning: a comprehensive review. *J Am Med Assoc* **2005,** *294* (18), 2342-51.
8. Bailon, P.; Won, C. Y. PEG-modified biopharmaceuticals. *Exper Opin Drug Del* **2009,** *6* (1), 1-16.
9. Hermeling, S.; Crommelin, D. J.; Schellekens, H.; Jiskoot, W. Structure-immunogenicity relationships of therapeutic proteins. *Pharm Res* **2004,** *21* (6), 897-903.
10. Sharma, B. Immunogenicity of therapeutic proteins. Part 1: impact of product handling. *Biotechnol Adv* **2007,** *25* (3), 310-7.
11. Sharma, B. Immunogenicity of therapeutic proteins. Part 2: impact of container closures. *Biotechnol Adv* **2007,** *25* (3), 318-24.
12. Schellekens, H. Immunogenicity of therapeutic proteins: clinical implications and future prospects. *Clin Ther* **2002,** *24* (11), 1720-40; discussion 19.
13. Goldenberg, D. M.; Griffiths, G. L.; Hansen, H. J.; Lentine-Jones, A. Therapeutic conjugates of toxins and drugs **1997**.
14. Youn, Y. S.; Na, D. H.; Yoo, S. D.; Song, S. C.; Lee, K. C. Carbohydrate-specifically polyethylene glycol-modified ricin A-chain with improved therapeutic potential. *Int J Biochem Cell Biol* **2005,** *37* (7), 1525-33.
15. Arnold, U.; Ulbrich-Hofmann, R. Natural and engineered ribonucleases as potential cancer therapeutics. *Biotechnol Lett* **2006,** *28* (20), 1615-22.

16. Schrama, D.; Reisfeld, R. A.; Becker, J. C. Antibody targeted drugs as cancer therapeutics. *Nat Rev Drug Discov* **2006,** *5* (2), 147-59.

17. Townsend, S. A.; Evrony, G. D.; Gu, F. X.; Schulz, M. P.; Brown, R. H., Jr.; Langer, R. Tetanus toxin C fragment-conjugated nanoparticles for targeted drug delivery to neurons. *Biomaterials* **2007,** *28* (34), 5176-84.

18. Stumpp, M. T.; Binz, H. K.; Amstutz, P. DARPins: a new generation of protein therapeutics. *Drug Discov Today* **2008,** *13* (15-16), 695-701.

19. Foster, K. A. Engineered toxins: new therapeutics. *Toxicon* **2009,** *54* (5), 587-92.

20. Arruebo, M.; Valladares, M.; González-Fernández, Á. Antibody-Conjugated Nanoparticles for Biomedical Applications. *J Nanomater* **2009,** *2009*, 1-24.

21. Irache, J. M.; Esparza, I.; Gamazo, C.; Agueros, M.; Espuelas, S. Nanomedicine: novel approaches in human and veterinary therapeutics. *Vet Parasitol* **2011,** *180* (1-2), 47-71.

22. Naumann, M.; Boo, L. M.; Ackerman, A. H.; Gallagher, C. J. Immunogenicity of botulinum toxins. *J Neural Transm* **2013,** *120* (2), 275-90.

23. Ansari, S. A.; Husain, Q. Potential applications of enzymes immobilized on/in nano materials: A review. *Biotechnol Adv* **2012,** *30* (3), 512-23.

24. Lord, M. S.; Foss, M.; Besenbacher, F. Influence of nanoscale surface topography on protein adsorption and cellular response. *Nano Today* **2010,** *5* (1), 66-78.

25. Lynch, I.; Dawson, K. A. Protein-nanoparticle interactions. *Nano Today* **2008,** *3* (1-2), 40-47.

26. Lundqvist, M.; Sethson, I.; Jonsson, B. H. Protein adsorption onto silica nanoparticles: conformational changes depend on the particles' curvature and the protein stability. *Langmuir* **2004,** *20* (24), 10639-47.

27. Vertegel, A. A.; Siegel, R. W.; Dordick, J. S. Silica nanoparticle size influences the structure and enzymatic activity of adsorbed lysozyme. *Langmuir* **2004,** *20* (16), 6800-7.

28. Peter, B.; Hans, E.; Uno, C. Studies on the Conformation of Adsorbed Proteins with the Use of Nanoparticle Technology. In *Biopolymers at Interfaces, Second Edition*, Malmsten, M., Ed.; CRC Press, 2003.

29. Niemeyer, C. M. Nanoparticles, proteins, and nucleic acids: biotechnology meets materials science. *Angew Chem Int Ed* **2001,** *40* (22), 4128-58.

30. Lei, C.; Shin, Y.; Liu, J.; Ackerman, E. J. Synergetic effects of nanoporous support and urea on enzyme activity. *Nano Lett* **2007,** *7* (4), 1050-3.

31. Schellekens, H.; Jiskoot, W. Erythropoietin-Associated PRCA: Still an Unsolved Mystery. *J Immunotoxicol* **2006,** *3* (3), 123-30.

32. Mathes, J. M. Protein adsorption to vial surfaces: quantification, structural and mechanistic studies. Ludwig Maximilian University of Munich, **2010**.

33. Höger, K. Investigations on protein adsorption to coated glass vials. Ludwig Maximilian University of Munich, **2014**.

34. Wood, J. *2007 Workshop on Decontamination,Cleanup and Associated Issues for Sites Contaminated with Chemical, Biological, or Radiological Materials* . U.S. Environmental Protection Agency: Washington, DC, **2008**.

35. Wood, J.; Lemieux, P.; Ryan, S.; Adams, N. *Persistence, Decontamination, and Disposal Issues Related to the Foot and Mouth Disease Virus and Ricin*; EPA/OSC Readiness Training; USEPA, NHSRC: San Diego, CA, **2008**.

36. Lillie, S. H.; Hanlon, E.; Kelly, J.; Rayburn, B. B. *Potential Military Chemical/Biological agents and compounds* FM 3-11.9, MCRP 3-37.1B, NTRP 3-11.32, AFTTP(I) 3-2.55; U. S. Army Chemical School Ft. Leonard Wood, MO, **2005**, p 200.

37. Latour, R. A. Biomaterials: Protein-Surface Interactions. In *The Encyclopedia of Biomaterials and Bioengineering*, 2 ed.; Bowlin, G. E. W. a. G. L., Ed.; Informa Healthcare, **2008**; Vol. 1, pp 270-84.

38. Gray, J. J. The interaction of proteins with solid surfaces. *Curr Opin Struct Biol* **2004,** *14* (1), 110-5.

39. Rabe, M.; Verdes, D.; Seeger, S. Understanding protein adsorption phenomena at solid surfaces. *Adv Colloid Interface Sci* **2011,** *162* (1-2), 87-106.

40. Talbert, J. N.; Goddard, J. M. Enzymes on material surfaces. *Colloids Surf B Biointerfaces* **2012,** *93* (0), 8-19.

41. Jandt, K. D. Evolutions, Revolutions and Trends in Biomaterials Science – A Perspective. *Adv Eng Mater* **2007,** *9* (12), 1035-50.

42. Ratner, B. D. *Biomaterials Science: An Introduction to Materials in Medicine*; Elsevier Academic Press2004.

43. Latour, R. A. Perspectives on the simulation of protein-surface interactions using empirical force field methods. *Colloids Surf B Biointerfaces* **2014,** *124* (0), 25-37.

44. Fears, K. P.; Latour, R. A. Assessing the influence of adsorbed-state conformation on the bioactivity of adsorbed enzyme layers. *Langmuir* **2009,** *25* (24), 13926-33.

45. Sivaraman, B.; Latour, R. A. Delineating the roles of the GPIIb/IIIa and GP-Ib-IX-V platelet receptors in mediating platelet adhesion to adsorbed fibrinogen and albumin. *Biomaterials* **2011,** *32* (23), 5365-70.

46. Sivaraman, B.; Latour, R. A. The relationship between platelet adhesion on surfaces and the structure versus the amount of adsorbed fibrinogen. *Biomaterials* **2010,** *31* (5), 832-9.

47. Sivaraman, B.; Latour, R. A. The adherence of platelets to adsorbed albumin by receptor-mediated recognition of binding sites exposed by adsorption-induced unfolding. *Biomaterials* **2010,** *31* (6), 1036-44.

48. Sivaraman, B.; Fears, K. P.; Latour, R. A. Investigation of the effects of surface chemistry and solution concentration on the conformation of adsorbed proteins using an improved circular dichroism method. *Langmuir* **2009,** *25* (5), 3050-6.

49. Amine, A.; Mohammadi, H.; Bourais, I.; Palleschi, G. Enzyme inhibition-based biosensors for food safety and environmental monitoring. *Biosens Bioelectron* **2006,** *21* (8), 1405-23.

50. Wang, J. Carbon-nanotube based electrochemical biosensors: A review. *Electroanalysis* **2005,** *17* (1), 7-14.

51. Prodromidis, M. I.; Karayannis, M. I. Enzyme based amperometric biosensors for food analysis. *Electroanalysis* **2002,** *14* (4), 241.

52. Chaubey, A.; Malhotra, B. D. Mediated biosensors. *Biosens Bioelectron* **2002,** *17* (6-7), 441-56.

53. Wilson, G. S.; Hu, Y. Enzyme-based biosensors for in vivo measurements. *Chem Rev* **2000,** *100* (7), 2693-704.

54. Johnson, I. Review: Fluorescent probes for living cells. *The Histochemical Journal* **1998,** *30* (3), 123-40.

55. Pihlasalo, S.; Puumala, P.; Hänninen, P.; Härmä, H. Sensitive Method for Determination of Protein and Cell Concentrations Based on Competitive Adsorption to Nanoparticles and Time-Resolved Luminescence Resonance Energy Transfer between Labeled Proteins. *Anal Chem* **2012,** *84* (11), 4950-56.

56. Daniel, R. M.; Dunn, R. V.; Finney, J. L.; Smith, J. C. The role of dynamics in enzyme activity. *Annu Rev Biophys Biomol Struct* **2003,** *32*, 69-92.

57. *Assay Guidance Manual* [Online]; Eli Lilly & Company and the National Center for Advancing Translational Sciences: Bethesda (MD), **2004**.

58. Emanuel, P. A.; Chue, C.; Kerr, L.; Cullin, D. Validating the performance of biological detection equipment: the role of the federal government. *Biosecur Bioterror* **2003,** *1* (2), 131-7.

59. Hlady, V.; Buijs, J. Local and global optical spectroscopic probes of adsorbed proteins. In *Biopolymers at Interfaces*, Malmsten, M., Ed.; Marcel Dekker: New York, **1998**; Vol. 75, pp 181-220.

60. Li, C. H.; Nguyen, X.; Narhi, L.; Chemmalil, L.; Towers, E.; Muzammil, S.; Gabrielson, J.; Jiang, Y. Applications of circular dichroism (CD) for structural analysis of proteins: qualification of near- and far-UV CD for protein higher order structural analysis. *J Pharm Sci* **2011,** *100* (11), 4642-54.

61. Sreerama, N.; Woody, R. W. Estimation of protein secondary structure from circular dichroism spectra: comparison of CONTIN, SELCON, and CDSSTR methods with an expanded reference set. *Anal Biochem* **2000,** *287* (2), 252-60.

62. Kelly, S. M.; Jess, T. J.; Price, N. C. How to study proteins by circular dichroism. *Biochim Biophys Acta* **2005,** *1751* (2), 119-39.

63. Greenfield, N. J. Using circular dichroism spectra to estimate protein secondary structure. *Nat Protoc* **2006,** *1* (6), 2876-90.

64. Wallace, B. A.; Lees, J. G.; Orry, A. J.; Lobley, A.; Janes, R. W. Analyses of circular dichroism spectra of membrane proteins. *Protein Sci* **2003,** *12* (4), 875-84.

65. Kelly, S. M.; Price, N. C. The use of circular dichroism in the investigation of protein structure and function. *Curr Protein Pept Sci* **2000,** *1* (4), 349-84.

66. McMillin, C. R.; Walton, A. G. A circular dichroism technique for the study of adsorbed protein structure. *J Colloid Interface Sci* **1974,** *48* (2), 345-49.

67. Arteaga, O.; Freudenthal, J.; Wang, B.; Nichols, S.; Kahr, B. Circular dichroism with multiple photoelastic modulators. *Chimica Oggi* **2012,** *30* (5), 6-9.

68. Engel, M. F.; Visser, A. J.; van Mierlo, C. P. Conformation and orientation of a protein folding intermediate trapped by adsorption. *Proc Natl Acad Sci USA* **2004,** *101* (31), 11316-21.

69. Ronda, L.; Bruno, S.; Viappiani, C.; Abbruzzetti, S.; Mozzarelli, A.; Lowe, K. C.; Bettati, S. Circular dichroism spectroscopy of tertiary and quaternary conformations of human hemoglobin entrapped in wet silica gels. *Protein Sci* **2006,** *15* (8), 1961-7.

70. Vogel, R.; Siebert, F. Vibrational spectroscopy as a tool for probing protein function. *Curr Opin Chem Biol* **2000,** *4* (5), 518-23.

71. Kneipp, J.; Kneipp, H.; Kneipp, K. SERS--a single-molecule and nanoscale tool for bioanalytics. *Chem Soc Rev* **2008,** *37* (5), 1052-60.

72. Chandra, G.; Ghosh, K. S.; Dasgupta, S.; Roy, A. Evidence of conformational changes in adsorbed lysozyme molecule on silver colloids. *Int J Biol Macromol* **2010,** *47* (3), 361-5.

73. Pelton, J. T.; McLean, L. R. Spectroscopic methods for analysis of protein secondary structure. *Anal Biochem* **2000,** *277* (2), 167-76.

74. Jos, B.; Vladimir, H. Local and Global Optical Spectroscopic Probes of Adsorbed Proteins. In *Biopolymers at Interfaces, Second Edition*, Malmsten, M., Ed.; CRC Press, **2003**.

75. Deighan, M.; Weidner, T.; Pfaendtner, J. Structural Insights on the Statherin N-Terminal Binding Domain in the Adsorbed State. *Biophys J* **2014,** *106* (2), 38a.

76. Weidner, T.; Castner, D. G. SFG analysis of surface bound proteins: a route towards structure determination. *PCCP* **2013,** *15* (30), 12516-24.

77. Baio, J. E.; Weidner, T.; Baugh, L.; Gamble, L. J.; Stayton, P. S.; Castner, D. G. Probing the orientation of electrostatically immobilized Protein G B1 by time-of-flight secondary ion spectrometry, sum frequency generation, and near-edge X-ray adsorption fine structure spectroscopy. *Langmuir* **2012,** *28* (4), 2107-12.

78. Baugh, L.; Weidner, T.; Baio, J. E.; Nguyen, P. C.; Gamble, L. J.; Stayton, P. S.; Castner, D. G. Probing the orientation of surface-immobilized protein G B1 using ToF-SIMS, sum frequency generation, and NEXAFS spectroscopy. *Langmuir* **2010,** *26* (21), 16434-41.

79. Baio, J. E.; Weidner, T.; Samuel, N. T.; McCrea, K.; Baugh, L.; Stayton, P. S.; Castner, D. G. Multi-technique Characterization of Adsorbed Peptide and Protein Orientation: LK3 and Protein G B1. *J Vac Sci Technol B Microelectron Nanometer Struct Process Meas Phenom* **2010,** *28* (4), C5D1.

80. Kastantin, M.; Langdon, B. B.; Schwartz, D. K. A bottom-up approach to understanding protein layer formation at solid-liquid interfaces. *Advances in Colloid and Interface Science* **2014,** *207*, 240-52.

81. Daly, S. M.; Przybycien, T. M.; Tilton, R. D. Coverage-Dependent Orientation of Lysozyme Adsorbed on Silica. *Langmuir* **2003,** *19* (9), 3848-57.

82. Robert, T. Mobility of Biomolecules at Interfaces. In *Biopolymers at Interfaces, Second Edition*, Malmsten, M., Ed.; CRC Press, **2003**.

83. Bhogale, A.; Patel, N.; Sarpotdar, P.; Mariam, J.; Dongre, P. M.; Miotello, A.; Kothari, D. C. Systematic investigation on the interaction of bovine serum albumin with ZnO nanoparticles using fluorescence spectroscopy. *Colloids Surf B Biointerfaces* **2013,** *102* (0), 257-64.

84. Axelrod, D. Chapter 7: Total internal reflection fluorescence microscopy. *Methods Cell Biol* **2008,** *89*, 169-221.

85. Kim, J.; Seidler, P.; Fill, C.; Wan, L. S. Investigations of the effect of curing conditions on the structure and stability of amino-functionalized organic films on silicon substrates by Fourier transform infrared spectroscopy, ellipsometry, and fluorescence microscopy. *Surf Sci* **2008,** *602* (21), 3323-30.

86. Benesch, J.; Hungerford, G.; Suhling, K.; Tregidgo, C.; Mano, J. F.; Reis, R. L. Fluorescence probe techniques to monitor protein adsorption-induced conformation changes on biodegradable polymers. *J Colloid Interface Sci* **2007,** *312* (2), 193-200.

87. Yamamoto, T.; Fukui, N.; Hori, A.; Matsui, Y. Circular dichroism and fluorescence spectroscopy studies of the effect of cyclodextrins on the thermal stability of chicken egg white lysozyme in aqueous solution. *J Mol Struct* **2006,** *782* (1), 60-66.

88. Kim, J.; Somorjai, G. A. Molecular packing of lysozyme, fibrinogen, and bovine serum albumin on hydrophilic and hydrophobic surfaces studied by infrared-visible sum frequency generation and fluorescence microscopy. *J Am Chem Soc* **2003,** *125* (10), 3150-8.

89. Czeslik, C.; Jackler, G.; Royer, C. Driving forces for the adsorption of enzymes at the water/silica interface studied by total internal reflection fluorescence spectroscopy and optical reflectometry. *Spectroscopy* **2002,** *16* (3), 139.

90. Griko, Y.; Sreerama, N.; Osumi-Davis, P.; Woody, R. W.; Woody, A. Y. Thermal and urea-induced unfolding in T7 RNA polymerase: calorimetry, circular dichroism and fluorescence study. *Protein Sci* **2001,** *10* (4), 845-53.

91. Wu, X.; Narsimhan, G. Effect of surface concentration on secondary and tertiary conformational changes of lysozyme adsorbed on silica nanoparticles. *Biochim Biophys Acta* **2008,** *1784* (11), 1694-701.

92. Yan, X.; Watson, J.; Ho, P. S.; Deinzer, M. L. Mass spectrometric approaches using electrospray ionization charge states and hydrogen-deuterium exchange for determining protein structures and their conformational changes. *Mol Cell Proteomics* **2004,** *3* (1), 10-23.

93. Suckau, D.; Mak, M.; Przybylski, M. Protein surface topology-probing by selective chemical modification and mass spectrometric peptide mapping. *Proc Natl Acad Sci USA* **1992,** *89* (12), 5630-4.

94. Fears, K. P.; Sivaraman, B.; Powell, G. L.; Wu, Y.; Latour, R. A. Probing the conformation and orientation of adsorbed enzymes using side-chain modification. *Langmuir* **2009,** *25* (16), 9319-27.

95. Ovod, V.; Scott, E. A.; Flake, M. M.; Parker, S. R.; Bateman, R. J.; Elbert, D. L. Exposure of the lysine in the gamma chain dodecapeptide of human fibrinogen is not enhanced by adsorption to poly(ethylene terephthalate) as measured by biotinylation and mass spectrometry. *J Biomed Mater Res* **2012,** *100* (3), 622-31.

96. Scott, E. A.; Elbert, D. L. Mass spectrometric mapping of fibrinogen conformations at poly(ethylene terephthalate) interfaces. *Biomaterials* **2007,** *28* (27), 3904-17.

97. Xu, J.; Bowden, E. F. Determination of the orientation of adsorbed cytochrome C on carboxyalkanethiol self-assembled monolayers by in situ differential modification. *J Am Chem Soc* **2006,** *128* (21), 6813-22.

98. Means, G. E.; Feeney, R. E. Chemical modifications of proteins: history and applications. *Bioconjugate Chem* **1990,** *1* (1), 2-12.

99. Lundblad, R. L. Some Reagents Used in the Modification of Proteins. In *Chemical Reagents for Protein Modification, Third Edition*; CRC Press, **2004**.

100. Iwasaki, Y.; Nakano, Y.; Mochizuki, K.; Nomoto, M.; Takahashi, Y.; Ito, R.; Saito, K.; Nakazawa, H. A new strategy for ionization enhancement by derivatization for mass spectrometry. *J Chromatogr B* **2011,** *879* (17-18), 1159-65.

101. Apte, J. S.; Collier, G.; Latour, R. A.; Gamble, L. J.; Castner, D. G. XPS and ToF-SIMS investigation of alpha-helical and beta-strand peptide adsorption onto SAMs. *Langmuir* **2010,** *26* (5), 3423-32.

102. Apte, J. S.; Gamble, L. J.; Castner, D. G.; Campbell, C. T. Kinetics of leucine-lysine peptide adsorption and desorption at -CH3 and -COOH terminated alkylthiolate monolayers. *Biointerphases* **2010,** *5* (4), 97-104.

103. Michel, R.; Pasche, S.; Textor, M.; Castner, D. G. Influence of PEG architecture on protein adsorption and conformation. *Langmuir* **2005,** *21* (26), 12327-32.

104. Sally, M.; Hans, G.; Matthew, W.; David, C.; Keith, M.; Peter, K. XPS, ToF-SIMS, and MALDI-MS for Characterizing Adsorbed Protein Films. In *Biopolymers at Interfaces, Second Edition*; CRC Press, **2003**.

105. Belu, A. M.; Graham, D. J.; Castner, D. G. Time-of-flight secondary ion mass spectrometry: techniques and applications for the characterization of biomaterial surfaces. *Biomaterials* **2003,** *24* (21), 3635-53.

106. Tidwell, C. D.; Castner, D. G.; Golledge, S. L.; Ratner, B. D.; Meyer, K.; Hagenhoff, B.; Benninghoven, A. Static time-of-flight secondary ion mass spectrometry and x-ray photoelectron spectroscopy characterization of adsorbed albumin and fibronectin films. *Surf Interface Anal* **2001,** *31* (8), 724-33.

107. Yearley, E. J.; Zarraga, I. E.; Shire, S. J.; Scherer, T. M.; Gokarn, Y.; Wagner, N. J.; Liu, Y. Small-angle neutron scattering characterization of monoclonal antibody conformations and interactions at high concentrations. *Biophys J* **2013,** *105* (3), 720-31.

108. Gabel, F.; Jensen, M. R.; Zaccai, G.; Blackledge, M. Quantitative modelfree analysis of urea binding to unfolded ubiquitin using a combination of small angle X-ray and neutron scattering. *J Am Chem Soc* **2009,** *131* (25), 8769-71.

109. Adya, A. K.; Zarbakhsh, A.; Bowers, J.; Shcherbakov, M. V.; Webster, J. R. P. Neutron reflectivity study of grafted poly(ethylene glycol) in the presence of an

aqueous bovine serum albumin solution. *J Indian Chem Soc* **2005,** *82* (12), 1133-40.

110. Lu, J. Neutron Reflection Study of Protein Adsorption at the Solid-Solution Interface. In *Biopolymers at Interfaces, Second Edition*, Malmsten, M., Ed.; CRC Press, **2003**.

111. Jackler, G.; Steitz, R.; Czeslik, C. Effect of Temperature on the Adsorption of Lysozyme at the Silica/Water Interface Studied by Optical and Neutron Reflectometry. *Langmuir* **2002,** *18* (17), 6565-70.

112. Su, T. J.; Lu, J. R.; Thomas, R. K.; Cui, Z. F. Effect of pH on the Adsorption of Bovine Serum Albumin at the Silica/Water Interface Studied by Neutron Reflection. *J Phys Chem B* **1999,** *103* (18), 3727-36.

113. Lu, J. R.; Su, T. J.; Thirtle, P. N.; Thomas, R. K.; Rennie, A. R.; Cubitt, R. The Denaturation of Lysozyme Layers Adsorbed at the Hydrophobic Solid/Liquid Surface Studied by Neutron Reflection. *J Colloid Interface Sci* **1998,** *206* (1), 212-23.

114. Su, T. J.; Lu, J. R.; Thomas, R. K.; Cui, Z. F.; Penfold, J. The Effect of Solution pH on the Structure of Lysozyme Layers Adsorbed at the Silica−Water Interface Studied by Neutron Reflection. *Langmuir* **1998,** *14* (2), 438-45.

115. Su, T. J.; Lu, J. R.; Thomas, R. K.; Cui, Z. F.; Penfold, J. The Adsorption of Lysozyme at the Silica-Water Interface: A Neutron Reflection Study. *J Colloid Interface Sci* **1998,** *203* (2), 419-29.

116. Petrash, S.; Liebmann-Vinson, A.; Foster, M. D.; Lander, L. M.; Brittain, W. J.; Majkrzak, C. F. Neutron and X-ray reflectivity studies of human serum albumin adsorption onto functionalized surfaces of self-assembled monolayers. *Biotechnol Progr* **1997,** *13* (5), 635-9.

117. Goobes, G.; Goobes, R.; Shaw, W. J.; Gibson, J. M.; Long, J. R.; Raghunathan, V.; Schueler-Furman, O.; Popham, J. M.; Baker, D.; Campbell, C. T.; Stayton, P. S.; Drobny, G. P. The structure, dynamics, and energetics of protein adsorption-lessons learned from adsorption of statherin to hydroxyapatite. *Magn Reson Chem* **2007,** *45 Suppl 1*, S32-47.

118. Breen, N. F.; Weidner, T.; Li, K.; Castner, D. G.; Drobny, G. P. A solid-state deuterium NMR and sum-frequency generation study of the side-chain dynamics of peptides adsorbed onto surfaces. *J Am Chem Soc* **2009,** *131* (40), 14148-9.

119. Sonesson, A. W.; Callisen, T. H.; Brismar, H.; Elofsson, U. M. A comparison between dual polarization interferometry (DPI) and surface plasmon resonance (SPR) for protein adsorption studies. *Colloids Surf B Biointerfaces* **2007,** *54* (2), 236-40.

120. Noto, M.; Keng, D.; Teraoka, I.; Arnold, S. Detection of protein orientation on the silica microsphere surface using transverse electric/transverse magnetic whispering gallery modes. *Biophys J* **2007,** *92* (12), 4466-72.

121. Leung, B. O.; Hitchcock, A. P.; Cornelius, R.; Brash, J. L.; Scholl, A.; Doran, A. X-ray spectromicroscopy study of protein adsorption to a polystyrene-polylactide blend. *Biomacromolecules* **2009,** *10* (7), 1838-45.

122. Oleinikova, A.; Smolin, N.; Brovchenko, I.; Geiger, A.; Winter, R. Formation of spanning water networks on protein surfaces via 2D percolation transition. *J Phys Chem B* **2005,** *109* (5), 1988-98.

123. Smolin, N.; Oleinikova, A.; Brovchenko, I.; Geiger, A.; Winter, R. Properties of spanning water networks at protein surfaces. *J Phys Chem B* **2005,** *109* (21), 10995-1005.

124. Nakagawa, H.; Kataoka, M. Percolation of Hydration Water as a Control of Protein Dynamics. *J Phys Soc Jpn* **2010,** *79* (8), 083801.

125. Dill, K. A. Dominant forces in protein folding. *Biochemistry (Mosc)* **1990,** *29* (31), 7133-55.

126. Leckband, D. Measuring the forces that control protein interactions. *Annu Rev Biophys Biomol Struct* **2000,** *29*, 1-26.

127. Chothia, C. Principles that Determine the Structure of Proteins. *Annu Rev Biochem* **1984,** *53* (1), 537-72.

128. Jaenicke, R. Stability and stabilization of globular proteins in solution. *J Biotechnol* **2000,** *79* (3), 193-203.

129. Norde, W. Driving forces for protein adsorption at solid surfaces. In *Biopolymers at Interfaces*, Malmsten, M., Ed.; Marcel Dekker: New York, 1998; Vol. 75, pp 27-54.

130. Ebbinghaus, S.; Kim, S. J.; Heyden, M.; Yu, X.; Heugen, U.; Gruebele, M.; Leitner, D. M.; Havenith, M. An extended dynamical hydration shell around proteins. *Proc Natl Acad Sci USA* **2007,** *104* (52), 20749-52.

131. Frauenfelder, H.; Chen, G.; Berendzen, J.; Fenimore, P. W.; Jansson, H.; McMahon, B. H.; Stroe, I. R.; Swenson, J.; Young, R. D. A unified model of protein dynamics. *Proc Natl Acad Sci USA* **2009,** *106* (13), 5129-34.

132. Swenson, J.; Jansson, H.; Hedström, J.; Bergman, R. Properties of hydration water and its role in protein dynamics. *J Phys: Condens Matter* **2007,** *19* (20), 205109.

133. Chen, S. H.; Liu, L.; Fratini, E.; Baglioni, P.; Faraone, A.; Mamontov, E. Observation of fragile-to-strong dynamic crossover in protein hydration water. *Proc Natl Acad Sci USA* **2006,** *103* (24), 9012-6.

134. Cheung, M. S.; Garcia, A. E.; Onuchic, J. N. Protein folding mediated by solvation: water expulsion and formation of the hydrophobic core occur after the structural collapse. *Proc Natl Acad Sci USA* **2002,** *99* (2), 685-90.

135. Hildebrandt, A.; Blossey, R.; Rjasanow, S.; Kohlbacher, O.; Lenhof, H. P. Electrostatic potentials of proteins in water: a structured continuum approach. *Bioinformatics* **2007,** *23* (2), e99-103.

136. Kim, G.; Gurau, M.; Kim, J.; Cremer, P. S. Investigations of Lysozyme Adsorption at the Air/Water and Quartz/Water Interfaces by Vibrational Sum Frequency Spectroscopy. *Langmuir* **2002,** *18* (7), 2807-11.

137. Fan, Y.; Chen, X.; Yang, L.; Cremer, P. S.; Gao, Y. Q. On the structure of water at the aqueous/air interface. *J Phys Chem B* **2009,** *113* (34), 11672-9.

138. Flores, S. C.; Kherb, J.; Konelick, N.; Chen, X.; Cremer, P. S. The Effects of Hofmeister Cations at Negatively Charged Hydrophilic Surfaces. *The Journal of Physical Chemistry C* **2012,** *116* (9), 5730-34.

139. Gurau, M. C.; Kim, G.; Lim, S. M.; Albertorio, F.; Fleisher, H. C.; Cremer, P. S. Organization of water layers at hydrophilic interfaces. *Chemphyschem* **2003,** *4* (11), 1231-3.

140. Jung, S. Y.; Lim, S. M.; Albertorio, F.; Kim, G.; Gurau, M. C.; Yang, R. D.; Holden, M. A.; Cremer, P. S. The Vroman effect: a molecular level description of fibrinogen displacement. *J Am Chem Soc* **2003,** *125* (42), 12782-6.

141. Chen, X.; Flores, S. C.; Lim, S. M.; Zhang, Y.; Yang, T.; Kherb, J.; Cremer, P. S. Specific anion effects on water structure adjacent to protein monolayers. *Langmuir* **2010,** *26* (21), 16447-54.

142. Chen, X.; Yang, T.; Kataoka, S.; Cremer, P. S. Specific ion effects on interfacial water structure near macromolecules. *J Am Chem Soc* **2007,** *129* (40), 12272-9.

143. Ballet, T.; Boulange, L.; Brechet, Y.; Bruckert, F.; Weidenhaupt, M. Protein conformational changes induced by adsorption onto material surfaces: an important issue for biomedical applications of material science. *Bulletin of the Polish Academy of Sciences: Technical Sciences* **2010,** *58* (2), 303-15.

144. Wang, W. Instability, stabilization, and formulation of liquid protein pharmaceuticals. *Int J Pharm* **1999,** *185* (2), 129-88.

145. Wei, T.; Kaewtathip, S.; Shing, K. Buffer Effect on Protein Adsorption at Liquid/Solid Interface†. *J Phys Chem C* **2009,** *113* (6), 2053-62.

146. Wendorf, J. R.; Radke, C. J.; Blanch, H. W. The role of electrolytes on protein adsorption at a hydrophilic solid-water interface. *Colloids Surf B Biointerfaces* **2010,** *75* (1), 100-6.

147. Parmar, A. S.; Muschol, M. Hydration and hydrodynamic interactions of lysozyme: effects of chaotropic versus kosmotropic ions. *Biophys J* **2009,** *97* (2), 590-8.

148. Kunz, W.; Henle, J.; Ninham, B. W. 'Zur Lehre von der Wirkung der Salze' (about the science of the effect of salts): Franz Hofmeister's historical papers. *Curr Opin Colloid In* **2004,** *9* (1-2), 19-37.

149. Zhang, Y.; Cremer, P. S. Interactions between macromolecules and ions: The Hofmeister series. *Curr Opin Chem Biol* **2006,** *10* (6), 658-63.

150. Zhang, Y.; Cremer, P. S. Chemistry of Hofmeister anions and osmolytes. *Annu Rev Phys Chem* **2010,** *61*, 63-83.

151. Zhang, Y.; Cremer, P. S. The inverse and direct Hofmeister series for lysozyme. *Proc Natl Acad Sci USA* **2009,** *106* (36), 15249-53.

152. Gurau, M. C.; Lim, S. M.; Castellana, E. T.; Albertorio, F.; Kataoka, S.; Cremer, P. S. On the mechanism of the hofmeister effect. *J Am Chem Soc* **2004,** *126* (34), 10522-3.

153. Nakanishi, K.; Sakiyama, T.; Imamura, K. On the Adsorption of Proteins on Solid Surfaces, a Common but Very Complicated Phenomenon. *J Biosci Bioeng* **2001,** *91* (3), 233-44.

154. Wertz, C. F.; Santore, M. M. Fibrinogen Adsorption on Hydrophilic and Hydrophobic Surfaces: Geometrical and Energetic Aspects of Interfacial Relaxations. *Langmuir* **2002,** *18* (3), 706-15.

155. Sethuraman, A.; Han, M.; Kane, R. S.; Belfort, G. Effect of surface wettability on the adhesion of proteins. *Langmuir* **2004,** *20* (18), 7779-88.

156. Paul, A. Chemical durability of glasses; a thermodynamic approach. *J Mater Sci Mater Med* **1977,** *12* (11).

157. Wei, Y.; Latour, R. A. Correlation between desorption force measured by atomic force microscopy and adsorption free energy measured by surface plasmon resonance spectroscopy for peptide-surface interactions. *Langmuir* **2010,** *26* (24), 18852-61.

158. Rao, F.; Garrett-Roe, S.; Hamm, P. Structural inhomogeneity of water by complex network analysis. *J Phys Chem B* **2010,** *114* (47), 15598-604.

159. Hopkins, A. J.; McFearin, C. L.; Richmond, G. L. Investigations of the solid–aqueous interface with vibrational sum-frequency spectroscopy. *Curr Opin Solid State Mater Sci* **2005,** *9* (1-2), 19-27.

160. Suresh, S. J. Disruption of hydrogen bond structure of water near charged electrode surfaces. *J Chem Phys* **2007,** *126* (20), 204705.

161. Stokely, K.; Mazza, M. G.; Stanley, H. E.; Franzese, G. Effect of hydrogen bond cooperativity on the behavior of water. *Proc Natl Acad Sci USA* **2010,** *107* (4), 1301-6.

162. Stanley, H. E.; Kumar, P.; Han, S.; Mazza, M. G.; Stokely, K.; Buldyrev, S. V.; Franzese, G.; Mallamace, F.; Xu, L. Heterogeneities in confined water and protein hydration water. *J Phys Condens Matter* **2009,** *21* (50), 504105.

163. Mezger, M.; Reichert, H.; Schoder, S.; Okasinski, J.; Schroder, H.; Dosch, H.; Palms, D.; Ralston, J.; Honkimaki, V. High-resolution in situ x-ray study of the hydrophobic gap at the water-octadecyl-trichlorosilane interface. *Proc Natl Acad Sci USA* **2006,** *103* (49), 18401-4.

164. Patel, A. J.; Varilly, P.; Chandler, D. Fluctuations of water near extended hydrophobic and hydrophilic surfaces. *J Phys Chem B* **2010,** *114* (4), 1632-7.

165. Nihonyanagi, S.; Yamaguchi, S.; Tahara, T. Water hydrogen bond structure near highly charged interfaces is not like ice. *J Am Chem Soc* **2010,** *132* (20), 6867-9.

166. Sedlmeier, F.; Janecek, J.; Sendner, C.; Bocquet, L.; Netz, R. R.; Horinek, D. Water at polar and nonpolar solid walls. *Biointerphases* **2008,** *3* (3), FC23-39.

167. Wertz, C. F.; Santore, M. M. Adsorption and Relaxation Kinetics of Albumin and Fibrinogen on Hydrophobic Surfaces: Single-Species and Competitive Behavior. *Langmuir* **1999,** *15* (26), 8884-94.

168. Wei, Y.; Latour, R. A. Benchmark experimental data set and assessment of adsorption free energy for peptide-surface interactions. *Langmuir* **2009,** *25* (10), 5637-46.

169. Evers, F.; Shokuie, K.; Paulus, M.; Sternemann, C.; Czeslik, C.; Tolan, M. Exploring the interfacial structure of protein adsorbates and the kinetics of protein adsorption: an in situ high-energy X-ray reflectivity study. *Langmuir* **2008,** *24* (18), 10216-21.

170. Rechendorff, K.; Hovgaard, M. B.; Foss, M.; Zhdanov, V. P.; Besenbacher, F. Enhancement of protein adsorption induced by surface roughness. *Langmuir* **2006,** *22* (26), 10885-8.

171. Minelli, C.; Kikuta, A.; Tsud, N.; Ball, M. D.; Yamamoto, A. A micro-fluidic study of whole blood behaviour on PMMA topographical nanostructures. *J Nanobiotechnology* **2008,** *6*, 3.

172. Roach, P.; Farrar, D.; Perry, C. C. Interpretation of protein adsorption: surface-induced conformational changes. *J Am Chem Soc* **2005,** *127* (22), 8168-73.

173. Roach, P.; Farrar, D.; Perry, C. C. Surface tailoring for controlled protein adsorption: effect of topography at the nanometer scale and chemistry. *J Am Chem Soc* **2006,** *128* (12), 3939-45.

174. Roach, P.; Eglin, D.; Rohde, K.; Perry, C. C. Modern biomaterials: a review - bulk properties and implications of surface modifications. *Journal of Materials Science Materials in Medicine* **2007,** *18* (7), 1263-77.

175. Jones, G.; Jones, L. B.; Thibault-Starzyk, F.; Seddon, E. A.; Raval, R.; Jenkins, S. J.; Held, G. The local adsorption geometry and electronic structure of alanine on Cu{110}. *Surf Sci* **2006,** *600* (9), 1924-35.

176. Zaia, D. A. A review of adsorption of amino acids on minerals: was it important for origin of life? *Amino Acids* **2004,** *27* (1), 113-8.

177. Addadi, L.; Weiner, S. Interactions between acidic proteins and crystals: stereochemical requirements in biomineralization. *Proc Natl Acad Sci USA* **1985,** *82* (12), 4110-14.

178. Han, M.; Sethuraman, A.; Kane, R. S.; Belfort, G. Nanometer-Scale Roughness Having Little Effect on the Amount or Structure of Adsorbed Protein. *Langmuir* **2003,** *19* (23), 9868-72.

179. Wertz, C. F.; Santore, M. M. Effect of Surface Hydrophobicity on Adsorption and Relaxation Kinetics of Albumin and Fibrinogen: Single-Species and Competitive Behavior. *Langmuir* **2001,** *17* (10), 3006-16.

180. Sethuraman, A.; Vedantham, G.; Imoto, T.; Przybycien, T.; Belfort, G. Protein unfolding at interfaces: slow dynamics of alpha-helix to beta-sheet transition. *Proteins* **2004,** *56* (4), 669-78.

181. Sethuraman, A.; Belfort, G. Protein structural perturbation and aggregation on homogeneous surfaces. *Biophys J* **2005,** *88* (2), 1322-33.

182. Fears, K. P.; Creager, S. E.; Latour, R. A. Determination of the surface pK of carboxylic- and amine-terminated alkanethiols using surface plasmon resonance spectroscopy. *Langmuir* **2008,** *24* (3), 837-43.

183. Kosmulski, M. Confirmation of the Differentiating Effect of Small Cations in the Shift of the Isoelectric Point of Oxides at High Ionic Strengths. *Langmuir* **2002,** *18* (3), 785-87.

184. Hunt, N. T.; Kattner, L.; Shanks, R. P.; Wynne, K. The dynamics of water-protein interaction studied by ultrafast optical Kerr-effect spectroscopy. *J Am Chem Soc* **2007,** *129* (11), 3168-72.

185. Agashe, M.; Raut, V.; Stuart, S. J.; Latour, R. A. Molecular simulation to characterize the adsorption behavior of a fibrinogen gamma-chain fragment. *Langmuir* **2005,** *21* (3), 1103-17.

186. Tamerler, C.; Oren, E. E.; Duman, M.; Venkatasubramanian, E.; Sarikaya, M. Adsorption kinetics of an engineered gold binding Peptide by surface plasmon

resonance spectroscopy and a quartz crystal microbalance. *Langmuir* **2006,** *22* (18), 7712-8.

187. Vernekar, V. N.; Latour, R. A. Adsorption thermodynamics of a mid-chain peptide residue on functionalized SAM surfaces using SPR. *Mater Res Innovations* **2005,** *9* (2), 53-55.

188. Wei, Y.; Latour, R. A. Determination of the adsorption free energy for peptide-surface interactions by SPR spectroscopy. *Langmuir* **2008,** *24* (13), 6721-9.

189. Liu, L.; Yang, C.; Guo, Q. X. A study on the enthalpy-entropy compensation in protein unfolding. *Biophys Chem* **2000,** *84* (3), 239-51.

190. Basiuk, V. A. Thermodynamics of adsorption of amino acids, small peptides, and nucleic acid components on silica adsorbents. In *Biopolymers at Interfaces*, Malmsten, M., Ed.; Marcel Dekker: New York, **1998**; Vol. 75, pp 55-87.

191. Dill, K. A. Additivity principles in biochemistry. *J Biol Chem* **1997,** *272* (2), 701-4.

192. Singh, N.; Husson, S. M. Adsorption thermodynamics of short-chain peptides on charged and uncharged nanothin polymer films. *Langmuir* **2006,** *22* (20), 8443-51.

193. Toscano, A.; Santore, M. M. Fibrinogen adsorption on three silica-based surfaces: conformation and kinetics. *Langmuir* **2006,** *22* (6), 2588-97.

194. Street, A. G.; Mayo, S. L. Intrinsic -sheet propensities result from van der Waals interactions between side chains and the local backbone. *Proc Natl Acad Sci USA* **1999,** *96* (16), 9074-76.

195. Matsuoka, D.; Nakasako, M. Probability distributions of hydration water molecules around polar protein atoms obtained by a database analysis. *J Phys Chem B* **2009,** *113* (32), 11274-92.

196. Seker, U. O.; Wilson, B.; Sahin, D.; Tamerler, C.; Sarikaya, M. Quantitative affinity of genetically engineered repeating polypeptides to inorganic surfaces. *Biomacromolecules* **2009,** *10* (2), 250-7.

197. Roth, C. M.; Lenhoff, A. M. Quantitative modeling of protein adsorption. In *Biopolymers at Interfaces*, Malmsten, M., Ed.; Marcel Dekker: New York, **1998**; Vol. 75, pp 89-118.

198. Zhang, M.; Horbett, T. A. Tetraglyme coatings reduce fibrinogen and von Willebrand factor adsorption and platelet adhesion under both static and flow conditions. *Journal of Biomedical Materials Research Part A* **2009,** *89* (3), 791-803.

199. Santos, O.; Nylander, T.; Schillén, K.; Paulsson, M.; Trägårdh, C. Effect of surface and bulk solution properties on the adsorption of whey protein onto steel surfaces at high temperature. *J Food Eng* **2006,** *73* (2), 174-89.

200. Szabelski, P.; Cavazzini, A.; Kaczmarski, K.; Liu, X.; Van Horn, J.; Guiochon, G. Experimental studies of pressure/temperature dependence of protein adsorption equilibrium in reversed-phase high-performance liquid chromatography. *J Chromatogr A* **2002,** *950* (1-2), 41-53.

201. Gruber, K.; Klintschar, G.; Hayn, M.; Schlacher, A.; Steiner, W.; Kratky, C. Thermophilic xylanase from Thermomyces lanuginosus: high-resolution X-ray structure and modeling studies. *Biochemistry (Mosc)* **1998,** *37* (39), 13475-85.

202. Baxter, R. L.; Baxter, H. C.; Campbell, G. A.; Grant, K.; Jones, A.; Richardson, P.; Whittaker, G. Quantitative analysis of residual protein contamination on reprocessed surgical instruments. *J Hosp Infect* **2006,** *63* (4), 439-44.

203. Bagchi, D.; Kumar, A.; Menon, R. Tuning phase transitions and realization of special thermodynamic states in alcohol–water mixtures by the addition of ions. *Physica A: Statistical Mechanics and its Applications* **2007,** *384* (1), 1-9.

204. Thomas, P. D.; Dill, K. A. Local and nonlocal interactions in globular proteins and mechanisms of alcohol denaturation. *Protein Sci* **1993,** *2* (12), 2050-65.

205. Yoshida, K.; Kawaguchi, J.; Lee, S.; Yamaguchi, T. On the solvent role in alcohol-induced α-helix formation of chymotrypsin inhibitor 2. *Pure Appl Chem* **2008,** *80* (6), 1337-47.

206. Voets, I. K.; Cruz, W. A.; Moitzi, C.; Lindner, P.; Areas, E. P.; Schurtenberger, P. DMSO-induced denaturation of hen egg white lysozyme. *J Phys Chem B* **2010,** *114* (36), 11875-83.

207. Pirzer, T.; Geisler, M.; Scheibel, T.; Hugel, T. Single molecule force measurements delineate salt, pH and surface effects on biopolymer adhesion. *Phys Biol* **2009,** *6* (2), 025004.

208. Yu, I.; Nagaoka, M. Slowdown of water diffusion around protein in aqueous solution with ectoine. *Chem Phys Lett* **2004,** *388* (4-6), 316-21.

209. Vinh, N. Q.; Allen, S. J.; Plaxco, K. W. Dielectric spectroscopy of proteins as a quantitative experimental test of computational models of their low-frequency harmonic motions. *J Am Chem Soc* **2011,** *133* (23), 8942-7.

210. Graziano, G. Contrasting the denaturing effect of guanidinium chloride with the stabilizing effect of guanidinium sulfate. *PCCP* **2011,** *13* (25), 12008-14.

211. Heyda, J.; Lund, M.; Oncak, M.; Slavicek, P.; Jungwirth, P. Reversal of Hofmeister ordering for pairing of NH4(+) vs alkylated ammonium cations with halide anions in water. *J Phys Chem B* **2010,** *114* (33), 10843-52.

212. Schwierz, N.; Horinek, D.; Netz, R. R. Reversed anionic Hofmeister series: the interplay of surface charge and surface polarity. *Langmuir* **2010,** *26* (10), 7370-9.

213. Zhang, Y.; Furyk, S.; Bergbreiter, D. E.; Cremer, P. S. Specific ion effects on the water solubility of macromolecules: PNIPAM and the Hofmeister series. *J Am Chem Soc* **2005,** *127* (41), 14505-10.

214. Boström, M.; Williams, D. R. M.; Ninham, B. W. Specific Ion Effects: Why the Properties of Lysozyme in Salt Solutions Follow a Hofmeister Series. *Biophys J* **2003,** *85* (2), 686-94.

215. Horinek, D.; Serr, A.; Bonthuis, D. J.; Bostrom, M.; Kunz, W.; Netz, R. R. Molecular hydrophobic attraction and ion-specific effects studied by molecular dynamics. *Langmuir* **2008,** *24* (4), 1271-83.

216. Lund, M.; Jungwirth, P. Patchy proteins, anions and the Hofmeister series. *J Phys: Condens Matter* **2008,** *20* (49), 494218.

217. Kosmulski, M. pH-dependent surface charging and points of zero charge. III. Update. *J Colloid Interface Sci* **2006,** *298* (2), 730-41.

218. Vanzi, F.; Madan, B.; Sharp, K. Effect of the Protein Denaturants Urea and Guanidinium on Water Structure: A Structural and Thermodynamic Study. *J Am Chem Soc* **1998,** *120* (41), 10748-53.

219. England, J. L.; Haran, G. Role of solvation effects in protein denaturation: from thermodynamics to single molecules and back. *Annu Rev Phys Chem* **2011,** *62*, 257-77.

220. Camilloni, C.; Rocco, A. G.; Eberini, I.; Gianazza, E.; Broglia, R. A.; Tiana, G. Urea and guanidinium chloride denature protein L in different ways in molecular dynamics simulations. *Biophys J* **2008,** *94* (12), 4654-61.

221. Mason, P. E.; Neilson, G. W.; Dempsey, C. E.; Barnes, A. C.; Cruickshank, J. M. The hydration structure of guanidinium and thiocyanate ions: implications for protein stability in aqueous solution. *Proc Natl Acad Sci USA* **2003,** *100* (8), 4557-61.

222. Salis, A.; Bilanicova, D.; Ninham, B. W.; Monduzzi, M. Hofmeister effects in enzymatic activity: weak and strong electrolyte influences on the activity of Candida rugosa lipase. *J Phys Chem B* **2007,** *111* (5), 1149-56.

223. Godawat, R.; Jamadagni, S. N.; Garde, S. Unfolding of hydrophobic polymers in guanidinium chloride solutions. *J Phys Chem B* **2010,** *114* (6), 2246-54.

224. Dempsey, C. E.; Mason, P. E.; Jungwirth, P. Complex ion effects on polypeptide conformational stability: chloride and sulfate salts of guanidinium and tetrapropylammonium. *J Am Chem Soc* **2011,** *133* (19), 7300-3.

225. Panuszko, A.; Bruzdziak, P.; Zielkiewicz, J.; Wyrzykowski, D.; Stangret, J. Effects of urea and trimethylamine-N-oxide on the properties of water and the secondary structure of hen egg white lysozyme. *J Phys Chem B* **2009,** *113* (44), 14797-809.

226. Das, A.; Mukhopadhyay, C. Reply to the “Comment on 'Urea-Mediated Protein Denaturation: A Consensus View'”. *J Phys Chem B* **2011,** *115* (5), 1327-28.

227. Heyda, J.; Kozisek, M.; Bednarova, L.; Thompson, G.; Konvalinka, J.; Vondrasek, J.; Jungwirth, P. Urea and guanidinium induced denaturation of a Trp-cage miniprotein. *J Phys Chem B* **2011,** *115* (28), 8910-24.

228. Zhou, R.; Li, J.; Hua, L.; Yang, Z.; Berne, B. J. Comment on "urea-mediated protein denaturation: a consensus view". *J Phys Chem B* **2011,** *115* (5), 1323-6; discussion 27-8.

229. Canchi, D. R.; Paschek, D.; Garcia, A. E. Equilibrium study of protein denaturation by urea. *J Am Chem Soc* **2010,** *132* (7), 2338-44.

230. Hedoux, A.; Krenzlin, S.; Paccou, L.; Guinet, Y.; Flament, M. P.; Siepmann, J. Influence of urea and guanidine hydrochloride on lysozyme stability and thermal denaturation; a correlation between activity, protein dynamics and conformational changes. *PCCP* **2010,** *12* (40), 13189-96.

231. Das, A.; Mukhopadhyay, C. Urea-mediated protein denaturation: a consensus view. *J Phys Chem B* **2009,** *113* (38), 12816-24.

232. Sagle, L. B.; Zhang, Y.; Litosh, V. A.; Chen, X.; Cho, Y.; Cremer, P. S. Investigating the hydrogen-bonding model of urea denaturation. *J Am Chem Soc* **2009,** *131* (26), 9304-10.

233. Zangi, R.; Zhou, R.; Berne, B. J. Urea's action on hydrophobic interactions. *J Am Chem Soc* **2009,** *131* (4), 1535-41.

234. Hua, L.; Zhou, R.; Thirumalai, D.; Berne, B. J. Urea denaturation by stronger dispersion interactions with proteins than water implies a 2-stage unfolding. *Proc Natl Acad Sci USA* **2008,** *105* (44), 16928-33.

235. Chen, X.; Sagle, L. B.; Cremer, P. S. Urea orientation at protein surfaces. *J Am Chem Soc* **2007,** *129* (49), 15104-5.

236. Hayashi, Y.; Katsumoto, Y.; Omori, S.; Kishii, N.; Yasuda, A. Liquid structure of the urea-water system studied by dielectric spectroscopy. *J Phys Chem B* **2007,** *111* (5), 1076-80.

237. Hermida-Ramon, J. M.; Ohrn, A.; Karlstrom, G. Planar or nonplanar: what is the structure of urea in aqueous solution? *J Phys Chem B* **2007,** *111* (39), 11511-5.

238. Kokubo, H.; Pettitt, B. M. Preferential solvation in urea solutions at different concentrations: properties from simulation studies. *J Phys Chem B* **2007,** *111* (19), 5233-42.

239. Stumpe, M. C.; Grubmuller, H. Interaction of urea with amino acids: implications for urea-induced protein denaturation. *J Am Chem Soc* **2007,** *129* (51), 16126-31.

240. Stumpe, M. C.; Grubmuller, H. Aqueous urea solutions: structure, energetics, and urea aggregation. *J Phys Chem B* **2007,** *111* (22), 6220-8.

241. Rezus, Y. L.; Bakker, H. J. Effect of urea on the structural dynamics of water. *Proc Natl Acad Sci USA* **2006,** *103* (49), 18417-20.

242. Otzen, D. Protein-surfactant interactions: a tale of many states. *Biochim Biophys Acta* **2011,** *1814* (5), 562-91.

243. Tobias, D. J.; Hemminger, J. C. Chemistry. Getting specific about specific ion effects. *Science* **2008,** *319* (5867), 1197-8.

244. Hunger, J.; Niedermayer, S.; Buchner, R.; Hefter, G. Are nanoscale ion aggregates present in aqueous solutions of guanidinium salts? *J Phys Chem B* **2010,** *114* (43), 13617-27.

245. Jha, S. K.; Udgaonkar, J. B. Direct evidence for a dry molten globule intermediate during the unfolding of a small protein. *Proc Natl Acad Sci USA* **2009,** *106* (30), 12289-94.

246. Kaushik, J. K.; Bhat, R. Thermal Stability of Proteins in Aqueous Polyol Solutions: Role of the Surface Tension of Water in the Stabilizing Effect of Polyols. *J Phys Chem B* **1998,** *102* (36), 7058-66.

247. Kaushik, J. K.; Bhat, R. Why is trehalose an exceptional protein stabilizer? An analysis of the thermal stability of proteins in the presence of the compatible osmolyte trehalose. *J Biol Chem* **2003,** *278* (29), 26458-65.

248. Banks, D. D. Non-specific shielding of unfavorable electrostatic intramolecular interactions in the erythropoietin native-state increase conformational stability and limit non-native aggregation. *Protein Sci* **2015**, n/a-n/a.

249. Dempsey, C. E.; Piggot, T. J.; Mason, P. E. Dissecting contributions to the denaturant sensitivities of proteins. *Biochemistry (Mosc)* **2005,** *44* (2), 775-81.

250. Hamada, H.; Arakawa, T.; Shiraki, K. Effect of additives on protein aggregation. *Curr Pharm Biotechnol* **2009,** *10* (4), 400-7.

251. Sasaki, Y.; Akiyoshi, K. Development of an artificial chaperone system based on cyclodextrin. *Curr Pharm Biotechnol* **2010,** *11* (3), 300-5.

252. Eiberle, M. K.; Jungbauer, A. Technical refolding of proteins: Do we have freedom to operate? *Biotechnology journal* **2010,** *5* (6), 547-59.

253. Chaudhuri, R. G.; Paria, S. Dynamic contact angles on PTFE surface by aqueous surfactant solution in the absence and presence of electrolytes. *J Colloid Interface Sci* **2009,** *337* (2), 555-62.

254. Zdziennicka, A.; Janczuk, B. Effect of anionic surfactant and short-chain alcohol mixtures on adsorption at quartz/water and water/air interfaces and the wettability of quartz. *J Colloid Interface Sci* **2011,** *354* (1), 396-404.

255. Tomi, T.; Maeda, T.; Satake, I.; Hayakawa, K. Micelle formation of a cationic surfactant in the presence of 1,n-alkanediol and the miscibility of alcohols in micelles. *Colloids Surf Physicochem Eng Aspects* **2009,** *346* (1-3), 28-33.

256. Bohnert, J. L.; Horbett, T. A. Changes in adsorbed fibrinogen and albumin interactions with polymers indicated by decreases in detergent elutability. *J Colloid Interface Sci* **1986,** *111* (2), 363-77.

257. Elwing, H.; Gölander, C.-G. Protein and detergent interaction phenomena on solid surfaces with gradients in chemical composition. *Adv Colloid Interface Sci* **1990,** *32* (4), 317-39.

258. Elwing, H.; Welin, S.; Askendal, A.; Nilsson, U.; LundstrÖm, I. A wettability gradient method for studies of macromolecular interactions at the liquid/solid interface. *J Colloid Interface Sci* **1987,** *119* (1), 203-10.

259. Zhang, R.; Somasundaran, P. Advances in adsorption of surfactants and their mixtures at solid/solution interfaces. *Adv Colloid Interface Sci* **2006,** *123-126*, 213-29.

260. Billsten, P.; Carlsson, U.; Elwing, H. Studies on the conformation of adsorbed proteins with the use of nanoparticle technology. In *Biopolymers at Interfaces*, Malmsten, M., Ed.; Marcel Dekker: New York, 1998; Vol. 75, pp 627-50.

261. Kotsmar, C.; Pradines, V.; Alahverdjieva, V. S.; Aksenenko, E. V.; Fainerman, V. B.; Kovalchuk, V. I.; Kragel, J.; Leser, M. E.; Noskov, B. A.; Miller, R. Thermodynamics, adsorption kinetics and rheology of mixed protein-surfactant interfacial layers. *Adv Colloid Interface Sci* **2009,** *150* (1), 41-54.

262. Joshi, O.; McGuire, J. Adsorption behavior of lysozyme and Tween 80 at hydrophilic and hydrophobic silica-water interfaces. *Appl Biochem Biotechnol* **2009,** *152* (2), 235-48.

263. Aurora, R.; Creamer, T. P.; Srinivasan, R.; Rose, G. D. Local interactions in protein folding: lessons from the alpha-helix. *J Biol Chem* **1997,** *272* (3), 1413-6.

264. Selvaraj, S.; Gromiha, M. M. Role of hydrophobic clusters and long-range contact networks in the folding of (alpha/beta)8 barrel proteins. *Biophys J* **2003,** *84* (3), 1919-25.

265. Chakrabartty, A.; Kortemme, T.; Baldwin, R. L. Helix propensities of the amino acids measured in alanine-based peptides without helix-stabilizing side-chain interactions. *Protein Sci* **1994,** *3* (5), 843-52.

266. Nick Pace, C.; Martin Scholtz, J. A Helix Propensity Scale Based on Experimental Studies of Peptides and Proteins. *Biophys J* **1998,** *75* (1), 422-27.

267. Pagel, K.; Wagner, S. C.; Samedov, K.; von Berlepsch, H.; Bottcher, C.; Koksch, B. Random coils, beta-sheet ribbons, and alpha-helical fibers: one peptide adopting three different secondary structures at will. *J Am Chem Soc* **2006,** *128* (7), 2196-7.

268. Zhmurov, A.; Kononova, O.; Litvinov, R. I.; Dima, R. I.; Barsegov, V.; Weisel, J. W. Mechanical transition from alpha-helical coiled coils to beta-sheets in fibrin(ogen). *J Am Chem Soc* **2012,** *134* (50), 20396-402.

269. Dong, H.; Hartgerink, J. D. Role of hydrophobic clusters in the stability of α-helical coiled coils and their conversion to amyloid-like β-sheets. *Biomacromolecules* **2007,** *8* (2), 617-23.

270. Bennion, B. J.; Daggett, V. The molecular basis for the chemical denaturation of proteins by urea. *Proc Natl Acad Sci USA* **2003,** *100* (9), 5142-7.

271. Moglich, A.; Krieger, F.; Kiefhaber, T. Molecular basis for the effect of urea and guanidinium chloride on the dynamics of unfolded polypeptide chains. *J Mol Biol* **2005,** *345* (1), 153-62.

CHAPTER THREE

SPECIFIC AIMS

3.1. Aim 1: Development of experimental methods to gain molecular-level insight on the effects of an adsorbed protein's orientation and the shifts in its secondary and tertiary structure on its solution-state bioactivity.

Protein adsorption on material surfaces is a common phenomenon that is of critical importance in many biotechnological and pharmaceutical applications. The structure and function of adsorbed proteins are tightly interrelated and play a key role in the communication and interaction of adsorbed proteins with the surrounding environment. Because the bioactive state of a protein on a surface is a function of the orientation, conformation, and accessibility of its bioactive site(s), the isolated determination of just one or two of these factors will typically not be sufficient to understand the structure-function relationships of the adsorbed layer. Rather a combination of methods is needed to address each of these factors in a synergistic manner to provide a complementary data set to characterize and understand the bioactive state of adsorbed proteins. Therefore the first objective of this dissertational work was to develop a set of complementary methods to address this need. The developed methods include (a) adsorbed-state circular dichroism spectropolarimetry to determine adsorption-induced changes in protein secondary structure, (b) amino-acid labeling/mass spectrometry to assess adsorbed protein orientation and changes in tertiary structure by monitoring adsorption-induced changes in residue solvent accessibility, and (c) bioactivity assays to assess adsorption-induced changes in protein bioactivity.

3.2 Aim 2: Delineating the individual and combined role of protein-surface interactions, protein-protein interactions, and inherent internal protein stability on adsorbed protein structure and bioactivity.

The adsorption-induced shifts in the native-state structure and bioactivity of a protein is an effective representation of the influence of protein-surface interactions, protein-protein interactions, and internal stability of a protein. Though the influence of protein-surface interactions on the structure and bioactivity of adsorbed proteins have been widely studied, the contribution of protein-protein interactions and internal protein stability on these adsorption responses are often inseparable from the effects of protein-surface interactions. Therefore, using the techniques developed in Aim 1, the subsequent objective of this research work was to delineate the individual and combined roles of protein-surface interactions, protein-protein interactions, and inherent internal protein stability on the structure of adsorbed proteins. Towards this purpose, the strategy used in this work was to tease out the effects of protein-surface interactions and protein-protein interactions on protein structure and bioactivity. This was studied by varying experimental conditions in a manner to obtain a broad range of surface coverages of protein on the surface, with protein-protein interaction effects assumed to be directly related to the adsorbed surface coverages of the protein. This was accomplished by varying the bulk solution concentration that the protein was adsorbed from, the adsorption time of the proteins on the surface, and the residence time of the protein on the surface in protein-free buffer. The role of internal stability on the protein structure and bioactivity were subsequently studied by using two similar sized proteins that catalyzed the substrate in similar fashion but differed in its sequence composition and solution-state

stability. In this dissertational work, the adsorption responses of two model proteins (hen egg-white lysozyme (HEWL) and bovine pancreatic ribonuclease-A (RNase-A)), on three model surfaces (flat surfaces of silica glass (glass), poly(methyl methacrylate) (PMMA), and high density polyethylene (HDPE)), were studied.

3.3 Aim 3: Evaluating the molecular mechanisms involved in the interaction of an aqueous solution of chemical excipients with adsorbed protein and their influence on protein structure and bioactivity

Strategies to stabilize and destabilize the structure and bioactivity of an adsorbed or an immobilized protein is an effective way for controlling its biological response with the surrounding environment and influencing the operational stability of an engineered system involving adsorbed or immobilized proteins. While many such strategies have been developed for proteins that are in solution, it not clear how effective these same strategies are when applied to adsorbed or immobilized proteins. Therefore, the final aim of this research was to evaluate the mode of interaction of different chemical excipients (i.e., surfactants and denaturants) on the surface coverage, adsorbed structure, and bioactivity of a protein. For this purpose, I tested the influence of two type of chemical excipients (salts and surfactants) of fixed concentration on HEWL and RNase A pre-adsorbed adsorbed on silica glass, PMMA, and HDPE. The excipient agents included ionic and non-ionic salts (guanidium hydrochloride and urea, respectively) and a set of detergents (sodium dodecyl sulphate (SDS, ionic detergent), 3-[(3-Cholamidopropyl) dimethyl-ammonio]-1-propanesulfonate (CHAPS, zwitterionic detergent), and octyl glucoside (Octyl, non-ionic detergent)).

CHAPTER FOUR

EXPERIMENTAL CHARACTERIZATION OF ADSORBED PROTEIN ORIENTATION, CONFORMATION, AND BIOACTIVITY

Based on the Published Article: Thyparambil A.A., Wei Y., and Latour R.A., Experimental Characterization of Adsorbed Protein Orientation, Conformation, and Bioactivity, Biointerphases, 2015, 10(1): 019002.

4.1 INTRODUCTION

The interaction of proteins with material surfaces constitutes one of the most prominently studied areas within the field of biomaterials and is of considerable interest for many applications of biotechnology and biomedical engineering, including biosensors,[1-2] enzyme based technologies,[3-4] tissue engineering and regenerative medicine,[5-6] implants,[7-9] and biodefense.[10-11]. These interactions typically occur spontaneously as a protein-containing solution contacts a solid material surface, which can result in a substantial shift in the protein's structure as well as changes in the solvent accessibility of its amino acid residues,[12-15] often leading to a reduction in bioactivity.[13-15]

When a protein adsorbs from solution onto a material surface, the interactions between the amino acid residues of the protein and the functional groups of the surface typically result in a situation where the native state of the protein no longer represents the low free energy state of the combined protein-surface-solution system. This situation can lead to substantial shifts in the protein away from its native-state structure. If these changes influence the structure of the bioactive site in the protein such that its intended

substrate or receptor can no longer bind to that site, bioactivity will be lost. Likewise, if the protein adsorbs to a surface such that accessibility to the binding site is sterically blocked, bioactivity can be lost as well. These effects are depicted in Fig. 2.2 in the Chapter 2 of this dissertation.[16] Unfortunately, bioactivity assays are unable to distinguish between these two factors when adsorption causes a loss in bioactivity (i.e., loss due to conformational distortion vs. steric hindrance of the bioactive site), thus making it difficult to determine how a given system should be redesigned to correct the problem. To address this situation, experimental methods are needed to characterize how adsorption influences both the orientation and the structure of protein on a surface in addition to adsorption-induced changes in bioactivity. With these combined datasets, assessment can then be made regarding the actual factor(s) that are responsible for a loss in bioactivity if it occurs.

Relative few methods have been developed to probe the orientation and structure of an adsorbed proteins.[15, 17] Some of the methods that can provide information on adsorbed protein orientation and tertiary (and quaternary) structure include fluorescence,[18-21] time-of-flight secondary-ion mass spectrometry (ToF-SIMS),[22-24] nuclear magnetic resonance spectroscopy (NMR),[25-26] and amino acid labeling/mass spectrometry (AAL/MS).[27-31] Methods for the determination of the secondary structure of adsorbed proteins include Fourier transform infra-red spectroscopy (FTIR),[32-33] surface enhanced Raman scattering (SERS),[34-35] and circular dichroism spectropolarimetry (CD).[27, 36-39] Unfortunately, as the size of the protein increases, many of the spectral signatures that are needed for tertiary structure determination using fluorescence and

NMR overlap, introducing much subjectivity into the analyses, thus making it difficult to accurately interpret the configuration of the adsorbed protein. In contrast, mass spectrometry (MS) has shown great promise in characterizing the adsorbed configuration of both large and small proteins at a molecular level, especially when used with amino acid labeling (AAL).[27-31] After evaluating several of these types of methods, our group has specifically focused on the development and adaptation of CD and AAL/MS for the characterization of adsorbed protein orientation and structure, and we will therefore focus on these methods for this paper. Readers are encouraged to refer to the above cited references for the application of the other types of methods that are noted above.

Circular dichroism spectropolarimetry (CD) has been extensively used to spectroscopically study the structure of biomolecules in solution and when absorbed to surfaces due to its characteristics of being non-destructive, relative easy to perform, requirement of small sample volume, and providing fast, reliable data analysis.[40-42] In particular, CD provides a very convenient experimental method for quantifying the secondary structure and environmentally induced structural changes in proteins since the different forms of the main secondary structural elements found in proteins (e.g., α-helix, β-sheet, and random loop) each exhibits a distinctly different CD spectrum.[42-43] Though, CD has been usually reported with proteins in solution or with proteins adsorbed to colloidal particles, its use with flat transparent material surfaces was reported as early as 1974 by McMillin and Walton.[44] However, unlike then, the modern versions of CD spectropolarimeters are equipped with photo-elastic modulators (PEM) instead of Pockel's cells, which have much improved signal-to-noise ratio and place less stringent

requirement on the minimum amount of protein that is needed for adsorption studies on planar surfaces.[38, 45-46] In addition to quantifying the secondary structural elements, the shifts in the near UV CD spectral range (260–320 nm) have been used to qualitatively determine the ‘‘molten globule’’ states in many adsorbed proteins, which reflect the protein’s tertiary structure.[40, 42, 46-47] Similarly, in many proteins containing co-factors as an important functional part of the bioactive site, such as metal ions, shifts in the spectral features in the visible light related to the cofactor’s position have also been used as indicators of the integrity of the binding site.[48-49] However, since the shape and magnitude of near-UV CD spectra are influenced by the type of protein, and strategies to quantify the tertiary structural shifts using CD techniques are lacking, CD is primarily used for secondary structural determination. Alternative techniques, such as AAL/MS, are thus required to provide insight into higher order structure.[42]

The AAL/MS technique combines the use of side-chain-selective chemical modification of amino acids within the proteins (i.e., AAL) along with MS to provide a readout of the sites susceptible to covalent modifications upon reaction with a labeling reagent.[50-51] The chemical labeling is conducted under mild reaction conditions to minimize any possible alterations to the protein structure, which can be confirmed by CD. The proteins are separately labeled in solution and after adsorption, following which the labeled proteins are digested to peptide fragments and the specific sites that are labeled are identified by MS. The amino acid residues that are found to be labeled in solution but unlabeled following adsorption indicate regions of the protein that are sterically blocked by the surface (i.e., indicative of adsorbed orientation) or by

neighboring proteins (i.e., indicative of protein-protein interactions). Although it is not possible to distinguish between these two causes, protein-protein interactions can be expected to have a higher probability of causing a loss in amino acid residue solvent accessibility when the protein is adsorbed from high solution concentration where the protein adsorbs with high packing density on the surface. In contrast to this, when a protein is adsorbed from low solution concentration, it generally undergoes a greater degree of unfolding and spreading out on the surface with lower adsorbed surface density, with a loss in solvent accessibility subsequently having greater probability for being caused by steric hindrance from the surface. Alternatively, amino acids that are unlabeled in solution but become labeled following adsorption are indicative of the sites in the protein that underwent adsorption-induced tertiary unfolding, thus exposing the side-chains of amino acids that are not solvent accessible in the protein's native-state. Thus by the application of AAL/MS to multiple different amino acid types that are distributed throughout a protein, a fairly comprehensive picture can be generated regarding the distribution of sites in the protein that are tightly adsorbed to the surface (or blocked by neighboring proteins) and the sites that undergo adsorption-induced tertiary unfolding.

In this chapter, I present the experimental methods that we have developed and/or adapted to gain amino-acid-residue-level information on adsorbed protein orientation and adsorption-induced changes in a protein's secondary and tertiary structure using CD and AAL/MS. When coupled with measurements of adsorption-induced changes in bioactivity, these data can provide insights regarding whether a measured loss in

bioactivity is due to adsorbed protein orientation or adsorption-induced changes in protein structure. Following the presentation of our CD and AAL/MS methods, I demonstrate their application to characterize the adsorption behavior of hen egg-white lysozyme (HEWL) on materials exhibiting three distinctly different types of surface chemistry (silica glass, poly(methyl methacrylate), and high-density polyethylene) to show how these methods can be used to provide insights into the cause of adsorption-induced changes in bioactivity.

4.2 EXPERIMENTAL SET UP AND METHODOLOGY

This section contains the overview of the protocols and the critical considerations taken by the authors when using CD,[36, 38, 52] AAL/MS,[51-52] and spectrophotometric techniques to gain quantitative information on the adsorbed structure and bioactivity of proteins on flat material surfaces with relatively low surface area.[36-37, 52] The reader is referred to our referenced original papers for additional details on the specific application of each of these methods to specific protein adsorption systems.[27, 36-38, 51-53]

4.2.1 Material Surface Characterization and Protein Adsorption

Characterization of the chemical, physical, and morphological properties of a material surface is important prior to structure determination of the adsorbed protein in order to validate and document that the material surface is of the type expected and to provide a basis for evaluating how various surface properties influence the adsorption processes. Because of the need for a material that exhibits negligible absorbance over the wavelengths that we use for CD (i.e., 190 – 250 nm), we use fused silica glass slides as our

base substrate for each of our material surfaces. The glass slides can subsequently be modified by coating them with thin films of polymer by spin coating, metal/metal oxide by vapor deposition, or self-assembled monolayers (SAMs) to present different surface functional groups. We typically characterize each type of surface for chemical composition via X-ray photoelectron spectroscopy (NESAC/BIO, University of Washington), surface roughness by atomic force microscopy (Asylum Research, MFP–3D), surface wettability by static contact angle (Krüss, DSA–20E), film thickness by variable angle spectroscopic ellipsometry (Sopra Inc., GES–5), and surface charge density using a streaming potential method (SurPASS, Anton Paar GmbH, Austria).[54] Prior to surface analysis and protein adsorption, standard cleaning procedures are followed, which vary depending on the type of surface being used,[36, 51-52, 55] and the respective substrates are then stored under buffered aqueous solution at room temperature until use.

We typically purchase protein for our studies from commercial vendors in crystallized form with at least 95% purity. The proteins are subsequently dissolved in a low-salt buffer to minimize absorbance (e.g., 10 mM phosphate buffered saline; PPB), with the protein concentration verified by the biuret method (Thermo Scientific, 23225) or absorbance at 205 nm (A_{205}).[36, 51-52] Prior to protein adsorption, the surfaces are equilibrated in buffer for several hours and then protein solution is added to the buffer as necessary to obtain the desired net solution concentration. The placement of the surface samples under pure buffer (i.e., in the absence of proteins) prior to adding the protein solution is very important. Since the air-water interface effectively acts as a hydrophobic surface, proteins tend to adsorb to this interface to form a relatively thick film of denatured

protein. Therefore, if the adsorbent surface is placed in the buffer solution after the protein is added, the surface will pass through this denatured film of protein at the air-water interface, which will subsequently coat the surface with a layer of this denatured protein. This adsorbed layer of protein will thus be very different from what would adsorb from the solution itself. Similarly, when pipetting the protein solution into the pure buffer solution, it is important to position the pipette tip beneath the air-water interface. This step thus minimizes the exposure of the stream of protein solution to an air-water interface, which can also induce protein denaturation. Likewise, removal of the adsorbent sample from the solution after adsorbing the protein should be done by first infinitely diluting the solution over the sample to remove the denatured film of protein at the air-water interface. This can be done by gently flowing pure buffer into the solution container for several minutes to remove all of the protein from solution. This process will also desorb any loosely bound protein from the surface leaving behind the strongly bound, effectively irreversibly adsorbed protein layer. Following this process, the surface with the sample can then be removed from the sample well without the presence of protein at the air-water interface.

4.2.2. Quantification of the Secondary Structure in Adsorbed Protein Using CD Spectropolarimetry

We use a Jasco J-810 spectrophotometer to determine the secondary structures of protein both in solution and after adsorption on surfaces. Prior to spectral scans, cuvettes are calibrated and the performance of the instrument is evaluated using freshly prepared 1S-(+)-10-camphorsulphonic acid (Aldrich, C2107) as the calibration standard over the spectral range of 190-320 nm and the ratio of the absolute signals at 192.5 nm and 290.5

nm are checked to ensure a value of ≥ 2, thereby confirming that CD instrument is performing within recommended standards.[42].[42]

4.2.2.1. Cuvette and Scan Settings for Acquiring the Spectra

The scan settings for acquiring the spectra of proteins in solution or in the adsorbed state are determined based on the total absorbance of the test sample, which in turn is directly related to the high-tension voltage (HTV, the voltage applied to the photomultiplier). In all our studies with the protein in solution or in its adsorbed state, the HTV is kept < 700 V.[42, 56] In the event, that the spectrum is too noisy or too weak, the concentration of protein and/or the pathlength of the cuvettes are adjusted. Generally, for determining the solution structure of protein we use protein concentrations of 1.0 mg/mL for a 0.01 cm pathlength cuvette (Starna Cells), or 0.1 mg/mL for a cuvette of 0.1 cm pathlength (Starna Cells). The protein structure determination in more dilute solutions should be avoided, as a significant proportion of the CD signal may be due to the protein adsorption on the surfaces of the cuvette instead of the protein that is in the solution.

For the determination of the structure of adsorbed proteins, we had previously used a custom designed cuvette that was capable of supporting four individual slides by gluing two quartz windows to a poly(ether-ether-ketone) (PEEK) polymer holder.[38] However, technical difficulties imposed by gluing the quartz windows to PEEK, and the limited reusability of these cuvettes, prompted us to improve the cuvette design used for our adsorption studies. The assembled set-up of the improved cuvette design that we currently use for protein adsorption studies is shown in Fig 4.1.

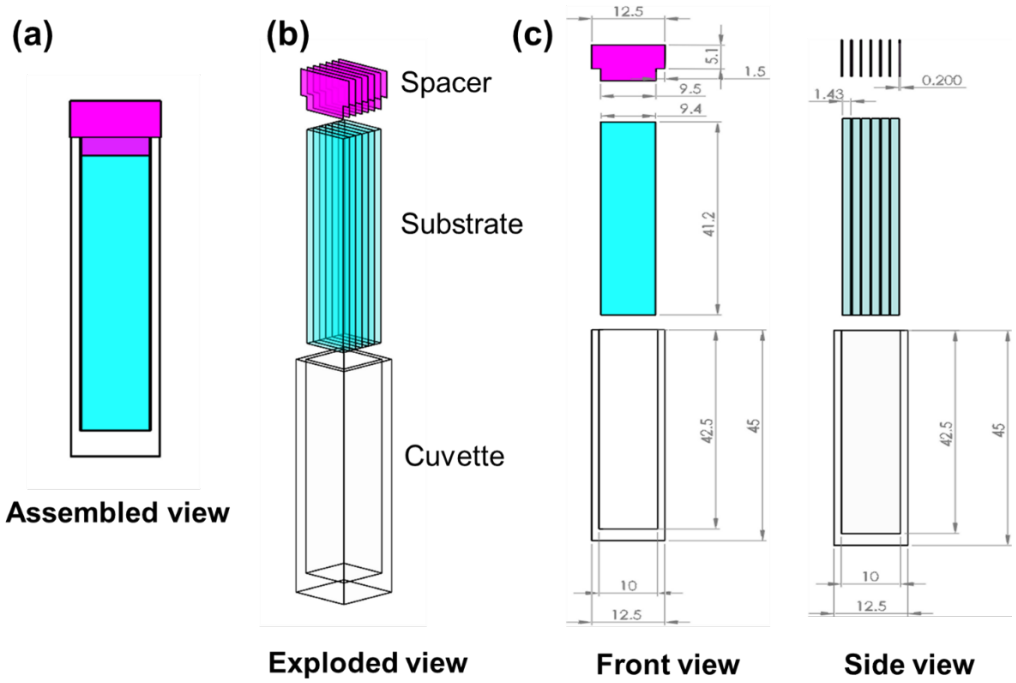

Figure 4.1: An improved CD cuvette Design.[16] An improved experimental set-up to investigate the effect of bulk surface properties on the structure of adsorbed proteins is shown in panels (a) – (c). The assembled view of the improved set-up is shown in panel (a) with the individual components within the set-up (1 standard spectroscopic grade quartz cuvette (Starna Cells, 1-Q-10), six custom-cut fused silica substrates (Custom order CU-1005-041JS, ChemGlass Life sciences) and, seven vinyl polymeric spacers being shown in the exploded view of panel (b). The dimensions of each individual component: the standard spectroscopic grade quartz cuvette of path length 1 cm (External dimension: 12.5 mm × 12.5 mm × 45 mm; Internal dimension: 42.5 mm × 10 mm × 10 mm), fused silica substrates (9.4 mm × 1.43 mm × 41.2 mm) and, T-spacers (Base: 1.5 mm × 9.5 mm × 0.2 mm; Head: 5.1 mm × 12.5 mm × 0.2 mm) are shown in the front and side views of the set-up. Reproduced with permission from Ref.16. Copyright 2015 AVS.

The relative advantages of this new construct over our old one lie in its relative simplicity, lower absorbance of the incident beam, and the prolonged reusability of the cuvettes. For example, the background absorbance at 190 nm for the old and new cuvettes at their full capacity of loading of six fused silica glass slides is about 2.1 and 1.7, respectively. In terms of percent transmission (%T), these absorbance values correspond to about 0.79% (% T = $10^{(2-A190)}$) and 2.00%, respectively, of the deep UV-

spectra for the old and new designs. These values result in 153% improvement in beam transmission as well as decreased pathlength of the new cuvette (0.14 cm as opposed to 0.16 cm). These changes provide the new design with an enhanced limit of detection that is equivalent to the absorbance of 0.03 mg/mL of protein solution concentration in a 1 cm cuvette at 195 nm.

Because of the differences in the light throughput in the cuvettes used for solution and adsorbed studies, we typically use two types of settings in our CD studies.[42, 56] When the light throughput from the instrument is high (%T > 5), the CD spectra are recorded from 190 nm to 300 nm at a scan rate of 100 nm/min, bandwidth of 0.5 nm, with a response time of 0.25 s. But, for all other cases, the CD spectra are recorded from 190 nm to 300 nm at a scan rate of 10 nm/min with a response time of 2 s, and a bandwidth of 0.5 nm. In each case, a spectrum of protein in solution or in the adsorbed state represents the data averaged over six (n = 6) accumulations. These scan parameters are set so as to optimize the contribution of shot and systematic noise in the acquired spectra. For example, lengthening the response time of the instrument will increase the number of photons reaching the detector (minimizing the shot noise), but require a longer time to complete a scan, thereby increasing the effect of baseline drift (systematic noise). Similarly, severely shortening the response time will minimize the systematic noise, but increase the shot noise. Therefore, the noise from these two sources is kept minimal by optimizing the response time and scan rates, and any residual effects on the spectra are off-set by averaging the spectra over multiple scans (n), which will reduce the signal error due to noise as a function of the square root of n.

4.2.2.2. Scaling of CD Spectra

The CD spectrum (θ, in mdeg) is dependent on the pathlength and the molar concentration of the proteins and needs to be appropriately scaled to its molar elliptical units ([θ], deg·cm^2/dmol) using the equation 4.1 (for proteins in solution) and equation 4.2 (for adsorbed proteins) prior to quantifying the secondary structural elements within the protein of interest.

$$[\theta] = \frac{\theta \times M_0}{10000 \times C_{\text{soln}} \times L} \tag{4.1}$$

$$[\theta] = \frac{\theta \times M_0}{10000 \times Q_{ads}} \tag{4.2}$$

where M_0 is the mean residue molecular weight of protein (≈ 112 g/mole) and is obtained by averaging the molecular weight of the protein over the overall sequence length, C_{soln} is concentration of protein in solution (g/ml), L is the pathlength of cuvette (cm), and Q_{ads} is the surface coverage of adsorbed protein (g/cm^2). Values for C_{soln} and Q_{ads} are calculated from equations 3 and 4:

$$C_{\text{soln}} = \frac{A_w}{\varepsilon_w \times L} \tag{4.3}$$

$$Q_{ads} = \frac{A_w}{\varepsilon_w} \tag{4.4}$$

where, A_{w} is the absorbance of the protein containing solution at wavelength (w) and ε_{w} (units of cm^{2}g^{-1} or (g/ml)$^{-1}$ cm^{-1}) is the molar extinction coefficient corresponding to wavelength, w.

The unknown concentration of proteins is typically determined using the absorbance at 280 nm,[42] and the extinction coefficient at 280 nm for 1% (w/v) protein solutions (ε_{280} (1%), units of $(g/100\ ml)^{-1}\ cm^{-1}$) are usually reported by the commercial vendors. However, if proteins in solution are denatured, (e.g., by chemical additives, or by thermal- or pH-induced unfolding), the red shifts associated with the protein can introduce significant errors in these estimate.[57] As a result, the extinction coefficient at far UV wavelengths, like those of 195 nm or 205 nm, are preferred due to the lesser influence of red-shifts and better sensitivity due to peak absorbance of the protein at 205 nm.[36, 51] The extinction coefficients ε_{205} or ε_{195} are determined from the slope of the calibration curve for A_{205} or A_{195} plotted vs. solution concentration (C_{soln}, units of g/ml) using serial dilutions of fresh stock solutions of protein, with the concentration verified using ε_{280} (1%) or the biuret method. Alternatively, the use of absorbance at 230 nm has also been shown to be better than 280 nm in determining the unknown concentration of proteins. Absorbance at 230 nm is useful when the solution contains strongly absorbing chemical additives like urea or guanidium hydrochloride, which tend to mask the signal from protein absorbance at wavelengths less than 230 nm.[57]

Once a spectrum is appropriately scaled, the quality of spectra for designated proteins in their native state in solution obtained over the 190 nm – 260 nm range can be verified by comparison to reference spectra for the respective proteins using online databases like the Protein Circular Dichroism Data bank (PCDDB), which contains synchrotron CD spectra (higher resolution spectra) for many proteins in their native

state.[58] Additionally, these spectra can be used to provide indicators of the structural integrity of the proteins in solution.

As a cautionary note regarding the determination of the structure of adsorbed proteins, it is important that the surfaces with the adsorbed protein are gently rinsed to remove loosely bound protein before they are mounted in the cuvette and that the remaining protein is effectively irreversible adsorbed. Otherwise, protein may desorb from the surface into the surrounding solution after the slides are placed under pure buffer solution in the cuvette, with the contribution of any desorbed protein in solution causing artifacts in the measured adsorbed-state structure. To insure that protein did not desorb from the surfaces during CD measurement, the amount of protein on the surface should be determined both before and after CD measurement, with the buffer solution replaced with pure buffer (protein-free buffer) for the after-scan measurement.

4.2.2.3. Quantification of Secondary Structure

To quantify the relative proportion of each associated secondary structure contained in a protein sample, the resulting CD spectrum acquired between wavelengths of 190 to 240 nm is typically empirically interpreted as a sum of fractional multiples of the reference spectrum for each type of secondary structure.[43] This deconvolution process is conducted using a variety of mathematical tools (like CONTIN/LL, SELCON3, and CDSStr methods provided with the CDPro software package)[59] that fit the acquired spectra with the spectra of reference datasets of highly resolved protein structures (i.e., the protein structures within the SP43 and SP48

datasets obtained using X-ray crystallography and NMR spectroscopy).[46] The quality of the fit is typically assessed by analyzing the R-fit using non-linear regression. With different algorithms and different reference datasets obtained over a larger wavelength range, such as 175–260 nm (SP-175 or MP-180, provided with Dichroweb), there can be slight variations in the estimated secondary structure content, and thus some discrepancies in the fitting parameters can be expected.[59-63] The analysis is usually considered reliable if different mathematical tools give similar results, at which point the values obtained from the different fitting algorithms can be averaged and confidently reported.[42]

One of the limitations of the deconvolution algorithms is that they depend on the availability of ellipticity values over the full range of wavelengths from 190-240 nm. Thus, these methods cannot be used in the presence of additives in solution that strongly adsorb wavelengths below 220 nm. In this case, alternative methods like the 222 nm, 225 nm, 228 nm, or 230 - 240 nm slope method can be used to quantify the helical content of proteins in solution or in the adsorbed state.[42, 64] Unfortunately, similar alternative methods are not available for quantifying the β-sheet structures in a protein.

4.2.3. Protein Structure Determination Using Amino Acid Side-Chain Modification with Mass Spectrometry (AAL/MS)

The AAL/MS technique is used to identify the sites susceptible to covalent modifications upon reaction with a labeling reagent and, in turn, assess the solvent exposure of these sites.[51] Although, the applicability of this technique on adsorbed

protein has been previously investigated by many groups, its use has been restricted to determining the labeling profile of just one type of amino acid because of problems related to differences in MS intensities that result from each of the different labeling processes.[27-30] However, the labeling profile for a single amino acid type provides very limited information for the assessment of the orientation and conformational changes of an adsorbed protein. Therefore, to provide more complete coverage for a given protein, our group recently developed methodology to combine labeling results from multiple target amino acid types applied to a single protein.[51] In our approach, we label an individual amino acid residue type for the protein in solution and after adsorption to a surface. Samples are then prepared for MS by digesting the protein using various proteolytic enzymes and then analyzed to identify which of the targeted amino acids are labeled and which are not. For this purpose, we use the Mass Spectrometry Center at Auburn University (Dr. Yonnie Wu, Director), which uses electrospray ionization quadrupole time-of-flight mass spectrometry (Q-ToF MS, Waters) for MS analysis. An overview of our AAL/MS method is provided in Fig. 4.2, with further details provided in the following paragraphs.

To minimize these complications, we chose a straightforward approach of labeling different amino acid types in a given protein, in solution and in its adsorbed state, under a common set of reactive conditions by targeting only one single type of amino acid at a time.[51-52] CD analysis is also then used to verify that the applied reactive conditions do not alter the protein's structure. Then, to overcome the inherent problem of different MS intensities occurring for each of the different labeling schemes, the

combined MS results are analyzed to identify a common peptide fragment that does not contain one of the targeted residues. The MS intensities of each sample are then normalized by the respective intensity of that untargeted fragment, thus adjusting the MS profiles to a common intensity level so that the MS results from each labeling process can be combined on an equal basis.[51]

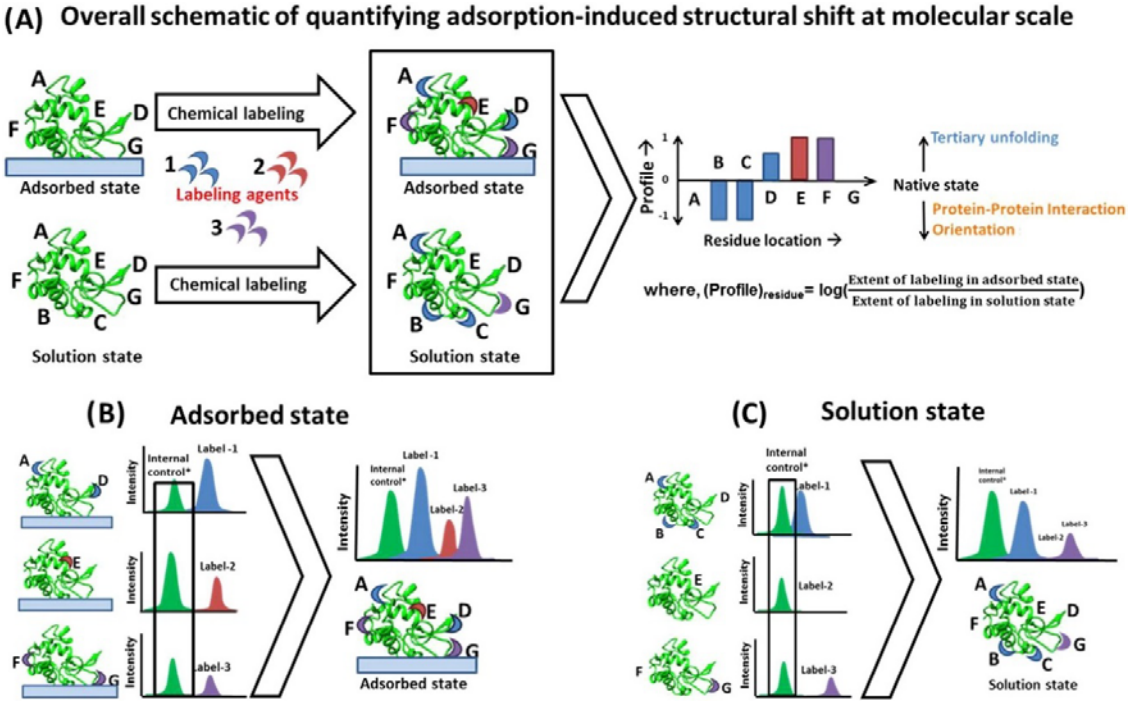

Figure 4.2. Schematic for quantifying the adsorption-induced structural shifts at a molecular level using the AAL/MS technique.[51] Panel A shows the overall scheme of the methodology while the specific approach to directly compare the labeling from multiple sites within the adsorbed and solution state are shown in panels B and C, respectively. The extent of amino acid labeling by a labeling agent is directly related to its solvent exposure. After being labeled for each individual amino acid residue type, the proteins are digested off of the surface, and the mass spectrum from each labeling process is acquired. The mass spectra from different batch labeling processes are then directly compared after normalizing them with the mass spectra of an internal control peptide fragment that does not contain one of the targeted amino acids to adjust for batch-to-batch differences in MS intensities. Subsequently, the profile of a residue relates to the extent of its solvent exposure in the adsorbed state relative to the solution state. When the protein is adsorbed from a very low solution concentration, a negative shift in an amino

acid profile can be considered to be primarily related to adsorbed orientation, while a positive shift infers areas of tertiary unfolding. When the protein is adsorbed from high solution concentration, the negative shift in an amino acid's profile can also be due to protein–protein interaction effects on the surface. Reproduced with permission from Ref. 51. Copyright 2014 Acta Materialia Inc., published by Elsevier Ltd.

4.2.3.2. Digestion of Labeled Proteins and Mass Spectrometric Analysis

The digestion of labeled proteins to peptide fragments is an essential step in identifying the sites of modification and quantifying the extent of labeling in the protein. This procedure is usually done after reducing and acetylating any disulphide bonds in the protein using iodoacetamide.[51] Currently, the two main strategies to cleave proteins in solution or in their adsorbed state are using either a sequence-grade proteolytic agent (typically, trypsin) and/or chemical agents like cyanogen bromide (CNBr), all of which are site-specific. Peptide digestion for the adsorbed protein can be done directly on the surface, or the protein can first be desorbed off the surface and then digested into peptide fragments in solution. However, since desorption of proteins from most surfaces requires the use of detergents, which can interfere with the ionization process of the peptides, digestion directly from the surface is usually used as the preferred method.

Most of the specific recognition sites within a protein that can be recognized by proteolytic agents are susceptible to alteration by the chemical labeling process, resulting in missed cleavages by the otherwise site-specific peptide digesting agents. Additionally, the specificity of cleaving agents can be altered or missed when the target site are sterically blocked by the adsorbent surface. Online resources like PeptideMass[65] are available to help with these issues, which contain a repository of different protein cleaving/digesting agents and their preferences to a recognition site within the protein.

These resources provide valuable tools for optimizing the selection of the types of amino acid labeling to be used, the number of modifications per peptide fragment (preferably 1-2 of the target residues within a peptide fragment), the type of cleaving agent, and suggested settings for the mass spectrometry scan procedures.[65]

When possible, it is best to use a cleaving agent that has multiple recognition sites as opposed to those digestive agents that are specific to limited sites, as this eliminates the usage of different cleaving agents for different batch labeling processes, and also minimizes the occurrence of peptide fragments with widely varying lengths. For example, enzymes like trypsin are specific to the carboxyl side of both Lys and Arg, (except when either one is followed by Pro) in any protein, and can be used for proteolytic cleavage when either of these amino acids are targeted.[66] Also, since each of these amino acids are relatively abundant within a protein sequence, approximately equal sized peptide fragments can be obtained following trypsin treatment. In contrast, CNBr is very specific to Met, which is very sensitive to oxidation and occurs much less frequently in proteins, resulting in higher probabilities of missed cleavages and unequally sized peptide fragments.[66] Peptide fragments that are too short result in difficulty in distinguishing the modification-induced mass increase from background noise. In contrast, the modification process on the peptides that are too long results in longer retention in the chromatographic columns and increased difficulty to be ionized by the ionization unit of the MS.[50, 66]

Once the protein is digested into peptide fragments, the sites of labeling are identified by measuring the mass-to-charge (m/z) ratios of the proteolytic fragments. The

fragments whose m/z ratios differ from the theoretical mass of the unlabeled peptide by the mass of the applied label (within 0.1% precision) are then identified using software typically provided by the MS system. The intensities obtained from mass matching are subsequently used to quantify the extent of labeling for each individual targeted amino acid.

4.2.3.3. Correlating Mass Spectra to Protein Configuration

The sample-to-sample variation in the ionization process, even within unmodified peptide digests, is typically high, and this variability is further compounded when amino acids within the peptide fragments are modified by chemical labels.[50, 66] These problems result in differences in the MS peptide intensity values from sample to sample, especially between proteins subjected to different treatments to label different targeted amino acid residue types. To overcome these problems, we have adapted a method to normalize out the differences in MS intensities between different datasets, thus enabling the MS results for multiple targeted amino acids within a given protein to be combined on an equivalent basis. This is accomplished by normalizing the MS intensities of each of the peptide fragments of a given protein sample by the MS intensity of an unlabeled peptide fragment of the protein that is present in the protein dataset for each of the different labeling processes applied. When selecting the unlabeled peptide fragment for MS-intensity normalization, care should be taken to select a fragment that is as identical as possible (i.e., same amino acid sequence) between each of the batch-labeled datasets to provide a common basis for MS intensity normalization. After this normalization procedure, we determine a labeling intensity parameter for each of the targeted amino acids. The

labeling intensity is calculated by dividing the number of times the designated targeted amino acid residue is present in the MS spectrum in its modified state divided by the total number of times the amino acid is present in all of the identified fragments (i.e., including both its labeled and unlabeled states). We then calculate a relative ratio of the extent of modification for each targeted amino acid residue of the protein by dividing its labeling intensity in its adsorbed state (I_{ads}) by its labeling intensity in its solution state (I_{soln}). Finally, we take the base-10 logarithm of this ratio to represent what we refer to as the amino acid's 'residue profile' as indicated in equation 5.

$$\text{Profile} = \log_{10}\left(\frac{I_{ads}}{I_{soln}}\right) \qquad (4.5)$$

If the value of either I_{soln} or I_{ads} is found to be less than 0.10 (which is considered to be the limit of detection), a low ceiling threshold value of 0.10 is designated for the respective intensity value instead of zero to avoid the mathematical problems of dividing by zero or taking the log(0) in equation (5).[51] Similarly, the maximum value for I_{soln} and I_{ads} is 1.0, which occurs when the targeted amino acid residue it found to be modified in every peptide fragment in the MS results.[51] Thus, the range of possible I_{ads}/I_{soln} values is from 0.1 to 10, with the values of the residue profiles for each targeted amino acid thus ranging from −1.0 to +1.0.[51] Accordingly, a given residue's profile is representative of the ensemble average change in its solvent accessibility when it is adsorbed on a given surface relative to its state in solution.

By sequentially mapping the positive and negative profile shifts of the multiple residues, the effect of adsorption on the protein structure can be analyzed. The orientation

of the protein on an adsorbent surface and the effect of neighboring proteins on the protein's structure can be inferred by hierarchically mapping the negative shift in residues' profiles. Similarly, indications of the sites in the protein's structure undergoing adsorption-induced tertiary unfolding are then determined from the locations of the amino acids with positive profile values. Accordingly, the profile values for the combined set of targeted amino acids for a given protein can be mapped onto the native-state structure of the protein for visualization, which can be represented by an appropriate tertiary structure model from the Protein Data Bank;[67] preferably using a model that is provided within the PCDDB,[58] as these share similarity in the predicted and theoretical secondary structural content of the protein.

4.2.3.4. Spectrophotometric Assay to Assess the Bioactive State of Adsorbed Proteins

There are variety of ways in which assays for assessing the bioactivity of proteins, especially enzymes, can be carried out.[68] These methods can be broadly classified as continuous or discontinuous assays. For most of our studies, spectrophotometric assays (a type of continuous assay) have been used to measure the changes in the absorbance of an incident beam following the addition of a ligand to the protein in solution or in its adsorbed state.[36-37] For this purpose, a working mass range of the protein (based on an estimate of the adsorbed amount of protein on a given surface) is determined for a fixed substrate concentration over which the change in absorbance for a designated wavelength is expected to be linear over time. The specific activity for the protein in solution is then determined under these conditions. Similarly for the adsorbed protein, the same general procedures are followed to determine the change in absorbance for the same substrate-to-

protein stoichiometry over time to determine its specific activity. Since the bioactivity of enzymes are critically affected by the environmental conditions, identical conditions (preferably those used in the adsorption and equilibration of the adsorbed protein) should be maintained while assaying the bioactivity of the protein in both its solution and adsorbed states to avoid any influence of the reaction kinetics on the bioactivity assay. The amount of adsorbed protein should be quantified before and after the bioactivity assays to ensure that the applied assay does not cause a measureable amount of the protein to be desorbed from the adsorbent surface. We typically measure this using the method of absorbance at 205 nm (A_{205}).[36, 51-52]

The bioactive state of the proteins can be expressed in either enzymatic units or in terms of its kinetic activity, whichever method suits the intended application. For example, while the specific activity of the proteins are generally used to express the enzyme's purity in a mixture, the Michaelis constant (K_M) is used as an indicator of the binding strength of the protein to its natural ligand. In our studies, we have preferred to express the bioactivity of the proteins in terms of its specific activity, as an indicator of the loss of its native-state activity rather than the K_M because of the use of highly purified one-component protein systems. Additionally, the specific activity of the native-state protein at a given purity is constant. Therefore, the relative shifts in the specificity of these highly purified enzymes following adsorption can be directly related to the adsorbed protein orientation or adsorption-induced changes in protein structure. As part of these assays, it is important to ensure that the adsorbed systems are not diffusion-limited, which can be verified when determining the working range for the study from

preliminary measurements of the reaction rate as a function of substrate concentration. The relative bioactivity (units of %) are subsequently calculated, which we represent as the ratio of the protein's specific activity in its adsorbed state relative to its specific activity in solution. The resulting relative bioactivity values can then be used as indicators of either the amount of adsorbed proteins that retain their native-state-like activity or, equivalently, the average degree of adsorption-induced loss in bioactivity.

4.3 CHAPTER SUMMARY AND CONCLUSIONS

In this paper we present an overview of the methodology that we have developed and/or adapted to quantitatively characterize the orientation, structure, and bioactivity of adsorbed protein using CD, AAL/MS, and adsorbed-state spectrophotometric assays. CD provides the ability to document the effect of adsorption on the secondary structure of a protein, while AAL/MS provides the ability to probe adsorption-induced changes in amino acid residue solvent accessibility, which can be related to adsorbed orientation, protein-protein interactions, and tertiary unfolding. The molecular-level understanding of adsorption processes that these methods provide can thus be very helpful to guide the design and development of surfaces for a broad range of applications in biotechnology and biomedical engineering. Examples include the design of substrate surfaces for biosensors to optimally preserve the bioactivity of enzymes that are either adsorbed or tethered to the surface; or, alternatively, the design of filters and decontamination systems for biodefense to purposely deactivate adsorbed protein toxins or the protein capsid of virus particles by surface-induced protein unfolding or steric blockage of bioactive sites. These methods are extremely important as well to provide the kinds of data that are

needed for the evaluation and validation of molecular modeling methods that are being developed to predict protein adsorption behavior through molecular simulation.

While our applications have primarily involved the investigation of protein adsorption on flat surfaces, these methods are certainly not limited to these type of substrates, but can be readily extended to other types of substrates as well, including micro-to-nanoscale-sized particles, fibers, and meshes. However, the presented techniques do have the limitation of not being capable of resolving the full atomistic structure of adsorbed protein, thus emphasizing the need for the further development of new methods to provide greater detail for the characterization of the effect of adsorption on the structure-bioactivity relationships of proteins on surfaces.

4.4 REFERENCES

1. Itamar, W.; Azalia, R.; Benjamin, S.; Dalia, R.; Eugenii, K. Development of novel biosensor enzyme electrodes: Glucose oxidase multilayer arrays immobilized onto self-assembled monolayers on electrodes. *Adv Mater* **1993,** *5* (12), 912-15.

2. Larsson, A.; Ekblad, T.; Andersson, O.; Liedberg, B. Photografted poly(ethylene glycol) matrix for affinity interaction studies. *Biomacromolecules* **2007,** *8* (1), 287-95.

3. Czeslik, C.; Jackler, G.; Royer, C. Driving forces for the adsorption of enzymes at the water/silica interface studied by total internal reflection fluorescence spectroscopy and optical reflectometry. *Spectroscopy* **2002,** *16* (3), 139.

4. Knowles, J. R. Enzyme catalysis: not different, just better. *Nature* **1991,** *350* (6314), 121-4.

5. Shard, A. G.; Tomlins, P. E. Biocompatibility and the efficacy of medical implants. *Regen Med* **2006,** *1* (6), 789-800.

6. Tsapikouni, T. S.; Missirlis, Y. F. Protein–material interactions: From micro-to-nano scale. *Materials Science and Engineering: B* **2008,** *152* (1-3), 2-7.

7. Kasemo, B.; Gold, J. Implant surfaces and interface processes. *Adv Dent Res* **1999,** *13*, 8-20.

8. Latkany, R.; Tsuk, A.; Sheu, M. S.; Loh, I. H.; Trinkaus-Randall, V. Plasma surface modification of artificial corneas for optimal epithelialization. *J Biomed Mater Res* **1997,** *36* (1), 29-37.

9. Wisniewski, N.; Moussy, F.; Reichert, W. M. Characterization of implantable biosensor membrane biofouling. *Fresenius J Anal Chem* **2000,** *366* (6-7), 611-21.

10. Bramwell, V. W.; Eyles, J. E.; Oya Alpar, H. Particulate delivery systems for biodefense subunit vaccines. *Adv Drug Deliv Rev* **2005,** *57* (9), 1247-65.

11. Herr, A. E. Protein Microarrays for the Detection of Biothreats. Dill, K.; Liu, R. H.; Grodzinski, P., Eds.; Springer New York, **2009**, pp 169-90.

12. Norde, W. Driving forces for protein adsorption at solid surfaces. In *Biopolymers at Interfaces*, Malmsten, M., Ed.; Marcel Dekker: New York, **1998**; Vol. 75, pp 27-54.

13. Nakanishi, K.; Sakiyama, T.; Imamura, K. On the Adsorption of Proteins on Solid Surfaces, a Common but Very Complicated Phenomenon. *J Biosci Bioeng* **2001,** *91* (3), 233-44.

14. Latour, R. A. Biomaterials: Protein-Surface Interactions. In *The Encyclopedia of Biomaterials and Bioengineering*, 2 ed.; Bowlin, G. E. W. a. G. L., Ed.; Informa Healthcare, **2008**; Vol. 1, pp 270-84.

15. Rabe, M.; Verdes, D.; Seeger, S. Understanding protein adsorption phenomena at solid surfaces. *Adv Colloid Interface Sci* **2011,** *162* (1-2), 87-106.

16. Latour, R. A. Perspectives on the simulation of protein-surface interactions using empirical force field methods. *Colloids Surf B Biointerfaces* **2014,** *124* (0), 25-37.

17. Horbett, T.; Brash John, L.; Norde, W. *Proteins at Interfaces III State of the Art*. American Chemical Society: **2012**; Vol. 1120, p 0.

18. Lynch, I.; Dawson, K. A. Protein-nanoparticle interactions. *Nano Today* **2008,** *3* (1-2), 40-47.

19. Benesch, J.; Hungerford, G.; Suhling, K.; Tregidgo, C.; Mano, J. F.; Reis, R. L. Fluorescence probe techniques to monitor protein adsorption-induced conformation changes on biodegradable polymers. *J Colloid Interface Sci* **2007,** *312* (2), 193-200.

20. Kastantin, M.; Langdon, B. B.; Schwartz, D. K. A bottom-up approach to understanding protein layer formation at solid-liquid interfaces. *Advances in Colloid and Interface Science* **2014,** *207*, 240-52.

21. Tsai, D. H.; DelRio, F. W.; Keene, A. M.; Tyner, K. M.; MacCuspie, R. I.; Cho, T. J.; Zachariah, M. R.; Hackley, V. A. Adsorption and conformation of serum albumin protein on gold nanoparticles investigated using dimensional measurements and in situ spectroscopic methods. *Langmuir* **2011,** *27* (6), 2464-77.

22. Baio, J. E.; Weidner, T.; Baugh, L.; Gamble, L. J.; Stayton, P. S.; Castner, D. G. Probing the orientation of electrostatically immobilized Protein G B1 by time-of-flight secondary ion spectrometry, sum frequency generation, and near-edge X-ray adsorption fine structure spectroscopy. *Langmuir* **2012,** *28* (4), 2107-12.

23. Apte, J. S.; Collier, G.; Latour, R. A.; Gamble, L. J.; Castner, D. G. XPS and ToF-SIMS investigation of alpha-helical and beta-strand peptide adsorption onto SAMs. *Langmuir* **2010,** *26* (5), 3423-32.

24. Weidner, T.; Castner, D. G. SFG analysis of surface bound proteins: a route towards structure determination. *PCCP* **2013,** *15* (30), 12516-24.

25. Goobes, G.; Goobes, R.; Shaw, W. J.; Gibson, J. M.; Long, J. R.; Raghunathan, V.; Schueler-Furman, O.; Popham, J. M.; Baker, D.; Campbell, C. T.; Stayton, P. S.; Drobny, G. P. The structure, dynamics, and energetics of protein adsorption-lessons learned from adsorption of statherin to hydroxyapatite. *Magn Reson Chem* **2007,** *45 Suppl 1*, S32-47.

26. Roehrich, A.; Drobny, G. Solid-state NMR studies of biomineralization peptides and proteins. *Acc Chem Res* **2013,** *46* (9), 2136-44.

27. Fears, K. P.; Sivaraman, B.; Powell, G. L.; Wu, Y.; Latour, R. A. Probing the conformation and orientation of adsorbed enzymes using side-chain modification. *Langmuir* **2009,** *25* (16), 9319-27.

28. Xu, J.; Bowden, E. F. Determination of the orientation of adsorbed cytochrome C on carboxyalkanethiol self-assembled monolayers by in situ differential modification. *J Am Chem Soc* **2006,** *128* (21), 6813-22.

29. Ovod, V.; Scott, E. A.; Flake, M. M.; Parker, S. R.; Bateman, R. J.; Elbert, D. L. Exposure of the lysine in the gamma chain dodecapeptide of human fibrinogen is not enhanced by adsorption to poly(ethylene terephthalate) as measured by biotinylation and mass spectrometry. *J Biomed Mater Res* **2012,** *100* (3), 622-31.

30. Scott, E. A.; Elbert, D. L. Mass spectrometric mapping of fibrinogen conformations at poly(ethylene terephthalate) interfaces. *Biomaterials* **2007,** *28* (27), 3904-17.

31. Yan, X.; Watson, J.; Ho, P. S.; Deinzer, M. L. Mass spectrometric approaches using electrospray ionization charge states and hydrogen-deuterium exchange for determining protein structures and their conformational changes. *Mol Cell Proteomics* **2004,** *3* (1), 10-23.

32. Roach, P.; Farrar, D.; Perry, C. C. Interpretation of protein adsorption: surface-induced conformational changes. *J Am Chem Soc* **2005,** *127* (22), 8168-73.

33. Krishnan, C. Proteins on Surfaces. In *Biopolymers at Interfaces, Second Edition*, Malmsten, M., Ed.; CRC Press, **2003**.

34. Chandra, G.; Ghosh, K. S.; Dasgupta, S.; Roy, A. Evidence of conformational changes in adsorbed lysozyme molecule on silver colloids. *Int J Biol Macromol* **2010,** *47* (3), 361-5.

35. Huang, H.; Xie, J.; Liu, X.; Yuan, L.; Wang, S.; Guo, S.; Yu, H.; Chen, H.; Zhang, Y.; Wu, X. Conformational changes of protein adsorbed on tailored flat substrates with different chemistries. *Chemphyschem* **2011,** *12* (18), 3642-6.

36. Wei, Y.; Thyparambil, A. A.; Latour, R. A. Quantification of the influence of protein-protein interactions on adsorbed protein structure and bioactivity. *Colloids and Surfaces B: Biointerfaces* **2013,** *110* (0), 363-71.

37. Fears, K. P.; Latour, R. A. Assessing the Influence of Adsorbed-State Conformation on the Bioactivity of Adsorbed Enzyme Layers. *Langmuir* **2009,** *25* (24), 13926-33.

38. Sivaraman, B.; Fears, K. P.; Latour, R. A. Investigation of the effects of surface chemistry and solution concentration on the conformation of adsorbed proteins using an improved circular dichroism method. *Langmuir* **2009,** *25* (5), 3050-6.

39. Sivaraman, B.; Latour, R. A. Delineating the roles of the GPIIb/IIIa and GP-Ib-IX-V platelet receptors in mediating platelet adhesion to adsorbed fibrinogen and albumin. *Biomaterials* **2011,** *32* (23), 5365-70.

40. Li, C. H.; Nguyen, X.; Narhi, L.; Chemmalil, L.; Towers, E.; Muzammil, S.; Gabrielson, J.; Jiang, Y. Applications of circular dichroism (CD) for structural

analysis of proteins: qualification of near- and far-UV CD for protein higher order structural analysis. *J Pharm Sci* **2011,** *100* (11), 4642-54.

41. Sreerama, N.; Woody, R. W. Estimation of protein secondary structure from circular dichroism spectra: comparison of CONTIN, SELCON, and CDSSTR methods with an expanded reference set. *Anal Biochem* **2000,** *287* (2), 252-60.

42. Kelly, S. M.; Jess, T. J.; Price, N. C. How to study proteins by circular dichroism. *Biochim Biophys Acta* **2005,** *1751* (2), 119-39.

43. Greenfield, N. J. Using circular dichroism spectra to estimate protein secondary structure. *Nat Protoc* **2006,** *1* (6), 2876-90.

44. McMillin, C. R.; Walton, A. G. A circular dichroism technique for the study of adsorbed protein structure. *J Colloid Interface Sci* **1974,** *48* (2), 345-49.

45. Arteaga, O.; Freudenthal, J.; Wang, B.; Nichols, S.; Kahr, B. Circular dichroism with multiple photoelastic modulators. *Chimica Oggi* **2012,** *30* (5), 6-9.

46. Kelly, S. M.; Price, N. C. The use of circular dichroism in the investigation of protein structure and function. *Curr Protein Pept Sci* **2000,** *1* (4), 349-84.

47. Engel, M. F.; Visser, A. J.; van Mierlo, C. P. Conformation and orientation of a protein folding intermediate trapped by adsorption. *Proc Natl Acad Sci USA* **2004,** *101* (31), 11316-21.

48. Ronda, L.; Bruno, S.; Viappiani, C.; Abbruzzetti, S.; Mozzarelli, A.; Lowe, K. C.; Bettati, S. Circular dichroism spectroscopy of tertiary and quaternary conformations of human hemoglobin entrapped in wet silica gels. *Protein Sci* **2006,** *15* (8), 1961-7.

49. Devineau, S.; Zanotti, J. M.; Loupiac, C.; Zargarian, L.; Neiers, F.; Pin, S.; Renault, J. P. Myoglobin on silica: a case study of the impact of adsorption on protein structure and dynamics. *Langmuir* **2013,** *29* (44), 13465-72.

50. Mendoza, V. L.; Vachet, R. W. Probing protein structure by amino acid-specific covalent labeling and mass spectrometry. *Mass Spectrom Rev* **2009,** *28* (5), 785-815.

51. Thyparambil, A. A.; Wei, Y.; Wu, Y.; Latour, R. A. Determination of orientation and adsorption-induced changes in the tertiary structure of proteins on material surfaces by chemical modification and peptide mapping. *Acta Biomaterialia* **2014,** *10* (6), 2404-14.

52. Wei, Y.; Thyparambil, A. A.; Wu, Y.; Latour, R. A. Adsorption-induced changes in ribonuclease A structure and enzymatic activity on solid surfaces. *Langmuir* **2014,** *30* (49), 14849-58.

53. Sivaraman, B.; Latour, R. A. The relationship between platelet adhesion on surfaces and the structure versus the amount of adsorbed fibrinogen. *Biomaterials* **2010,** *31* (5), 832-9.

54. Ladner, D. A.; Steele, M.; Weir, A.; Hristovski, K.; Westerhoff, P. Functionalized nanoparticle interactions with polymeric membranes. *J Hazard Mater* **2012,** *211-212*, 288-95.

55. Thyparambil, A. A.; Wei, Y.; Latour, R. A. Determination of Peptide–Surface Adsorption Free Energy for Material Surfaces Not Conducive to SPR or QCM using AFM. *Langmuir* **2012,** *28* (13), 5687-94.

56. DiNitto, J. M.; Kenney, J. M. Noise characterization in circular dichroism spectroscopy. *Appl Spectrosc* **2012,** *66* (2), 180-7.

57. Liu, P. F.; Avramova, L. V.; Park, C. Revisiting absorbance at 230nm as a protein unfolding probe. *Anal Biochem* **2009,** *389* (2), 165-70.

58. Whitmore, L.; Woollett, B.; Miles, A. J.; Klose, D. P.; Janes, R. W.; Wallace, B. A. PCDDB: the Protein Circular Dichroism Data Bank, a repository for circular dichroism spectral and metadata. *Nucleic Acids Res* **2011,** *39* (Database issue), D480-6.

59. Wallace, B. A.; Lees, J. G.; Orry, A. J.; Lobley, A.; Janes, R. W. Analyses of circular dichroism spectra of membrane proteins. *Protein Sci* **2003,** *12* (4), 875-84.

60. Abdul-Gader, A.; Miles, A. J.; Wallace, B. A. A reference dataset for the analyses of membrane protein secondary structures and transmembrane residues using circular dichroism spectroscopy. *Bioinformatics* **2011,** *27* (12), 1630-36.

61. Whitmore, L.; Wallace, B. A. DICHROWEB, an online server for protein secondary structure analyses from circular dichroism spectroscopic data. *Nucleic Acids Res* **2004,** *32* (Web Server issue), W668-73.

62. Whitmore, L.; Wallace, B. A. Protein secondary structure analyses from circular dichroism spectroscopy: methods and reference databases. *Biopolymers* **2008,** *89* (5), 392-400.

63. Lees, J. G.; Miles, A. J.; Wien, F.; Wallace, B. A. A reference database for circular dichroism spectroscopy covering fold and secondary structure space. *Bioinformatics* **2006,** *22* (16), 1955-62.

64. Wei, Y.; Thyparambil, A. A.; Latour, R. A. Protein helical structure determination using CD spectroscopy for solutions with strong background absorbance from 190 to 230nm. *Biochim Biophys Acta* **2014,** *1844* (12), 2331-37.

65. Wilkins, M. R.; Lindskog, I.; Gasteiger, E.; Bairoch, A.; Sanchez, J. C.; Hochstrasser, D. F.; Appel, R. D. Detailed peptide characterization using

PEPTIDEMASS--a World-Wide-Web-accessible tool. *Electrophoresis* **1997,** *18* (3-4), 403-8.

66. Duncan, M. W.; Aebersold, R.; Caprioli, R. M. The pros and cons of peptide-centric proteomics. *Nat Biotechnol* **2010,** *28* (7), 659-64.

67. Berman, H. M.; Westbrook, J.; Feng, Z.; Gilliland, G.; Bhat, T. N.; Weissig, H.; Shindyalov, I. N.; Bourne, P. E. The Protein Data Bank. *Nucleic Acids Res* **2000,** *28*, 235-42.

68. Lundblad, R. L. The Chemical Cleavage of Peptide Bonds. In *Chemical Reagents for Protein Modification, Third Edition*; CRC Press, **2004**.

CHAPTER FIVE

QUANTIFICATION OF THE INFLUENCE OF PROTEIN-PROTEIN INTERACTIONS ON ADSORBED PROTEIN STRUCTURE AND BIOACTIVITY

Based on the Published Article: Wei Y., Thyparambil A.A., and Latour R.A., Quantification of the influence of protein-protein interactions on adsorbed protein structure and bioactivity, Colloids and Surfaces B: Biointerfaces, 110(1): 363-371 (2013);

5.1 . INTRODUCTION

The interaction of proteins with material surfaces is of primary importance in many areas of biotechnology and biomedical engineering, including biosensors, enzyme based technologies, tissue engineering and regenerative medicine, implants, and biodefense. The key element in all of these applications is the bioactive state of the protein, which can be strongly influenced by adsorption-induced changes in a protein's structure on an adsorbent surface. While much work on this topic has already been reported, a fundamental understanding on the role of different material surfaces on the conformational state, packing arrangement, and bioactivity of adsorbed proteins is still not well understood. These limitations are partly due to the complexities introduced by protein-protein interactions on the adsorption responses of proteins with various levels of internal protein stability in combination with protein-surface interactions.[1-3]

As previously described by Norde[4-6] and others,[7-11] when a material is exposed to a protein-containing solution, proteins rapidly adsorb to its surfaces. Once adsorbed, forces between the protein, surface, and solvent (e.g., electrostatic, hydrogen bonding,

hydrophobic, and/or dispersion interactions) can alter the thermodynamic state of the system leading to spontaneous shifts in an adsorbed protein's structure from its native state and subsequent unfolding and spreading out on the surface. The amount that an adsorbed protein will unfold and spread out on a surface is largely determined by the strength of the protein-surface interactions relative to the internal stability of the protein. The extent to which unfolding will occur is also influenced by whether or not the adjacent areas of the surface are occupied by other adsorbed proteins and subsequent interactions with such neighboring proteins; which, when present, result in protein-protein interactions that tend to sterically block further unfolding and spreading. The degree to which protein-protein interaction (PPI) effects limit the unfolding or spreading of a protein on a surface can thus be simply controlled by adjusting the concentration of the protein in solution, which influences the rate that neighboring sites are filled.

At surface saturation, the conformational state of the final resulting adsorbed layer of protein will thus be dependent on the combined influences of internal protein stability, protein-surface interaction, and PPI effects. PPI effects are the least understood of these types of interactions and can be generally expected to be proportional to the amount of the protein adsorbed on the surface (i.e., surface coverage of the protein on the surface).[2].Based on this assumption, the influence of PPI effects on the structure of adsorbed protein for a given type of surface should be able to be assessed by adsorbing the protein to the surface under conditions that will provide different degrees of surface coverage, which can be controlled for a given surface by varying the protein solution concentration from which the protein is adsorbed, with higher solution concentrations

generally resulting in higher surface coverage at surface saturation.[12] The objective of this research was therefore to study the influence of PPI effects on the structural changes and corresponding bioactivity of two different type of adsorbed protein with different internal stability on three different surface chemistries, each with the potential to interact with proteins through a distinctly different molecular mechanism.

The experimental approach that we designed to address these issues was to first adsorb the protein from varying solution concentrations for a period of time previously determined to be sufficient to saturate the surface (adsorption time) in order to vary the initial surface coverage of protein on the surface and the subsequent degree of PPI effects occurring within the adsorbed layer of protein. We then rinsed the surfaces with protein-free buffer to remove weakly adsorbed proteins, replaced the protein solution with protein-free buffer solution to remove the ability of new proteins to adsorb to the surface, and allowed the adsorbed protein layers to equilibrate under protein-free buffer conditions while monitoring their surface coverage and conformational structure by measuring the shift in absorbance and circular dichroism (CD), respectively, until they stabilized to an apparent equilibrated state (equilibration time). Following equilibration, bioactivity studies were then finally conducted to quantify the influence of the applied adsorption processes on the bioactive state of the adsorbed protein. Under these experimental conditions, differences in the optical characteristics of the adsorbed protein layers with different surface coverage on a given surface can be considered to occur under constant internal protein stability and protein-surface interaction conditions, thus isolating the influence of PPI effects on the structural and bioactive response of the adsorbed protein.

5.2 EXPERIMENTAL SETUP AND METHODLOGY

5.2.1 Protein and Material Surfaces

Hen egg white lysozyme (HEWL) and bovine pancreatic ribonuclease A (RNase A) were selected for use in this study as two of the most well characterized protein model systems.[12-19] Being small (MW ~ 14 kDa) relatively 'hard' protein with 4 disulfide bonds stabilizing its structure, both proteins are generally considered to be of relatively high internal stability.[2, 18]

The selected material surfaces included fused silica glass (glass), high density polyethylene (HDPE), and poly(methyl methacrylate) (PMMA). These three materials were chosen to represent some of the most commonly used materials in biotechnological and biomedical engineering applications.[19-25] They were also selected because their chemical compositions provide them with the potential to interact with proteins by three distinctly different mechanisms.

Being composed of a silicon-oxygen network with a high density of hydroxyl groups on the surface, the glass surface has strong potential to form both accepting and donating-type hydrogen bonds (H-bonds) with hydrogen bondable groups of a protein as well as ionic groups for electrostatic interactions. Because H-bonds stabilize the secondary structures of a protein (as well as playing a role in tertiary structural stability), this type of surface has the potential to substantially destabilize a protein's secondary and tertiary structures by competing with H-bonds that serve to stabilize a protein's internal structure.

In contrast to glass, HDPE is entirely composed of saturated nonpolar alkane chains, thus lacking the ability to interact with a protein via either hydrogen bonding or electrostatic effects, while having the potential to exhibit strong hydrophobic interactions with a protein's hydrophobic amino acid residues. Given the fact that the tertiary structure of a protein is generally stabilized by hydrophobic interactions, HDPE thus has the potential to strongly induce tertiary unfolding of a protein, which in turn can be expected to potentially destabilize the native secondary structures as well.

Our third surface, PMMA, can be considered to have much lower potential to interact with the secondary structure of proteins compared to the glass surfaces since it has a much lower density of H-bondable groups, with these representing only hydrogen-bond-accepting groups but not H-bond-donating groups. In addition, because the H-bondable groups that are present in PMMA subsequently reduce the hydrophobicity of the surface, it can be expected to exhibit weaker hydrophobic interactions with proteins compared with HDPE. Therefore, theoretically, PMMA should exhibit lower protein-surface interaction effects than either glass or HDPE, with the greater protein-surface interaction effects from glass and HDPE occurring through different mechanisms.

5.2.2 Material Surface Preparation and Characterization

5.2.2.1. Preparation of Material Surfaces

Custom cut glass slides (0.375″ × 1.625″ × 0.0625″, Chemglass Life Sciences) were procured to fit our custom designed CD cuvettes[12]. HDPE and PMMA surfaces were spin–coated onto glass slides from dodecalin (0.5% (w/w) at 1500 rpm for 60s) and chloroform solutions (1.5% (w/w) at 1000 rpm for 60s), respectively. All chemicals

including the HDPE (M_w =125,000, Sigma 181900) and PMMA (M_w=350,000, Sigma 445746) and the solvents such as dodecalin (Sigma 294772) and chloroform (EMD Chemicals, CX 1054) were used as supplied by the manufacturer. Glass substrates used for adsorption studies were cleaned by sonicating in "piranha" (7:3 (v/v) H_2SO_4 (EMD Chemicals, SX 1244)/H_2O_2 (Ricca Chemicals, 3821) and basic solution (1:1:3 (v/v/v) NH_4OH (BDH Chemicals, BDH3016)/ H_2O_2/ H_2O) at 50°C for 1 minute. Prior to adsorption studies, all the substrates were rinsed in absolute ethanol, followed by nano-pure water and then dried under a steady stream of nitrogen gas.

5.2.2.2. Characterization of Material Surfaces.

Surface characterization was performed to determine the static air–water contact angle, atomic composition, film thickness, and surface roughness of the substrates used. For all the surfaces, the static air–water contact angle values were analyzed using a contact–angle goniometer (Kruss, DSA-20E). Similarly, the atomic compositions were verified via X–ray photoelectron spectroscopy (NESCA/BIO, University of Washington) and the average surface roughness was analyzed using atomic force microscopy (Asylum Research, MFP–3D) over an area of 5μm×5μm. The thicknesses of the polymer films were characterized using variable angle spectroscopic ellipsometry (Sopra Inc., GES–5).

5.2.3. Protein Adsorption and Equilibration

5.2.3.1 Protein Adsorption

Stock solutions of 5.0 mg/ml HEWL (Sigma, L6876) and 5.0 mg/ml RNase-A (Sigma, L6513) were prepared in 10 mM potassium phosphate buffer (PPB) and filtered to remove any insoluble aggregates. The final protein concentrations were verified via biuret

method (Thermo scientific, 23225) or absorbance at 205 nm (A_{205}).[14, 26] PPB was prepared by mixing appropriate amounts of monobasic potassium phosphate (Sigma, P8708) and dibasic potassium phosphate (Sigma, P8508) to a final solution pH of 7.4.

All adsorbent surfaces were first stored in PPB at room temperature and then the required amount of protein stock solution was pipetted into the buffer to make up to the desired bulk solution concentration, with care taken to ensure that the pipet tip was below the air−water interface during injection to avoid denaturation of the protein at this interface. As previously mentioned, the effects of PPI on the adsorption responses of protein on glass, PMMA and HDPE surfaces were then varied by controlling the adsorption-desorption kinetic parameters, namely (i) the protein concentration in solution from which the protein was adsorbed, (ii) the time that the surfaces were exposed to the protein solution, and (iii) the equilibration time following adsorption with the adsorbed protein layers immersed in protein-free buffer solution.

5.2.3.2. Bulk Concentrations of Protein for Adsorption Studies

Protein adsorption was conducted at room temperature from eight different solution concentrations of HEWL (0.03 mg/mL, 0.05 mg/mL, 0.10 mg/mL, 0.20 mg/mL, 0.40 mg/mL, 0.60 mg/mL, 0.80 mg/mL, and 1.00 mg/mL) and RNase A (0.03 mg/mL, 0.05 mg/mL, 0.10 mg/mL, 0.20 mg/mL, 0.40 mg/mL, 0.80 mg/mL, 1.00 mg/mL, and 1.60 mg/mL).

5.2.3.3. Adsorption Time in Protein Solution

For the protein solution concentrations used in this study, an adsorption time of 2 h was determined to be sufficient to saturate the surface for each material and protein

solution concentration, which is consistent with the previous reports on the adsorption time required by HEWL and RNase A to saturate an adsorbent surface for a wide range of solution concentrations.[13, 15]

5.2.3.4. Equilibration Time in Pure Buffer Solution

Following the adsorption process in the respective protein solution concentrations, the material surfaces were subsequently washed under a steady gentle flow (12 mL/min) of protein-free buffer for five minutes in order to remove the bulk protein solution and to desorb loosely adherent proteins. The surfaces with the adsorbed layer of protein were then immersed in protein-free buffer solutions for 15 h to allow the adsorbed protein layers to structurally equilibrate.

5.2.4. Analysis of Adsorbed Proteins Using CD Spectroscopy

The structure of protein in solution, the amount of protein adsorbed on each surface, and the subsequent adsorption-induced conformational changes on these proteins on each material surface were determined using CD spectropolarimetry following our standardized methods as covered in Chapter 4.[12] The CD spectra (consisting of the ellipticity and absorbance values over wavelengths ranging from 190 nm to 300 nm) were obtained at room temperature using a Jasco J-810 spectropolarimeter. The solution structure of the proteins was determined in quartz cuvettes (Starna Cells) while the structure of the adsorbed proteins was determined using a custom-designed cuvette, which has been previously described.[12] The CD instrument as well as the path length of the cuvettes used in this study were calibrated to be within the recommend standards,[14] prior to these analyses (see section B.2 in the appendix).

5.2.4.1. Determination of Molar Extinction Coefficient of Protein at 205 nm and Structure of Protein in Solution

The molar extinction coefficient of the protein (ε_{205}) in solution at 205 nm was determined by recording the background corrected absorbance at this wavelength (A_{205}) for five different solution concentrations (0.20 mg/ml, 0.40 mg/ml, 0.60 mg/ml, 0.80 mg/ml and 1.00 mg/ml) in 0.10 mm pathlength (L) demountable quartz cuvettes (Starna). The solution concentrations (C_{soln}) were first verified using the biuret method (Thermo scientific, 23225),[26] following which the molar extinction coefficient of protein in solution at 205 nm was obtained from the slope of the absorbance (A_{205}) vs (C_{soln}*L) plot.

The CD spectrum for protein in solution was then measured in the same 0.10 mm pathlength demountable quartz cuvette (Starna) at 1.00 mg/ml solution concentration using parameters and techniques previously described.[12] Briefly, the background-corrected solution CD spectra were recorded from 190 nm to 300 nm at a scan rate of 50 nm/min with a response time of 0.25 s using six accumulations, with the CD spectra then analyzed using the methods described in section 5.2.4.3 below.

5.2.4.2. Determination of the Surface Coverage of Adsorbed Protein (Q_{ads}) and Adsorbed Protein Structure

The slides supporting the material surfaces with the adsorbed protein layers were transferred into custom-designed cuvettes and the CD spectra were recorded before and after protein adsorption. Throughout the study, slides remained hydrate in buffer solution. Following our established methods,[12] the absorbance is dependent only on the total mass

of protein per unit area that the polarized light beam passes through. The surface coverage of protein (Q_{ads}) was estimated by the following equation:

$$Q_{ads} = \frac{A_{205}}{\varepsilon_{205}} \qquad (5.1)$$

where A_{205} is the background-corrected absorbance at 205 nm, and ε_{205} is the molar extinction coefficient that was determined for the protein solution at a wavelength of 205 nm in section 5.2.4.1.

5.2.4.3. Quantification of Secondary Structure in Solution and Adsorbed State of Protein

The background corrected CD signals that were obtained as described above in sections 5.2.4.1 and 5.2.4.2 were converted to molar ellipticity (θ_{mol}) using equations 5.2 and 5.3, respectively:

$$\theta_{mol} = \frac{\theta_{raw} * M}{10000 * C_{soln} * L} \qquad (5.2)$$

$$\theta_{mol} = \frac{\theta_{raw} * M}{10000 * Q_{ads}} \qquad (5.3)$$

where θ_{raw} is the background corrected raw CD signal, L is the path length of the cuvette (cm), C_{soln} is the solution concentration of the protein (g/mL), Q_{ads} is the surface coverage of adsorbed protein (g/cm^2), and M is the mean residue molecular weight of 112 g/mol.

Once the CD signals were converted to their respective molar ellipticity units, the spectra were then deconvoluted to predict secondary structure using the CONTIN/LL,

SELCON3, and CDSStr methods provided with the CDPro package using the SP43 and SP48 protein reference datasets.[16] Each of the deconvoluted spectra was then assessed for quality by analyzing the R-fit using non-linear regression.[16] The final secondary structures represent the averaged structures obtained from all of the reliable outputs (R-fit < 10) resulting from the above described data analysis methods, which are consistent with the data analysis recommendations for CD.[14, 17] For the purposes of this study, we were primarily interested in the percent helical structure of HEWL and RNase A as a sensitive indicator of adsorption-induced changes in the protein's structure.

5.2.4. Estimation of Internal Stability Two Unrelated Proteins Using CD

The thermodynamic stability of the native state of a protein is reflected by a change in the standard-state Gibbs free energy, $\Delta G°$, of unfolding and is usually estimated by the chemical and thermal denaturation of these proteins.[27] In the current study, thermal-induced denaturation of the proteins was done using an external water bath (Neslab, RTE-111) over a temperature range from 5 to 90°C. The T_m of a protein can be determined experimentally by applying a temperature ramp to the protein in solution and identifying the temperature at which the folded fraction of a protein at equilibrium is equal to the unfolded fraction (i.e., folded and unfolded fractions corresponding to 0.5).Temperature control within the CD instrument was done using the Peltier temperature control device that is integrated within our instrument. The data was acquired at a bandwidth of 0.5 nm, response time of 4 s over the heating rate of 0.5°C/min and an averaged over 6 times. Data was collected after every 1°C rise in temperature over 220 nm to 300 nm. Similarly, chemical denaturation of the proteins was

done using 0-9 M of urea (Fisher Scientific, U15500) and 0-6 M guanidium hydrochloride (GdmHCl, Sigma, G3272) at 25°C.

In either type of denaturation, the reversibility of the unfolding process was verified. Subsequently, the change in molar ellipticity at 222 nm was measured for each denaturant concentration. Assuming a two-state transition of the protein, the fraction of denatured protein (f_d) at each denaturant concentration was obtained by equation 5.4

$$f_d = \frac{Y_{obs} - Y_n}{Y_d - Y_n} \qquad (5.4)$$

Where Y_{obs} is the observed physical quantity (absorbance or molar ellipticity), Y_n and Y_d are values for the native and fully denatured proteins at each of the denaturant concentrations, respectively, and were obtained from the least square fit of the sigmoid shaped plot. Y_n is obtained from the least square fit of the curve prior to transition, and Y_d was obtained from the least square fit of the curve post transition.[27-28]

Subsequently, f_d is plotted as a function of the denaturant concentration, and the equilibrium constant, K, and standard-state free energy change, $\Delta G°$, were estimated using equations 5.5 and 5.6 respectively.

$$K = \frac{f_d}{1 - f_d} = \frac{Y_{obs} - Y_n}{Y_d - Y_{obs}} \qquad (5.5) \quad \text{and,}$$

$$\Delta G^\circ = -RT \ln(K) \qquad (5.6)$$

where R is the ideal gas constant (8.314 $Jmol^{-1}K^{-1}$), T is the absolute temperature. f_d is fraction denatured. If the protein unfolding was reversible at lower dilutions of the

denaturants, the conformational stability of protein in the absence of denaturant, $\Delta G°$, can be obtained by linearly extrapolating to the Y-intercept in the plot of ΔG against denaturant concentration using the following equation 5.7 and equation 5.8.[27]

$$\Delta G = \Delta G^0 - m[denaturant] \qquad (5.7)$$

$$\Delta G^0 = m[denaturant]_{1/2} \qquad (5.8)$$

where m is a measure of the dependence of ΔG on denaturant concentration, and $\Delta G°$ is the standard-state change in free energy, with the denaturant concentration at the midpoint of the unfolding curve given by $[denaturant]_{1/2}$.

5.2.5 Bioactivity Assays of Solution-State and Adsorbed-State of HEWL

We used a turbidometric assay to measure the enzymatic activity of HEWL, which was carried out using a custom-designed cuvette that was previously described (see Chapter 4).[12, 29] Bioactive substrates were prepared in PPB to a final concentration of 60 mg/liter *Micrococcus lysodeikticus* (Sigma M3770) and the assays to determine the enzymatic bioactivity were done at pH 7.4 for a time period of 10 min at 450 nm. Prior to performing the assay, samples were incubated with the bioactive substrate at room temperature for 1 min before the decreases in absorbance at 450 nm (ΔA_{450}) were recorded.

Typically, the solution state assays are directly done on proteins in solutions. However, as the kinetics of proteins on immobilized and adsorbed proteins on surfaces are influenced by the diffusion gradients, adsorption of ligands to the surface, as well as the adsorbed configuration of protein,[30-31] it was of utmost importance in our studies to

minimize the influence of factors other than the structural shifts on the activity profile of the adsorbed proteins. For this purpose, the solution-state activity assays were determined over a fixed time interval by estimating the activity rate of HEWL when injected immediately into the custom designed cuvette containing bare substrates (i.e for glass, HDPE, and PMMA) without any adsorbed protein but saturated with a fixed concentration of target ligand. For the bioactive substrate concentration and the experimental conditions that were used in our current study, the activity profile of the native enzyme was found to be linear over the protein mass range of 0.1 µg – 30 µg, suggesting that the system was not diffusion-limited (see section B.3 in the appendix B). The specific activities of the proteins in solution were subsequently calculated by normalizing ΔA_{450} to the amount of protein in solution, with the values found to be constant over the working mass range

Due to concerns that the bioactivity assay may have some unappreciated influence on the layers of adsorbed protein, bioactivity assays were only performed at the end of the experiment for the HEWL layers after the 15 h equilibration period under protein-free buffer conditions. The bioactivities of the adsorbed proteins were then assayed after the completion of the CD analyses. The amount of adsorbed protein was quantified by the layer's absorbance at 205 nm (A_{205}), both before and after the bioactivity assays were performed to ensure that the bioactivity assays did not cause a measureable amount of the protein to be desorbed from the adsorbent surface. The specific activities of the adsorbed proteins were then calculated by normalizing the ΔA_{450} absorbance values by the total amount of protein adsorbed on the surface (Q_{ads}* area of adsorbent surface).

The relative bioactivities (%) of the adsorbed proteins were then determined by normalizing the measured adsorbed-state specific activity to the protein's solution-state specific activity, thus providing a measure for adsorption-induced change in HEWL activity.

5.2.6 Bioactivity Assays of Solution-State and Adsorbed-State of RNase A

Similar to methods that were applied to HEWL activity assays, a spectrophotometric assay was also used to measure the enzymatic activity of RNase A in a CD cuvette.[32] Briefly, ribonucleic acid, which is the substrate for RNase A, was prepared in PPB to a final concentration of 20 mg/mL (Baker's yeast, Sigma R6750) and exposed to RNase A in both solution and following RNase A adsorption. An initial calibration plot for solution-state bioactivity was obtained for a working range of 0.1 µg – 30 µg of RNAse A (based on the equivalently adsorbed amount of protein on different surfaces) by monitoring the absorbance at 300 nm (ΔA_{300}) at pH 7.4. A time period of 10 min was found to be sufficient for complete catalysis. The amount of adsorbed protein was quantified by the layer's absorbance at 205 nm (A_{205}), both before and after the bioactivity assays were performed to ensure that the bioactivity assay did not cause a measureable amount of the protein to be desorbed from the adsorbent surface.

The relative enzymatic activities (%) of adsorbed RNase A enzymes were determined by normalizing the measured adsorbed-state specific activity by the solution-state specific activity, thus providing a measure adsorption-induced changes in RNase A activity.

5.2.7. Statistical Analysis

The results from this study are presented as the mean values ± 95% confidence intervals (C.I.). The statistical significance of differences between mean values for different samples/conditions was evaluated using either the Student's t-test or a nonparametric sign test,[33-34] with values of $p < 0.05$ being considered as statistically significant.

5.3. RESULTS AND DISCUSSION

5.3.1. Surface Characterization

Table 5.1 presents the results analyzed by the characterization techniques applied to the surfaces used in this study. All of the measured values reported in Table 5.1 fall within the expected range.[20-24]

Table 5.1. Surface characterization: Atomic composition, static contact angle, film thickness, and surface roughness analyses for each surface. (Mean ± 95% C.I., N = 3.)

Surface	C (%)	S (%)	N (%)	O (%)	Roughness (nm)	Contact Angle (°)	Thickness (nm)
GLASS**	25.4 (2.3)	*	0.6 (0.5)	49.2 (2.2)	< 10.0	23 (4)	NA
HDPE	96.3 (2.7)	*	*	3.4 (2.6)	< 8.0	97 (5)	100 (10)
PMMA	75.6 (1.3)	*	*	23.7 (1.4)	< 1.5	63 (3)	90 (10)

*indicates a negligible value; ** Fused glass slide also contains Zn (<1%), Al (<1%) and Si (22.0±1.0%). The presence of extra carbon composition is believed to be originating from surface contamination due to the exposure of samples to air after the cleaning procedure. These are the typical adventitious and unavoidable hydrocarbon impurities that adsorb spontaneously from ambient air onto the GLASS surfaces,[22] NA refers to the thickness of the GLASS slides described in 5.2.2.1.

5.3.2. Internal Stabilities of the Native Structures of HEWL and RNase-A

As presented above, the adsorption behavior of two proteins, HEWL and RNase A, were compared in this current study. Both these proteins are small and similar in size. Moreover, both these proteins catalyze their respective substrate in similar fashion.

However, the sequence compositions of these proteins are very different with RNase A being composed of more than 50% polar residues (57%) and HEWL being composed of more than 50% non-polar residues (53%), thus resulting in differences in their internal structural stability. An understanding of the difference in stability of these proteins, as represented by the standard-state free energy of protein unfolding ($\Delta G°$) at room temperature, provides insight into their adsorption behavior in terms of their inherent resistance to adsorption-induced unfolding.

Generally, when comparing two dissimilar proteins, the stability rankings are usually presented in terms of T_m, which is often substantially higher than room temperature.[27, 35-40] Conceptually, proteins with higher T_m would be more stable at room temperature and thus have lesser tendency to unfold at room temperatures as opposed to proteins with lower T_m. But as the thermal stability of a protein is a function of enthalpy, entropy and heat capacity changes, it is not necessarily true that proteins with higher T_m are more stable at room temperature.[27, 35, 37, 41] For example, two proteins with the same T_m can have very different stabilities at room temperature depending on the magnitude of heat capacity changes. Heat capacity changes are in turn proportional to the degree of solvent exposure of the hydrophobic core within the protein upon denaturation.[27, 38] The more hydrophobic the core, the lower the stability at lower temperatures despite higher T_m.[38, 41] As a result, $\Delta G°$ for unfolding at room temperature is a more reliable estimate of a protein's internal stability.[38]

But as shown in Fig. 5.1a, temperature-induced denaturation for many proteins like HEWL and RNase A represents an irreversible process, which makes estimation of

$\Delta G°$ from these plots error prone. As a result, the estimation of $\Delta G°$ for proteins in PPB at 25°C were obtained from the denaturation curves with chemical denaturants (because of the reversibility in structural transitions at lower denaturant concentrations (Fig 5.1 b and Fig 5.1 c) and not from the thermal unfolding curves, under the empirical assumption of a 2-state co-operative transition between the folded and unfolded states. For this purpose, the internal stability of HEWL and RNase A was characterized by estimating $\Delta G°$ at 298 K from different chemical denaturants, and T_m from thermal unfolding. The unfolding transitions in these two unrelated proteins were obtained by monitoring the change in CD ellipticity at 222 nm when exposed to thermal and chemical denaturation. Table 5.2 lists these parameters for HEWL and RNase A in PPB (pH 7.4), determined using our CD technique.

Table 5.2 Thermodynamic estimation of the parameters to characterize the internal stability of HEWL and RNase-A determined using the CD technique. $\Delta G°$ values for the proteins in PPB were obtained at 25°C under the assumption of a two-state unfolding process.[27-28, 36, 41]

Proteins	**T_m (K)**	**Urea**			**GdmCl**		
		m (kcal/mol/M)	$[urea]_{1/2}$ (M)	**ΔG^0** at 298 K (kcal/mol)	m (kcal/mol/M)	$[GdmCl]_{1/2}$ (M)	**ΔG^0** at 298 K (kcal/mol)
HEWL	347 (2)	NA	NA	NA	1.88	3.4 (0.3)	8.9
RNase-A	327 (2)	1.89	6.6 (0.2)	7.4	2.50	2.5 (0.3)	7.3

*NA indicates indeterminate value due to the incomplete unfolding of HEWL at pH 7.4 even at 9M urea.

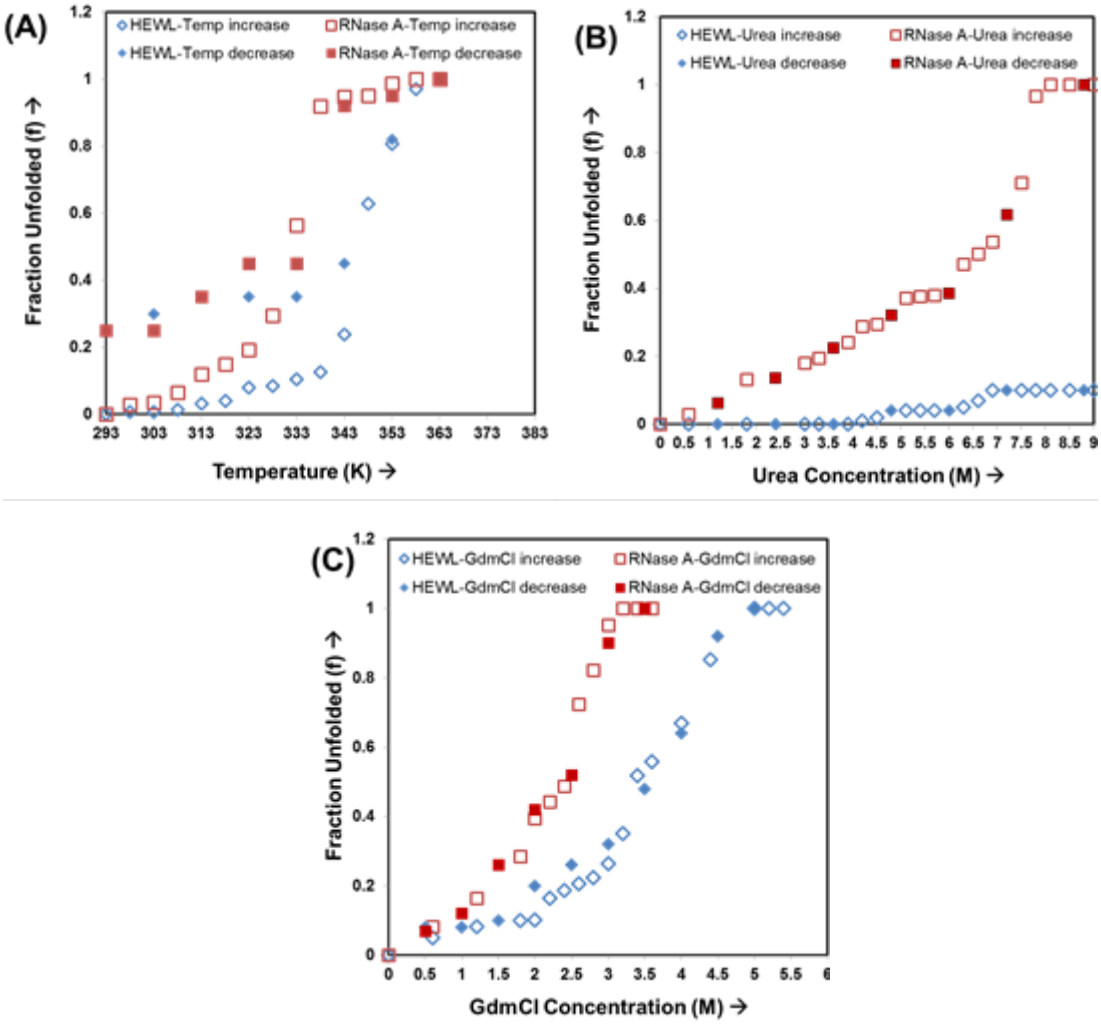

Figure 5.1: Effect of (a) thermal treatment, (b) urea treatment and (c) GdmCl treatments on the unfolded fractions of HEWL and RNase A. The unfolding transition in these protein were estimated by monitoring the change in ellipticity at 222 nm. The open red and blue circles represents the increasing influence of chemical and thermal treatments on the unfolded fractions of HEWL and RNase A respectively. Similarly, the colored red and blue circles represent the decreasing influence of chemical and thermal treatments on the unfolded fractions of HEWL and RNase A respectively. Chemical treatments were done at 25°C. Fractional unfolding corresponding to 0 represents fully folded and 1 represents complete unfolding.

The thermodynamic estimates obtained in Fig 5.2 are in general agreement with the literature estimates.[27, 36-40, 42] The T_m values for HEWL and RNase A in PPB were 347 K (≈ 74°C) and 327 K (≈ 54°C) respectively, which indicates that HEWL was

thermally more stable than RNase A. Similarly, the $\Delta G°$ estimates for HEWL and RNase A at room temperatures were obtained for each individual chemical treatment, except for HEWL treated with urea as these treatments resulted in incomplete unfolding of the protein. But considering that the $\Delta G°$ estimates are expected to be similar for a protein system irrespective of the type of chemical treatment, and the unfolding tendency of HEWL in GdmCl was reversible, it was safely concluded from these estimates that HEWL is more stable than RNase-A in PPB at room temperatures equivalent to 25°C.

5.3.3. Surface Coverage of Adsorbed Protein and Protein-Protein Effects

5.3.3.a Surface coverage of HEWL on different surfaces

Fig. 5.2 presents a plot of the surface coverage of adsorbed HEWL on each of our three surfaces for each solution concentration as a function of exposure time. From these plots, it is evident that the initial surface coverage at 2 h and final surface coverages post 15 h exposure to protein-free buffer solution on each of the surfaces were significantly different, suggesting that varying the solution concentration and equilibration time in buffer provided an effective method to vary the surface coverage of the adsorbed protein on the surface.[33-34]

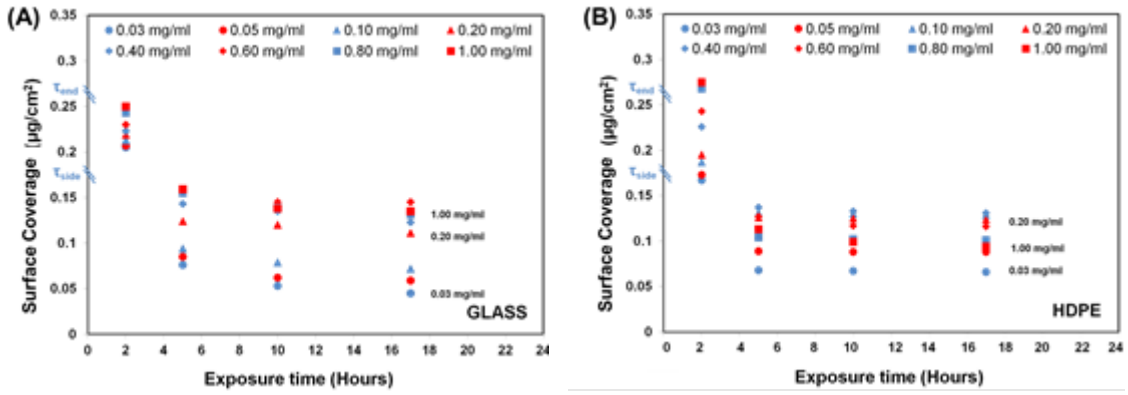

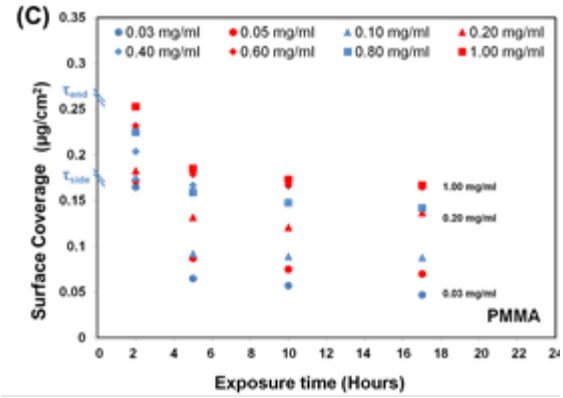

Figure 5.2: Effect of varying exposure time on the surface coverage of HEWL adsorbed on (A) glass, (B) HDPE, and (C) PMMA surfaces. (Exposure time point (e.g., n hours; $n \geq 2$) represents 2 h exposure under the designated protein solution concentration followed by (n−2) hours of equilibration in PPB) (N=3; averaged 95% C.I. was ± 0.018 µg/cm^2 for surface coverage measurements).τ_{side} (0.17 µg/cm^2) and τ_{end} (0.26 µg/cm^2) refers to the theoretical full surface coverage of HEWL for adsorption in 'side-on' and 'end-on' orientations, respectively.[13] The decrease in surface coverage on each of the surface from 2-5 h, 5-10 h, and 10-17 h are statistically significant at $p < 0.05$ per the non-parametric sign-rank test. See Table B.1 in the appendix for the raw data of Fig 5.1.

The 2 h of exposure to the protein solutions resulted in very similar surface coverages on each surface, which fall within the surface coverages corresponding to the theoretical limits for a saturated surface for a monolayer of HEWL organized in a close-packed side-on orientation (0.17 µg/cm^2) and close-packed end-on orientation (0.26 µg/cm^2).[13] It is also important to note that the surface coverages at this time-point generally increased with increasing solution concentration for each surface between these two theoretical values, with PPI effects considered to increase in magnitude with increased surface coverage. The fact that the distribution of initial surface coverage of adsorbed HEWL was quite similar for each of our three materials also indicates that, on average, the PPI effects were initially quite similar for each type of surface.

But at 5-h time point in Fig.5.2, when the layers of adsorbed HEWL were allowed to relax for 3 h under protein-free buffer solution conditions, the surface coverages of each layer spontaneously decreased to values at or below that for a close-packed side-on orientation. Following these shifts, the surface coverages were still found to be widely distributed, thus continuing to provide a range of PPI for each surface type. The surface coverages then appeared to stabilize with relatively little further change with continued exposure time. However, comparison of the mean values of the concentrations on each of the surfaces between the 5–10 h and 10–17 h time points using a nonparametric sign test,[33-34] reveals that the consistent slight decreases in surface coverages over time do actually represent a statistically significant difference ($p \leq 0.05$), thus showing that the HEWL continued to desorb from the surface at a very slow rate. But, most importantly, the results for each time point during this equilibration phase of the experiments continued to provide a broad range of surface coverage, which we assume to proportionally correspond to a broad range of PPI effects within the adsorbed protein layers.

5.3.3. b Surface coverage of RNase A on different surfaces

Fig. 5.3 presents a plot of the surface coverage of the adsorbed RNase A on each of our three surfaces for each solution concentration. As these plots show, the exposure of each surfaces to protein solutions for different exposure time resulted in very similar surface coverages. But, unlike the strikingly evident differences in the initial and final surface coverages of HEWL on different surfaces, the differences in initial (at 2 h) and final (at 17 h) surface coverages of RNase A on each of the surfaces were less evident, especially at 0.03 mg/ml and 0.05 mg/ml.[33-34] Despite this result, the significant differences

observed in the surface coverages of RNase A at different exposure time for most of the other bulk solution concentrations is suggestive that varying the bulk solution concentration and equilibration time in buffer is an effective strategy to vary the surface coverage of the adsorbed RNase A on these surfaces.[33-34]

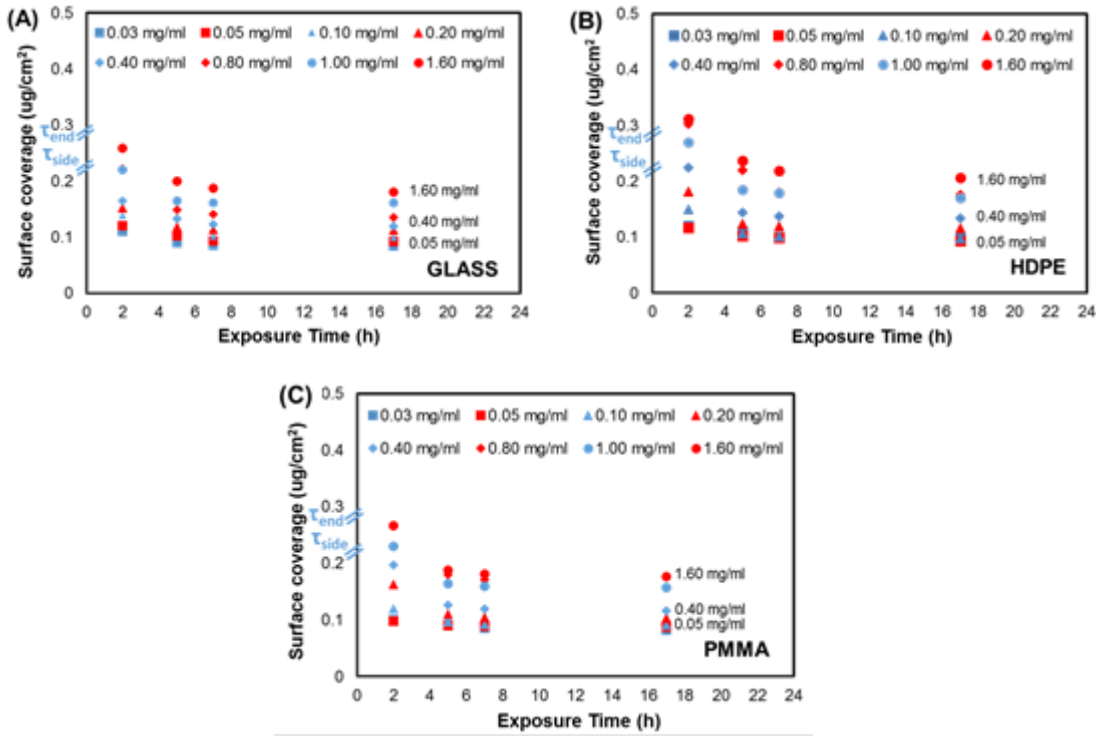

Figure 5.3: Effect of varying exposure time on the surface coverage of RNase A adsorbed on (A) glass, (B) HDPE, and (C) PMMA surfaces. (Exposure time point (e.g., n hours; n ≥ 2) represents 2 h exposure under the designated protein solution concentration followed by (n-2) hours of equilibration in PPB) (N=3; averaged 95% C.I. was ± 0.016 μg/cm^2 for surface coverage measurements). τ_{side} (0.21 μg/cm^2) and τ_{end} (0.28 μg/cm^2) refers to the theoretical full surface coverage of RNase-A for adsorption in 'side-on' and 'end-on' orientations, respectively. See Table B.2 in the appendix for the raw data of Fig 5.3.

The theoretical limits for a saturated surface with a monolayer of RNase A organized in a close-packed side-on orientation and close-packed end-on orientation are 0.21 μg/cm^2 and 0.26 μg/cm^2 respectively.[13] The 2 h of exposure of different solution

concentrations of RNase A resulted in wide variations in the initial surface coverage on each of the surface, with solution concentrations less than 0.40 mg/ml often resulting in surface coverages less than 0.21 μg/cm^2 while solution concentrations 0.80 mg/ml, 1.00 mg/ml and 1.60 mg/ml, resulted in surface coverages less than the 0.26 μg/cm^2. Although 2 h of adsorption from protein solution was found sufficient to saturate the adsorbent surfaces, the fact that the initial surface coverages of RNase A were considerably lower than that for a close-packed side-on orientation suggest that each protein occupied a larger footprint on the surface than provided by the side-on adsorption of the protein in its native-state structure. This is quite different from the adsorption behavior of HEWL which tend to adsorb on surfaces at initial surface coverages closer to the footprint of native structure. The increased footprint of RNase A on different surfaces at initial surface coverage compared to HEWL suggests that RNase A undergoes a greater degree of structural unfolding on the adsorbent surfaces, presumably due to its lowered internal stability. However, it is also important to note that these tendencies tend to reduce at increasing solution concentration, as evident by the general increase in surface coverages at this time-point with increasing solution concentration. Also, these general trends in the distribution of initial surface coverage of adsorbed RNase A at 2 h was quite similar for each of our three material surfaces, which indicates that, on average, the PPI effects were initially quite similar for each type of surface.

At the 5-h time point in Fig.5.3, when the layers of adsorbed RNase A were allowed to relax for 3 h under protein-free buffer solution conditions, the surface coverages of all layers decreased to values at or below that for a close-packed side-on

orientation. Though the surface coverages for RNase A at the 5-h time point were less distributed than that of HEWL, these surface coverages were still found to vary with each solution concentration and were considered to provide a range of PPI for each surface type. On further equilibrating the adsorbed RNase A in PPB, the surface coverages appeared to stabilize with relatively little further change at the exposure time of 5–7 h and 7–17 h. However, comparison of the mean values of the concentrations on each of the surfaces between the 5–7 h and 7–17 h time points using a nonparametric sign test,[33-34] indicates that the consistent slight decreases in surface coverages over time do actually represent a statistically significant difference ($p \leq 0.05$), thus showing that the RNase A desorbed from the surface at a very slow rate. As desired, the broad range of surface coverage during this equilibration period corresponds to a broad range of PPI effects within the adsorbed protein layers.

5.3.4 Adsorption-Induced Changes in Protein Helical Structure

5.3.4.1 Effect of Surface Coverage and PPI on the Secondary Structure of HEWL

The influence of adsorption conditions on the secondary structure of the adsorbed HEWL is presented in Fig. 5.4. The percent helical structure shown in Fig. 5.4 corresponding to the 0 h exposure times represents the native helical content of the protein in solution (38 ± 2% helix), with the subsequent time points representing the average helical structure of the protein layers in the adsorbed state. The 2 h time point represents the structure of the saturated layers of the adsorbed protein after 2 h exposure to their respective protein solution concentrations followed by rinsing in pure buffer to remove loosely bound proteins, while the time points after 2 h represent the time given

the protein to equilibrate following adsorption while immersed in pure buffer solution (e.g., 5 h time point represents 2 h exposure under the designated protein solution concentration followed by 3 h of equilibration in PPB).

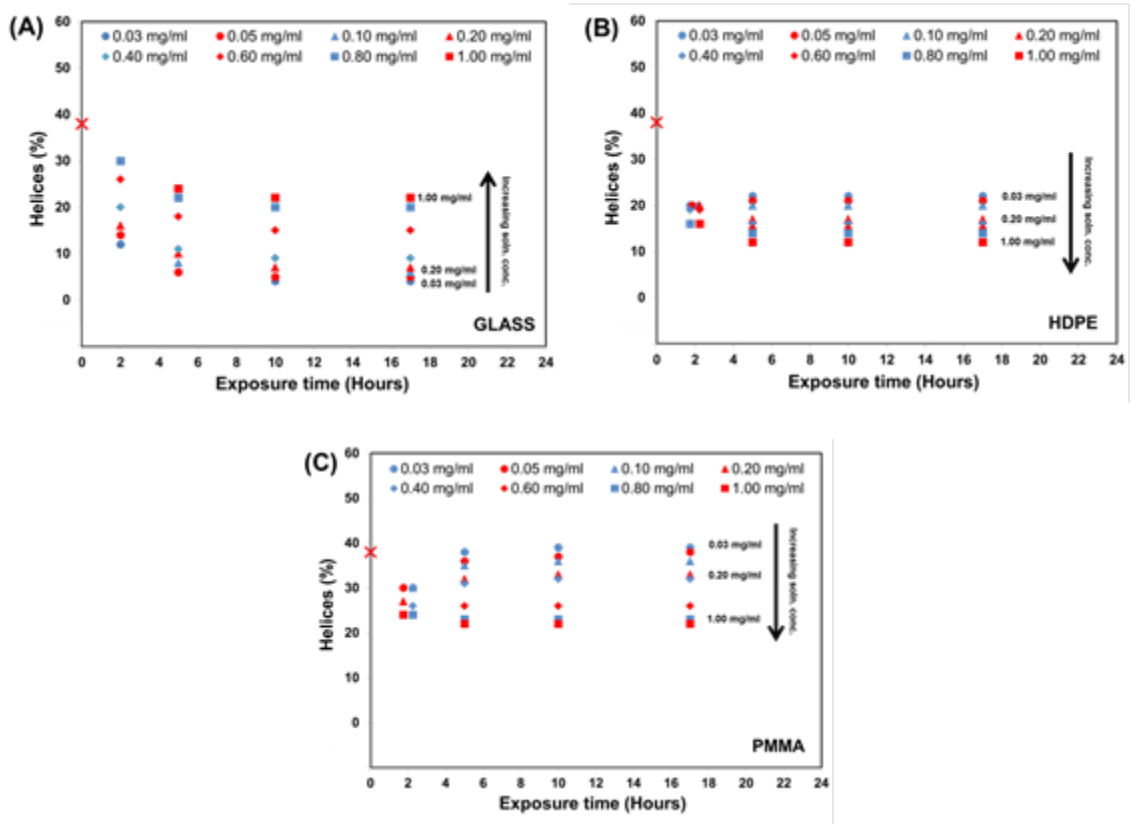

Figure 5.4 Helical content of adsorbed HEWL on (a) glass, (b) HDPE, and (c) PMMA surface as a function of exposure time. Symbols represent the different protein solution concentrations that were used to adsorb the HEWL to each surface. Zero time point represents the native helical structure of HEWL in solution, which was 38% (± 2%), consistent with the reported secondary structure. (N = 3, averaged 95% C.I. values = ± 4 % helicity for each data point). Data points for the 2 h time point for (b) and (c) have been shifted slightly for visualization due to overlap. The black arrows indicate the direction of increasing solution concentration from which the protein was adsorbed. (Table B.3 provides the raw data of Fig. 5.3).

As shown in Fig 5.4, adsorption of HEWL to each surface following 2 h exposure to the protein solution resulted in a significant reduction of helical secondary structure for each

surface and for each solution concentration, which reflects the combined influences of protein-surface interaction, PPI, and internal protein stability effects upon HEWL. Comparisons of the adsorption response at 2 h between these three surfaces show some interesting differences. In particular, the solution concentration from which HEWL was adsorbed had a very strong influence on the adsorbed structure on glass, with greater helicity being retained for adsorption from increased solution concentration. In distinct contrast to this, while a significant loss in helical structure upon adsorption also occurred on the HDPE and PMMA surfaces, the range of the influence of solution concentration was much reduced. In addition, the increase in solution concentration had very different effects on the protein's structure on these surfaces compared to the glass surface. On PMMA, there was actually significantly reduction in the helical structure for the HEWL layers adsorbed from solutions of higher protein concentration, while there was no significant difference in the drop in the percent helical structure between layers adsorbed from different solution concentrations for the HDPE surface.

The data shown in Fig. 5.4 for the exposure times of 5, 10, and 17 h represent the structural response of HEWL during the 15 h of equilibration in the pure buffer following the 2 h adsorption period. As shown in Fig. 5.4, the structure of the HEWL on each of these surfaces underwent significant further changes between the 2 h and 5 h overall exposure times. Subsequent changes in the percent helicity between the 5 h, 10 h, and 17 h time points was not significantly different ($p > 0.05$) for any of our surfaces except for the transition from the 5 h to the 10 h time exposures times for HEWL on glass, which showed slight but still statistically significant further decreases in helicity. ($p < 0.01$; nonparametric sign test[33-34]).

As with the 2 h results, comparisons of the structural behavior of HEWL between our three surfaces for the 5, 10, and 17 h time points suggest that HEWL behaved distinctly differently on each different type of surface, with the influence of the protein solution concentration from which the HEWL was adsorbed having the opposite effect on PMMA as it did on glass, with relatively little effect on HDPE. In order explore the influence of PPI effects more directly based on our assumption that the degree of PPI effects within the adsorbed HEWL layers is directly proportional to the surface coverage of the layer, the values of the percent helical structure for the data shown in Fig 5.4 were replotted against the surface coverage for the HEWL layers from Fig. 5.2, with these plots presented in Fig 5.5

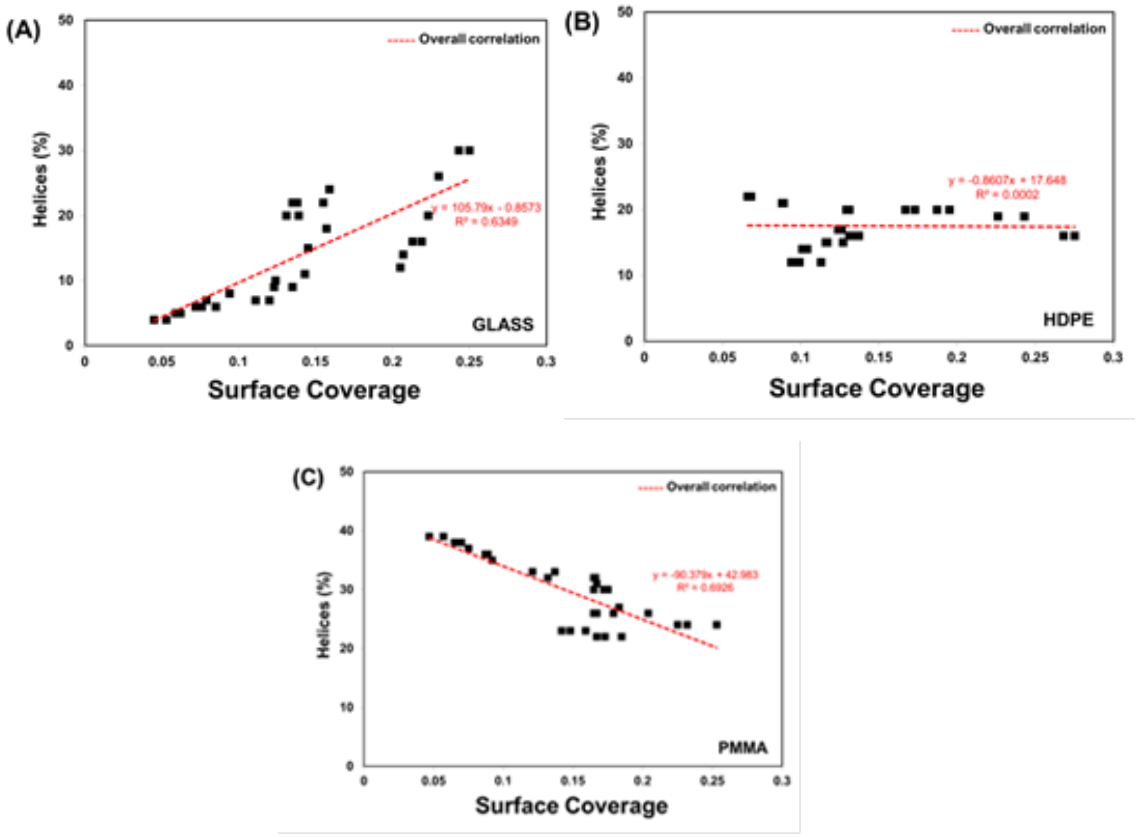

Figure 5.5. HEWL % helicity (y-axis) vs. surface coverage (x-axis) of the adsorbed HEWL layers on (a) glass, (b) HDPE, and (c) PMMA. (N = 3; averaged 95% C.I. values

of ± 4% for helicity and ± 0.032 μg/cm^2 for surface coverage.) (Table B.5 provides the raw data of Fig. 5.4).

The data presented in Fig. 5.5 provide a much clearer picture of the influence of PPI effects (as represented by the surface coverage) on the stability of the adsorbed HEWL (as represented by the percent helicity) for each of our three surfaces. On the glass surface, increased surface coverage of the adsorbed protein layer is clearly shown to stabilize the protein against protein-surface interaction-induced unfolding with only a 20% decrease in the native-state % helicity (38% to 30%) for the highest surface coverage (0.25 μg/cm^2, reflecting a close-packed end-on structure; see Fig. 5.3), while at the lowest surface coverage (0.045 mg/cm^2, reflecting an areal density 4x lower than that for a close-packed side-on structure) the helicity decreased all the way down to only 4% (i.e., 90% loss in helicity). As shown in Fig. 5.4.b, changes in surface coverage of HEWL on HDPE had minimal influence on its helical structure with the percent helicity ranging from 12 to 22% with an average of about 18% helicity (53% loss in % helicity). As the most interesting (and unexpected) result, PPI effects are shown to have the opposite effect on HEWL on the PMMA surface compared with glass. On the PMMA surface, when PPI effects were decreased by the displacement of proteins from the surface from their initial saturated condition, HEWL actually refolded to regain the percentage of helicity lost following the initial adsorption process to attain a percent helicity equal to its native-state solution structure.

5.3.4.2 Effect of Surface Coverage and PPI on the Secondary Structure of RNase A

The influence of adsorption conditions on the secondary structure of the adsorbed RNase A is presented in Fig. 5.6. The percent helical structure shown in Fig. 5.6 corresponding to the 0 h exposure times represents the native helical content of the protein in

solution (20 ± 2% helix), with the subsequent time points representing the average helical structure of the protein layers in the adsorbed state. The 2 h time point represents the structure of the saturated layers of the adsorbed protein after 2 h exposure to their respective protein solution concentrations followed by rinsing in protein-free buffer to remove loosely bound proteins, while the time points after 2 h represent the time given the protein to equilibrate following adsorption while immersed in protein-free buffer solution (e.g., 5 h time point represents 2 h exposure under the designated protein solution concentration followed by 3 h of equilibration in PPB).

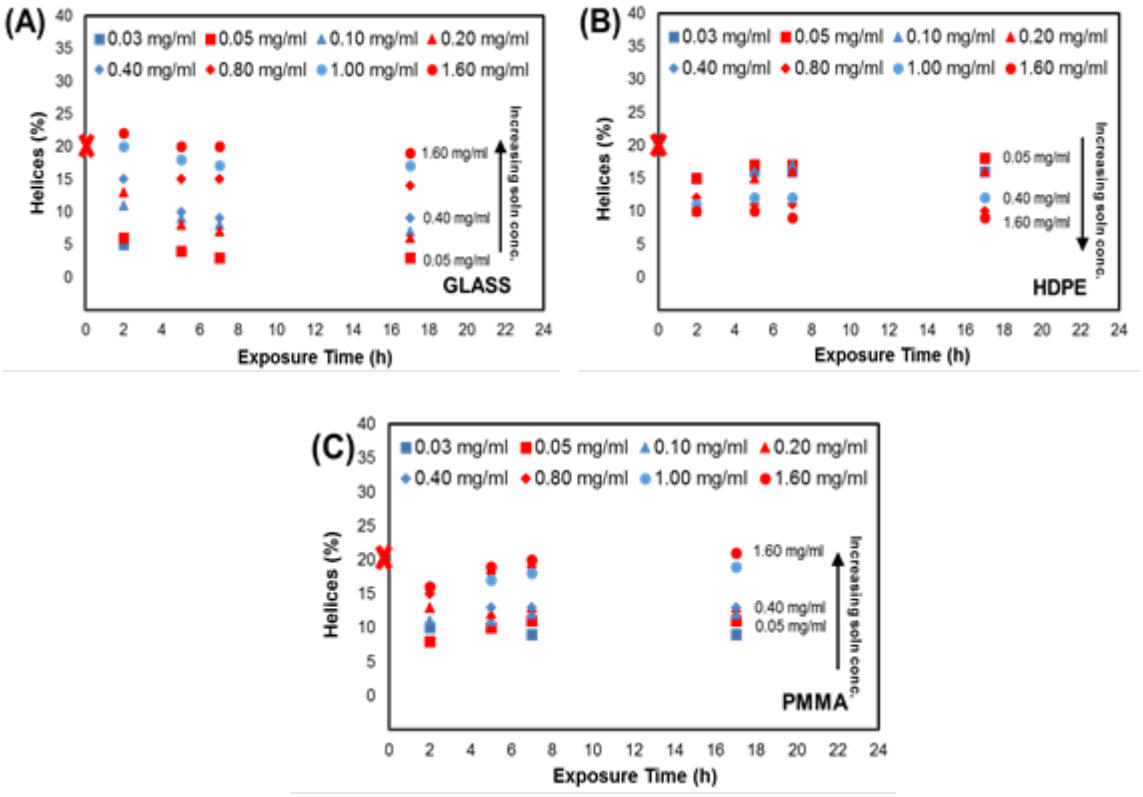

Figure 5.6: Helical content of adsorbed RNase-A on (a) glass, (b) HDPE, and (c) PMMA surface as a function of exposure time. Symbols represent different protein solution concentrations that were used to adsorb the RNase-A to each surface. Zero time point represents the native helical structure of RNase-A in solution, which was 20 % (± 2%), consistent with the reported secondary structure. (N = 3, averaged 95% C.I. values = ± 4 % helicity for each data point). The black arrows indicate the

direction of increasing solution concentration from which the protein was adsorbed. (Table B.4 provides the raw data of Fig. 5.6).

As shown in Fig 5.6, adsorption of RNase A to each surface following 2 h exposure to the protein solution showed some interesting differences. In particular, the solution concentration from which RNase A was adsorbed had a very strong influence on the adsorbed structure on glass, with greater helicity being retained for adsorption from increased solution concentration. In distinct contrast to this, while a significant loss in helical structure upon adsorption also occurred on the HDPE and PMMA surfaces, the range of the influence of solution concentration was much reduced. In addition, the increase in solution concentration had very different effects on the protein's structure on these surfaces compared to the glass surface. On the PMMA surface, there was a significantly increase in the helical content of RNase A layers when adsorbed from solutions of higher protein concentration, while there was a significant drop in the percent helical structure between the layers adsorbed from higher solution concentrations on the HDPE surface.

The data shown in Fig. 5.6 for the exposure times of 5, 7, and 17 h represent the structural response of RNase A during the 15 h of equilibration in the protein-free buffer following the 2 h adsorption period. As shown in Fig. 5.6, the structure of RNase A on each of these surfaces underwent significant further changes between the 2 h and 5 h overall exposure times. While on the glass surfaces, RNase A underwent statistically significantly drop in helical structure ($p < 0.01$; nonparametric sign test[33-34]), these adsorbed layers underwent statistically significant increase in its helical content on the PMMA and HDPE surfaces over the time period. However, over the time period of 5-7 h and 7-17 h, there was

not significantly different ($p > 0.05$) for any of our surfaces except for the transition from the 5 h to the 10 h time exposures times for HEWL on glass, which showed slight but still statistically significant further decreases in helicity ($p < 0.01$; nonparametric sign test[33-34]). In order explore the influence of PPI effects more directly based on our assumption that the degree of PPI effects within the adsorbed RNase A layers is directly proportional to the surface coverage of the layer, the values of the percent helical structure for the data shown in Fig 5.6 were replotted against the surface coverage for the HEWL layers from Fig. 5.3, with these plots presented in Fig 5.7

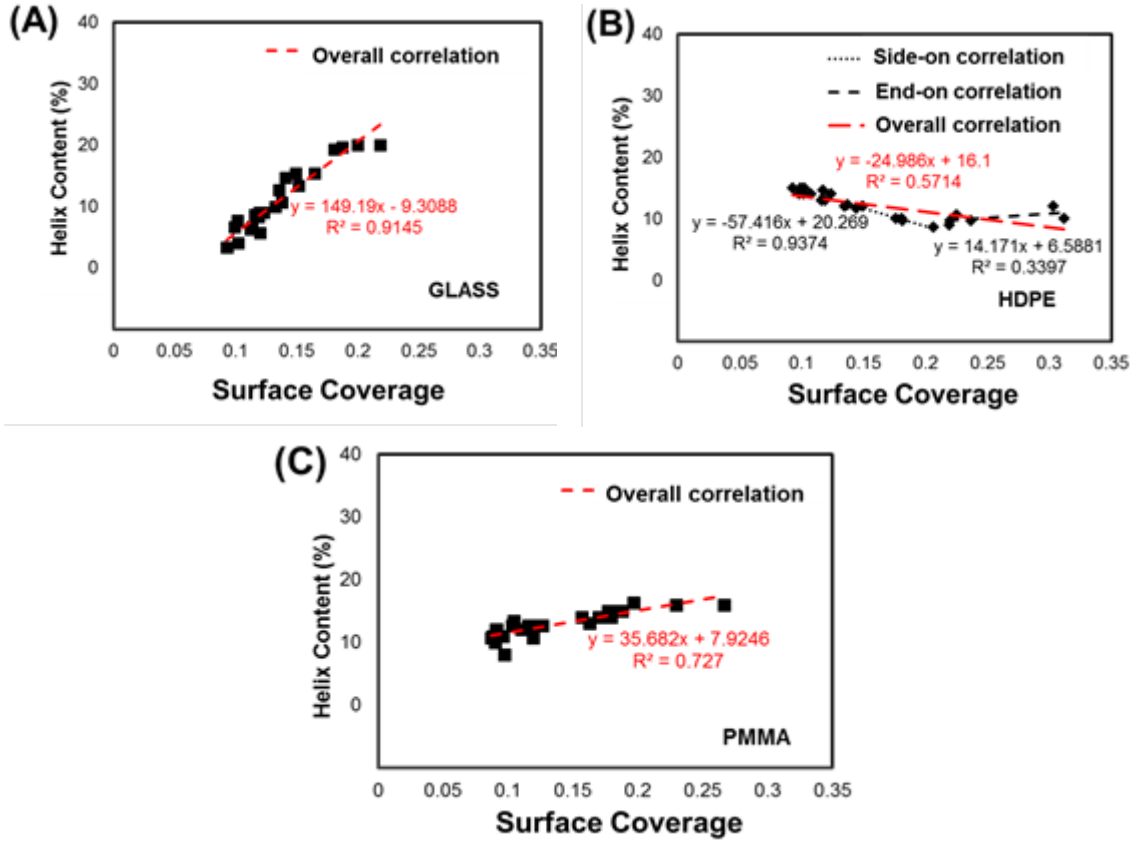

Figure 5.7: RNase A % helicity (y-axis) vs. surface coverages (x-axis) of the adsorbed RNase A layers on (a) glass, (b) HDPE, and (c) PMMA. (N = 3; averaged 95% C.I. values of ± 4 % for helicity and ± 0.032 mg/cm^2 for surface coverage.) (Table B.6 provides the raw data of Fig. 5.7)

The data presented in Fig. 5.7 provide a much clearer picture of the influence of PPI effects (as represented by the surface coverage) on the stability of adsorbed RNase A (as represented by the percent helicity) for each of our three surfaces. Like the HEWL on glass surfaces, increased surface coverage of RNase A on these surfaces was found to stabilize the protein ($R^2 = 0.91$) against protein-surface interaction-induced unfolding. The PPI effects were shown to stabilize the protein with complete restoration of its retained helical content to that of native-state (20 %) at the highest surface coverage (0.22 μg/cm^2, reflecting a close-packed end-on structure) while at the lowest surface coverage (0.09 μg/cm^2, reflecting a surface coverage about 2x lower than that for a close-packed side-on structure) the retained helical content decreased all the way down to 3 % (i.e., 85 % loss in helicity). The PPI were also found to stabilize the protein structure on the PMMA surface ($R^2 = 0.73$), with the retained % helicity being restored to near native state (20 % to 16 %, i.e., 20 % loss in helicity) at the highest surface coverage (0.26 μg/cm^2, reflecting a close-packed end-on structure; see Fig. 5.7c), while there was about 45 % loss in helicity (absolute content of retained helical content was about 11 %) at the lower surface coverages (0.09 μg/cm^2, about 2x lower than that of a close-packed side-on structure).

In direct contrast to the stabilizing effects of PPI on the structure of RNase A on glass and PMMA surfaces, the overall correlation between the surface coverage and the helical content of RNase A ($R^2 = 0.57$) on HDPE surface was suggestive of a slight destabilizing influence of PPI on the helical content of adsorbed RNase A on HDPE surface. Among these interactions, more prominent destabilizing influence of

PPI on the helical structure of RNase A on HDPE surface was evident at surface coverages lower than closed packed side on orientations (R^2 = 0.94), but had relatively no influence (R^2 = 0.33) on the helical structure of RNase A when adsorbed at surface coverages near or equal to closed packed end on orientation (R^2 = 0.94) (Fig 5.7b). The helical content of the RNase A on the HDPE surface at the highest and lowest surface coverages were 9% (55% loss in native helical structure) and 15% (i.e. 25% loss in native helical content) respectively.

5.3.4.3 Molecular Mechanisms Influencing the Adsorbed Protein Structure on Different Surfaces

Based on these combined results, we hypothesize the following general molecular-level relationships between protein-surface, internal protein stability, and PPI effects in order to explain the observed behavior presented in Fig. 5.5 and Fig. 5.6.

On surfaces with a large density of hydrogen bondable and ionic groups, such as glass, protein-surface interaction effects will occur in the form of competition of the surface hydrogen bondable groups with the hydrogen bonds that stabilize the secondary helical structure of the protein,[43] thus tending to destabilize the helical structures of the protein on the surface. PPI effects, in turn, tend to restrict the conformational freedom of neighboring proteins thus providing a stabilizing force that helps to inhibit the unfolding process induced by protein-surface interaction effects. Therefore under low surface coverage conditions when PPI effects are minimized, protein-surface interaction effects tend to overcome internal protein stability effects, leading to substantial unfolding of the protein on this type of surface. Similarly, under high surface coverage conditions, PPI

effects couple with the internal protein stability effects to help stabilize the protein, thus limiting the degree of unfolding that occurs.

In contrast to surfaces with a high density of hydrogen-bondable and ionic groups on the surface, highly hydrophobic surfaces, such as HDPE, which do not have hydrogen bonding capability, have the potential to strongly interact with the hydrophobic amino acid residues that typically stabilize a protein's tertiary structure.[43] Because of the substantial thermodynamic driving force behind hydrophobic interactions in aqueous solution, this type of protein-surface interaction effect dominates over both internal protein stability and PPI effects for HEWL, with PPI effects then having relatively little influence on the degree of protein unfolding that occurs upon adsorption.

As a third category of surface chemistry, surfaces with moderate density of hydrogen-bondable and/or charged groups have only moderate capability to form hydrogen bonds with the protein, while also tending to be only moderately hydrophobic. These types of surfaces can thus be expected to exhibit relatively weak protein-surface interaction effects, with only moderate tendency to disrupt both the hydrogen bonds that stabilize the helical secondary structures of the adsorbed protein and moderate tendency to compete with the hydrophobic interactions that tend to stabilize the protein's tertiary structure. In proteins like HEWL that are stabilized by more than 50% non-polar amino acids, the increasing influence of PPI along with protein-surface interaction tend to destabilize the local helical structure by weakening the internal stability of the proteins (40% loss in native structure). We propose that the presence of high PPI effects on PMMA surface for a more hydrophobic protein

like HEWL acts like an in-plane compressive force that tend to destabilize and unfold the helix content in these protein. But, in proteins like RNase-A, which are stabilized by more than 50% of the polar residues, the PPI effects on these surfaces inhibit the initial destabilizing influence on the helical structure by restricting its conformational freedom, thus inhibiting the unfolding process induced by protein-surface interaction effects. Although speculative at this time, this hypothesized interplay between internal protein stability, protein-surface interaction, and PPI effects is consistent with the results obtained from this present study.

5.3.5 Adsorption-Induced Changes in Protein Bioactivity

The key element in most applications where protein-surface interactions are important is the bioactive state of the adsorbed protein. Protein bioactivity is primarily determined by the structure and accessibility of a protein's bioactive site, both of which are influenced by the combination of protein-surface interaction, PPI, and internal protein stability effects in an adsorbed protein layer. In this section, results for the influence of these interactions on the conformation and bioactivity of adsorbed HEWL and of adsorbed RNase A on our three material surfaces are presented

5.3.5.1 Relationship between the Conformation and Bioactivity of Adsorbed HEWL under Varying Protein-Protein Interaction and Protein-Surface Interaction Conditions.

Fig 5.8 presents the bioactivities of the adsorbed HEWL expressed as a percentage of its solution bioactivity vs. its percent helicity for each of our three surfaces for the layers of adsorbed HEWL at the 17 h exposure time (i.e., 2 h immersion in protein solution followed by 15 h equilibration in pure buffer solution).

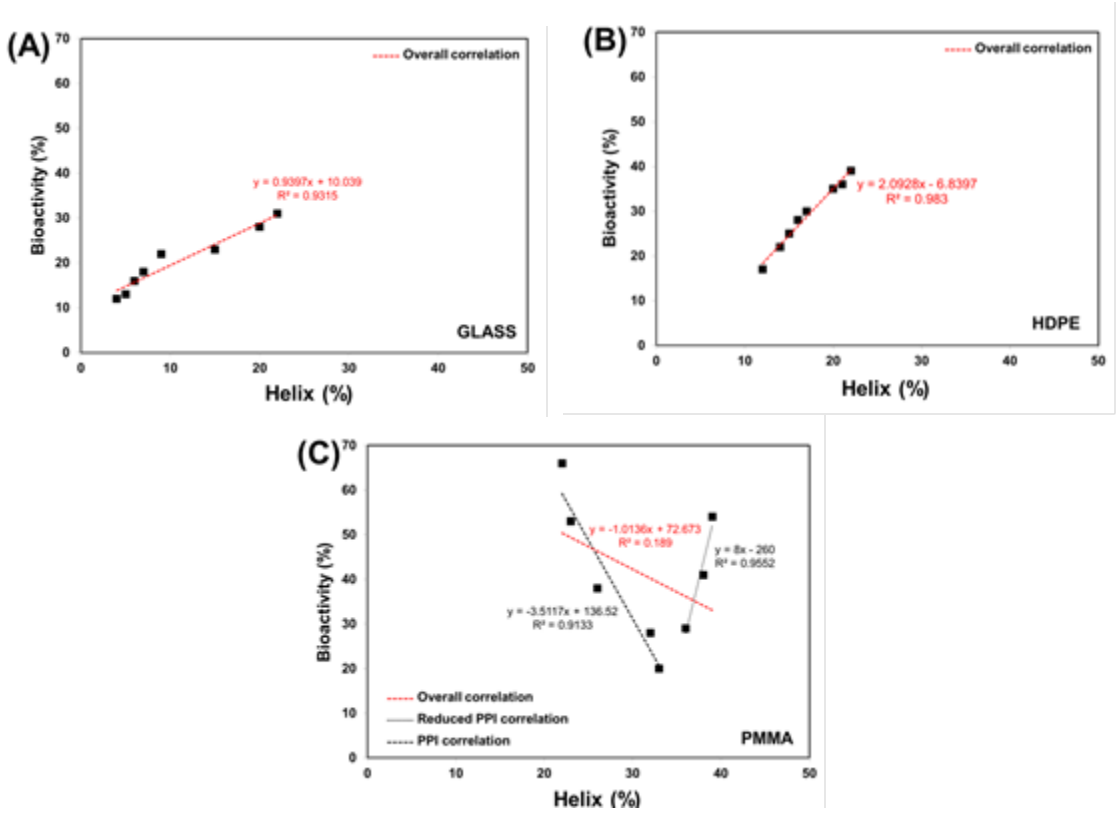

Figure 5.8. Bioactivity vs. percent helicity for adsorbed HEWL on (a) glass, (b) HDPE, and (c) PMMA for 17 h exposure time period. Three separate correlation lines given in (c) represent the correlation between bioactivity and percent helical structure of lysozyme for percent helicity < 35%, > 35%, and overall. (N=3; averaged 95% C.I. values (*N* = 3; averaged 95% C.I. values of ± 4% for helicity and ± 9% for bioactivity.).

As shown in Fig. 5.8a (glass) and 5.8b (HDPE), HEWL loses more than 60% of its bioactivity following adsorption, with an apparent direct linear correlation between the retained relative bioactivity of adsorbed HEWL and its percent helicity. These results suggest that on both of these surfaces, HEWL bioactivity is primarily being influenced by the structure of the bioactive site, with loss in helical structure from the native state structure (38% helicity) reflecting the degree of conformational distortion of the bioactive site. Comparing these results to the results shown in Fig. 5.5 (% helicity vs. surface

coverage), suggests that on glass, PPI effects primarily influence HEWL bioactivity by acting to inhibit protein-surface interaction-induced unfolding, which in turn helps preserve the structure of the bioactive site. Alternatively, on HDPE, for which the adsorption response was found to be dominated by protein-surface interaction effects, the loss in percent helicity of HEWL results in loss of bioactivity, presumably through concomitant structural distortions in the structure of the bioactive site, but with little influence from PPI effects.

The bioactive response of HEWL vs. percent helicity when adsorbed on PMMA was again quite surprising and distinctly different from the behavior of HEWL on either glass or HDPE. As indicated from the results presented in Fig. 5.5c, when PPI effects were minimized, HEWL was able to regain a percent helicity that was not significantly different than that of its native structure (38% helicity). As shown in Fig. 5.8c, the adsorbed HEWL retained up to 55% of its solution-state bioactivity under these conditions, but with its percent bioactivity rapidly decreasing to as low as only 20% for relatively small decreases in % helicity from that point. A strong correlation is indicated between bioactivity and helicity as the % helicity decreased, but only down to a value of about 35%. The apparent correlation then reversed, with bioactivity rapidly increasing as helicity further decreased down to a value as low as about 20%. Thus, as indicated in Fig. 5.7c, while a low correlation is found between the overall results for bioactivity and % helicity, the data suggests two subdomains within the overall data set that exhibit strong correlation, but in the opposite directions to one another. Surprisingly, HEWL exhibited the highest percent bioactivity at its lowest percent helicity, which, as shown in Fig. 5.5c,

corresponds to conditions of the strongest PPI effects. These results suggest that the loss in bioactivity of HEWL on PMMA is not just a result of adsorption-induced structural changes in its bioactive site. Other factors are evidently playing a substantial role, such as possibly the influence of PPI effects on the protein's orientation on the surface and the subsequent accessibility of the bioactive site for the substrate used in the bioactive assay. It is also, of course, possible that the combination of protein-surface interaction, protein-protein interaction, and internal protein stability effects on this surface result in structural distortions of the bioactive site in HEWL that are not directly reflected by the overall helicity of the protein on this surface. At this time, we can only speculate on explanations for this behavior and further studies are required to provide additional understanding of these intriguing results.

5.3.5.2 Relationship between the Conformation and Bioactivity of Adsorbed RNase A under Varying PPI and Protein-Surface Interaction Conditions.

Fig 5.9 presents the activity profile of the adsorbed RNase A expressed as a percentage of its solution bioactivity vs. its percent helicity for each of our three surfaces for the layers of adsorbed RNase A at the 17 h exposure time (i.e., 2 h immersion in protein solution followed by 15 h equilibration in protein free buffer solution). As evident from Fig 5.3 and Fig 5.6, the surface coverage corresponding to these helical content on all surfaces were below that for a close-packed side-on orientation.

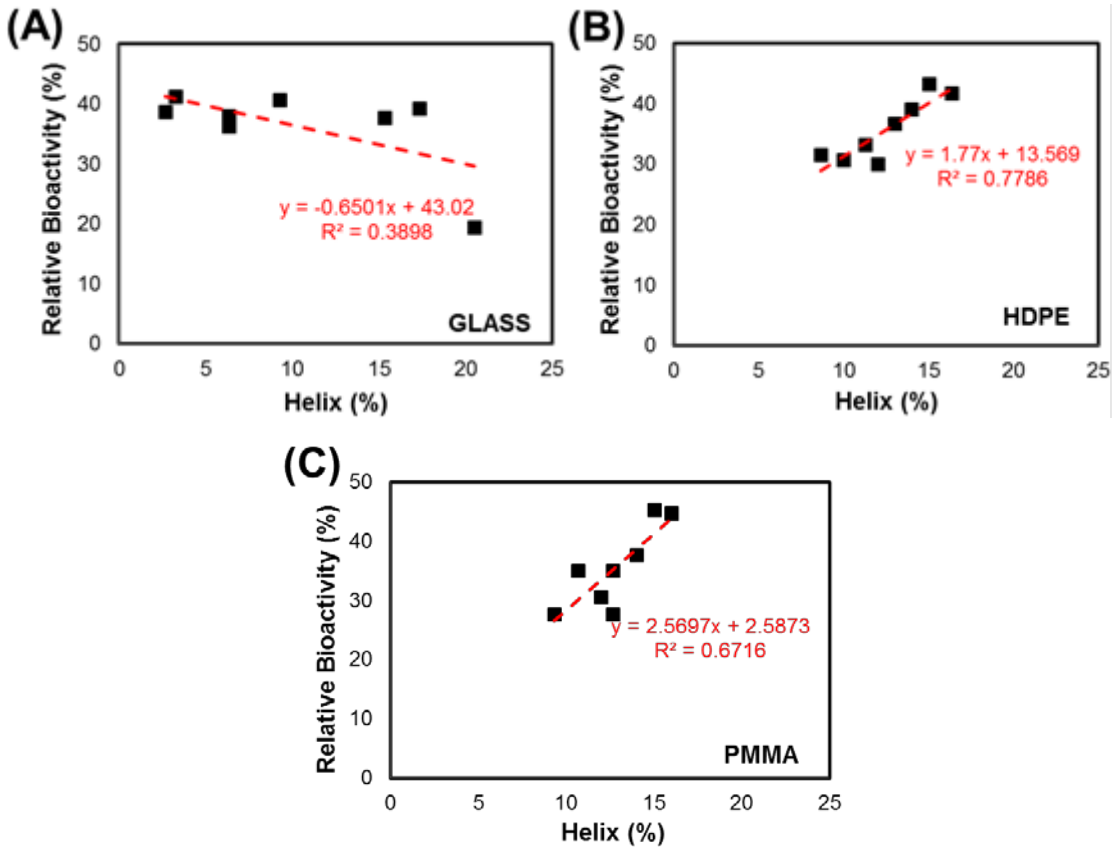

Figure 5.9. Bioactivity vs. percent helicity for adsorbed RNAse A on (a) glass, (b) HDPE, and (c) PMMA for 17 h exposure time period (15 hours of incubation following 2 hours of adsorption). (N=3; averaged 95% C.I. values of ± 2% for helicity and ± 6% for bioactivity.)

As indicated from the results presented in Fig 5.9, the bioactivity of RNase A on glass decreased with increased helicity suggesting that the loss of bioactivity is not directly related to the degree of adsorption-induced unfolding, but rather may be more directly related to adsorbed orientation or blocking by PPIs.

However, the bioactivity response of RNase A vs. percent helicity when adsorbed on PMMA or HDPE surfaces was distinctly different from the behavior of RNase A on the glass surface, with a positive correlation between retained bioactivity and protein structure. These results suggest that on both PMMA and HDPE surfaces, the bioactivity

of RNase A is primarily being influenced by the helical conformation of the bioactive site, with the higher degree of conformational distortion of the bioactive site resulting in greater reduction of its native state bioactivity.

5.4. CONCLUSION

A new experimental approach has been developed and applied to study the combined influence of protein-surface interactions, protein-protein interactions, and internal protein stability on the conformational behavior and bioactivity of adsorbed protein. In this paper, we present the first application of the developed methods to characterize the adsorption response of HEWL and RNase A on glass, HDPE and PMMA surfaces, with these surfaces selected to provide three characteristically different molecular mechanisms for their interactions with the protein.

The results from these structural studies indicate that the internal stabilities of the protein affect the initial surface coverage on the adsorbent surface, which in turn affects the PPI on the adsorbent surface. Subsequently these PPI effects were found to (1) stabilize the structure of proteins on a silica glass surface, which can be expected to exhibit strong hydrogen bond and electrostatic interactions with proteins; (2) have little influence on the structure of proteins on strongly hydrophobic surfaces, such as HDPE; and (3) can either stabilize or destabilize the structure of proteins on a PMMA surface (which has only moderate hydrogen bonding and hydrophobic character), depending on the amino acid composition of the adsorbing proteins. Furthermore, the results of the

bioactivity studies indicate that PPI effects play an indirect role on the bioactivity of adsorbed proteins through their influence on the adsorbed protein's structure (i.e., % helicity), with bioactivity reducing in direct proportion to the degree of adsorption-induced disruption of the protein's structure for most, but not all, of the protein-surface systems studied in this research. However, PPI effects may also influence adsorbed-state bioactivity by affecting the accessibility of the protein's bioactive site, either by directly blocking access or by influencing the orientation of the protein such that access to the bioactive site is blocked by the surface itself. We speculate that these later effects may be responsible for the lack of a clear overall correlation between bioactivity and adsorbed structure of HEWL on PMMA surfaces or RNase A on a glass surface.

5.5 REFERENCES

1. Latour, R. A. Molecular simulation of protein-surface interactions: benefits, problems, solutions, and future directions. *Biointerphases* **2008,** *3* (3), FC2-12.

2. Rabe, M.; Verdes, D.; Seeger, S. Understanding protein adsorption phenomena at solid surfaces. *Adv. Colloid Interface Sci.* **2011,** *162* (1-2), 87-106.

3. Vogler, E. A. Protein adsorption in three dimensions. *Biomaterials* **2012,** *33* (5), 1201-37.

4. Zoungrana, T.; Findenegg, G. H.; Norde, W. Structure, Stability, and Activity of Adsorbed Enzymes. *J. Colloid Interface Sci.* **1997,** *190* (2), 437-48.

5. Norde, W.; Giacomelli, C. E. In *Conformational changes in proteins at interfaces: from solution to the interface, and back*, Macromolecular Symposia, 1999; Wiley Online Library, pp 125-136.

6. Norde, W.; Lyklema, J. Interfacial behaviour of proteins, with special reference to immunoglobulins. A physicochemical study. *Adv. Colloid Interface Sci.* **2012,** *179-182*, 5-13.

7. Hlady, V. V.; Buijs, J. Protein adsorption on solid surfaces. *Curr. Opin. Biotechnol.* **1996,** *7* (1), 72-7.

8. Seigel, R. R.; Harder, P.; Dahint, R.; Grunze, M.; Josse, F.; Mrksich, M.; Whitesides, G. M. On-line detection of nonspecific protein adsorption at artificial surfaces. *Anal. Chem.* **1997,** *69* (16), 3321-3328.

9. Latour, R. A. Biomaterials: Protein-Surface Interactions. In *The Encyclopedia of Biomaterials and Bioengineering*, 2 ed.; Bowlin, G. E. W. a. G. L., Ed.; Informa Healthcare, 2008; Vol. 1, pp 270-284.

10. Szott, L. M.; Horbett, T. A. Protein interactions with surfaces: cellular responses, complement activation, and newer methods. *Curr. Opin. Chem. Biol.* **2011,** *15* (5), 677-82.

11. Horbett, T.; Brash John, L.; Norde, W. *Proteins at Interfaces III State of the Art*. American Chemical Society: 2012; Vol. 1120, p 0.

12. Sivaraman, B.; Fears, K. P.; Latour, R. A. Investigation of the effects of surface chemistry and solution concentration on the conformation of adsorbed proteins using an improved circular dichroism method. *Langmuir* **2009,** *25* (5), 3050-6.

13. Wertz, C. F.; Santore, M. M. Adsorption and Reorientation Kinetics of Lysozyme on Hydrophobic Surfaces. *Langmuir* **2002,** *18* (4), 1190-1199.

14. Kelly, S. M.; Jess, T. J.; Price, N. C. How to study proteins by circular dichroism. *Biochimica Et Biophysica Acta-Proteins and Proteomics* **2005,** *1751* (2), 119-139.

15. van der Veen, M.; Stuart, M. C.; Norde, W. Spreading of proteins and its effect on adsorption and desorption kinetics. *Colloids Surf. B. Biointerfaces* **2007,** *54* (2), 136-42.

16. Sreerama, N.; Woody, R. W. Computation and analysis of protein circular dichroism spectra. *Numerical Computer Methods, Pt D* **2004,** *383*, 318-351.

17. Greenfield, N. J. Using circular dichroism spectra to estimate protein secondary structure. *Nat Protoc* **2006,** *1* (6), 2876-90.

18. Norde, W. Driving forces for protein adsorption at solid surfaces. In *Biopolymers at Interfaces*, Malmsten, M., Ed.; Marcel Dekker: New York, 1998; Vol. 75, pp 27-54.

19. Fears, K. P.; Latour, R. A. Assessing the Influence of Adsorbed-State Conformation on the Bioactivity of Adsorbed Enzyme Layers. *Langmuir* **2009,** *25* (24), 13926-13933.

20. Ton-That, C.; Shard, A. G.; Daley, R.; Bradley, R. H. Effects of Annealing on the Surface Composition and Morphology of PS/PMMA Blend. *Macromolecules* **2000,** *33* (22), 8453-8459.

21. Banik, I.; Kim, K. S.; Yun, Y. I.; Kim, D. H.; Ryu, C. M.; Park, C. S.; Sur, G. S.; Park, C. E. A closer look into the behavior of oxygen plasma-treated high-density polyethylene. *Polymer* **2003,** *44* (4), 1163-1170.

22. Serra, J.; González, P.; Liste, S.; Serra, C.; Chiussi, S.; León, B.; Pérez-Amor, M.; Ylänen, H. O.; Hupa, M. FTIR and XPS studies of bioactive silica based glasses. *J. Non-Cryst. Solids* **2003,** *332* (1-3), 20-27.

23. Oiseth, S. K.; Krozer, A.; Lausmaa, J.; Kasemo, B. Ultraviolet light treatment of thin high-density polyethylene films monitored with a quartz crystal microbalance. *J. Appl. Polym. Sci.* **2004,** *92* (5), 2833-2839.

24. De Geyter, N.; Morent, R.; Van Vlierberghe, S.; Dubruel, P.; Leys, C.; Gengembre, L.; Schacht, E.; Payen, E. Deposition of polymethyl methacrylate on polypropylene substrates using an atmospheric pressure dielectric barrier discharge. *Prog. Org. Coat.* **2009,** *64* (2-3), 230-237.

25. Sharma, S.; Berne, B. J.; Kumar, S. K. Thermal and structural stability of adsorbed proteins. *Biophys. J.* **2010,** *99* (4), 1157-65.

26. Smith, P. K.; Krohn, R. I.; Hermanson, G. T.; Mallia, A. K.; Gartner, F. H.; Provenzano, M. D.; Fujimoto, E. K.; Goeke, N. M.; Olson, B. J.; Klenk, D. C. Measurement of protein using bicinchoninic acid. *Anal. Biochem.* **1985,** *150* (1), 76-85.

27. Pace, C. N.; Scholtz, J. M. Measuring the conformational stability of a protein. *Protein structure: A practical approach* **1997,** *2*, 299-321.

28. Pace, C. N.; Shaw, K. L. Linear extrapolation method of analyzing solvent denaturation curves. *Proteins* **2000,** *Suppl 4* (S4), 1-7.

29. Fears, K. P.; Sivaraman, B.; Powell, G. L.; Wu, Y.; Latour, R. A. Probing the conformation and orientation of adsorbed enzymes using side-chain modification. *Langmuir* **2009,** *25* (16), 9319-27.

30. Talbert, J. N.; Goddard, J. M. Enzymes on material surfaces. *Colloids Surf. B. Biointerfaces* **2012,** *93* (0), 8-19.

31. Tischer, W.; Wedekind, F. Immobilized Enzymes: Methods and Applications. In *Biocatalysis - From Discovery to Application*, Fessner, W.-D.; Archelas, A.; Demirjian, D. C.; Furstoss, R.; Griengl, H.; Jaeger, K. E.; Morís-Varas, E.; Öhrlein, R.; Reetz, M. T.; Reymond, J. L.; Schmidt, M.; Servi, S.; Shah, P. C.; Tischer, W.; Wedekind, F., Eds.; Springer Berlin Heidelberg, 1999; Vol. 200, pp 95-126.

32. Wei, Y.; Thyparambil, A. A.; Latour, R. A. Quantification of the influence of protein-protein interactions on adsorbed protein structure and bioactivity. *Colloids and Surfaces B: Biointerfaces* **2013,** *110* (0), 363-371.

33. Snedecor, G. W.; Cochran, W. G. *Statistical methods*; Iowa State University Press1980.

34. Whitley, E.; Ball, J. Statistics review 6: Nonparametric methods. *Critical Care* **2002,** *6* (6), 509-13.

35. Scholtz, J. M.; Grimsley, G. R.; Pace, C. N. Solvent denaturation of proteins and interpretations of the m value. *Methods Enzymol.* **2009,** *466*, 549-65.

36. Pace, C. N.; Grimsley, G. R.; Scholtz, J. M. Denaturation of proteins by urea and guanidine hydrochloride. *Protein Science Encyclopedia* **2005**.

37. Huyghues-Despointes, B. M.; Scholtz, J. M.; Pace, C. N. Protein conformational stabilities can be determined from hydrogen exchange rates. *Nat. Struct. Mol. Biol.* **1999,** *6* (10), 910-912.

38. Freire, E.; Schon, A.; Hutchins, B. M.; Brown, R. K. Chemical denaturation as a tool in the formulation optimization of biologics. *Drug Discov. Today* **2013,** *18* (19-20), 1007-13.

39. Ahmad, F.; Yadav, S.; Taneja, S. Determining stability of proteins from guanidinium chloride transition curves. *Biochem. J* **1992,** *287 (Pt 2)* (Pt 2), 481-5.

40. Ahmad, F.; Bigelow, C. C. Estimation of the free energy of stabilization of ribonuclease A, lysozyme, alpha-lactalbumin, and myoglobin. *J. Biol. Chem.* **1982,** *257* (21), 12935-8.

41. Myers, J. K.; Pace, C. N.; Scholtz, J. M. Denaturant m values and heat capacity changes: relation to changes in accessible surface areas of protein unfolding. *Protein Sci.* **1995,** *4* (10), 2138-48.

42. Hedoux, A.; Krenzlin, S.; Paccou, L.; Guinet, Y.; Flament, M. P.; Siepmann, J. Influence of urea and guanidine hydrochloride on lysozyme stability and thermal denaturation; a correlation between activity, protein dynamics and conformational changes. *PCCP* **2010,** *12* (40), 13189-96.

43. Branden, C.; Tooze, J. *Introduction to protein structure*; Garland Pub.1991.

CHAPTER SIX

DETERMINATION OF ORIENTATION AND ADSORPTION-INDUCED CHANGES IN THE TERTIARY STRUCTURE OF PROTEINS ON MATERIAL SURFACES BY CHEMICAL MODIFICATION AND PEPTIDE MAPPING

Based on the Published Articles:

1. Thyparambil A.A., Wei Y., Wu Y., and Latour R.A., Determination of orientation and adsorption-induced changes in the tertiary structure of proteins on material surfaces by chemical modification and peptide mapping, Acta Biomaterialia, 10(6): 2404-2414 (2014);
2. Thyparambil A.A., Wei Y., and Latour R.A., Experimental Characterization of Adsorbed Protein Orientation, Conformation, and Bioactivity, Biointerphases, 10, 019002, pp. 1-14 (2015).

6.1 INTRODUCTION

The interaction of proteins with adsorbent surfaces is a fundamental process involved in many emerging scientific and industrial fields such as biomaterials, bioseparation technology and bionanotechnology. In each of these applications, a key factor that is central to mediating a biological response specific to a given surface is the localized structural shifts and orientation adopted by the protein on the adsorbent surface.[1-2] Spectroscopic techniques that can detect the shifts in spectral signatures of a protein such as fluorescence, nuclear magnetic resonance or vibrational motion have been previously used to study a protein's adsorbed configuration on a given surface.[2-3] However, as the size of the protein increases, many of these spectral signatures overlap and introduce much subjectivity into the analyses,

thus making it difficult to accurately interpret the configuration of the adsorbed protein..[4] In contrast, mass spectrometry (MS) has shown great promise in characterizing the adsorbed configuration of both large and small proteins at a molecular level.[5-7]

Shifts in mass spectra can be related to adsorbed protein configuration if the structural information of the protein is encoded by changing its overall mass in a structure-dependent manner.[8] In this regard, although hydrogen–deuterium exchange when used along with MS may seem a very attractive option, the back-exchange associated with the processing of adsorbed proteins on surfaces severely limits the reliable application of this technique to study changes in the adsorption-induced protein structure.[9] An alternative strategy to encode this information is by covalently labeling the side-chains of selected amino acid residues in the protein to generate a labeling profile that can be used to map localized structural shifts in the protein from the changes in the solvent-exposed domains of the labeled residues.[5-8] Because labeling of an amino acid or a residue is localized to a very small portion in the overall protein structure, detailed information on its adsorbed configuration would require sampling of the labeling profile from multiple localized regions within a protein. However, the spatial distribution of a given amino acid within a protein is generally not uniform and varies greatly from one protein to another, with polar and charged amino acids mostly occupying the outer surface and fewer polar amino acids forming the inner core of the protein.[10] Therefore, to effectively represent the overall shift in a given protein configuration, multiple amino acid types in both the inner and outer core of the protein must be targeted.

Ideally, it would be desirable to directly compare the labeling profile of multiple amino acids modified using different modifying agents to map the adsorbed configuration of

a protein. Unfortunately, such a strategy is associated with considerable difficulties. Amino acid labeling can influence the protein's proteolytic digestion pattern and kinetics, and can also alter the hydrophobicity and ionization efficiency of the peptide-fragment digests, all of which can affect the signal intensities of the target peptides in ways that are difficult to predict.[8, 11-12] This problem is even more pronounced when different amino acid types are labeled on the same peptide, which further complicates the quantification of modified peptide fragments by MS. Additionally, when amino acid labeling of each type of amino acid is done under its respective optimal conditions (e.g. temperature, pH, concentration of reactants), the resulting labeling profile is a function not only of the configuration of the adsorbed protein, but also of the reaction kinetics. To avoid these complications, we chose a straightforward approach of labeling different amino acid types in a given protein in solution and in its adsorbed state under a common set of reactive condition by targeting only a single type of amino acid at a time. The resulting labeling profiles from each targeted amino acid type could then be combined by normalizing the signal intensities from each set of experiments using an internal standard. By following these procedures, the variability in the resulting labeling profile of each type of amino acid can be overcome and the results combined to provide detailed information of the adsorbed structure of the protein.

In the current study, the amino acid labeling and mass spectrometry (AAL/MS) technique was used to comprehensively identify the configuration of hen egg white lysozyme (HEWL) adsorbed on fused silica glass, high-density polyethylene (HDPE) and poly(methyl methacrylate) (PMMA) by combining the labeling profiles of modified arginine (Arg), lysine (Lys), tryptophan (Trp) and carboxylic groups (Asp, Glu). The resulting labeling profiles of

the targeted amino acid residues provide molecular-level insights regarding adsorbed protein orientation, areas of the protein that are involved in protein–protein interactions, and areas of the protein undergoing tertiary unfolding.

6.2 EXPERIMENTAL SETUP AND METHODOLOGY

6.2.1. Material Surface Preparation and Characterization.

The selected material surfaces include fused silica glass (glass), high density polyethylene (HDPE), and poly(methyl methacrylate) (PMMA). Custom cut glass discs (4" diameter, Chemglass Life Sciences) were procured and were cleaned by sonicating in "piranha" solution (7:3 (v/v) H_2SO_4 (EMD Chemicals, SX 1244)/H_2O_2 (Ricca Chemicals, 3821) and basic solution (1:1:3 (v/v/v) NH_4OH (BDH Chemicals, BDH3016)/ H_2O_2/ H_2O) at 50°C for 1 minute. HDPE and PMMA surfaces were spin–coated onto silicon wafers (6" diameter, University Wafer) from dodecalin (0.5% (w/w) at 1500 rpm for 60s) and chloroform (1.5% (w/w) solutions at 1000 rpm for 60s), respectively. All chemicals including the monomers of HDPE (Mw =125,000, Sigma 181900) and PMMA (Mw=350,000, Sigma 445746) and the solvents such as dodecalin (Sigma 294772) and chloroform (EMD Chemicals, CX 1054) were used as supplied by the manufacturer. Prior to adsorption studies, all the substrates were rinsed in absolute ethanol followed by nanopure water, and then were dried under a steady stream of nitrogen gas.

Surface characterization of the material surfaces was performed to determine the static air–water contact angle, atomic composition, film thickness, and surface roughness of the substrates used. For all the surfaces, the static air–water contact angle values were

analyzed using a contact-angle goniometer (Kruss, DSA-20E). The atomic compositions were verified via X-ray photoelectron spectroscopy (NESCA/BIO, University of Washington) and the average surface roughness was analyzed using atomic force microscopy (Asylum Research, MFP–3D) over an area of 5μm×5μm. The thicknesses of the polymer films were characterized using variable angle spectroscopic ellipsometry (Sopra Inc., GES–5).

6.2.2. Protein Adsorption and Structure Equilibration

Hen egg white lysozyme (HEWL) was procured from Sigma, (L6876). A stock solution of 5.0 mg/mL of HEWL was prepared in 10 mM potassium phosphate buffer (PPB), pH 7.4, and filtered to remove any insoluble aggregates. The final protein concentrations were verified via absorbance at 205 nm. All adsorbent surfaces were first incubated in PPB and then the required amount of protein stock solution was pipetted into the buffer to make up to the desired bulk solution concentration by taking care to ensure that pipet tip was below the air−water interface to avoid denaturation of the protein at this interface. The adsorption of HEWL on material surfaces was then carried out in a manner to vary the amount of adsorbed protein on each surface in order to investigate the effects of protein-protein interactions on the labeling pattern of amino acids in the adsorbed protein.[13] Briefly, protein adsorption was conducted under a protein bulk concentration of 0.03 mg/mL and 1.00 mg/mL for 2 h, after which the material surfaces were gently rinsed under a steady flow (12 mL/min) of protein-free buffer for 5 min to remove the bulk protein solution. The surfaces with the adsorbed layer of protein were then immersed in protein-free buffer solutions for 15 h to allow the adsorbed protein layers to structurally

equilibrate. In the case of protein adsorbed from lower solution concentrations, the protein-protein interactions effects should diminish due to the much lower surface coverage of the adsorbed protein layer, while the protein-protein interactions effects can be considered to be significant when proteins are adsorbed from high solution concentrations.[13]

6.2.3. Quantifying Adsorption-Induced Effects at a Molecular Level.

Proteins are known to adsorb to a surface in varied conformations and orientations,[1-2] resulting in varying degrees of solvent exposure for a given residue in the adsorbed protein population. Thus, instead of basing the results on a single amino acid type, combining the solvent exposure of residues from multiple amino acid types in the protein can provide a much better understanding of its predominant configuration on an adsorbent surface. Additionally, since the amino acids within a protein are generally not uniformly distributed, information from multiple sites within the inner and outer core of the protein is required to give a more comprehensive understanding of the extent of adsorption-induced configurational shifts in a protein.

Fig. 4.2 outlines the_methodology used in the current study to identify the predominant configuration of protein on an adsorbent surface by this AAL/MS technique.

6.2.3.1. Quantifying the Labeling from Multiple Sites using AAL/MS Technique

It has been previously shown that the AAL/MS technique is directly related to the extent of the solvent exposure of the targeted amino acids.[5] However, when multiple amino acids within a protein are targeted in batch experiments, two major issues need to be addressed in order to be compared on an equivalent basis. Firstly, since the ionization

efficiency of peptides between different batch experiments can vary, a common baseline reference is required in order to estimate the absolute extent of labeling from the peptide intensities of each of the batch experiments.[8, 14] Secondly, since the estimate on the absolute extent of labeling of residues for different labeling agents is influenced by the reaction kinetics, even under a common set of reactive conditions,[8] a relative ratio of the absolute extent of modification of protein in its adsorbed state to its solution state is necessary to define the residue profile. These combined methods were subsequently used to determine the adsorbed configuration of the protein.

6.2.3.2. Batch Labeling of Target Amino Acids

Arg, Lys, Trp, Asp and Glu in HEWL were labeled under a common reactive condition to facilitate direct comparison of the labeling profiles from each of these amino acids using previously developed methods (see section C.2. in the appendix).[7, 15-17] For consistency between treatments, the reaction between labeling agent and its targeted amino acid was carried out at 5x the overall molar concentration of the targeted amino acid type contained within the protein in the dark at 25°C for 3h in 10 mM potassium phosphate buffer (PPB). The sole criterion for choosing the labeling agent concentration and the duration of the modification was the maximal amount of labeling agent concentration and minimal time that would be required for modifying the most abundant amino acid (i.e. Arg) within the protein without any significant conformational shift. Reacting conditions such as temperature and pH were chosen to minimize any variability in the protein structure due to changes in the solution conditions. The solution pH was

maintained at 7.4 by adding required amounts of monobasic potassium phosphate (Sigma, P8708) or dibasic potassium phosphate (Sigma, P8508).

6.2.3.3. Spectral Acquisition of Labeled Proteins by Mass Spectrometry

Proteolytic digestion of modified and unmodified HEWL in its solution as well as in its adsorbed state was done using sequence-grade porcine trypsin (Promega) as described in section C.3 of the appendix. Trypsin-digested peptides were subsequently analyzed using an Ultra Performance Liquid Chromatography System (UPLC, Waters) coupled with a quadruple time-of-flight mass spectrometer (Q-TOF MS, Waters) with electrospray ionization in ESI^+-MS mode operated by Masslynx software (V4.1). The intensities obtained from modified peptides were subsequently used in quantifying the extent of solvent exposure for the targeted residues in HEWL.

6.2.3.4. Baseline Reference to Directly Compare the Modification from Multiple Sites

The intensity of a selected peptide fragment that was generated as a byproduct of tryptic digestion and did not contain the target residue of interest was used as an internal control to normalize the intensities within a given mass spectrum. By this approach, the signal intensities from the different amino-acid labeling studies could be compared on an equivalent basis. Although it is highly desirable that the internal control used in a study remains unaltered between each of the targeted amino-acid modifications, variants to the internal control are inevitable, especially when Arg and Lys are modified or when proteins are adsorbed on different surfaces.[5-6, 11] These variants in the internal control are a result of changes in the accessibility and/or reactivity of the cleavage sites in the protein for tryptic digestion.

Trypsin is known to cleave peptide chains with high specificity at the carboxyl side of Lys and Arg, except when either one is followed by proline.[11] A central step essential to tryptic digestion of a given peptide with positively charged Lys and Arg amino acids involves the binding of the peptide to the negatively charged catalytic sites of the trypsin. However, most side-chain modifying agents that are available to label Lys or Arg in the protein neutralize the positive charge on these amino acids, resulting in the alteration of the specificity with which the peptides are cleaved.[8] Additional alterations in the specificity of trypsin can also be introduced when these positively charged amino acids are sterically blocked by the adsorbent surfaces. Following the methods presented by Xu and Bowden,[5] under these circumstances the baseline reference in the acquired mass spectra for the protein is determined as the effective sum of the intensities from the internal standard and its variants as represented by equation 6.1. The overall contribution of the intensities from internal standards was therefore accounted by considering the contribution of the internal standards generated as a result of tryptic digestion plus those generated as a result of missed cleavage. In the event of a missed cleavage, peptides undergoing a mass shift due to the modification process were given an added weighting to partially account for any variation in the ionization efficiency due to the labeling process, as represented by equation 6.2.[5]

$$\text{Baseline reference} = \Sigma \text{ Intensities from Internal Control} \quad (6.1)$$

$$\Sigma \text{ Intensities from Internal Control} = \Sigma(N * I)\text{modified} + \Sigma(I)\text{unmodified variants} \quad (6.2)$$

where N is the weighting factor and is defined as the number of the modifying agents on the peptide containing the residue of interest, which is estimated using equation 6.3.

$$N = \frac{\text{Mass of the modified peptide} - \text{Mass of the unmodified peptide}}{\text{Mass of the labeled product}} \quad (6.3)$$

The signal intensities for peptide fragments containing the residue of interest were subsequently normalized to obtain the normalized intensities (I_{norm}) using the baseline reference as shown in equation 6.4.

$$I_{norm} = \frac{\text{Intensity of the peptides with the residues of interest}}{\text{Baseline reference}} \quad (6.4)$$

The absolute extent of modification for a target residue in its solution (I_{soln}) and adsorbed state (I_{ads}) was subsequently estimated from a given mass spectrum by calculating the ratio of the weighted intensity of peptide fragments containing the labeled target amino acid to the total weighted intensities of all peptide fragments, as shown in equation 6.5.[5, 8]

$$I_{soln} \text{ or } I_{ads} = \frac{\Sigma(N * Inorm)\text{modified}}{\Sigma(N * Inorm)\text{modified} + \Sigma(Inorm)\text{unmodified}} \quad (6.5)$$

6.2.3.5. Determining the Labeling Profile of Target Residues from the Absolute Extent of Modification.

Although the reaction kinetics for different labeling reactions can be expected to differ,[7, 15-17] its effect on the absolute extent of modification can be considered to be minimal for a given amino-acid labeling, irrespective of whether the protein is modified in

solution or in adsorbed state. Accordingly, a shift in the solvent accessibility of a residue in an adsorbed protein can be characterized by its profile value as determined by equation 6.6.

$$\text{Profile} = \log\left(\frac{I_{ads}}{I_{soln}}\right) \tag{6.6}$$

If the I_{soln} from equation 6.5 was found to be less than 0.10 (which was considered to be the limit of detection), a low ceiling threshold value of 0.10 was designated in order to avoid dividing by zero in equation 6.6.

6.2.3.6. Relating the Profile of Target Amino Acids to the Configuration of Adsorbed Protein.

A given residue's profile must be understood to represent an averaged response of all the configurations that the adsorbed protein adopts on a given surface. A positive shift in the profile of a given residue indicates that on average it has more solvent exposure after being adsorbed compared to when in solution, while a negative shift in its profile indicates that on average it has lower solvent exposure in its adsorbed state compared to solution.

The expected range of I_{ads}/I_{soln} values is from 0.1 to 10. Ideally, if labeling within the adsorbed and native states of the protein is similar, the I_{ads}/I_{soln} value is expected to be equal to 1.0. However for modification of residues within the solution, variability in I_{soln} measurement of about 0.25 (95% confidence interval (C.I.) about the mean) was obtained. Since reacting conditions between different modifications in the adsorbed and solution state were kept identical, similar variability in labeling within solution was also expected in the adsorbed state of the protein. Therefore, we consider

I_{ads}/I_{soln} values beyond the range of 0.75 (i.e., 1 - C.I.) to 1.25 (i.e., 1 + C.I.) as representing a significant change in solvent accessibility. Among the I_{ads}/I_{soln} values that represent significant changes in solvent accessibility (i.e., 0.1 to 0.75 and 1.25 to 10), the I_{ads}/I_{soln} values 5x higher or lower than the native state were arbitrarily chosen to represent a greater degree of difference in labeling. These metrics are listed in Table 6.1.

Table 6.1. Metrics to determine the configuration of adsorbed protein based on its labeling profile. $\mathbf{I_{ads}/I_{soln}}$ values between 0.75 and 1.25 were considered to not be significantly different than the native solution-state structure. $\mathbf{I_{ads}/I_{soln}}$ values that were 5x higher or lower than the native solution-state condition are designated as undergoing a high level of change.

$\mathbf{I_{ads}/I_{soln}}$	$\mathbf{Profile = \log[I_{ads}/I_{soln}]}$	Solvent Exposure of Residues	Physical Meaning
≥ 5.0	≥ 0.70	More than the native state	Structural unfolding or Core Unfolding
1.25 – 5.0	0.10 – 0.70		
0.75 – 1.25	-0.12 – 0.10	Similar to the native state	Native structure
0.20 – 0.75	-0.12 – -0.70	Less than the native state	Structural refolding or Orientation shift
≤ 0.20	≤ -0.70		

As noted in Table 6.1, a positive profile value for a designated amino acid is indicative of an adsorption-induced increase in the solvent accessibility of its side group, which implies that, on average, a tertiary unfolding event has taken place in that location of the protein. In contrast, a negative shift in the profile indicates that adsorption has reduced the solvent accessibility of the designated amino acid's side chain, which implies that this part of the protein has been sterically blocked by either the surface (i.e.,

orientation effect) or a neighboring protein (i.e., protein-protein effect), causing this side chain to be covered by neighboring amino acid residues.[7, 18]

6.2.3.7. Visualization of the Adsorption Induced Structure of Protein

By sequentially mapping the positive and negative profile shifts in the protein following adsorption, the orientation of protein on an adsorbent surface can be inferred by hierarchically mapping the amino acid profiles for the protein, with the residues showing the most negative shift in profile being oriented towards the surface or towards a closely associated neighboring adsorbed protein. Indications of the sites in the protein's structure undergoing adsorption-induced tertiary unfolding are then determined from the locations of the amino acids with positive profile values. Accordingly, the profile values for the combined set of targeted amino acids for HEWL were mapped onto the native structure of the protein for visualization, which was represented by the Protein Data Bank's tertiary structure model of HEWL, 193l, with UCSF Chimera used as the visualization software.[19-21]

6.2.4. Statistical Analysis

The mean and 95% confidence interval (CI) for each measurement were calculated for each set of experimental data collected. Statistical differences were determined using a Student's unpaired t-test with values of $p \leq 0.05$ considered to be statistically significant.

6.3 RESULTS AND DISCUSSION

6.3.1. Surface Characterization.

Table 5.1 presents the results analyzed by the characterization techniques applied to the surfaces used in this study. All of the measured values reported in Table 5.1 fall within the expected range.

6.3.2. Protein Characterization

In this study, HEWL was adsorbed to glass, HDPE, and PMMA surfaces from two different solution concentrations (0.03 mg/ml and 1.00 mg/ml) to obtain different degrees of surface coverages and associated different degrees of protein-protein interaction effects on the surface. Each surface was exposed to HEWL in solution for 2 h to form the adsorbed layer of protein, gently rinsed to remove loosely bound protein, following which adsorbed layer of HEWL on each surface was placed under protein-free buffer solution for 15 h to allow the adsorbed protein to further equilibrate on the surface. Subsequently, CD, AAL/MS, and bioactivity assays were applied to characterize the adsorbed orientation and conformation of HEWL on these surfaces and these analyses were then used to provide insights into the causes of the measured loss of HEWL bioactivity following adsorption.

Surface coverage, secondary structural content and ternary structural shifts of adsorbed HEWL were characterized using circular dichroism (CD) and AAL/MS techniques. The effect of amino acid labeling on the HEWL structure were also assessed using CD. Unlabeled HEWL in PPB was used as the control.

6.3.2.1 Secondary Structural Content of Adsorbed Proteins

Table 6.2 presents the quantified results on the secondary structural content and amount of HEWL adsorbed on these surfaces. Fig. 6.1 shows the CD spectra for HEWL on glass, HDPE and PMMA surfaces when adsorbed from high (1.00 mg/mL) and low (0.03 mg/mL) solution concentrations.

Table 6.2. Secondary structure content, surface coverage, and relative enzymatic activity for adsorbed HEWL from two different protein solution concentrations (0.03 and 1.00 mg/ml) on (a) glass, (b) HDPE, and (c) PMMA (N=3; average ± 95% C.I. values). Retabulated with permission from Ref. 22. Copyright 2014 Acta Materialia Inc., published by Elsevier Ltd.

Surface	Solution concentration (mg/ml)	Helices* (%)	Sheets* (%)	Surface coverage (μg/cm^2)**	Relative Enzymatic Activity (%)
GLASS	0.03	4 (2)	42 (3)	0.045 (0.026)	12 ± 5
	1.00	22 (4)	30 (4)	0.135 (0.026)	31 ± 14
HDPE	0.03	22 (3)	28 (3)	0.066 (0.021)	39 ± 9
	1.00	12 (3)	33(4)	0.094 (0.036)	17 ± 8
PMMA	0.03	39 (3)	16 (4)	0.047 (0.011)	54 ± 22
	1.00	22 (4)	28 (3)	0.167 (0.032)	66 ± 9

*The helical and sheet content of HEWL in solution was found to be about 38% (± 2%) and 16 % (± 2%) respectively, which is very close to the reported solution-state secondary structure from the protein data bank (PDB ID: 193L: 40% helix, 10% sheet).[21, 23] **The theoretical full surface coverage of HEWL on adsorption in 'side-on' and 'end-on' orientations, was determined to be 0.17 μg/cm^2 (τ_{side}) and 0.26 μg/cm^2 (τ_{end}) respectively.

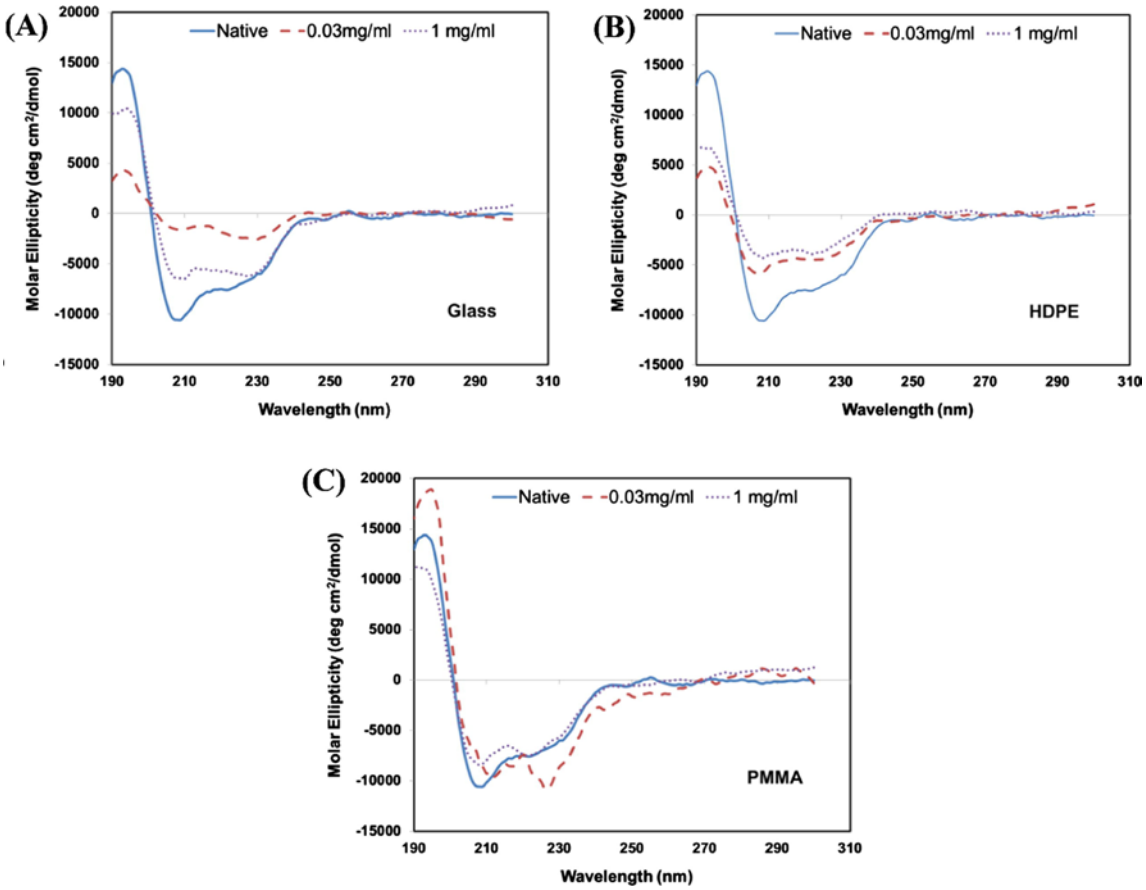

Figure 6.1. CD spectra for HEWL adsorbed on (A) glass, (B) HDPE, and (C) PMMA surfaces when adsorbed from 0.03 mg/ml and 1.00 mg/ml bulk solution concentrations. (Average of 3 spectra). Redrawn with permission from Ref. 22. Copyright 2014 Acta Materialia Inc., published by Elsevier Ltd.

As shown in Table 6.2, adsorption of HEWL resulted in a significant shift in its secondary structure on each surface and for each solution concentration. These results reflect the combined influences of protein–surface interactions, protein–protein interactions (PPI), and internal protein stability effects.[24] When HEWL was adsorbed from a 1.00 mg/ml solution concentration, the resulting surface coverage of adsorbed protein on each surface was within 53% of a saturated, close–packed monolayer with side–on protein orientation. In contrast to this, when adsorbed from 0.03 mg/ml solution

and equilibrated under protein-free buffer conditions, the surface coverage of the HEWL was about one third of that was adsorbed from 1.00 mg/ml solution conditions (e.g., 0.05 μg/cm^2, nearly 3x less than the closed-packed side-on arrangement of 0.17 μg/cm^2). These differences suggest that PPI effects have a much greater influence on the adsorbed state of the HEWL when it was adsorbed from the 1.00 mg/ml solution compared to 0.03 mg/ml.

As clearly evident from the results presented in Table 6.2, the surface coverage of HEWL and the type of surface that it was adsorbed on had a profound influence on both its secondary structure and bioactivity. Interestingly, the degree of surface coverage had a completely different effect on the adsorbed-state bioactivity on each of these three different surfaces, with increased surface coverage enhancing bioactivity on glass, decreasing bioactivity on HDPE, and having little effect on PMMA.

6.3.2.1.a Correlation between the Secondary Structure and Activity of Adsorbed HEWL

The key items of interest for an adsorbed enzyme is its activity and the factors influencing its activity. The native-state structure of the HEWL resembles a kidney shape, with three of the primary active site residues (E35, D52, and D101) laying in the concave cleft of the enzyme (Fig. 6.2a). As indicated by its PDB structure, one of the three residues involved in catalysis lies within α-helix in the protein structure (Fig. 6.2a; E35). Many studies have indicated that the loss in secondary structural content, especially helices, is associated with the loss in native-state activity. Fig. 6.2b plots the data from Table 6.2 to investigate the relationships between the adsorbed secondary structures (i.e.,

helix and the sheets) and the observed enzymatic activity of HEWL on our three different surfaces.

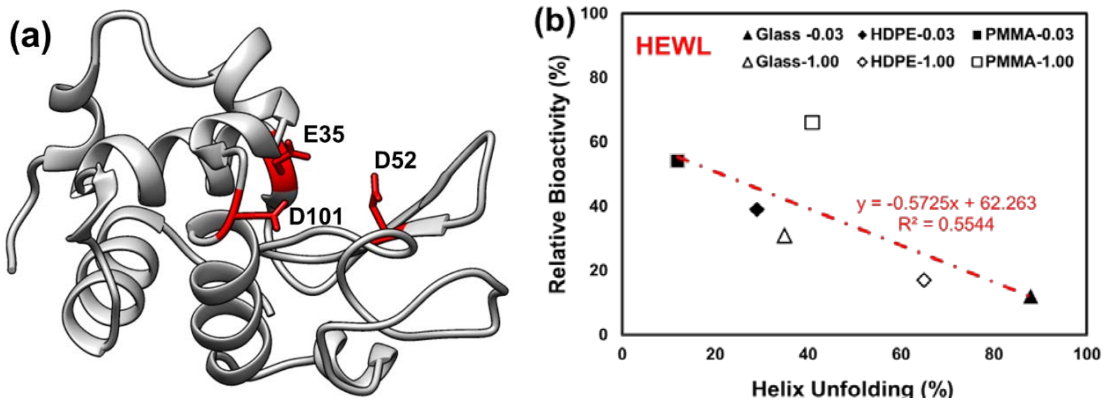

Figure 6.2: (a) Ribbon diagram of the three-dimensional structure of HEWL (PDB ID: 193L[21]).[25] The three residues most important for catalysis: E35, D52, and D101 are marked in red, and (b) % Relative bioactivity (y-axis) vs. % secondary structural content (helix and sheet) (x-axis) in the adsorbed HEWL layers on different surfaces. The helix and β-sheet content of HEWL in solution was found to be ~38% (± 2%) and 16% (± 2%) (N = 3, averaged 95% C.I. values = ± 4 % helicity for each data point, averaged 95% C.I. values = ± 9% for bioactivity).[13] Redrawn with permission from Ref 25. Copyright 2015 AVS.

As indicated from the results presented in Fig. 6.2b, the loss in native enzymatic activity of HEWL is correlated to the secondary structural content within the protein, with the enzyme tending to lose its native-state bioactivity as the adsorbed-state of the enzyme deviated more and more away from its native-state structure (i.e., loss in helicity). These results suggest that the enzymatic activity of HEWL on these three surfaces is primarily caused by conformational changes in the enzyme's bioactive site as opposed to adsorbed orientation. While these data provide important structural-level insights into the cause of the adsorption-induced loss of HEWL bioactivity, they do not provide any direct information regarding how these

structural changes may influence the actual active site of the enzyme. If conformational changes of the active site are indeed primarily causing this loss in bioactivity, then it can be expected that these changes may be detectable by measuring changes in the solvent accessibility of the three key amino acids that are involved in HEWL's catalytic site, which can be probed using AAL/MS.

6.3.2.2 Conformational Distortion of the Bioactive Site Probed by AAL/MS

AAL/MS provides an approach to identify areas in a protein that undergo adsorption-induced conformational changes and protein orientation as reflected in changes in the solvation profile of targeted amino acid residues. In particular, an increase in the solvent accessibility of amino acid residues that are present within the active site of a protein indicate conformational unfolding of the binding site as a likely cause of adsorption-induced loss in bioactivity. Alternatively, a decrease in solvent accessibility of the residues within the active site indicate loss of bioactivity due to steric hindrance from either the surface or neighboring adsorbed proteins.

In this section, the capability of AAL/MS technique to provide additional insights into the loss of HEWL bioactivity when adsorbed on surfaces to complement the data presented in the previous section, is demonstrated.

6.3.2.2.a.1 Effect of Labeling on the Structure of Proteins in Solution.

Fig. 6.3 shows the effect of amino acid labeling on the solution structure of HEWL under the reaction conditions used in the current study as assessed using CD. The effect of labeling agents on the solution structure of HEWL was found to be

negligible, thus indicated that the applied labeling processes did not significantly alter lysozyme's solution-state structure.

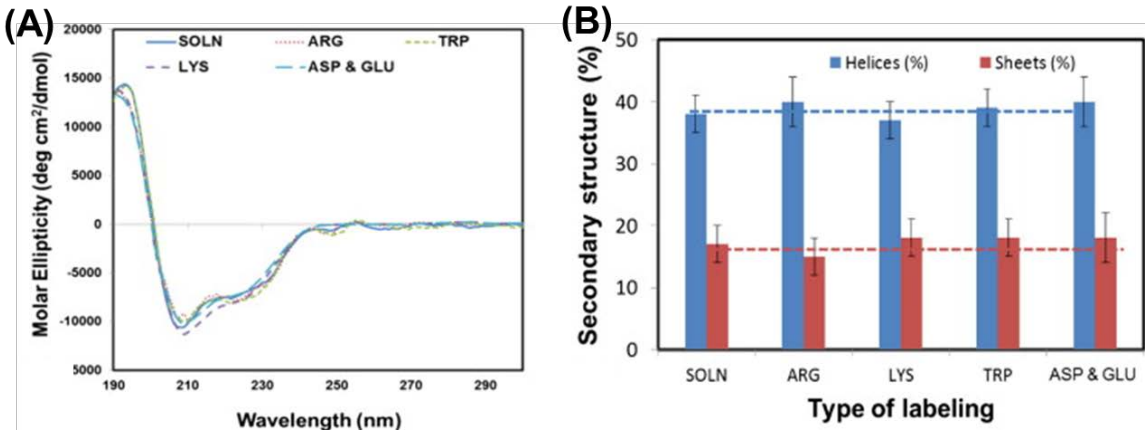

Figure 6.3. The effect of amino acid labeling (ARG-arginine, LYS-lysine, TRP-tryptophan, ASP-aspartic acid and GLU-glutamic acid) on the structure of HEWL in solution is shown. The native structure of HEWL is represented by the SOLN CD spectrum. (A) Average of 6 Spectra. (B) Quantification of the secondary structures within amino acid labeled HEWL. No significant difference in the structure of amino acid labeled HEWL was observed relative to its unlabeled solution state (N = 6, error bar presents the mean ± 95% confidence interval, C.I.). Redrawn with permission from Ref. 22. Copyright 2014 Acta Materialia Inc., published by Elsevier Ltd.

6.3.2.2.a.2 Solvent Accessibility of Residues in Solution.

A total of 32 residues which were distributed across the protein were labeled in solution (see Section C.1 in the appendix). The I_{soln} determined following the baseline correction for each of the target residues compared very well to its theoretical solvent exposure (see Table C.8 in the appendix). Based on the I_{soln}, charged residues like Arg (R5, R14, R21, R45, R68, R73, R112, R114, R125, and R128), Lys (K1, K13, K33, K97, and K116), Asp (D48, D87, D101, and D119) and, Glu (E7) were found to be highly solvent exposed as expected due to their presence on the outer surface of the protein. However some of the charged residues that have a specific role as a catalytic site were

found to be less solvent exposed or partially buried (D18, E35, D52, R61, D66, and K96).[26-28]

Most of the relatively hydrophobic Trp groups were found to be less solvent exposed or buried inside the protein structure (W28, W108, W111, and W123), while W62 and W63, which lie within the binding cleft of HEWL, were found to be moderately solvent exposed. The buried Trp groups help provide core stability for the protein through hydrophobic interactions, while those that are more solvent exposed (i.e., W62 and W63), are known to be important for substrate binding.[26-28] Fig. 6.4 illustrates these effects by presenting a space-filling model of HEWL with the targeted amino acid residues color coded by their degree of solvent exposure as determined by the AAL/MS results.

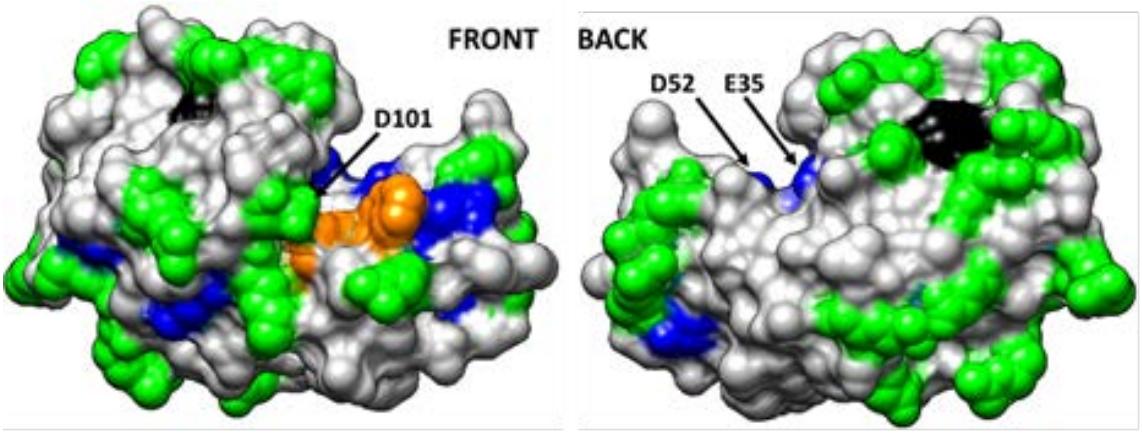

Figure 6.4. Spacefilled model of HEWL (PDB ID: 193L) with amino acid residues color coded by their solvent accessibility as determined from targeted amino acid labeling in solution.[21] Color coding: charged amino acid residues (Asp, Glu, Lys, Arg) with high solvent accessibility (green) and moderate solvent accessibility (blue), Trp residues with high solvent accessibility (orange) and low solvent accessibility (black). Non–targeted amino acid residues are color coded in light grey. This Figure is illustrated using UCSF Chimera.[19] The arrows point out the location of the three key amino acid residues that provide the catalytic function of the enzyme (E35, D52, D101). Redrawn with permission from Ref. 22. Copyright 2014 Acta Materialia Inc., published by Elsevier Ltd. See Table C.8 in the appendix.

6.3.2.2.b.1 Effect of Labeling on Structure of Adsorbed Proteins

Table 6.3 shows the effects of the labeling agents on the helical content of adsorbed HEWL. The effect of labeling agents on the adsorbed structure of HEWL on different surfaces was found to not significantly alter lysozyme's secondary structure compared to its unlabeled adsorbed state.

Table 6.3. Helical content (%) within the adsorbed HEWL before and after labeling (N = 3, error bar presents the mean ± 95% confidence interval, C.I. in parentheses). Retabulated with permission from Ref. 22. Copyright 2014 Acta Materialia Inc., published by Elsevier Ltd

Surface	Solution concentration (mg/ml)	No label (%)	Arg label (%)	Lys label (%)	Trp label (%)	Asp/Glu label (%)
GLASS	0.03	4 (2)	5 (2)	4 (2)	4 (2)	5 (3)
	1.00	22 (4)	23 (4)	22 (4)	22 (4)	21 (4)
HDPE	0.03	22 (3)	21 (4)	22 (3)	22 (3)	23 (3)
	1.00	12 (3)	13 (3)	12 (3)	12 (3)	13 (3)
PMMA	0.03	39 (3)	40 (4)	40 (3)	39 (3)	41 (4)
	1.00	22 (4)	23 (3)	23 (4)	22 (4)	21 (4)

6.3.2.2.b.2 Solvent Accessibility of Residues in Adsorbed HEWL

Profile values for each of the targeted amino acids in HEWL were determined from the mass spectrometry data through the application of equations 6.1-6.6. For each surface, ≥ 90% of the adsorbed proteins were removed and 100% sequence coverage was obtained following tryptic digestion (see Table C.2 in the appendix). Fig. 6.5 shows the labeling profile of the targeted residues in HEWL on each of the different surfaces when adsorbed from 0.03 mg/mL and 1.00 mg/mL protein solution concentrations, respectively. The data presented in Fig. 6.5 were further separated into Tables 6.4 and 6.5

for HEWL adsorbed from the 0.03 mg/ml and 1.00 mg/mL solution concentrations, respectively, according to the divisions listed in Table 6.1.

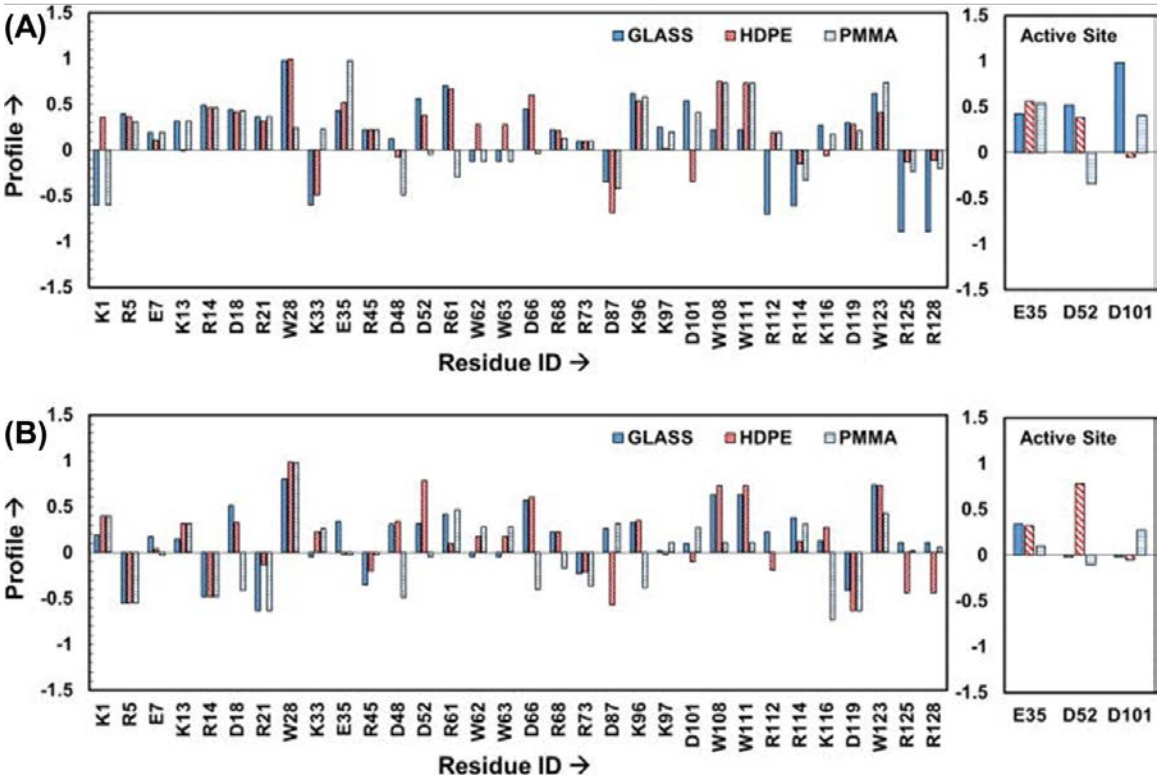

Figure 6.5: Labeling profile of the targeted residues in HEWL on glass, PMMA and HDPE surfaces when adsorbed from 0.03 mg/mL (top plot) and 1.00 mg/mL (bottom plot) protein solutions. Residue ID refers to the location of targeted amino acids in the primary sequence of the protein. The residues within the active site of HEWL are shown separately in the right-hand plot to more clearly show their response. Profiles within about ± 0.1 of zero can be considered to be not significantly different from the solution state (n = 3). Profiles beyond ± 0.5 represent greater than 3-fold change to the native-state solvent exposure, which is a highly significant difference (p-value < 0.0001). Residues showing no difference in their solvation between solution and the adsorbed states have profile values equal to 0. Redrawn with permission from Ref 25. Copyright 2015 AVS.

Table 6.4: Overview of the labeling profile in HEWL on each surface when adsorbed from 0.03 mg/mL solution concentration. The profiles are grouped according to the classification specified in Table 6.1 in the increasing order of solvent exposure (left to right). The single letter followed by the number represents the standard one letter amino acid notation for the targeted amino acids, i.e (R-arginine, K-lysine, E-glutamic acid, D-aspartic acid, W-tryptophan) along with the amino acid position in the proteome primary

sequence. Red text indicates a residue involved with the active site. Retabulated with permission from Ref. 22. Copyright 2014 Acta Materialia Inc., published by Elsevier Ltd.

Surface	Profile ≤ -0.72	-0.72 < Profile < -0.12	-0.12 ≤ Profile ≤ 0.1	0.1 < Profile < 0.7	Profile ≥ 0.7
GLASS	R112, R125, R128	K1, K33, D87, R114	D48, W62, W63, R73	R5, E7, K13, R14, D18, R21, E35, R45,D52, D66, R68, K96, K97, D101, W108, W111, K116, D119, W123	W28, R61
HDPE	D87	K33, D101, R114	E7, K13, D48, R73, K97, K116, R125, R128	K1, R5, R14, D18, R21, E35, R45, D52, W62, W63, D66, R68, K96, R112, D119, W123	W28, R61, W108, W111
PMMA		K1, D48, R61, D87, R114, R125, R128	D52, W62, W63, D66, R68, R73, K116	R5, E7, K13, R14, D18, R21, W28, K33, R45, K96, K97, D101, R112, D119	E35, W108, W111, W123

Table 6.5. Overview of the labeling profile in HEWL on each surface when adsorbed from 1.00 mg/mL solution concentration. The profiles are grouped according to the classification specified in Table 6.1 in the increasing order of solvent exposure (left to right). The single letter followed by the number represents the standard one letter amino acid notation for targeted amino acids, i.e (R-arginine, K-lysine, E-glutamic acid, D-aspartic acid, W-tryptophan) along with the amino acid position in the proteome primary sequence. Red text indicates a residue involved with the active site. Retabulated with permission from Ref. 22. Copyright 2014 Acta Materialia Inc., published by Elsevier Ltd.

Surface	Profile ≤ -0.72	-0.72 < Profile < -0.12	-0.12 ≤ Profile ≤ 0.1	0.1 < Profile < 0.7	Profile ≥ 0.7
GLASS		R5, R14, R21, R45,□R73, D119	K33, W62, W63, K97, D101, K116, R125, R128	K1, E7, K13, D18, E35, D48, D52, R61, D66, R68, D87, K96, W108, W111, R112, R114	W28, W123
HDPE		R5, R14, R45, R73, D87, R112, D119 R125, R128	E7, R21, E35, R61, K97, D101	K1, K13, D18, K33, D48, W62, W63, D66, R68, K96, R114, K116	W28, D52, W108, W111, W123
PMMA	K116	R5, R14, D18, R21, D48, D66, R73, K96, D119	E7, E35, R45, D52, R68, K97, W108, W111, R112, R125, R128	K1, K13, K33, R61, W62, W63, D87, D101, R114, W123	W28

The labeling agents for the reacting conditions used in the current study were not found to affect the structure of HEWL significantly in the solution or adsorbed state (Fig. 6.3 and Table 6.3, respectively). Thus the profile shifts can be considered to be solely

mediated by the shift in solvent exposure of the residue as a result of the adsorption process. As shown in Fig. 6.5, the labeling profiles reveal stark differences in residue solvent accessibility between each surface and when adsorbed from 0.03 mg/mL and 1.00 mg/mL solution conditions. The trends in HEWL behavior on the different surfaces and from different solution conditions were generally expected based on differences found in secondary structure behavior as demonstrated by our previous study using CD.[13] However, in contrast to CD, the AAL/MS technique is capable of providing molecular (or domain) level insights into the adsorbed configuration of a protein by correlating the resulting profile shifts to the known positions of the targeted amino acid residues within the protein's tertiary structure, while CD results only provide a scalar indication of the net change in secondary structural elements of the adsorbed protein layer.[13, 29]

When HEWL was adsorbed from a 1.00 mg/mL solution concentration followed by 15 h of equilibration in pure buffer, the resulting surface coverage of adsorbed protein on each surface was about equal to or slightly below that of a saturated close-packed monolayer with side-on orientation (Table 6.2). In contrast to this, when adsorbed from 0.03 mg/mL solution and equilibrated under pure buffer conditions, the surface coverage of the HEWL was about one third that of the HEWL adsorbed from the 1.00 mg/mL solution conditions (Table 6.3). Based on these surface coverage differences, we can thus expect a much greater degree of protein-protein effects blocking access to the amino acid residues on the ends and sides of HEWL adsorbed from the 1.00 mg/mL solution compared to the 0.03 mg/mL solution.

6.3.2.2.c. Visualizing the Shift in Solvent Accessibility of Residues and Correlating those Shifts to the Adsorbed Configuration of HEWL

In order to illustrate how the AAL/MS results can be used to provide insight into the amino acid-level mechanisms influencing the effect of adsorption on the activity of the enzyme, Figs. 6.6 and 6.7 presents the native-state structure of HEWL with the targeted amino acids color-coded according to the profile values specified in Tables 6.4 and 6.5, and represents areas in HEWL undergoing varying extent of solvation shift when adsorbed on different surfaces. Amino acid residues exhibiting more than a 5-fold increase in solvent accessibility compared to the solution-state accessibility are colored-coded in blue while residues exhibiting more than a 5-fold decrease in solvent accessibility are color-coded in yellow. Similarly, amino acid residues exhibiting moderate shift in solvent accessibility were color coded in orange and green to represent decrease or increase in solvent accessibility of the residues, respectively. All the other targeted residues with solvent accessibility within about ± 0.25 of zero were considered to be not significantly different from that of the native state, and were colored in grey. The non-targeted residues were colored in white.

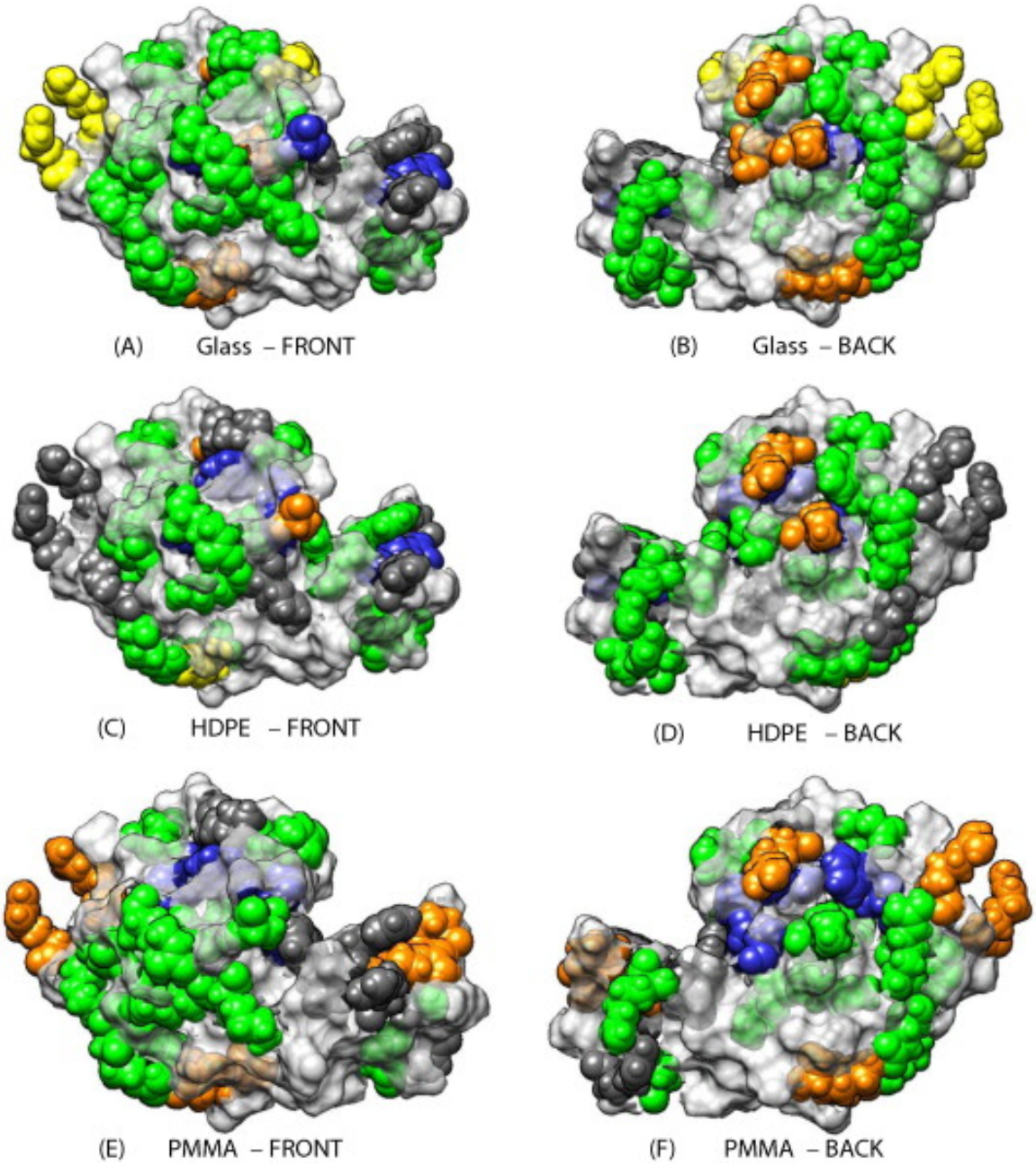

Figure 6.6. Representation of the solvation profiles in residues for space filled model of HEWL from protein data bank (PDB ID: 193l) when adsorbed from 0.03 mg/ml on (A, B) Glass, (C, D) HDPE and (E, F) PMMA surfaces.[20-21] Residue color code: yellow (--), orange (-), grey (native state), green (+), blue (++) and white (non-targeted). Illustrated using UCSF Chimera.[19] The arrows point out the location of the three key amino acid residues that provide the catalytic function of the enzyme (E35, D52, D101). Redrawn with permission from Ref. 22. Copyright 2014 Acta Materialia Inc., published by Elsevier Ltd.

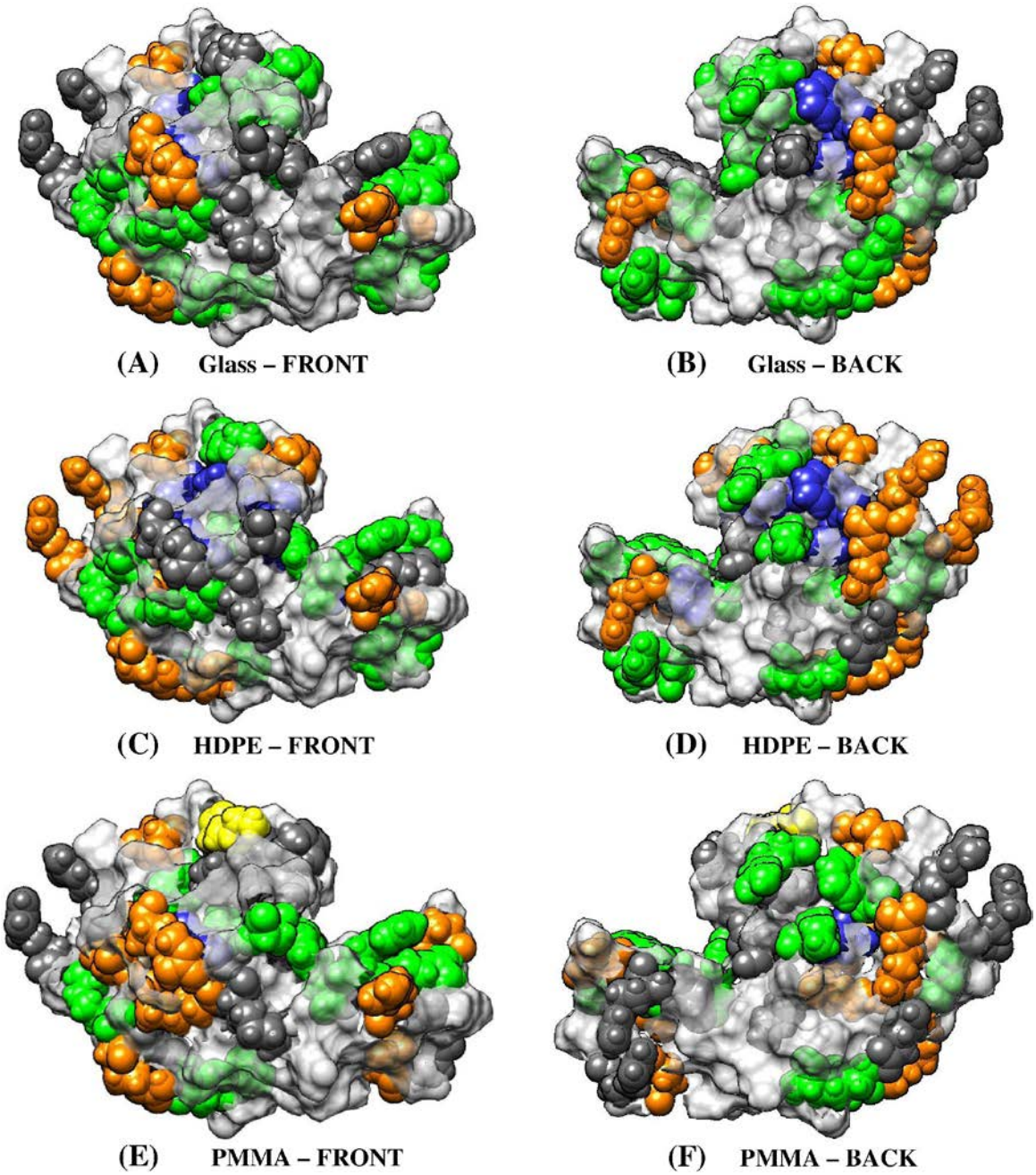

Figure 6.7. Representation of the solvation profiles in residues for space filled model of HEWL from protein data bank (PDB ID: 193l) when adsorbed from 1.00 mg/ml on (A, B) Glass, (C, D) HDPE and (E, F) PMMA surfaces.[20-21] Residue color code: yellow (--), orange (-), grey (native state), green (+), blue (++) and white (non-targeted). Illustrated using UCSF Chimera.[19] The arrows point out the location of the three key amino acid residues that provide the catalytic function of the enzyme (E35, D52, D101). Redrawn with permission from Ref. 22. Copyright 2014 Acta Materialia Inc., published by Elsevier Ltd.

The data presented in Tables 6.4 and 6.5 for the amino acids with negative profiles (i.e., loss in solvent accessibility) are visually depicted as color-coded by yellow and orange in Figs. 6.6 and 6.7 on the protein's native-state structure, respectively, with this loss in solvent accessibility caused by either close contact with the adsorbent surface or with neighboring adsorbed proteins. Comparing the results for the non-charged surfaces (HDPE and PMMA) between the 1.00 and 0.03 mg/mL samples clearly shows evidence of the additional blocking of amino acid solvent accessibility. As noted above, the HEWL adsorbed from 1.00 mg/mL solution had a surface coverage consistent with near-saturated close-packed side-on orientation while the HEWL layer adsorbed from 0.03 mg/mL had an surface coverage much lower than that for saturated monolayer coverage. (Table 6.2) The results presented in Fig. 6.6 and 6.7 thus suggest that the amino acid residues displaying negative profile values from the 1.00 mg/mL conditions (Fig. 6.7) can be considered to be a result of both protein-protein and adsorbed orientation effects blocking solvent accessibility (HDPE – 28% of the labeled residues, PMMA – 31% of the labeled residues), while those with a negative profile from the 0.03 mg/mL conditions (Fig. 6.6) can be considered to primarily represent amino acids with solvent accessibility blocked due to adsorbed protein orientation alone (HDPE – 13% of the labeled residues, PMMA – 22% of the labeled residues).

The distribution of amino acids with decreased solvent accessibility is distinctly different for HEWL on the negatively charged glass surface, with adsorption under low solution concentration conditions (22% of the labeled residues) resulting in HEWL adsorbing predominantly along one patch of positively charged amino acid residues that

are positioned both at one end and along one side of the protein. When adsorbed from the higher solution concentration, these profiles shift towards being more concentrated along the ends of the protein but with a lesser degree of loss of solvent accessibility (19% of the labeled residues), presumably due to protein-protein effects interfering with the ability of the HEWL to be oriented by the electrostatic attraction by the surface.

The data presented in Tables 6.4 and 6.5 and illustrated in Figs. 6.6 and 6.7 also depict the regions of the HEWL that underwent a high degree of adsorption-induced tertiary unfolding (color coded green and blue). As indicated by the number of amino acid residues with positive profiles, it is apparent that HEWL underwent a slightly greater degree of tertiary unfolding on the surfaces (glass – 66% of the labeled residues, HDPE – 63% of the labeled residues, PMMA – 56% of the labeled residues) when adsorbed from lower solution concentration conditions. This behavior can be understood based on the increased time that an individual protein has on average to undergo adsorption-induced unfolding prior to reposition of a neighboring molecule to blocking further spreading on the surface. In addition to these observations, the results also suggest that the glass (44% of the labeled residues) and HDPE surfaces (53% of the labeled residues) induce a greater degree of tertiary unfolding of HEWL than the PMMA surface (34% of the labeled residues), especially under high solution concentration conditions. These results are also intuitively very reasonable given that electrostatic and hydrophobic effects from the glass and HDPE surfaces, respectively, can be expected to exert greater perturbing forces upon the protein than those induced by the PMMA surface, which is neutrally charged and only moderately hydrophobic.

Similarly, the very same trend was observed with the residues E35, D52, and D101 in the active site, with these residues undergoing more solvent exposure at lower surface coverages than when adsorbed at higher surface coverages. These shifts in solvent exposure clearly indicate adsorption-induced conformational unfolding of the active site. Such conformational unfolding can lead to a loss in bioactivity. In addition, the fact that the profiles for the three key amino acids in the active site are all positive for HEWL on glass and HDPE surfaces indicate that access to the active site was not sterically blocked by either surface or neighboring proteins. But on the PMMA surface, the reduced bioactivity of HEWL at low surface coverage as opposed to the bioactivity of HEWL on these surfaces at higher surface coverage could also be explained by the conformational unfolding of the active site. At low surface coverages of HEWL on PMMA surface, the conformational shift lead to the steric blocking of the residue D52 and exposure of residues E35 and D101 within the catalytic site. However, at higher surface coverages, the solvent exposure of the residues within the HEWL on the PMMA surfaces were relatively nearer to its native state, and would explain the increased retention of its active state despite undergoing more unfolding on these surfaces at higher surface coverages.

The results presented in this chapter are directly in line with the observations obtained from many other experimental and theoretical studies by other groups on the adsorption behavior of HEWL.[2, 30-37] For example, it has been demonstrated previously that on negatively charged hydrophilic surfaces similar to glass, the orientation of HEWL on these surface at lower surface coverages is mediated by electrostatic interactions[2, 30]

and is capable of undergoing conformational loss.[32-34, 37] Similarly, the adsorption of HEWL on hydrophobic surfaces like polyethylene at low surface coverages is considered to be mediated by hydrophobic interactions and could induce conformation loss in the region surrounding the bioactive site.[31, 35-36] However, none of these prior studies have quantitatively connected the role of these individual molecular-level events on the bioactive state of adsorbed HEWL. As we have demonstrated in our combined set of studies, the synergistic use of CD, AAL/MS, and adsorbed-state spectrophotometric assays provide a powerful approach to investigate how adsorption influences the molecular structure of proteins and how this subsequently causes changes in bioactivity. Obviously these combined methods do not provide a fully comprehensive description of the influence of adsorption on protein structure and bioactivity and continued development work is certainly called for to provide further understanding of these complex issues.

6.4 CHAPTER SUMMARY AND CONCLUSION

This study demonstrates the expanded capability of AAL/MS to provide molecular-level information on the orientation and tertiary structure of proteins adsorbed on a surface. Using this technique, it was quantitatively demonstrated that adsorption-induced effects on the structure of HEWL at the amino acid residue level depends on the type of surface to which it is adsorbed and the surface coverage of the adsorbed protein layer. The results from our studies indicate that protein-protein interaction effects tend to (1) stabilize the structure of HEWL on a silica glass surface, which can be expected to exhibit strong hydrogen bond and electrostatic interactions with proteins; (2) have little

influence on the structure of HEWL on strongly hydrophobic surfaces, such as HDPE; and (3) actually destabilize the structure of HEWL on a PMMA surface, which has only moderate hydrogen bonding and hydrophobic character.

The results presented for HEWL on all the surfaces also both complement and support the CD-bioactivity results. These combined results indicate that the greater loss in HEWL activity on different surface when adsorbed at different solution concentrations is caused by greater adsorption-induced conformational unfolding of the active site. The AAL/MS results further indicate that the loss in bioactivity under both the low and high surface coverage conditions for glass and HDPE surfaces is not due to steric hindrance of the active site due to adsorbed orientation or PPI on the surface. However, the loss in bioactivity on the PMMA surfaces at lower surface coverages is probably due to the combined effects of tertiary structural shifts and steric hindrance.

Of particular importance, the developed technique allows the labeling profiles from multiple amino acids within an adsorbed protein to be combined together by normalizing their profiles to a common basis. This capability provides the potential to further expand this approach to a broader set of target amino acids so as to obtain additional detailed information to probe the structure of adsorbed protein layers on surfaces to further our understanding of protein adsorption behavior.

6.5 REFERENCES

1. Latour, R. A. Biomaterials: Protein-Surface Interactions. In *The Encyclopedia of Biomaterials and Bioengineering*, 2 ed.; Bowlin, G. E. W. a. G. L., Ed.; Informa Healthcare, 2008; Vol. 1, pp 270-284.

2. Rabe, M.; Verdes, D.; Seeger, S. Understanding protein adsorption phenomena at solid surfaces. *Adv. Colloid Interface Sci.* **2011,** *162* (1-2), 87-106.

3. Gray, J. J. The interaction of proteins with solid surfaces. *Curr. Opin. Struct. Biol.* **2004,** *14* (1), 110-5.

4. Pelton, J. T.; McLean, L. R. Spectroscopic methods for analysis of protein secondary structure. *Anal. Biochem.* **2000,** *277* (2), 167-76.

5. Xu, J.; Bowden, E. F. Determination of the orientation of adsorbed cytochrome C on carboxyalkanethiol self-assembled monolayers by in situ differential modification. *J. Am. Chem. Soc.* **2006,** *128* (21), 6813-22.

6. Scott, E. A.; Elbert, D. L. Mass spectrometric mapping of fibrinogen conformations at poly(ethylene terephthalate) interfaces. *Biomaterials* **2007,** *28* (27), 3904-17.

7. Fears, K. P.; Sivaraman, B.; Powell, G. L.; Wu, Y.; Latour, R. A. Probing the conformation and orientation of adsorbed enzymes using side-chain modification. *Langmuir* **2009,** *25* (16), 9319-27.

8. Mendoza, V. L.; Vachet, R. W. Probing protein structure by amino acid-specific covalent labeling and mass spectrometry. *Mass Spectrom. Rev.* **2009,** *28* (5), 785-815.

9. Yan, X.; Watson, J.; Ho, P. S.; Deinzer, M. L. Mass spectrometric approaches using electrospray ionization charge states and hydrogen-deuterium exchange for determining protein structures and their conformational changes. *Mol. Cell. Proteomics* **2004,** *3* (1), 10-23.

10. Gromiha, M. M.; Ahmad, S.; Suwa, M. Application of residue distribution along the sequence for discriminating outer membrane proteins. *Comput. Biol. Chem.* **2005,** *29* (2), 135-42.

11. Duncan, M. W.; Aebersold, R.; Caprioli, R. M. The pros and cons of peptide-centric proteomics. *Nat. Biotechnol.* **2010,** *28* (7), 659-64.

12. Iwasaki, Y.; Nakano, Y.; Mochizuki, K.; Nomoto, M.; Takahashi, Y.; Ito, R.; Saito, K.; Nakazawa, H. A new strategy for ionization enhancement by derivatization for mass spectrometry. *J. Chromatogr. B* **2011,** *879* (17-18), 1159-65.

13. Wei, Y.; Thyparambil, A. A.; Latour, R. A. Quantification of the influence of protein-protein interactions on adsorbed protein structure and bioactivity. *Colloids and Surfaces B: Biointerfaces* **2013,** *110*, 363-371.

14. Farkas, P.; Cizova, A.; Bekesova, S.; Bystricky, S. Comparison of EDC and DMTMM efficiency in glycoconjugate preparation. *Int. J. Biol. Macromol.* **2013,** *60* (0), 325-7.

15. Leitner, A.; Amon, S.; Rizzi, A.; Lindner, W. Use of the arginine-specific butanedione/phenylboronic acid tag for analysis of peptides and protein digests using matrix-assisted laser desorption/ionization mass spectrometry. *Rapid Commun. Mass Spectrom.* **2007,** *21* (7), 1321-30.

16. Suckau, D.; Mak, M.; Przybylski, M. Protein surface topology-probing by selective chemical modification and mass spectrometric peptide mapping. *Proc. Natl. Acad. Sci. USA* **1992,** *89* (12), 5630-4.

17. Rappsilber, J. The beginning of a beautiful friendship: cross-linking/mass spectrometry and modelling of proteins and multi-protein complexes. *J. Struct. Biol.* **2011,** *173* (3), 530-40.

18. Lins, L.; Thomas, A.; Brasseur, R. Analysis of accessible surface of residues in proteins. *Protein Sci.* **2003,** *12* (7), 1406-17.

19. Pettersen, E. F.; Goddard, T. D.; Huang, C. C.; Couch, G. S.; Greenblatt, D. M.; Meng, E. C.; Ferrin, T. E. UCSF Chimera--a visualization system for exploratory research and analysis. *J. Comput. Chem.* **2004,** *25* (13), 1605-12.

20. Bernstein, F. C.; Koetzle, T. F.; Williams, G. J. B.; Meyer, E. F.; Brice, M. D.; Rodgers, J. R.; Kennard, O.; Shimanouchi, T.; Tasumi, M. The protein data bank: A computer-based archival file for macromolecular structures. *J. Mol. Biol.* **1977,** *112* (3), 535-542.

21. Vaney, M. C.; Maignan, S.; Ries-Kautt, M.; Ducriux, A. High-resolution structure (1.33 A) of a HEW lysozyme tetragonal crystal grown in the APCF apparatus. Data and structural comparison with a crystal grown under microgravity from SpaceHab-01 mission. *Acta Crystallographica. Section D, Biological Crystallography* **1996,** *52* (Pt 3), 505-17.

22. Thyparambil, A. A.; Wei, Y.; Wu, Y.; Latour, R. A. Determination of orientation and adsorption-induced changes in the tertiary structure of proteins on material surfaces by chemical modification and peptide mapping. *Acta Biomaterialia* **2014,** *10* (6), 2404-2414.

23. Berman, H. M.; Westbrook, J.; Feng, Z.; Gilliland, G.; Bhat, T. N.; Weissig, H.; Shindyalov, I. N.; Bourne, P. E. The Protein Data Bank. *Nucleic Acids Research* **2000,** *28* (1), 235-242.

24. Wei, Y.; Thyparambil, A. A.; Latour, R. A. Quantification of the influence of protein-protein interactions on adsorbed protein structure and bioactivity. *Colloids and Surfaces B: Biointerfaces* **2013,** *110* (0), 363-371.

25. Thyparambil, A. A.; Wei, Y.; Latour, R. A. Experimental characterization of adsorbed protein orientation, conformation, and bioactivity. *Biointerphases* **2015,** *10* (1), 019002.

26. Levitt, M. Conformational preferences of amino acids in globular proteins. *Biochemistry (Mosc).* **1978,** *17* (20), 4277-85.

27. Fleming, P. J.; Richards, F. M. Protein packing: dependence on protein size, secondary structure and amino acid composition. *J. Mol. Biol.* **2000,** *299* (2), 487-98.

28. Redfield, C.; Dobson, C. M. Sequential proton NMR assignments and secondary structure of hen egg white lysozyme in solution. *Biochemistry (Mosc).* **1988,** *27* (1), 122-136.

29. Hlady, V. V.; Buijs, J. Protein adsorption on solid surfaces. *Curr. Opin. Biotechnol.* **1996,** *7* (1), 72-7.

30. Kubiak-Ossowska, K.; Mulheran, P. A. Mechanism of hen egg white lysozyme adsorption on a charged solid surface. *Langmuir* **2010,** *26* (20), 15954-65.

31. Sethuraman, A.; Vedantham, G.; Imoto, T.; Przybycien, T.; Belfort, G. Protein unfolding at interfaces: slow dynamics of alpha-helix to beta-sheet transition. *Proteins* **2004,** *56* (4), 669-78.

32. van der Veen, M.; Stuart, M. C.; Norde, W. Spreading of proteins and its effect on adsorption and desorption kinetics. *Colloids Surf. B. Biointerfaces* **2007,** *54* (2), 136-42.

33. Wu, X.; Narsimhan, G. Effect of surface concentration on secondary and tertiary conformational changes of lysozyme adsorbed on silica nanoparticles. *Biochim. Biophys. Acta* **2008,** *1784* (11), 1694-701.

34. Vertegel, A. A.; Siegel, R. W.; Dordick, J. S. Silica nanoparticle size influences the structure and enzymatic activity of adsorbed lysozyme. *Langmuir* **2004,** *20* (16), 6800-7.

35. Wei, T.; Carignano, M. A.; Szleifer, I. Lysozyme adsorption on polyethylene surfaces: why are long simulations needed? *Langmuir* **2011,** *27* (19), 12074-81.

36. Sharma, S.; Berne, B. J.; Kumar, S. K. Thermal and structural stability of adsorbed proteins. *Biophys. J.* **2010,** *99* (4), 1157-65.

37. Kim, D. T.; Blanch, H. W.; Radke, C. J. Direct imaging of lysozyme adsorption onto mica by atomic force microscopy. *Langmuir* **2002,** *18* (15), 5841-5850.

CHAPTER SEVEN

ADSORPTION-INDUCED CHANGES IN RIBONUCLEASE A STRUCTURE AND ENZYMATIC ACTIVITY ON SOLID SURFACES

Based on the published article: Wei Y., Thyparambil A.A., Wu Y., and Latour R.A., Adsorption-induced changes in ribonuclease A structure and enzymatic activity on solid surfaces, Langmuir, 30(49): 14849-14858 (2014);

7.1 INTRODUCTION

Ribonucleases, such as ribonuclease A (RNase A), which catalyzes the breakdown of the phosphodiester backbone of ribonucleic acid (RNA) into smaller components, are being investigated as potential chemotherapy agents.[1-3] RNase A has been shown to have a cytotoxic effect that is specific for many malignant tumor cells from in vitro experiments. Their effectiveness on tumor cells is believed to be due, in part, to this enzyme's exceptional stability even under harsh environmental conditions.[4-5] Aqueous solution stability of RNase A is recognized to be a result of its compact globular structure (14 kDa with four disulfide bonds) and from its hydrophilicity [6-8].

Unfortunately, the successful clinical application of RNase A has been limited by factors including its short half–life in vivo due to rapid glomerular filtration and inactivation by antibodies.[9-10] Attempts have been made to increase the in vivo residence time and delivery concentration by coupling it to material surfaces of various drug delivery platforms.[9, 11-13] However, studies have indicated that this has often causes loss of native-state enzyme activity, due to adsorption-induced changes in the structure and/or

stearic hindrance of the active site.[12-16] These findings indicate that greater understanding is needed regarding how interactions with material surfaces influence the adsorbed structure and enzymatic activity of RNase A in order to support the therapeutic use of this enzyme in anti–tumor drug delivery applications.

The effect of different material surfaces and adsorption conditions on the structure and enzymatic activity of adsorbed RNase A is not very well understood. Previous studies on the adsorption behavior of proteins have shown that the adsorbed orientation and adsorption-induced changes in protein conformation and enzymatic activity are a result of the combination of a protein's internal stability relative to the ability of protein-surface and protein-protein interactions (PPI) on the surface to perturb the protein's structure.[17-19] While many previous studies have been published that relate adsorption-induced loss in protein structure to loss of bioactivity, most of these studies were done using techniques like circular dichroism spectropolarimetry (CD), which though useful, are only scalar indicators of the molecular structure underlying the involved processes.[10, 19-23] Alternatively, techniques like amino acid labeling and mass spectrometry (AAL/MS), though localized, can be used to identify the shifts in the solvent exposure of the residues within the tertiary structure of adsorbed protein.[12, 23-29] Additionally, these type of techniques are especially relevant in applications that require molecular-scale understanding of the processes underlying the loss in the bioactivity of a protein, despite retaining its near-native secondary-structure.[29]

The objective of this study was therefore to investigate how different adsorption conditions would influence the structure and enzymatic activity of adsorbed RNase A.

Towards this purpose, we have used an AAL/MS technique along with CD to quantitatively investigate the effects of adsorption on bovine pancreatic ribonuclease-A (RNase A) when it is adsorbed on fused silica glass (glass), high-density polyethylene (HDPE), and poly(methyl–methacrylate) (PMMA) to further explore how surface chemistry influences the relationships between adsorbed conformation and enzymatic activity. The combined use of these techniques provide insights into the protein's adsorbed orientation, adsorption-induced changes in protein secondary and tertiary structure, and adsorption-induced effects on the solvent accessibility of RNase A's bioactive site.

7.2 EXPERIMENAL SET-UP AND METHODOLOGY

7.2.1 Material Surface Preparation and Characterization

The selected material surfaces include fused silica glass (glass), high density polyethylene (HDPE), and poly (methyl methacrylate) (PMMA). Custom cut glass (0.375″(L) × 0.0625″ (W)× 1.625″ (H), Chemglass Life Sciences) was procured and cleaned at 50°C by immersion in piranha solution (7:3 v/v H_2SO_4(EMD Chemicals, SX 1244)/H_2O_2) for at least 30 minutes, followed by basic wash (1:1:5 v/v NH_4OH (BDH Chemicals, BDH3016)/H_2O_2/H_2O), and this procedure was repeated twice. Standard safety procedures were followed during the handling, storage, and disposal of these wash solutions. HDPE and PMMA surfaces were spin–coated onto the silicon wafer (6" diameter, University Wafer) from dodecalin (0.5% (w/w) at 1500 rpm for 60s) and chloroform solutions (1.5% (w/w) at 1000 rpm for 60s), respectively. All chemicals including the polymers of HDPE (M_w =125,000 Da, Sigma 181900) and PMMA

(M_w=350,000 Da, Sigma 445746) and the solvents such as dodecalin (Sigma 294772) and chloroform (EMD Chemicals, CX 1054) were used as supplied by the manufacturer. Prior to conducting the adsorption studies, all the substrates were rinsed in absolute ethanol, followed by nanopure water, and then dried under nitrogen gas.

Characterization of the material surfaces was performed to determine the static air–water contact angle, surface composition, film thickness, and surface roughness of the substrates. For each of the surfaces, the static air–water contact angle was analyzed using a contact–angle goniometer (Krüss, DSA–20E). The surface composition was verified via X–ray photoelectron spectroscopy (NESCA/BIO, University of Washington), and the average RMS surface roughness was analyzed using atomic force microscopy (Asylum Research, MFP–3D) over an area of 5 × 5 μm. The thickness of the polymer films was characterized using variable angle spectroscopic ellipsometry (Sopra Inc., GES–5).

7.2.2 Protein Adsorption and Equilibration

The adsorption of ribonuclease A (RNAse A, Sigma R6513) on the material surfaces was carried out using previously described methods (see section 5.2.3 in chapter 5).[19] Briefly, 10 mM potassium phosphate buffer solution (PPB; pH 7.4) was prepared by mixing appropriate amounts of 1 M monobasic potassium phosphate (Sigma, P8708) or 1 M dibasic potassium phosphate (Sigma, P8508) following which the buffer concentration was verified by titrating against 0.065 M potassium hydrogen phthalate. Protein adsorption was conducted in 10 mM PPB under a protein concentrations of 0.03 and 1.00 mg/mL for 2 h in order to vary the surface coverage of adsorbed protein on each surface following which the material surfaces were gently rinsed under a steady gentle flow (12

mL/min) of PPB for 5 min to remove weakly adsorbed protein. The surfaces with the adsorbed layer of protein were then immersed in PPB for 15 h to allow the adsorbed protein layers to structurally equilibrate on the surface at room temperature (≈ 25° C). Control studies were conducted to ensure that RNase A itself did not undergo a significant change in structure and/or activity during this frame in PPB solution due to simple aging. The effect of adsorption time from protein solution and equilibration time in PPB for different surfaces on the surface coverage and structure of the protein when adsorbed from a given solution concentration is provided in Chapter 5. From these studies, it was determined that the designated times of 2 h for initial adsorption followed by 15 h of relaxation under PPB were sufficient for system equilibration for each of our treatment conditions.

7.2.3 . Characterization of Secondary Structure

The secondary structures of RNase A both in solution and on each surface were determined using CD spectropolarimetry described in Chapter 5.[30] Briefly, the CD spectra of RNase A in solution was obtained at room temperature using a Jasco J–810 spectropolarimeter in a 0.1 mm path-length quartz cuvette (Starna) from 190 to 300 nm in 10 mM PPB solution (pH 7.4). The structure of the adsorbed RNase A was determined under similar conditions but using a custom–made cuvette that was designed to hold four sets of the adsorbed surfaces perpendicular to the CD beam, which enhances the signal-to-noise ratio. The amount of protein on a given surface (Q_{ads}) was determined from equation 7.1 using the absorbance at 205 nm (A_{205}) [24]

$$Q_{ads} = \frac{A_{205}}{\varepsilon 205}\left(\frac{mg}{cm^2}\right) \quad (7.1)$$

where ε_{205} represents the molar extinction coefficient at 205 nm (units of $M^{-1}cm^{-1}$), which was determined from the calibration plot of standardized solution of RNase A at different concentrations. The solution concentrations (C_{soln}) of RNase A were standardized using the E (1%) of 7.0 $(g/100\ ml)^{-1}\ cm^{-1}$ at 280 nm method provided by the supplier.

7.2.4 Characterizing Orientation and Tertiary Structure of RNase A Using Amino Acid Labeling/Mass Spectrometry (AAL/MS)

AAL/MS uses amino-acid-specific, nonreversible chemical labeling to probe the adsorbed orientation and adsorption-induced changes in the tertiary structure of proteins.[24] This method is based on the principle that only solvent accessible amino acids can undergo chemical labeling. Mass spectrometry is then used to identify whether the targeted amino acids are labeled or not. Amino acid residues that are found to be labeled in solution but unlabeled following adsorption indicate regions of blockage by the surface (i.e., indicative of adsorbed orientation) or by neighboring proteins (i.e., indicative of protein-protein interactions). Alternatively, amino acids that are unlabeled in solution but become labeled following adsorption are indicative of sites in the protein that underwent adsorption-induced tertiary unfolding that exposed otherwise unavailable residues.

Application of AAL/MS to multiple different amino acid types that are distributed throughout a protein enables a fairly comprehensive picture to be generated regarding the primary distribution of sites in the protein that are tightly adsorbed to the surface (or

blocked by neighboring proteins) and sites undergoing adsorption-induced tertiary unfolding.

7.2.4.1 Batch Labeling of Target Amino Acids.

Arg, Lys, Asp, Glu, Tyr, and His in RNAse A were individually labeled under a common reactive condition to facilitate direct comparison of the labeling profiles from each of these amino acids using previously developed methods (see section C.2 in the appendix).[31-34] For consistency between treatments, the reaction between the labeling agent and its targeted amino acid was carried out at 5x the overall molar concentration of the targeted amino acid type contained within the protein in the dark at 25°C for 3 h in PPB. The solution pH was maintained at 7.4 by adding required amounts of 1 M monobasic potassium phosphate (Sigma, P8708) or 1 M dibasic potassium phosphate (Sigma, P8508), following which the buffer concentration was verified by titrating against 0.065 M potassium hydrogen phthalate.

7.2.4.2 Analysis by Mass Spectrometry

Proteolytic digestion of modified and unmodified RNAse A from in solution and adsorbed states was done using sequence–grade porcine trypsin (Promega) after being chemically labeled as described in section C.3 in appendix C. Trypsin–digested peptides were subsequently analyzed using an Ultra Performance Liquid Chromatography System (UPLC, Waters) coupled with a quadruple time–of–flight mass spectrometer (Q–TOF MS, Waters) with electrospray ionization in both ESI^+–MS and ESI^+–MS/MS (SetMass without fragmentation) mode operated by Masslynx software (V4.1). The intensities obtained from

mass matching were subsequently used in quantifying the extent of solvent exposure for the targeted residues, as described in 6.2.3.

7.2.4.3 Correlating Mass Spectra to Configuration of Adsorbed RNase A

It has been previously shown that the peak intensities of the mass spectra of trypsin digests of a protein following chemical labeling are directly related to the extent of the solvent exposure of the targeted amino acid.[26] These previous methods, however, were only developed for application to individual types of amino acid residues within a protein. Our group has developed a method to target multiple amino acids within a protein[24] by (*i*) using an unlabeled peptide sequence of the protein to normalize the absolute extent of labeling from the peptide intensities of each of the batch experiments to a common reference state,[35] and (*ii*) calculating a relative ratio of the normalized extent of modification for each targeted amino acid residue of the protein in its adsorbed state to its solution state, which we refer to as the 'residue profile'. These combined methods are subsequently used to probe the adsorbed configuration of a protein on a surface.

Accordingly, the normalized extents of modification (%) for a target residue in its solution (I_{soln}) and adsorbed (I_{ads}) states were subsequently estimated from a given mass spectrum by calculating the ratio of the weighted intensity of peptide fragments containing the labeled target amino acid to the total weighted intensities of all peptide fragments, as described in 6.2.3. Following which, the net intensity parameter of amino acid labeling in the protein's adsorbed state (I_{ads}) was determined by dividing it by its net intensity parameter in solution to obtain the overall relative degree of labeling in the

amino acid's adsorbed versus solution state. If the weighted intensity for a given residue in solution (I_{soln}) or in its adsorbed state (I_{ads}) was found to be less than 0.10 (which was considered to be the limit of detection), a low ceiling threshold value of 0.10 was designated for the respective intensity value instead of zero in order to avoid the mathematical problems of dividing by zero or taking the log(0) in equation (1).[24] Similarly, the maximum values that could be expected for I_{soln} and I_{ads} was 1.0, which corresponds to the condition when all the peptide fragments containing the target residues were labeled.[24] The base–10 logarithm of I_{ads}/I_{soln} was then taken to provide the residue profile value for each targeted amino acid, as indicated in equation (7.2). A given residue's profile could then be used to represent an averaged response of the ensemble of configurations that the adsorbed protein adopts on a given surface. A positive shift in the profile of a given residue indicates that on average it has more solvent exposure after being adsorbed compared to when in solution, while a negative shift in its profile indicates that on average it has lower solvent exposure in its adsorbed state compared to solution.

$$\text{Profile} = \log(I_{ads} / I_{soln}) \qquad 7.2$$

Thus, the expected range of I_{ads}/I_{soln} values is from 0.1 to 10 (using 0.1 and 1.0 as the minimum and maximum intensity values, respectively).[24] If the extent of labeling within the adsorbed and native states of the protein was similar, the I_{ads}/I_{soln} value would be close to 1.0. Modification of residues within the solution provided a measure of the variability in I_{soln} of about 0.25 (95% confidence interval (C.I.) about the mean). Since reacting conditions between different modifications in the adsorbed and solution state

were kept identical, similar variability in labeling was also expected in the adsorbed state of the protein. Therefore, we considered I_{ads}/I_{soln} values beyond the range of 0.75 (i.e., 1 - C.I.) to 1.25 (i.e., 1 + C.I.) as representing a significant change in solvent accessibility. However, among the residues showing significant change in solvent accessibility, residues with $I_{ads}/I_{soln} > 5.0$ and < 0.2 indicate a 5-fold shift in their state of solvation, with a corresponding log-ratio p-value[36] < 0.0001.[36-37] These metrics are listed in Table 7.1

Table 7.1. Metrics to determine the configuration of an adsorbed protein based on its labeling profile. I_{ads}/I_{soln} values between 0.75 and 1.25 are considered to not be significantly different than the native solution–state structure. I_{ads}/I_{soln} values that are 5x higher or lower than the native solution-state condition are designated as undergoing a high level of change. Retabulated with permission from Ref. [24]. Copyright 2014 Acta Materialia Inc., published by Elsevier Ltd.

I_{ads}/I_{soln}	Profile = $\log_{10}(I_{ads}/I_{soln})$	Solvent Exposure of Residues	Physical Meaning
≥ 5.0	≥ 0.70	More than the native state	Accessibility increased by tertiary unfolding
1.25 – 5.0	0.10 to 0.70		
0.75 – 1.25	–0.12 to 0.10	Similar to the native state	Native structure
0.20 – 0.75	–0.12 to–0.70	Less than the native state	Accessibility decreased by surface or protein-protein effects
≤ 0.20	≤ -0.70		

The labeling agents for the reacting conditions used in the current study did not significantly affect the secondary structure of RNase A in either the solution or in the adsorbed state as determined by CD (see Fig C.3 in the appendix). Thus the profile shifts can be considered to be solely mediated by the shift in solvent exposure

of the residue as a result of the adsorption process. The resulting profile values for the combined set of targeted amino acids for RNase A were determined accordingly and mapped onto the native structure of the protein for visualization, which was represented by the Protein Data Bank's[38] tertiary structure model of RNase A, 6RSA[39], with UCSF Chimera used as the visualization software.

7.2.5 Characterization of Enzymatic Activity

A spectrophotometric assay was used to measure the enzymatic activity of RNase A to complement the CD and AAL/MS data. Taken together, these combined methods enable correlations to be examined between adsorbed orientation and conformation with adsorption-induced changes in RNase A's enzymatic activity. These enzymatic activity studies were also carried out in CD cuvettes.[19] Briefly, ribonucleic acid, which is the substrate for RNase A, was prepared in PPB to a final concentration of 20 mg/mL (Baker's yeast, Sigma R6750) and exposed to RNase A in both solution and following RNase A adsorption. An initial calibration plot for solution-state enzymatic activity was obtained for a working range of 0.1 μg – 30 μg of RNAse A (based on the equivalently adsorbed amount of protein on different surfaces) by monitoring the absorbance at 300 nm (ΔA_{300}) at pH 7.4. A time period of 10 min was found to be sufficient for complete catalysis. The amount of adsorbed protein was quantified by the layer's absorbance at 205 nm (A_{205}), both before and after the bioactivity assays were performed to ensure that they did not cause a measureable amount of the protein to be desorbed from the adsorbent surface. The specific activities of the adsorbed proteins were then calculated by normalizing the

ΔA_{300} absorbance values by the total amount of protein adsorbed on the surface (Q_{ads}* area of adsorbent surface). The relative enzymatic activities (%) of the adsorbed RNase A enzymes were then determined by normalizing the measured adsorbed-state specific activity by the solution-state specific activity.

7.2.6 Statistical Analysis

The mean and 95% confidence interval (C.I.) for each measurement were calculated for each set of experimental data collected. Statistical differences were determined using a one-tailed Student's t–test with values of $p \leq 0.05$ considered to be statistically significant.

7.3 RESULTS AND DISCUSSION

7.3.1 Surface Characterization

Table 5.1 presents the results analyzed by the characterization techniques applied to the surfaces used in this study. All of the measured values reported in Table 5.1 fall within the expected range.

7.3.2 Role of Adsorbed Configuration of RNase A on the Enzymatic Activity

Unlike many proteins, RNase A is a very hydrophilic molecule. It is composed of more than 70% polar and charged amino acids, and therefore it was expected to interact more strongly with the glass and PMMA than the HDPE surface via hydrogen bonding and/or electrostatic effects. The influence of adsorption conditions on the secondary structure, surface coverage, and relative enzymatic activity of the adsorbed RNase A on each of our three surfaces for each solution concentration are presented in Table 7.2.

Table 7.2. Secondary structure content (%), surface coverage, and relative enzymatic activity (%) for adsorbed RNase A from two different protein solution concentrations (0.03 and 1.00 mg/mL) on (a) glass, (b) HDPE, and (c) PMMA (N=3; average ±95% C.I. values). For comparison, the helical and β-sheet content of RNaseA in solution was found to be 20% (±3%) and 42% (±4%), respectively. The theoretical full surface coverage of RNase A for adsorption in 'side–on' and 'end–on' orientations are τ_{side} (0.21 μg/cm^2) and τ_{end} (0.28 μg/cm^2), respectively.[40]

Surface	Solution Conc. (mg/mL)	Surface Coverage (ug/cm^2)	Avg. Distance Between Proteins (nm)*	Helices (%)	Sheets (%)	Relative Enzymatic Activity (%)
Glass	0.03	0.08 ± 0.01	5.8	5 ± 2	52 ± 8	38 ± 8
	1.00	0.16 ± 0.03	4.1	19 ± 4	26 ± 5	39 ± 9
HDPE	0.03	0.10 ± 0.01	5.2	18 ± 2	25 ± 3	43 ± 6
	1.00	0.17 ± 0.03	4.0	9 ± 2	29 ± 5	35 ± 8
PMMA	0.03	0.08 ± 0.02	5.8	8 ± 2	31 ± 3	33 ± 5
	1.00	0.16 ± 0.03	4.1	18 ± 3	24 ± 4	45 ± 9

*Average distance between the centers of adsorbed RNase A assuming monolayer coverage with the enzymes arranged in an evenly spaced hexagonal array.[41-42] For comparison sake, per the protein data bank (PDB) structure of RNase A (PDB #6RSA[39]), the long and short axis dimensions of RNase A are approximately 4.2 and 2.8 nm, respectively.

7.3.2.1 Role of Surface Coverage and Surface Chemistry on the Secondary Structural Content of Adsorbed RNase A

As shown in Table 7.2, adsorption of RNase A to each surface for 2 h of exposure in the protein solutions followed by 15 h of equilibration in buffer resulted in a significant shift in its secondary structure for each surface and for each solution concentration. These results reflect combined influences of protein–surface interactions, protein–protein interactions (PPI), and internal protein stability effects.[19] These timeframes (i.e., 2 h adsorption, 15 h relaxation) were selected to represent equilibrated conditions where the amount and structure

of the adsorbed protein was found to stabilize and undergo no further noticeable changes (See Fig 5.3 and Fig. 5.6 in chapter 5). In addition, control studies were conducted to measure the secondary structure of RNase A in solution over timeframes of at least 24 h and showed no significant change in either the secondary structure or enzymatic activity during this time, thus supporting that the changes in the structure of RNase A on the materials surfaces were due to interactions of the protein with the surface rather than being simply an aging phenomenon of the protein itself.

When RNase A was adsorbed from a 1.00 mg/mL solution concentration followed by 15 h of equilibration under pure PPB (i.e., protein-free PPB solution), the resulting surface coverage of the adsorbed protein on each surface was within 25% of a saturated, close–packed monolayer with side–on protein orientation. In contrast, when adsorbed from a 0.03 mg/mL solution and equilibrated, the resulting surface coverage of the RNase A was about half of that obtained when it was adsorbed from the 1.00 mg/mL solution. These results show that different degrees of surface coverage for RNase A were obtained in our studies by varying the protein solution concentration from which it is adsorbed. As intended, the higher solution concentration resulted in higher surface coverage, which can subsequently be associated with a greater degree of PPI effects on the surface.

As can be seen from the data presented in Table 7.2, when the coverage on the surfaces was low (e.g., 0.08 μg/cm^2, nearly 3x less than the closed-packed side-on arrangement of 0.21 μg/cm^2), in which case the effects of PPI can be expected to be relatively low, the protein-surface interactions induced about 70% and 85% loss in the native helical content of adsorbed RNase A on the PMMA and glass surfaces, respectively. We

hypothesize that these responses are indicative of the surface destabilizing the helical structures of RNase A by competing with the hydrogen bonding that stabilizes the helices of the native-state structure. However, at high surface coverages (0.16 μg/cm^2, close to the close-packed side-on arrangement), where PPI effects can be expected to be substantially greater, these effects apparently tend to inhibit surface-induced unfolding, and result in the native-state helical content being largely preserved with less than 1% loss in the native structure.

In contrast to the trends observed for PPI effects on the native state helical content of RNase A, changes in the surface coverage of RNase A on the HDPE and PMMA surfaces had minimal influence on the β–sheet content of the protein, with a general decrease in β-sheet structures, ranging from 24 to 31% with an average of about 28% β-sheet structure (or a 29% loss in the native state % β-sheet). However, on the silica glass surfaces, when PPI effects were minimized, it was observed that there was a large increase in the β–sheet content of the adsorbed RNase A (i.e., 24% gain in β-sheet), suggesting that the glass surface has a particularly strong tendency to act as a planar template for the alignment of the polypeptide chain segments as the protein unfolds, presumably mediated mainly by electrostatic effects.[43]

However, this trend was not observed at the higher protein surface coverage on glass, with PPI effects apparently inhibiting the ability of the protein to unfold and spread out on the surface. Thus while, it is relatively easy to predict that the competing influence of hydrogen-bondable groups in glass and PMMA for the hydrogen bonds that stabilize the helical secondary structure of the protein would induce a loss in helicity, its effect on the on β-sheet structure of RNase A are less predictable. The hydrogen-bonding groups of the surface can

either compete for the hydrogen bonds that stabilize the β-sheet structure, leading to a reduction in β-sheet content, or serve as a template to form new β-sheet-like structure by attracting and aligning peptide segments along the surface. Based on this understanding, we consider that the change in helical structure provides a more sensitive and straightforward indicator of the degree of adsorption-induced disruption of the native-state secondary structure of a protein.

In direct contrast to the stabilizing effect of PPIs on the helical content of adsorbed RNase A on PMMA and glass, it is apparent that PPI on the hydrophobic HDPE surface had a destabilizing effect on the helical structure—adsorption to HDPE induced more than 50% loss in native-state % helicity at higher surface coverage (0.17 μg/cm^2) compared to less than 1% loss at low surface coverage (0.10 μg/cm^2). As an explanation for these interesting results, we propose that in the absence of PPI effects, the adsorption of RNase A to HDPE results in the replacement of the hydrophobic interactions between the side-chains of the amino acid residues making up the helices and the β-sheet in the native-state structure with hydrophobic interactions with the HDPE surface. This process thus could result in the unfolding the tertiary structure while maintaining the stability of the helical secondary structure of the protein. We further propose that the presence of high PPI effects disrupts this process in RNase A, leading to the separation and destabilization of the helical and β-sheet structures, while inhibiting the helices from being re-stabilized by the hydrophobic surface. Obviously, these specific types of molecular-level interactions are speculative at this time. We hope to provide support for these hypothesized molecular-level events through molecular simulation studies in the near future.

7.3.2.1.a Impact of Loss in Secondary Structure on the Enzyme Activity of Adsorbed RNase A

The key element in the current study is the activity of the adsorbed RNase A, and the factors influencing its activity. In many studies the extent of helical unfolding has often been associated with the loss in activity for other proteins. Additionally, at least one of the three residues involved in catalysis are within the helical conformation of the protein structure (Fig. 7.1).[44] The native-state structure of the RNase A resembles a kidney shape, with the active site residues (H12, K41, and H119) laying in the concave cleft (Fig. 7.1).[44]

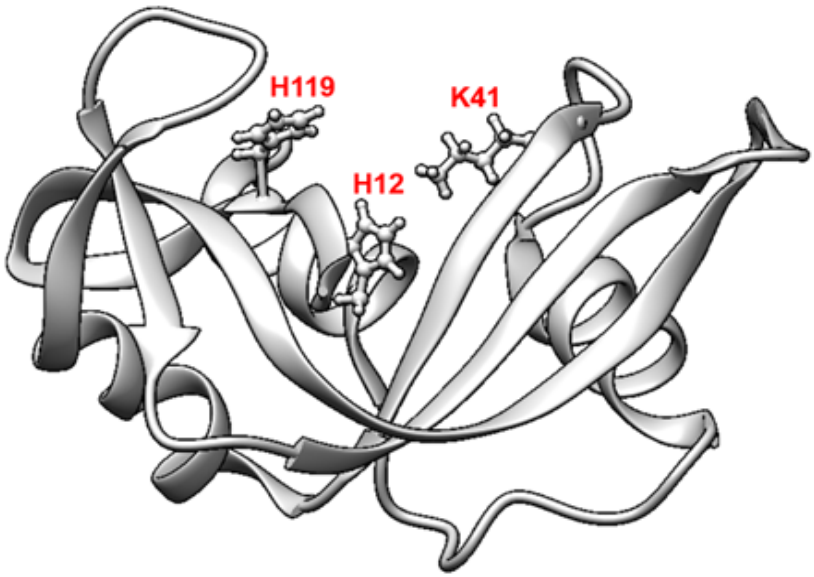

Figure 7.1. Ribbon diagram of the three-dimensional structure of ribonuclease A.[44-45] The three residues most important for catalysis: His12, His119, and Lys41 are marked in red. Reproduced with permission from Ref. 45. Copyright 2014 ACS.

As can be inferred from the results presented in Table 7.2, the loss in helix is not a clear indicator of the loss in enzymatic activity, especially since the relative enzymatic activity of RNase A was unchanged for a wide range of helical unfolding. Even when the helical content within the protein was equivalent to that of its native-state structure (i.e.,

when RNase A was adsorbed under minimal PPI conditions on the HDPE surface and when adsorbed under high PPI conditions on the glass and PMMA surfaces), there were no significant differences ($p > 0.05$) in its activity when compared to the unfolded states of RNase A under conditions exhibiting a large degree of unfolding. Thus it is evident that the reduction in helical content of RNase A does not correlate well with the loss in the native state activity. As a result, more sensitive assays that would provide molecular (or domain) level insights on the tertiary and orientation of the adsorbed RNase A might serve as a better indicator of how the adsorbed configuration of the protein might affect its enzymatic activity level.

7.3.2.2 AAL/MS Technique to Identify the Orientation and Tertiary Structural Shift in Adsorbed Protein

In our study, the AAL/MS technique was used to identify the areas within the protein that underwent orientation and tertiary structural shift by estimating the changes in the absolute extent of modification (%) in the adsorbed states of the protein relative to its solution state, or profile, using equation 2. The extent of modification (%) was assumed to be directly proportional to the solvent exposure of the target residues, as the labeling conditions used in the current study were not found to significantly affect the structure of protein structure in solution or the adsorbed state (see Fig C.3 and Table C.1 in appendix C). Additionally, sequence coverage of 100% was obtained with the tryptic digests in-solution and adsorbed RNase A. In our experiment, a total of 34 residues that were distributed throughout the protein were labeled in solution of which H12, K41, and H119, form the catalytic site in RNase A, and are utilized by these enzymes to cleave

phosphodiester bonds in RNA. The residues H12 and H119 act as an acid or a base to both accept and donate electrons while K41 stabilizes the transition state of the catalytic reaction.[44, 46]

7.3.2.2.a. Active Sites and Solvent Accessibility of Amino Acid Residues in Solution Phase of a Protein

Fig. 7.2 illustrates these effects in a space–filled model of RNase A with targeted amino acid residues color-coded by their degree of solvent exposure as determined by the side-chain modification experiment. Based on these results, two of the catalytic residues (K41 and H119) were solvent exposed while the third (H12) was buried in the solution-state structure.

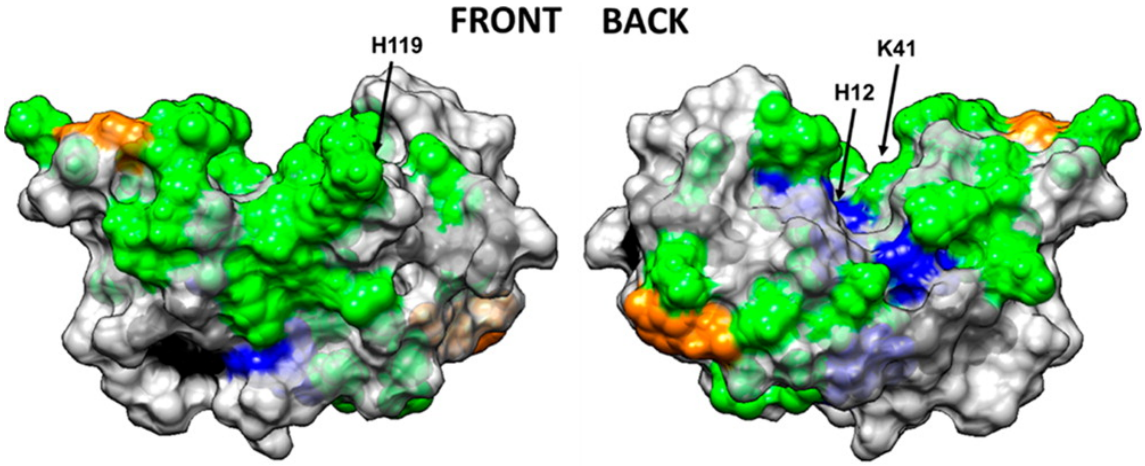

Figure 7.2. Spacefilled model of RNase A with amino acid residues color coded by their solvent accessibility as determined from targeted amino acid labeling in solution. Color coding: charged amino acid residues (Asp, Glu, Lys, Arg, His) with high solvent accessibility (green) and moderate solvent accessibility (blue), tyrosine residues with high solvent accessibility (orange) and low solvent accessibility (black). Non–targeted amino acid residues are color coded in light grey. Figure illustrated using UCSF Chimera. The arrows point out the location of the three key amino acid residues that provide the catalytic function of the enzyme (H12, K41, H119). See Table C.9 for the raw data. Reproduced with permission from Ref. 45. Copyright 2014 ACS.

Based on the absolute extent of modification (%) for a target residue in its solution state, I_{soln}, charged residues such as Arg (R10, R33, R39, and R85), Lys (K1, K7, K31, K37, K41, K61, K66, K91, K98, and K104), His (H105, H119), Asp (D10, D38, and D53) and Glu (E2, E9, E49, and E86) at physiological pH were found to be solvent exposed. However, some of the charged residues were found to be less solvent exposed or buried (D14, D121, D83, H12, and H48). In contrast to charged residues, most Tyr amino acids were found to be less solvent exposed or buried inside the protein structure (Y25, Y73, Y97, and Y115), while Y92 and Y76, which are located on the outer surface of the protein, were found to be solvent exposed (see Table C.9 in the appendix for raw data).

7.3.2.2.b. Active Sites and Solvent Accessibility of Amino Acid Residues in Adsorbed Phase of a Protein

The resulting profiles for each of the targeted amino acids were determined and are shown in Fig. 7.3 and Fig. 7.4 for each of the three different surfaces when adsorbed from 0.03 mg/mL and 1.00 mg/mL protein solutions, respectively. The data presented in Fig. 7.3 (0.03 mg/mL results) were separated according to the classification shown in Table 7.1 (i.e., surface type and solution concentration) and the resulting residues belonging to each group are presented in Table 7.3. Similarly, Fig. 7.4 presents the profile values for RNase A adsorbed from 1.00 mg/mL solution with the division of residues according to the Table 7.1 categories presented in Table 7.4.

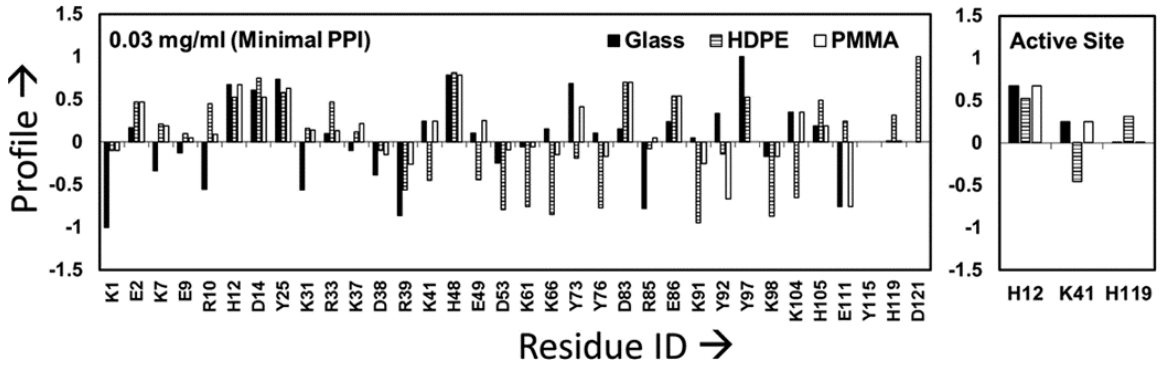

Figure 7.3: Labeling profile of the targeted residues in RNase A on glass, PMMA, and HDPE surfaces when adsorbed from 0.03 mg/mL protein solution. The residues within the active site of RNase A are shown separately in the right-hand plot to more clearly show their response. The profiles within about ± 0.1 of zero can be considered to be not significantly different from the solution state (n = 3). Residues showing no difference in their solvation between solution and the adsorbed states have profile values equal to 0 (e.g., Y115 for all three surfaces). See Table C.9 for the raw data. Reproduced with permission from Ref. 45. Copyright 2014 ACS.

Table 7.3: The labeling profile of RNase A on each surface when adsorbed from 0.03 mg/mL solution concentration. His12, Lys41, and His119 (in red) are the main catalytic residues. Reproduced with permission from Ref. 45. Copyright 2014 ACS.

Surface	Profile ≤ –0.72	–0.72 < Profile <– 0.12	–0.12 ≤ Profile ≤ 0.1	0.1 < Profile < 0.7	Profile ≥ 0.7
GLASS	K1, R39, R85, E111	K7, R10, K31, D38, D53, K98	E9, R33, K37, E49, K61, Y76, K91, Y115, H119, D121	E2, H12, D14, K41, K66, D83, E86, Y92, K104, H105	Y25, H48, Y73, Y97
HDPE	D53, K61, K66, Y76, K91, K98	K104, R39, K41, E49, Y73, Y92	K1, E9, D38, R85, Y115	E2, K7, R10, H12, H15, Y25, K31, R33, K37, D83, E86, Y97, E111, H119	D14, H48, D121
PMMA	E111	D38, R39, K66, Y76, K91, Y92, K98	K1, E9, R10, D53, K61, R85, Y97, Y115, H119, D121	E2, K7, H12, D14, Y25, K31, R33, K37, K41, E49, Y73, D83, E86, K104, H105	H48

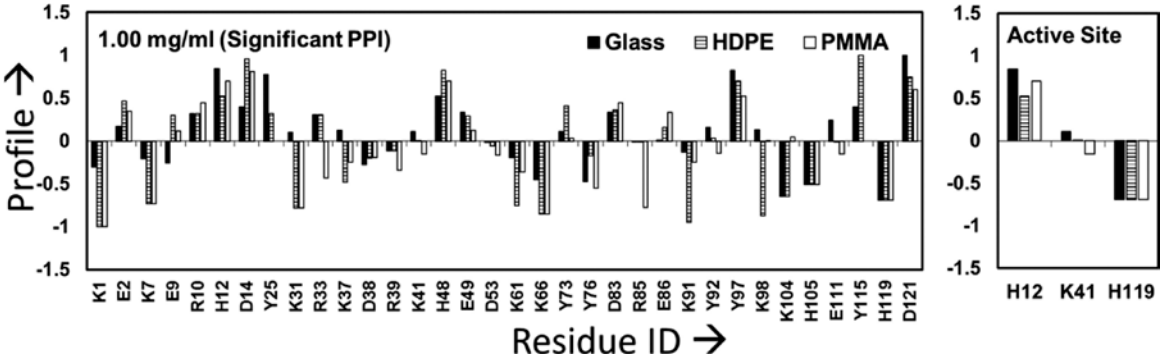

Figure 7.4: Labeling profile of the targeted residues in RNase A on glass, PMMA and HDPE surfaces when adsorbed from 1.00 mg/mL protein solutions. The residues within the active site of RNase A are shown separately in the right-hand plot to more clearly show their response. Profiles within about ± 0.1 of zero can be considered to be not significantly different from the solution state (n = 3). Residues showing no difference in their solvation between solution and the adsorbed states have profile values equal to 0 (e.g., R85 for the glass and HDPE surfaces). See Table C.9 for the raw data. Reproduced with permission from Ref. 45. Copyright 2014 ACS.

Table 7.4: The labeling profile of RNase A on each surface when adsorbed from 1.00 mg/mL solution concentration. His12, Lys41, and His119 (in red) are the main catalytic residues. Reproduced with permission from Ref. 45. Copyright 2014 ACS.

Surface	**Profile ≤ –0.72**	**–0.72 < Profile <–0.12**	**–0.12 ≤ Profile ≤ 0.1**	**0.1 < Profile < 0.7**	**Profile ≥ 0.7**
GLASS		K1, K7, E9, D38, K61, K66, Y76, K91,J104, H105,H119	K31, R39, K41, D53, Y73, R85, E86	E2, R10, D14, R33, K37, H48, E49, D83, Y92, K98, E111, Y115	H12, Y25, Y97, D121
HDPE	K1, K7, K31, K61, K66, K91, K98	K37, D38, Y76, K104, H105, H119	R39, K41, D53, R85, Y92, E111	E2, E9, R10, H12, Y25, R33, E49, Y73, D83, E86	D14, H48, Y97, Y115, D121
PMMA	K1, K66, K31, R85, K7	R33, K37, D38, R39, K41, D53, K61, Y76, K91, Y92, E111, H105, H119	Y25, Y73, K98, K104, Y115	E2, E9, R10, E49, D83, E86, Y97, D121	H12, D14, H48

As can be seen from Fig. 7.3 and Fig. 7.4, the labeling profiles reveal substantial differences in residue solvent accessibility between each surface when adsorbed in both 0.03 mg/mL and 1.00 mg/mL solutions. These data also reflect the combined influences of protein–surface interactions, PPI, and internal protein stability effects upon the adsorption configuration of adsorbed RNase A. As noted in Table 7.1, a positive profile value for a designated amino acid is indicative of an adsorption-induced increase in the solvent accessibility of its side group, which implies that, on average, a tertiary unfolding event has taken place in that location of the protein. In contrast, a negative shift in the profile indicates that adsorption has reduced solvent accessibility of the designated amino acid's side chain, which implies that this part of the protein has been sterically blocked by either the surface (i.e., orientation effect) or a neighboring protein (i.e., protein-protein effect).[33, 47] In order to provide a graphical understanding of the locations of the amino acid residues in RNase A that underwent adsorption-induced changes in their solvated state, Figs. 7.5-7.7 present images of the native-state structure of RNase A with the residues color coded by their respective profile values from Tables 7.3 and 7.4.

The data presented in Tables 7.3 and 7.4 for the amino acids with negative profiles (i.e., loss in solvent accessibility) are visually depicted as color coded by yellow and orange in Figs. 7.5-7.7 on the protein's native-state structure. The loss in solvent accessibility of the amino acid residues displaying a negative profile can be caused by close contact with either the adsorbent surface or neighboring adsorbed proteins (i.e., from PPI effects). The regions of the RNase A that underwent a high degree of

adsorption–induced tertiary unfolding as evidenced by increased solvent accessibility following adsorption are color-coded green and blue in Figs.7.5-7.7.

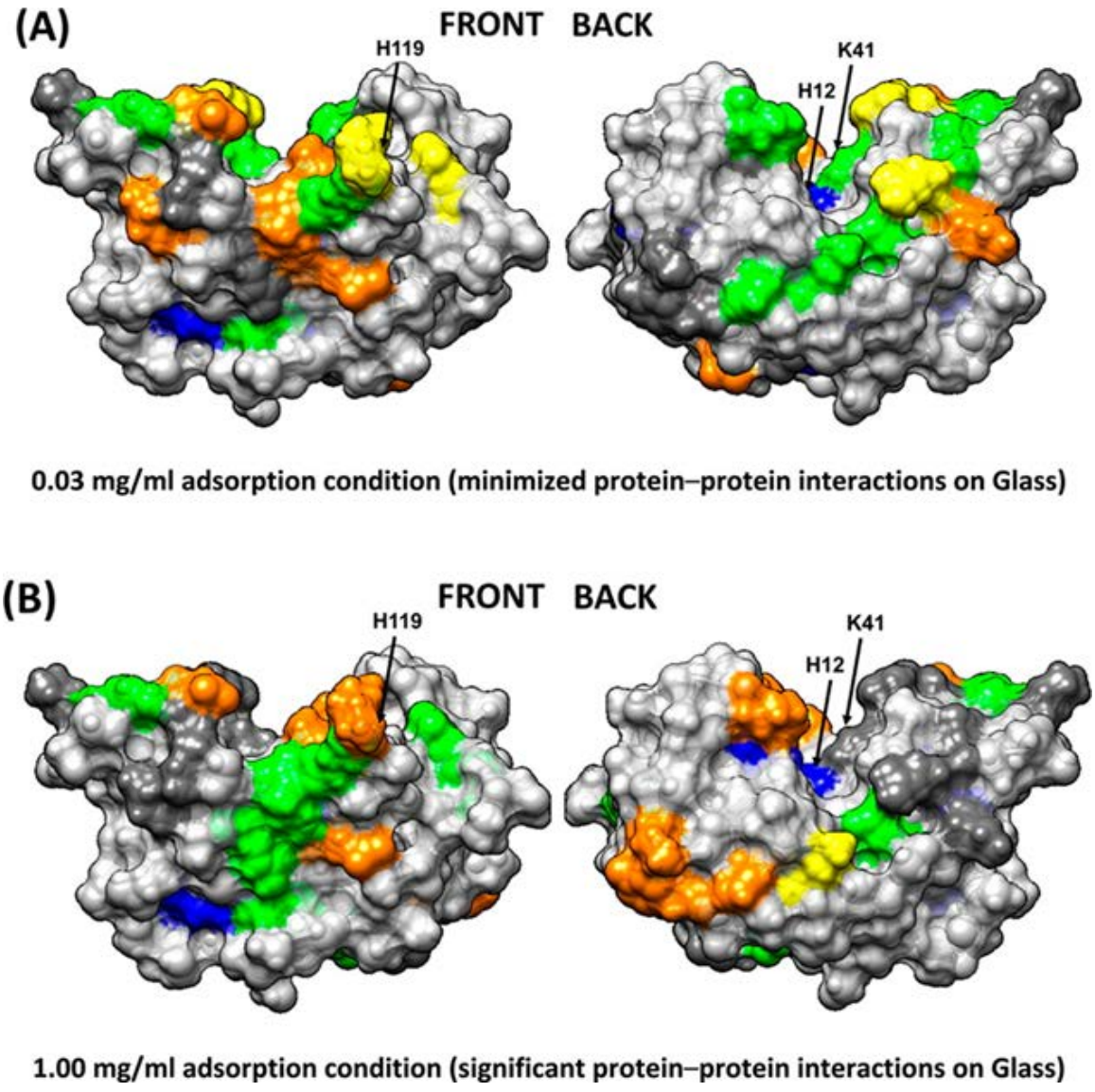

Figure 7.5. Solvation profile of residues in RNase A adsorbed from (A) 0.03 and (B) 1.00 mg/mL on the Glass surface. Residue color code: yellow (−−), orange (–), dark grey (native state), green (+), blue (++) and light grey (non–targeted). The arrows point to the location of the three key amino acid residues that provide the catalytic function of the enzyme (H12, K41, and H119). Reproduced with permission from Ref. 45. Copyright 2014 ACS.

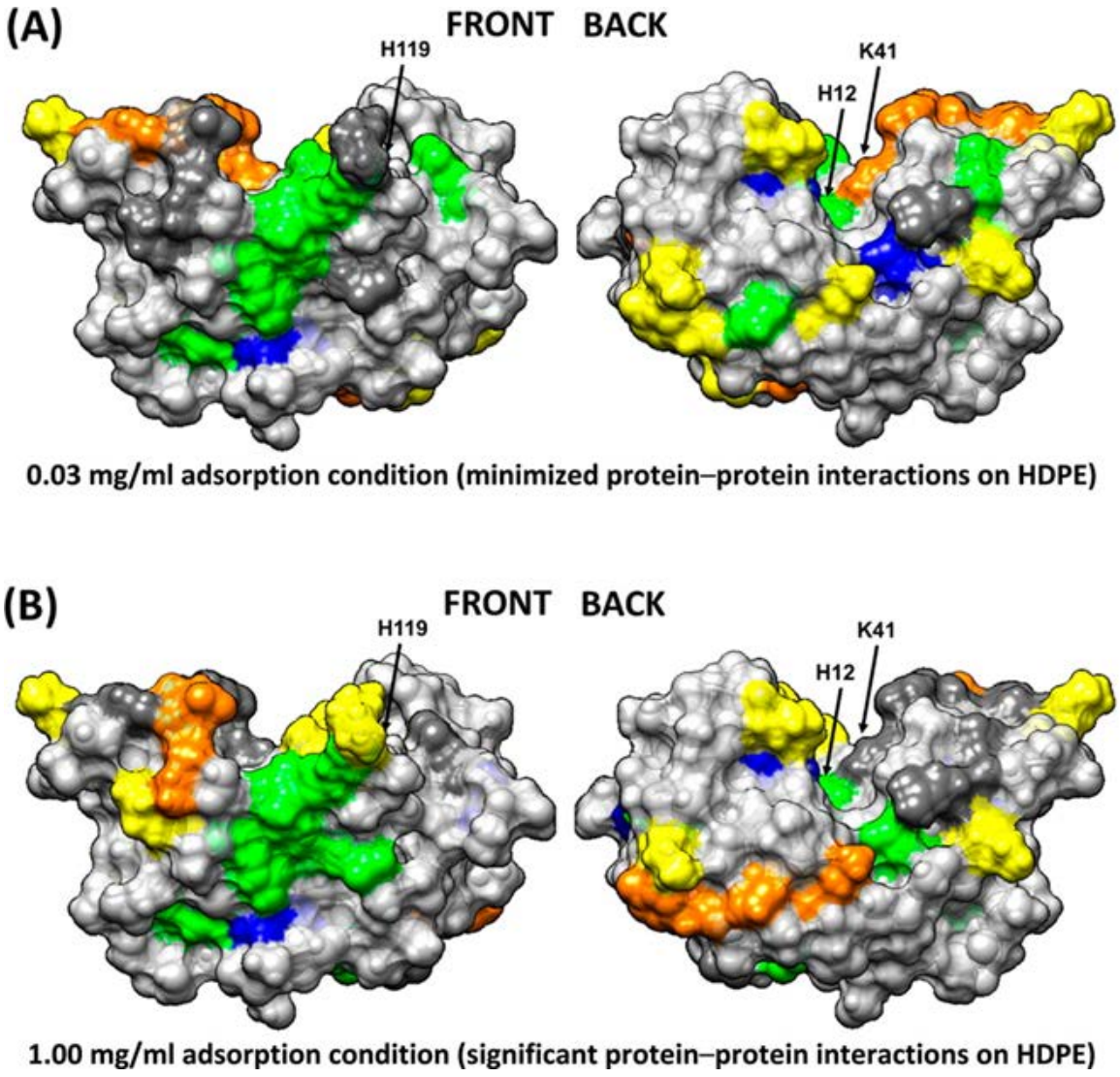

Figure 7.6. Solvation profile of residues in RNase A adsorbed in (A) 0.03 and (B) 1.00 mg/mL on the HDPE surface. Residue color code: yellow (−−), orange (–), grey (native state), green (+), blue (++) and white (non–targeted). The arrows point to the location of the three key amino acid residues that provide the catalytic function of the enzyme (H12, K41, and H119). Reproduced with permission from Ref. 45. Copyright 2014 ACS.

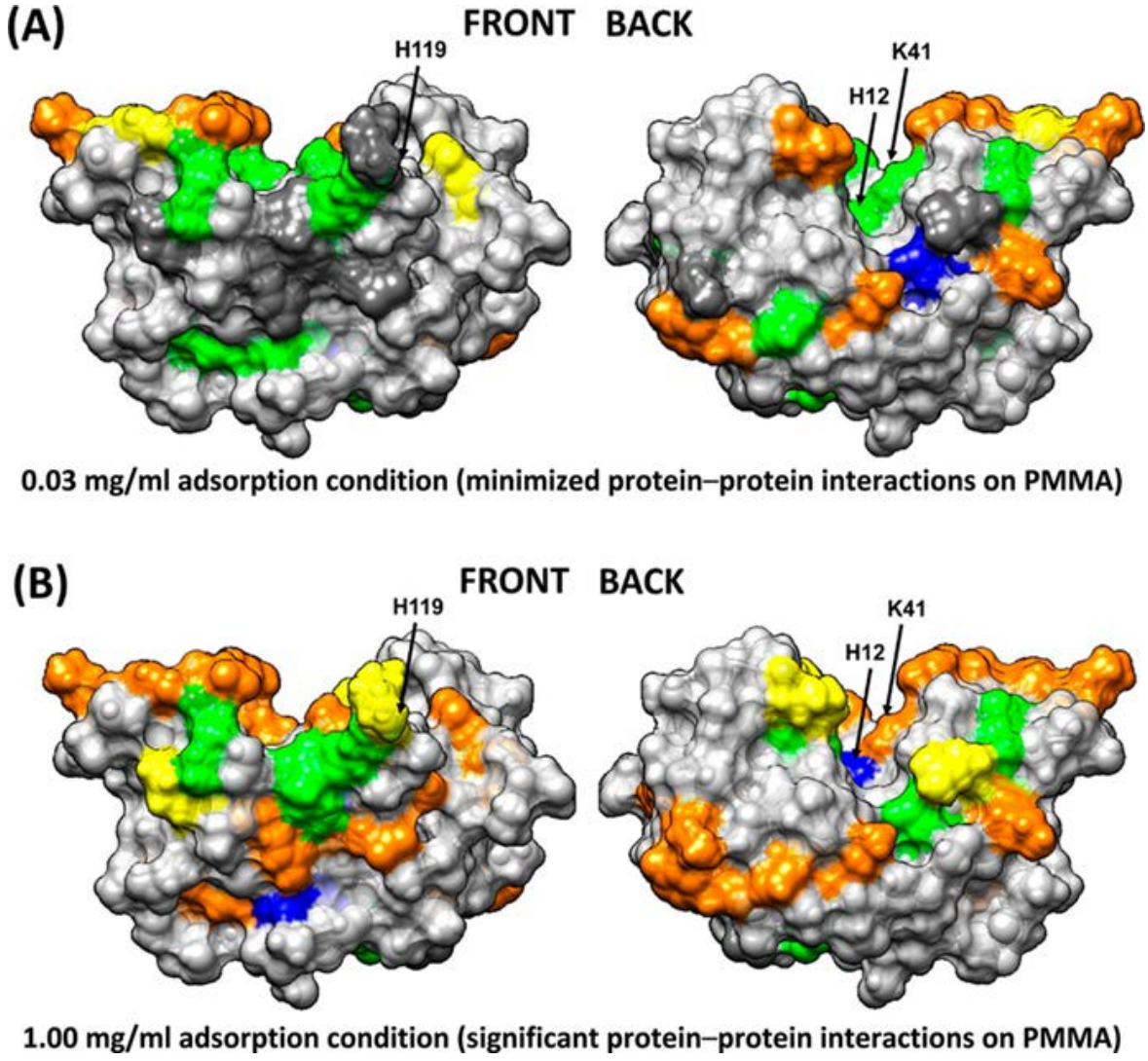

Figure 7.7. Solvation profiles of residues in RNase A adsorbed in (A) 0.03 and (B) 1.00 mg/mL on the PMMA surface. Residue color code: yellow (−−), orange (–), grey (native state), green (+), blue (++) and white (non–targeted). The arrows point to the location of the three key amino acid residues that provide the catalytic function of the enzyme (H12, K41, and H119). Reproduced with permission from Ref. 45. Copyright 2014 ACS.

7.3.2.2.c. Orientation and Configuration of Adsorbed RNase A

As evident from Fig. 7.3, Table 7.3, and Fig. 7.4, when adsorbed from the low solution concentration (i.e., low PPI effects) the adsorbed RNase A predominantly interacts with glass (Fig 7.5), along the positively charged patch of amino acid residues as shown by the residues with greatly reduced solvent accessibility in Table 7.3. These interactions are likely due to the electrostatic interactions between the negatively charged glass surface (determined by streaming potential technique) and the protein. However, when adsorbed from high protein solution concentration (Fig. 7.4, Table 7.4, and Fig. 7.5), the resulting increased PPI effects appear to have interfered with the ability of electrostatic interactions to orient RNase A on the surface, with the negative profiles being not as strong and shifted towards different positions that are more evenly distributed around the protein's surface, presumable due to closer contact with neighboring proteins and different orientations adopted by the protein when approaching surface saturation.

The strongly hydrophobic HDPE surface (Fig. 7.5), which does not have hydrogen bonding capability, has the potential to primarily interact with the hydrophobic side-chain functional groups of amino acids within RNase A. As shown in Fig. 5.A, when adsorbed from 0.03 mg/mL with minimal PPI effects, the amino acids showing the lowest solvent accessibility are all positioned along what we refer to as the 'back' surface of the protein with no apparent areas of lost solvent accessibility on the 'front' surface (Fig. 7.3, Table 7.3). These results provide evidence that RNase A adsorbs on HDPE with its 'back' face oriented towards the surface. When adsorbed from 1.00 mg/mL (Fig.

7.6.B), with higher PPI effects, a similar loss in solvent accessibility is indicated on the 'back' surface as with the low PPI effect case, but with a few additional areas on the 'front' surface showing substantial loss in solvent accessibility due to either altered orientation or blockage from neighboring proteins (Fig. 7.4, Table 7.4).

Comparing the results of a RNase A adsorbed on the neutral and moderately hydrophobic PMMA surface, Fig. 7.7.A shows areas of loss in solvation along the 'back' surface very similar to the HDPE surface, but with a lower degree of solvent accessibility loss compared to the HDPE surface (i.e., orange instead of yellow color coding in Fig. 7.7.A), which we assume to reflect the weaker degree of hydrophobic interactions on PMMA (Fig. 7.3, Table 7.3). Adsorption to PMMA under 1.00 mg/mL conditions, with a greater degree of PPI effects, showed a loss in solvent accessibility similar to the 0.03 mg/mL condition, but with a few additional areas of loss in solvent accessibility, due to either altered adsorbed orientation or blocking by neighboring adsorbed RNase A (Fig. 7.4, Table 7.4).

7.3.2.2.d Tertiary Unfolding of an Adsorbed RNase A

As shown in Figs 7.5-7.7, there are many similarities in the amino acid residues of RNase A that underwent increased solvent exposure, indicative of tertiary unfolding on each of our three model surfaces, with relatively minor differences indicated between these three surfaces (Figs. 7.3-7.7, Tables 7.3-7.4). We interpret these results to reflect regions in the RNase A structure that are less stable and prone to adsorption-induced unfolding. One point that is particularly relevant is that RNase A shows a substantial degree of increased solvent accessibility deep within its bioactive cleft for each surface

and solution concentration, as indicated by the solvent exposure of H12, which is not solvent accessible in solution (see Tables 7.3 and 7.4, and Figs 7.2, 7.5-7.7). These results suggest the disturbance of the structure of its binding site. This similarity may be responsible for the nearly equivalent loss in enzymatic activity that we measured for each adsorbed condition, which is addressed in the following section.

7.3.3 Molecular Mechanism Underlying the Enzymatic Activity of Adsorbed RNase A

The adsorption processes altered not only RNase A's native-state structure but also substantially reduced its enzymatic activity. As shown in Table 7.2, RNase A lost at least 60% of its solution-state activity on each of our three surfaces, which represent a broad range of surface chemistries, with no significant difference in the loss of activity for any of the applied adsorption conditions. The one common feature shown in Figs 7.4-7.6 for each of the adsorption conditions, which may explain these results, is a substantial increase in solvent accessibility of the H12 residue that is buried deep within the bioactive site pocket of RNase A, thus indicating that adsorption caused a substantial degree of tertiary unfolding to occur in this region of the protein. As shown in Fig. 7.1, H12 is one of the three key residues responsible for this enzyme's catalytic function. Based on these result, we propose that RNase A is susceptible to adsorption-induced unfolding of its binding site when adsorbed to a broad range of surface chemistries, and that this unfolding behavior causes substantial loss in its enzymatic activity.

The presented studies investigated the influence of adsorption on the structure and enzymatic activity of RNase A and are thus primarily relevant to protein-based drug delivery systems where proteins are adsorbed onto or within some sort of larger carrier

particles for the purpose of delivering higher pay-loads of a protein to a target. In such approaches, the outer surface of the carrier particles are often tethered with ‘stealth’ molecules, such as poly(ethylene glycol) (PEG), to enhance their residence time in the blood stream. Targeting molecules such as antibodies are then also typically linked to the drug delivery particles to selectively bind and concentrate the drug-bearing particles to their intended delivery site. As shown from the presented fundamental studies, adsorption of an enzyme to a material support can lead to a reduction in the enzyme’s activity by either structural unfolding or steric blocking of the enzyme’s active site. Other simpler approaches for the delivery of protein-based pharmaceutical agents have been taken such as the direct PEGylation of otherwise free enzymes to slow their clearance from the blood through mechanisms such as inhibiting their detection by phagocytic cells. However, this strategy can also reduce enzymatic activity by sterically blocking the binding of its intended substrate or receptor.[12, 29, 48] The key element in either of these strategies is to design the enzyme delivery system in such a manner as to preserve its activity so that it can perform its intended function once it is delivered to its intended target. This process requires a residue-level understanding of both the solvent accessibility and structural integrity of the enzyme’s active site along with the development and application of methods to make these types of assessments, such as the presented method of AAL/MS.

7.4 CHAPTER SUMMARY AND CONCLUSION

RNase A is known to be structurally robust in solution. However, our results demonstrate that it undergoes dramatic changes in both its structure and enzymatic

activity during adsorption on biomaterial surfaces with a broad range of surface chemistries and solution conditions. Using a complementary array of experimental techniques, which included circular dichroism, amino-acid side-chain modification and detection by mass spectrometry, we quantitatively demonstrated that the orientation and adsorption-induced changes in the secondary and tertiary structures of adsorbed RNase A are unique for each surface type and degree of PPI effects occurring in the adsorbed layer of protein. However, the effect of adsorption on the enzymatic activity of RNase A was not significantly different for any of the applied conditions, with about a 60% loss in enzymatic activity occurring irrespective of the type of adsorbent surface or degree of protein-protein interactions on the surface. Our results indicate that the similar loss in enzymatic activity observed with RNase A, despite undergoing varying extent of structural unfolding, is most likely due to the localized structural unfolding of the catalytic site. Therefore drug delivery systems must focus on retaining the native structure of catalytic site of RNase A in order to maintain a high level of enzymatic activity for applications such as anti-tumor chemotherapy.

7.5 REFERENCES

1. Rybak, S. M.; Newton, D. L. Natural and engineered cytotoxic ribonucleases: therapeutic potential. *Exp. Cell Res.* **1999,** *253* (2), 325-35.

2. Arnold, U.; Ulbrich-Hofmann, R. Natural and engineered ribonucleases as potential cancer therapeutics. *Biotechnol. Lett* **2006,** *28* (20), 1615-22.

3. Ilinskaya, O. N.; Makarov, A. A. Why ribonucleases induce tumor cell death. *Mol. Biol.* **2005,** *39* (1), 1-10.

4. Leland, P. A.; Raines, R. T. Cancer chemotherapy--ribonucleases to the rescue. *Chem. Biol.* **2001,** *8* (5), 405-13.

5. Klink, T. A.; Raines, R. T. Conformational stability is a determinant of ribonuclease A cytotoxicity. *J. Biol. Chem.* **2000,** *275* (23), 17463-7.

6. Poklar, N.; Petrovcic, N.; Oblak, M.; Vesnaver, G. Thermodynamic stability of ribonuclease A in alkylurea solutions and preferential solvation changes accompanying its thermal denaturation: a calorimetric and spectroscopic study. *Protein Sci.* **1999,** *8* (4), 832-40.

7. Townsend, M. W.; DeLuca, P. P. Stability of ribonuclease A in solution and the freeze-dried state. *J. Pharm. Sci.* **1990,** *79* (12), 1083-6.

8. Klink, T. A.; Woycechowsky, K. J.; Taylor, K. M.; Raines, R. T. Contribution of disulfide bonds to the conformational stability and catalytic activity of ribonuclease A. *Eur. J. Biochem.* **2000,** *267* (2), 566-72.

9. Daly, S. M.; Przybycien, T. M.; Tilton, R. D. Adsorption of poly(ethylene glycol)-modified ribonuclease A to a poly(lactide-co-glycolide) surface. *Biotechnol. Bioeng.* **2005,** *90* (7), 856-68.

10. Li, C.; Lin, Q.; Wang, J.; Shen, L.; Ma, G.; Su, Z.; Hu, T. Preparation, structural analysis and bioactivity of ribonuclease A-albumin conjugate: tetra-conjugation or PEG as the linker. *J. Biotechnol.* **2012,** *162* (2-3), 283-8.

11. Michaelis, M.; Cinatl, J.; Cinatl, J.; Pouckova, P.; Langer, K.; Kreuter, J.; Matousek, J. Coupling of the antitumoral enzyme bovine seminal ribonuclease to polyethylene glycol chains increases its systemic efficacy in mice. *Anticancer. Drugs* **2002,** *13* (2), 149-54.

12. Mathe, C.; Devineau, S.; Aude, J. C.; Lagniel, G.; Chedin, S.; Legros, V.; Mathon, M. H.; Renault, J. P.; Pin, S.; Boulard, Y.; Labarre, J. Structural determinants for protein adsorption/non-adsorption to silica surface. *PloS one* **2013,** *8* (11), e81346.

13. Pai, S. S.; Hammouda, B.; Hong, K.; Pozzo, D. C.; Przybycien, T. M.; Tilton, R. D. The conformation of the poly(ethylene glycol) chain in mono-PEGylated lysozyme

and mono-PEGylated human growth hormone. *Bioconjugate Chem.* **2011,** *22* (11), 2317-23.

14. Lee, C. S.; Belfort, G. Changing activity of ribonuclease A during adsorption: a molecular explanation. *Proc Natl Acad Sci U S A* **1989,** *86* (21), 8392-6.

15. Yi, C.; Fong, C. C.; Zhang, Q.; Lee, S. T.; Yang, M. The structure and function of ribonuclease A upon interacting with carbon nanotubes. *Nanotechnology* **2008,** *19* (9), 0957-4484.

16. Smith, B. D.; Soellner, M. B.; Raines, R. T. Synthetic surfaces for ribonuclease adsorption. *Langmuir* **2005,** *21* (1), 187-90.

17. Kastantin, M.; Langdon, B. B.; Schwartz, D. K. A bottom-up approach to understanding protein layer formation at solid-liquid interfaces. *Adv. Colloid Interface Sci.* **2014,** *207* (0), 240-52.

18. Lee, W. K.; McGuire, J.; Bothwell, M. K. Concentration effects on adsorption of bacteriophage T4 lysozyme stability variants to silica. *J. Colloid Interface Sci.* **2002,** *252* (2), 473-6.

19. Wei, Y.; Thyparambil, A. A.; Latour, R. A. Quantification of the influence of protein-protein interactions on adsorbed protein structure and bioactivity. *Colloids and Surfaces B: Biointerfaces* **2013,** *110* (0), 363-371.

20. Sivaraman, B.; Latour, R. A. The relationship between platelet adhesion on surfaces and the structure versus the amount of adsorbed fibrinogen. *Biomaterials* **2010,** *31* (5), 832-9.

21. Kim, J.; Somorjai, G. A. Molecular packing of lysozyme, fibrinogen, and bovine serum albumin on hydrophilic and hydrophobic surfaces studied by infrared-visible sum frequency generation and fluorescence microscopy. *J. Am. Chem. Soc.* **2003,** *125* (10), 3150-8.

22. Hu, Y.-J.; Ou-Yang, Y.; Dai, C.-M.; Liu, Y.; Xiao, X.-H. Site-selective binding of human serum albumin by palmatine: spectroscopic approach. *Biomacromolecules* **2009,** *11* (1), 106-112.

23. Rabe, M.; Verdes, D.; Seeger, S. Understanding protein adsorption phenomena at solid surfaces. *Adv. Colloid Interface Sci.* **2011,** *162* (1-2), 87-106.

24. Thyparambil, A. A.; Wei, Y.; Wu, Y.; Latour, R. A. Determination of orientation and adsorption-induced changes in the tertiary structure of proteins on material surfaces by chemical modification and peptide mapping. *Acta Biomaterialia* **2014,** *10* (6), 2404-2414.

25. Engel, M. F.; Visser, A. J.; van Mierlo, C. P. Conformation and orientation of a protein folding intermediate trapped by adsorption. *Proc. Natl. Acad. Sci. USA* **2004,** *101* (31), 11316-21.

26. Xu, J.; Bowden, E. F. Determination of the orientation of adsorbed cytochrome C on carboxyalkanethiol self-assembled monolayers by in situ differential modification. *J. Am. Chem. Soc.* **2006,** *128* (21), 6813-22.

27. Kastantin, M.; Langdon, B. B.; Schwartz, D. K. A bottom-up approach to understanding protein layer formation at solid-liquid interfaces. *Advances in Colloid and Interface Science* **2014,** *207*, 240-252.

28. Ovod, V.; Scott, E. A.; Flake, M. M.; Parker, S. R.; Bateman, R. J.; Elbert, D. L. Exposure of the lysine in the gamma chain dodecapeptide of human fibrinogen is not enhanced by adsorption to poly(ethylene terephthalate) as measured by biotinylation and mass spectrometry. *J. Biomed. Mater. Res.* **2012,** *100* (3), 622-31.

29. Mu, Q.; Hu, T.; Yu, J. Molecular insight into the steric shielding effect of PEG on the conjugated staphylokinase: biochemical characterization and molecular dynamics simulation. *PloS one* **2013,** *8* (7), e68559.

30. Sivaraman, B.; Fears, K. P.; Latour, R. A. Investigation of the effects of surface chemistry and solution concentration on the conformation of adsorbed proteins using an improved circular dichroism method. *Langmuir* **2009,** *25* (5), 3050-6.

31. Leitner, A.; Amon, S.; Rizzi, A.; Lindner, W. Use of the arginine-specific butanedione/phenylboronic acid tag for analysis of peptides and protein digests using matrix-assisted laser desorption/ionization mass spectrometry. *Rapid Commun. Mass Spectrom.* **2007,** *21* (7), 1321-30.

32. Suckau, D.; Mak, M.; Przybylski, M. Protein surface topology-probing by selective chemical modification and mass spectrometric peptide mapping. *Proc. Natl. Acad. Sci. USA* **1992,** *89* (12), 5630-4.

33. Fears, K. P.; Sivaraman, B.; Powell, G. L.; Wu, Y.; Latour, R. A. Probing the conformation and orientation of adsorbed enzymes using side-chain modification. *Langmuir* **2009,** *25* (16), 9319-27.

34. Rappsilber, J. The beginning of a beautiful friendship: cross-linking/mass spectrometry and modelling of proteins and multi-protein complexes. *J. Struct. Biol.* **2011,** *173* (3), 530-40.

35. Mendoza, V. L.; Vachet, R. W. Probing protein structure by amino acid-specific covalent labeling and mass spectrometry. *Mass Spectrom. Rev.* **2009,** *28* (5), 785-815.

36. Altman, D. G.; Bland, J. M. *How to obtain the P value from a confidence interval* [Journal Article]2011; Vol. 343.

37. Xiao, Y.; Hsiao, T. H.; Suresh, U.; Chen, H. I.; Wu, X.; Wolf, S. E.; Chen, Y. A novel significance score for gene selection and ranking. *Bioinformatics* **2014,** *30* (6), 801-7.

38. Berman, H. M.; Westbrook, J.; Feng, Z.; Gilliland, G.; Bhat, T. N.; Weissig, H.; Shindyalov, I. N.; Bourne, P. E. The Protein Data Bank. *Nucleic Acids Res.* **2000,** *28*, 235-242.

39. Borah, B.; Chen, C. W.; Egan, W.; Miller, M.; Wlodawer, A.; Cohen, J. S. Nuclear magnetic resonance and neutron diffraction studies of the complex of ribonuclease A with uridine vanadate, a transition-state analog. *Biochemistry (Mosc).* **1985,** *24* (8), 2058-2067.

40. Anand, G.; Sharma, S.; Dutta, A. K.; Kumar, S. K.; Belfort, G. Conformational transitions of adsorbed proteins on surfaces of varying polarity. *Langmuir* **2010,** *26* (13), 10803-11.

41. Ostuni, E.; Grzybowski, B. A.; Mrksich, M.; Roberts, C. S.; Whitesides, G. M. Adsorption of Proteins to Hydrophobic Sites on Mixed Self-Assembled Monolayers†. *Langmuir* **2003,** *19* (5), 1861-1872.

42. Konradi, R.; Textor, M.; Reimhult, E. Using complementary acoustic and optical techniques for quantitative monitoring of biomolecular adsorption at interfaces. *Biosensors* **2012,** *2* (4), 341-376.

43. Fears, K. P.; Latour, R. A. Assessing the influence of adsorbed-state conformation on the bioactivity of adsorbed enzyme layers. *Langmuir* **2009,** *25* (24), 13926-33.

44. Raines, R. T. Ribonuclease A. *Chem. Rev.* **1998,** *98* (3), 1045-1066.

45. Wei, Y.; Thyparambil, A. A.; Wu, Y.; Latour, R. A. Adsorption-induced changes in ribonuclease A structure and enzymatic activity on solid surfaces. *Langmuir* **2014,** *30* (49), 14849-58.

46. Chatani, E.; Hayashi, R. Functional and structural roles of constituent amino acid residues of bovine pancreatic ribonuclease A. *J. Biosci. Bioeng.* **2001,** *92* (2), 98-107.

47. Lins, L.; Thomas, A.; Brasseur, R. Analysis of accessible surface of residues in proteins. *Protein Sci.* **2003,** *12* (7), 1406-17.

48. Xue, X.; Li, D.; Yu, J.; Ma, G.; Su, Z.; Hu, T. Phenyl linker-induced dense PEG conformation improves the efficacy of C-terminally monoPEGylated staphylokinase. *Biomacromolecules* **2013,** *14* (2), 331-41.

CHAPTER EIGHT

PROTEIN HELICAL STRUCTURE DETERMINATION USING CD SPECTROSCOPY FOR SOLUTIONS WITH STRONG BACKGROUND ABSORBANCE FROM 190-230 NM

Based on the published article: Wei Y., Thyparambil A.A., and Latour R.A., Protein helical structure determination using CD spectroscopy for solutions with strong background absorbance from 190 to 230nm, BBA-Proteins and Proteomics, 1844(12): 2331-2337 (2014);

8.1 INTRODUCTION

Circular dichroism (CD) has been extensively used to spectroscopically study the structure of biomolecules in solution and when absorbed to surfaces due to its characteristics of being non-destructive, relatively easy to perform, requiring small sample volume, and providing fast, reliable data analyses.[1-2] In particular, CD provides a very convenient experimental method for the determination of the secondary structure and environmentally induced structural changes in proteins since the different forms of the primary secondary structural elements found in proteins (e.g., α-helix, β-sheet, and random loop) exhibit distinctly different CD spectrum.[3]

Most algorithms that have been developed for secondary structure determination of proteins by CD depend on the analysis of spectral features in the far UV range, primarily from 190 to 230 nm. Over this spectral range, the amides within the secondary structural components constituting a protein strongly absorb circularly polarized light and

undergo varying extents of n→π* and π→π* transitions for a given wavelength.[4] The CD spectrum (Fig 8.1) for a pure α-helical structure acquired between 190 to 250 nm exhibits a characteristic double minima at 208 nm (π →π*) and 222 nm (n→π*), and a stronger maxima at 191-193 nm (π→π*).[4] Similarly, β-sheet structure exhibits a characteristic minimum at 215 nm (n→π*) and a maximum at 198 nm (π→π*).[4] In contrast to these spectral features, random coil segments of protein tend to exhibit a maximum and a minimum that is essentially opposite from the minimum and maximum of the α-helical and β-sheet structures.[5]

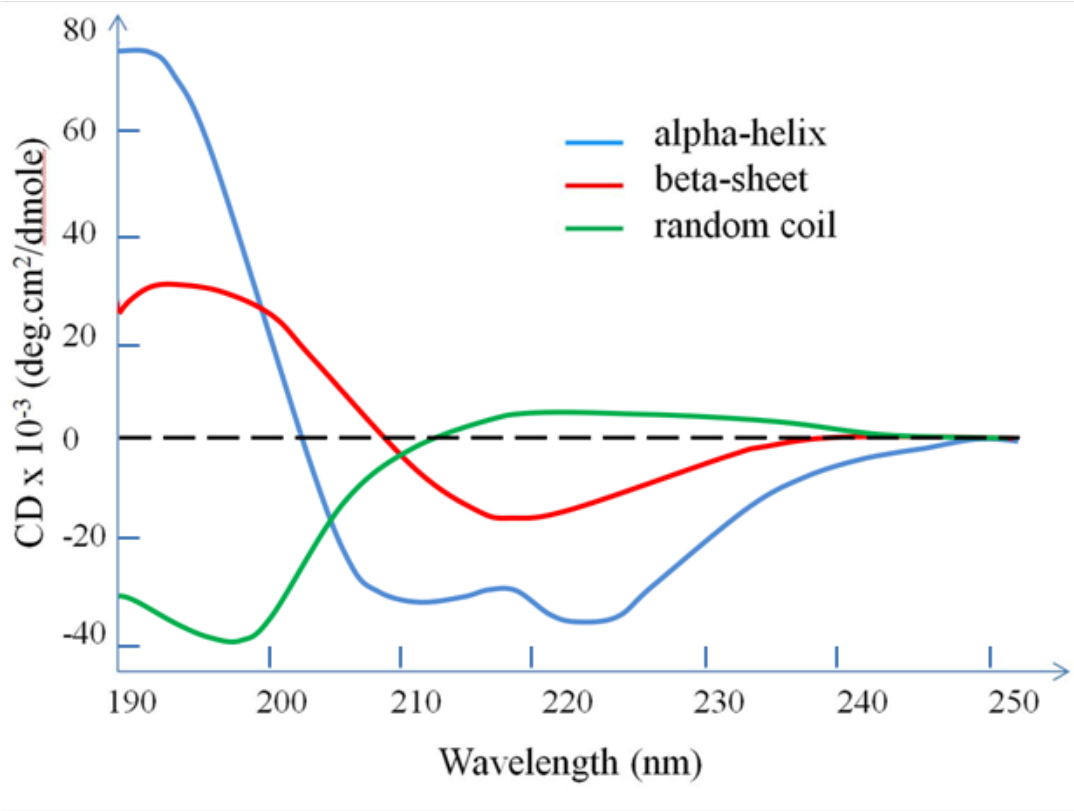

Figure 8.1. Standard CD spectra redrawn from Corrêa et al.[5-6] Each of the three basic secondary structures of a polypeptide chain (α-helix, β-sheet and random coil) show a distinctly different characteristic CD spectrum.[5] Redrawn with permission from Ref.6. Copyright 2014 BBA Inc., published by Elsevier Ltd.

To quantify the relative proportion of each associated secondary structure contained in a protein sample, the resulting CD spectrum acquired between wavelengths of 190 and 240 nm is typically empirically interpreted as a sum of fractional multiples of reference spectra for each type of secondary structure.[3] This process is conducted using a variety of mathematical tools[7] along with reference datasets of highly resolved protein structures (i.e., protein structures from X-ray crystallography and NMR spectroscopy).[8] As a result, these conventional algorithms cannot be used if the protein solution to be analyzed contains chemical species that strongly absorb at wavelengths below 230 nm, as commonly seen with various detergents and denaturants.[9-12] For example, Fig. 8.2, presents plots of the background absorbance for solutions containing various chemical additives using a 0.1 cm pathlength cuvette, which show saturating levels of absorbance (see for wavelengths below 225 nm). When this situation occurs, other methods are required for protein structural analysis.[1, 11, 13] This type of absorbance problem becomes increasingly problematic as the pathlength of the cuvette is increased, with pathlengths up to 1.0 cm being commonly used for temperature and titration experiments,[3, 14-23] and for the analysis of adsorbed proteins on nanoparticles or flat material surfaces in order to provide sufficient signal strength for analysis.[24-32]

Subsequently, conventional algorithms that rely on CD spectra over the range of 190-230 nm can only be used when the additives are present under extremely dilute conditions (e.g., < 50 mM urea), thus greatly limiting the ability to investigate the influence of such additives on a protein's secondary structure.

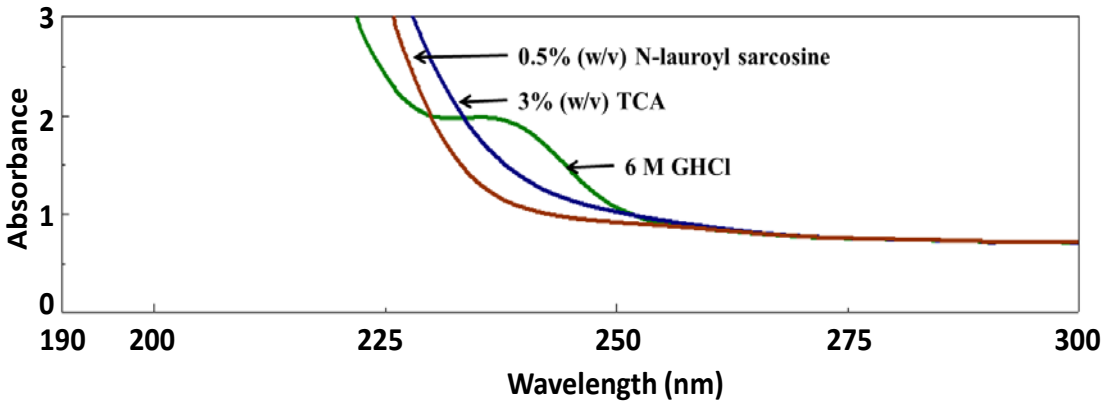

Figure 8.2. Effective absorbance spectra for different chemical additives (3% (w/v) trichloroacetic acid (TCA), 0.5% (w/v) N-lauroyl sarcosine solutions, and 6 M Guanidium hydrochloride (GHCl)) in a 0.1 cm pathlength cuvette. Strong absorbance results in signal saturation at high wavelengths, which can prohibit the use of conventional structural analysis algorithms that require CD signal sensitivity over the range of 190 to 230 nm.[1, 13] Redrawn with permission from Ref.6. Copyright 2014 BBA Inc., published by Elsevier Ltd.

To overcome this problem, a CD cell with shorter path-length is commonly used to minimize the background absorbance.[33] Alternatively, if CD data from wavelengths above 220 nm are available, the helical content of protein can at least still be estimated by choosing a single wavelength above 220 nm where the difference in signal between a folded and unfolded protein is large (unfortunately there are no analogous methods for estimating β-sheet or random coil structure).[34] For example, CD molar ellipticity data at 222 nm are commonly used for quantifying the helical content of protein (i.e., 222 nm method), where helical structure exhibits a characteristic minimum in ellipticity (Fig. 8.1).[5] Even higher wavelengths than 222 nm, such as 225 nm[11] or 228 nm,[34] have also been used for estimating helical content when the background absorbance has influenced the CD response at 222 nm. The situation, however, becomes particularly problematic when samples exhibit strong background absorbance all of the way up to 230 nm even when using CD cells of short path

length (Fig 8.2). In this case, there are presently no existing methods that can be used for the quantitative analysis of even the helical structure of a protein when in solution.

While seeking for alternative methods for the analysis of CD spectra for the determination of protein helical structure in the presence of strongly absorbing additives,[24-25] we observed that a linear region of varying slope typically occurs in CD spectrum between 230 nm to 240 nm. Based on this observation, we hypothesized that if the relative change in the molar ellipticity values between 230 nm to 240 nm were primarily caused by the helical structure of the protein, then the relative change in the slope, which can be simply derived from multiple CD points over this wavelengths range, may provide a sensitive method of estimating the helical content of protein in solution when the background absorbance occurs for wavelengths all of the way up to 230 nm.

The purpose of current chapter was therefore to investigate if a linear correlation exists between the slope of CD spectra over the range of 230-240 nm and protein fractional helicity determined by existing methods for a range of proteins and their conformational states in aqueous solution. The specific objective of this research was then to use this correlation (if found) to provide a method (i.e., the 230-240 nm slope method) that could be used to reliably quantify the helical content in proteins in solution with backgrounds exhibiting strong absorbance up to 230 nm.

8.2 ANALYTICAL MODEL

The 222 nm wavelength method for CD analysis of the helicity of protein structure uses the molar ellipticity CD data at 222 nm,[8] which is the wavelength corresponding to the characteristic minimum of the CD spectrum of the helical structure

of protein (see Fig. 8.1). Accordingly, the fractional helicity (*FH*) of a protein in solution can be estimated from the CD response at 222 nm, and similarly at other nearby wavelengths such as 225 and 228 nm,[11, 34] by equation (8.1): [5, 35]

$$FH = \frac{\left(\theta_{\lambda}^{\exp} - \theta_{\lambda}^{u}\right)}{\left(\theta_{\lambda}^{h} - \theta_{\lambda}^{u}\right)}, \tag{8.1}$$

where $\theta_{\lambda}^{\exp}$ is the experimentally observed mean residue ellipticity (usually given in deg.cm^2.dmol^{-1}) for a given wavelength (λ), and θ_{λ}^{u} and θ_{λ}^{h} correspond to the ellipticity for a protein with 0% and 100% helical content at wavelength λ, which are typically experimentally or theoretically estimated to be −3,000 and −39,500 deg.cm^2.dmole^{-1}, respectively, for a λ of 222 nm.[5, 36-37] Equation (8.1) can be rearranged to generally express $\theta_{\lambda}^{\exp}$ as a function of *FH* as designated by equation (8.2),

$$\theta_{\lambda}^{\exp} = FH\left(\theta_{\lambda}^{h} - \theta_{\lambda}^{u}\right) + \theta_{\lambda}^{u}. \tag{8.2}$$

Accordingly, by extending this relationship over a linear region of a CD spectrum in the region of 230-240 nm,[24-25] equation (8.2) can be expressed in terms of the change in ellipticity between two selected wavelengths, λ_1 and λ_2, as indicated by equation (8.3):

$$\Delta\theta^{\exp} = \theta_{\lambda 2}^{\exp} - \theta_{\lambda 1}^{\exp} = (\lambda_2 - \lambda_1)\nabla = \Delta\lambda\nabla = FH\left(\Delta\theta^{h} - \Delta\theta^{u}\right) + \Delta\theta^{u} \tag{8.3}$$

where '∇' represents the slope of the CD spectrum within this region of wavelengths and $\Delta\theta^{h}$ and $\Delta\theta^{u}$ represent the difference in molar ellipticity for 100% and 0% helical structure, respectively, at the two designated bracketing wavelengths, λ_1 and λ_2.

Equation (8.3) can subsequently be rearranged to express *FH* as a linear function of the slope, *A*, as presented in equation (8.4):

$$FH = \frac{(\Delta\lambda\nabla - \Delta\theta^u)}{(\Delta\theta^h - \Delta\theta^u)} - \left(\frac{\Delta\lambda}{\Delta\theta^h - \Delta\theta^u}\right)\nabla + \left(\frac{-\Delta\theta^u}{\Delta\theta^h - \Delta\theta^u}\right) - m\nabla + b \qquad (8.4)$$

where $\left(\frac{\Delta\lambda}{\Delta\theta^h - \Delta\theta^u}\right)$ and $\left(\frac{-\Delta\theta^u}{\Delta\theta^h - \Delta\theta^u}\right)$ should be constant for a designated pair of wavelengths in the linear portion of the CD spectrum, with '*m*' and '*b*' thus representing the slope and y-axis intercept for the linear relationship between *FH* and '∇'.

In this study, we investigate the correlation between values of *FH* provided by equation (8.4) and the values of *FH* obtained using both a conventional algorithm method and the 222 nm method, as provided by equation (8.1), for the estimation of the helicity of proteins in solution. If a strong correlation is shown, equation (8.4) then provides a method that should be useful for the estimation of the helical structure of proteins in solution with strong background of wavelengths up to 230 nm, which represents a condition that presently prohibits the use of conventional methods for the determination of the helicity of proteins either in solution or when adsorbed to a surface.

8.3 EXPERIMENTAL SETUP AND METHODOLOGY

8.3.1 Protein Solutions

The proteins used in the study were ribonuclease-A from bovine pancreas (RNase A, 13.7 kDa, 124 residues, Sigma, R5503), hen egg-white lysozyme (HEWL, 14 kDa, 129 residues, Sigma, L6876), human serum albumin (Albumin, 66 kDa, 585 residues,

Sigma, A3782), and human serum fibrinogen (Fibrinogen, 340 kDa, 269 residues, Sigma, F3879). Stock solutions (1.00 mg/ml) of each protein were first prepared in deionized water (D.I. water, 18.2 M Ω-cm, EMD Millipore, Milli Q Direct) and filtered to remove impurities. The final concentrations of protein in D.I. water or solutions with urea (Fisher Scientific, U15500) at different concentrations were verified via absorbance of protein solutions at 280 nm (A_{280}).[5, 11]

8.3.2 Acquisition of Spectrum Using CD Spectroscopy

The structure of each protein in solution (0.01 mg/ml) was determined in a quartz cuvette (Starna Cells) of 1.0 cm path length using a standardized methodology for CD spectropolarimeter (Jasco J-810) over a range of temperatures to induce various degrees of protein unfolding.[25] Briefly, each CD spectrum, consisting of the ellipticity and absorbance values, was obtained over a wavelength range from 190 to 300 nm, at a scan rate of 50 nm/min and a response time of 0.25 s. Each spectrum represented an accumulation of 6 scans. Temperature control within the CD instrument was done using the Peltier temperature control device that is integrated within our instrument. Thermal-induced denaturation of the proteins was done using an external water bath (Neslab, RTE-111) over a temperature range from 5 to 85°C.

In addition to the plain protein solutions, solutions of proteins with urea at different concentrations in a quartz cuvette (Starna Cells) of 0.01 cm path length were analyzed to provide samples exhibiting strong background absorbance over the range of 190–220 nm that could not be analyzed by conventional full-spectrum-based methods.

8.3.3 Algorithms to Quantify Protein Secondary Structure in Solution

The helical content of proteins in solution was determined using three different algorithms—the CONTIN program method,[2] the 222 nm method, and the proposed 230-240 nm slope method. Irrespective of the algorithm, the background-corrected CD signals were converted to molar ellipticity, $\theta_\lambda^{\exp}$, given in deg.cm^2/(dmol)), using equation (8.5):

$$\theta_\lambda^{\exp} = \frac{\theta_\lambda^{raw} \times M}{1000 \times C_{\text{soln}} \times L}, \tag{8.5}$$

where $\theta_\lambda^{\text{raw}}$ is the background corrected raw CD signal (degrees), L is the path length of the cuvette (mm), C_{soln} is the solution concentration of the protein (mg/mL), M is the mean residue molecular weight of 115 g/mol.

8.3.3.1 222 nm Method

The *FH* values of the proteins in solution were estimated from the mean residue ellipticity values at 222 nm according to equation (8.1).

8.3.3.2 CONTIN Program Method

The CONTIN program method, introduced by Provencher and Glöckner, determines the *FH* of a sample from the direct analysis of a CD spectrum over the full far-UV range from 190 to 240 nm as a linear combination of the CD spectrum from a library of 16 proteins whose structures have been determined to high resolution by X-ray crystallography.[2] In this method, the contribution of each reference spectrum is kept small unless it contributes to good agreement between the theoretical best-fit curve and the raw spectrum.[8]

8.3.3.3 230-240 nm Slope Method

The slope ('∇') over the wavelength range of 230 to 240 nm was first measured directly from the CD spectrum. As further addressed below, the slope ('*m*') and y-intercept ('*b*') characterizing the linear relationship between '∇' and *FH* (see equation (8.4) above) were then determined from a plot of '∇' vs. the *FH* values provided by the CONTIN program method. This linear relationship was then subsequently applied for the determination of the *FH* for solutions exhibiting high background absorbance up to 220 nm such that the CONTIN program method could not be used. A detailed protocol on FH determination using this method is provided in (section D.1 in appendix D)

8.3.4 Correlations Between Methods for Determination of Helical Structure of Protein in Solution

The helical structure of each protein under each solution condition was first determined using both the CONTIN and 222 nm methods, and the slope '∇' was calculated for each CD spectrum over the wavelength range from 230-240 nm. The slope '∇' from each CD spectrum was then plotted against the *FH* values estimated by the CONTIN program to assess the level of correlation between these two parameters, with values of '*m*' and '*b*' from equation (8.4) determined from the resulting linear relationship. Similarly, *FH* values obtained from the CONTIN program and 222 nm methods were then compared in order to confirm the correlation between these two conventional methods for our set of protein solutions.

The *FH* values obtained from the 230-240 nm slope method were then plotted against *FH* values estimated by the 222 nm method for proteins in solution containing 4

M and 8 M urea, which prohibited the direct use of the CONTIN method due to the strong background absorbance caused by these additives over the wavelength range of 190-220 nm. These comparisons were then used to assess the validity of using the proposed new 230-240 nm slope method for the estimation of the percentage of helical secondary structure of proteins including α-helix and 3_{10}-helix in solution in the presence of additives exhibiting strong background absorbance for wavelengths below 230 nm.

8.3.5 Statistical Analysis

The results from this study are presented as mean values ± 95% confidence intervals (C.I.) for each data point presented. The statistical significance of differences between calculated parameters was evaluated using Student's t test, with values of $p < 0.05$ being considered as statistically significant.

8.4 RESULTS and DISCUSSION

8.4.1 Determination of the Designated Values of 'm' and 'b' in Equation (8.4)

As shown in Fig. 8.3 for a set of four very structurally different proteins, a linear relationship is found between molar ellipticity and wavelength over the wavelength region from 230 to 240 nm. Furthermore, as indicated by equation (8.4), the slope of this linear portion of CD spectrum should be linearly related to the *FH* if molar ellipticity responses over this range are primarily determined by helical content of the protein (i.e., $FH = m\nabla + b$).

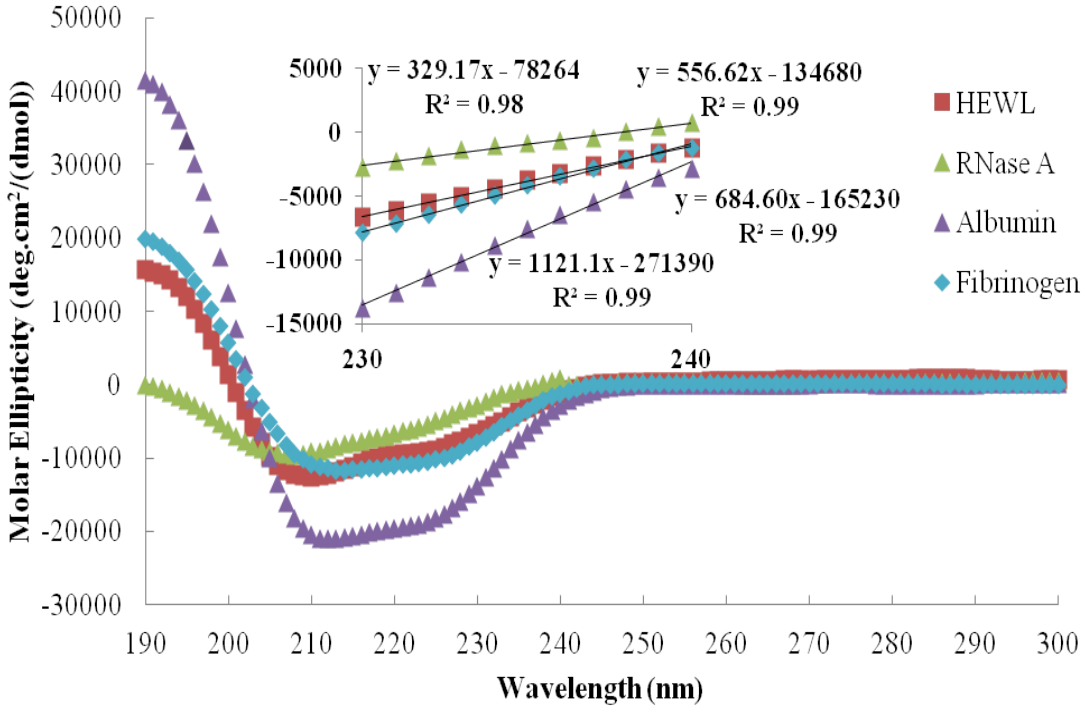

Figure 8.3. CD spectra showing a linear relationship over the wavelength range from 230 to 240 nm for four different types of protein. Inset: Enlargement of the molar ellipticities over the wavelength range of 230-240 nm from each overall CD spectrum with the linear regression equation provided for each plot. The slope of linear region between 230-240 nm is empirically determined to represent the parameter '∇' according to equation (8.3). For example '∇'= 329.17 (molar ellipticity/nm) for RNase A. Redrawn with permission from Ref.6. Copyright 2014 BBA Inc., published by Elsevier Ltd.

Since the CONTIN program is considered to be one of the 'gold standards' for protein structural determination by CD, if a linear relationship can be shown between '∇' and *FH* determined from the CONTIN program, then values of '*m*' and '*b*' can be determined from that plot to provide the ability to predict *FH* directly from '∇' for a given CD spectrum of protein in solution. Fig. 8.4 presents the solution structure data for *FH* values ranging from 0.03 to 0.58 estimated from the CONTIN program method vs. the empirical parameter '∇' for four different protein solutions.

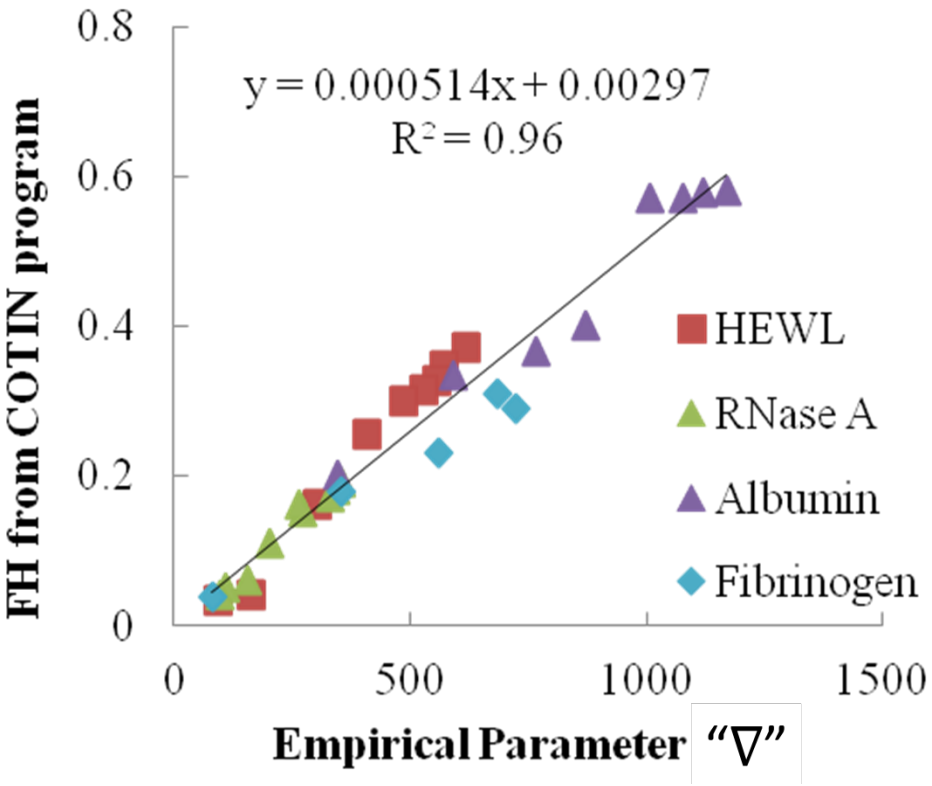

Figure 8.4. Correlation between the *FH* calculated by the CONTIN program method and the empirical parameter '∇' (i.e., the slope indicated in Eqn. (8.3) for each CD spectrum over the wavelength range from 230-240 nm; see Fig. 8.3). As indicated, the slope ('*m*') and y-intercept ('*b*') of the linear correlation line are equal to 0.000514 *FH*/(molar ellipticity/nm) and 0.00297 molar ellipticity, respectively, according to Eqn. (8.4). The value of '*b*' is not significantly different from zero. Raw data is provided in Table D.1 in Appendix D. Redrawn with permission from Ref.6. Copyright 2014 BBA Inc., published by Elsevier Ltd.

The wide range of helical content was achieved for these proteins by thermal denaturation in solution for temperatures ranging from 5°C to 85°C.[38] As shown, a strong linear correlation with $R^2 = 0.96$ is obtained between these two parameters (i.e., *FH* and '∇'), with the y-intercept (i.e., '*b*') of the linear correlation line not being significantly different from zero ($p = 0.65$). The strong linear relationship between *FH* and '∇' supports our hypothesis that the 230-240 nm slope method can be used to provide a reliable approach for the determination of *FH*. Based on the linear relationship shown in Fig. 8.4, the designated

values of '*m*' and '*b*' representing the slope and y-axis intercept for the linear relationship between *FH* and *A* are 5.14×10^{-3} *FH*/(molar ellipticity/nm) and 2.97×10^{-3} *FH*, respectively.

8.4.2 Reliability of the Helical Analysis Using CD Response at 222 nm

In this section, the *FH* estimated by equation (8.1) using CD at 222 nm (i.e., 222 nm method) is compared with *FH* estimated from the CONTIN program method in order to validate the use of the 222 nm method for the estimation of protein helical structure for our set of protein solutions. Once validated, the 222 nm method can then be used as a basis to evaluate the reliability of the 230-240 nm slope method for *FH* determination for samples with high background absorbance over wavelengths below 220 nm, for which the CONTIN method cannot be applied.

As shown in Fig. 8.5, a strong linear correlation with $R^2 = 0.96$ is found between the *FH* values from both algorithms for the same protein reference set. However, the 222 nm and CONTIN methods are not in perfect agreement, which would be indicated if the linear regression of the data plot shown in Fig. 8.5 had a slope = 1 and a y-axis intercept = 0. Statistical analyses of the data presented in Fig. 8.5 indicate that the slope of the linear regression line is significantly different from one ($p < 0.0001$) and we can directly conclude that these two lines (i.e., $y = 0.815x + 0.0875$ and $y = x$) are significantly different without comparing the intercepts. Compared to the CONTIN program method, the 222 nm method is thus shown to slightly overestimate helix content when $FH < 0.47$ and slightly underestimate helicity when $FH > 0.47$ for this set of samples. Additionally, as noted in the preceding section, statistical analysis of the y-axis intercept of the linear correlation line in Fig. 8. 4 shows that it is not significantly different from zero while having an equivalent R^2 value as

the correlation line in Fig. 8.5. These results suggest that 230-240 nm slope method actually has the potential to provide closer agreement with the CONTIN program method over a wider range of *FH* than the 222 nm method.

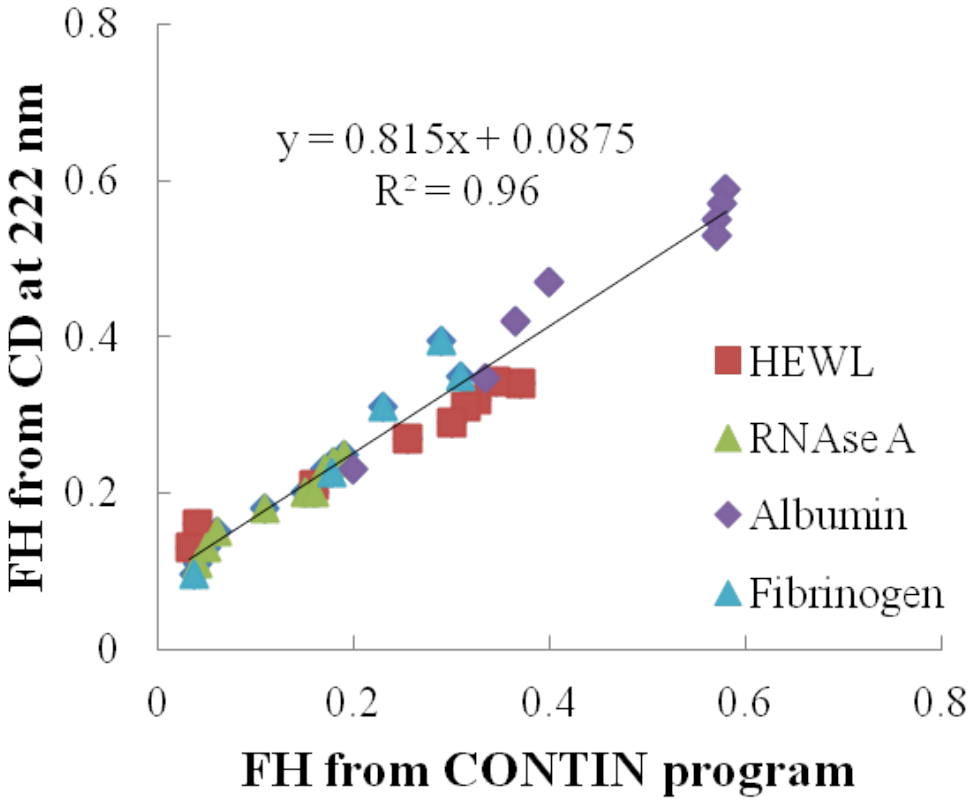

Figure 8.5. The correlation for calculated *FH* values between two popular CD algorithms: the 222 nm method and the CONTIN program method. The slope of the linear correlation line is significantly different from one and the y-intercept is significantly different from zero, thus showing some deviation between the CONTIN program and the 222 nm methods for the calculation of *FH*. Raw data is provided in Table D.1. Redrawn with permission from Ref.6. Copyright 2014 BBA Inc., published by Elsevier Ltd.

8.4.3 Comparison Between *FH* Values Calculated by the 222 nm and 230-240 nm Slope Methods for Protein Solutions with Strong Background Absorbance from 190-220 nm

Fig. 8.6 presents solution structure data for *FH* values ranging from 0.03 to 0.58 calculated from equation (8.1) using the 222 nm method versus *FH* values calculated from

equation (8.4) using the 230-240 nm slope method with '*m*' and '*b*' values determined in Section 8.4.1 ($m = 5.14\times10^{-3}$ *FH*/(molar ellipticity/nm) and $b = 2.97\times10^{-3}$ *FH*). In addition to the *FH* values from the set of proteins in D.I. water shown in Fig. 8.5, data points are added in Fig. 8.6 for protein in solution with 4 M and 8 M urea, which caused strong background absorbance over the range of 190-220 nm, thus prohibiting application of the CONTIN program method to determine *FH*.

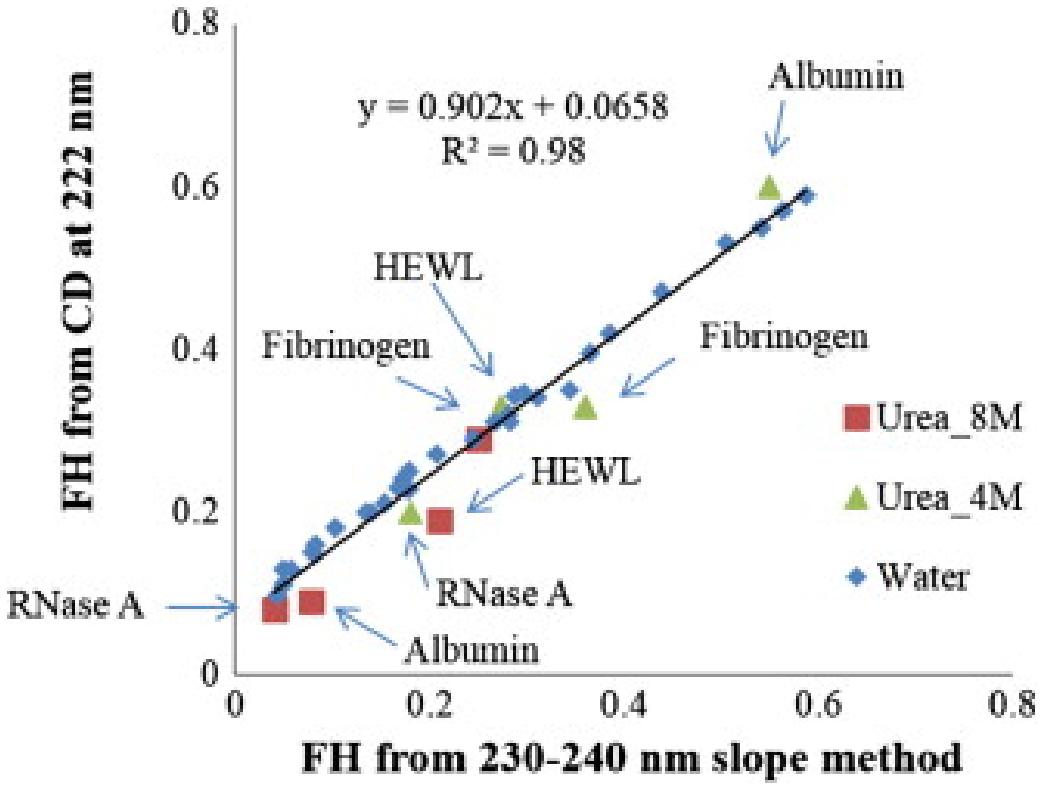

Figure 8.6. *FH* calculated from 222 nm method versus the 230-240 nm slope method for four different proteins in D.I. water and in the presence of 4 M and 8 M urea. The trend line is created considering all of the data points. Raw data is provided in Table D.1 and Table D.2 in the Appendix D. Redrawn with permission from Ref.6. Copyright 2014 BBA Inc., published by Elsevier Ltd.

As shown in Fig. 8.6, a strong linear correlation with $R^2 = 0.98$ is obtained between the 222 nm and 230-240 nm slope methods. This result is expected given that the '*m*' and '*b*' parameters of the slope method were calculated to fit the *FH* values determined by the

CONTIN program method, which is shown to correlate well with the 222 nm method in Fig. 8.5. More importantly, however, the 230-240 nm slope method is shown in Fig. 8.6 to provide *FH* values in close agreement with values calculated using the 222 nm method even for protein solutions with a high concentration of urea over the full range of *FH*. These results thus support the ability to use the 230-240 nm slope method for the estimation of the percentage of helical secondary structure of proteins in solution, with specific application for samples exhibiting strong background absorbance over wavelengths up to 230 nm, thus preventing the application of either the 222 nm or the CONTIN program method for *FH* determination.

8.4.4 Limitation of 230-240 nm slope method in estimating helical content of protein

Much like the 222 nm method, the helix content obtained using the 230–240 nm slope method should be used with caution and only when more robust methods cannot be applied due to high background absorbance. Secondary structural assignments within a CD spectrum and their quantification are dependent on both the algorithm used and the dataset available to fit the spectral features[3, 39] In this present study, the fitting parameters for determining the *FH* of the proteins using the 230–240 nm slope method were obtained using the CONTIN algorithm that is provided with the CDPro package using protein spectra obtained between 190 and 240 nm as the reference dataset. Of course, different algorithms and reference datasets may provide different estimates of helical content, resulting in a different set of fitting parameters than those presented in this work for application of the proposed 230–240 nm slope method. [39-42]

To investigate the broader applicability of the presented 230–240 nm slope

method beyond our limited dataset, we applied the method to analyze the large CD reference set of proteins with known 3D structures contained in the Protein Circular Dichroism Data Bank (PCDDB),[43] which is an excellent resource for structural biology. Fig. 8.7 presents the plot of 230-240 nm slopes measured from the CD spectra of 71 soluble proteins and 30 membrane proteins that comprise SP175 [44] and MP180 [41] datasets within the PCDDB, vs. the fractional helicity for each of these proteins.[43] The fractional helicity for each of these proteins included the contribution from α-, and 3_{10}helices as estimated using the DSSP algorithm.[43]

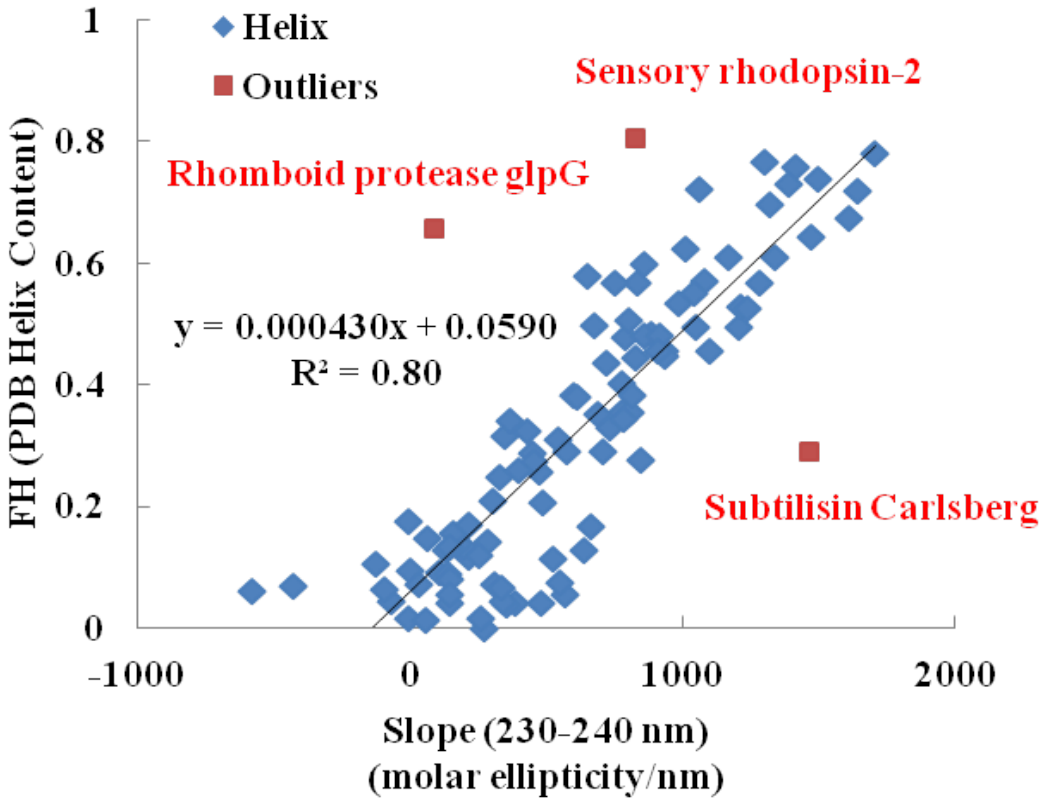

Figure 8.7. The helix content as a function of the 230-240 nm slopes on the proteins of the SP175 and MP 180 CD reference set (downloadable form PCDDB). Outlier data points were marked in red with protein names provided and analyzed by the Studentized–Residual method.[45] Raw data is provided in Table D.3 of the Appendix D. Redrawn with permission from Ref.6. Copyright 2014 BBA Inc., published by Elsevier Ltd.

As shown in Fig 8.7, the majority of the data points indicate very good correlation between the 230–240 nm slope and *FH*. However, there are a few obvious exceptions in the dataset indicative of proteins that do not follow this correlation. These data points, which were identified as outliers of the overall dataset using the Studentized-Residual method,[45] are labeled in red in Fig 8.7 along with the name of the associated protein. When these outliers are removed from the dataset, the resulting correlation line is not significantly different ($p > 0.05$) from the correlation line obtained for our experimental dataset that is shown in Fig. 8.4 (slope comparison: $p = 0.14$; intercept comparison: $p = 0.49$). Thus, the 230–240 nm methods are shown to be generally reliable for the estimation of the helical content of proteins even for this much larger reference set of proteins aside from a few clear exceptions.

Because Fig. 8.7 presents clear examples where the 230–240 nm slope method does not closely predict the helical content of the protein (e.g., the outliers), before this method is applied to analyze the structure of a given protein for a case where chemical agents are present that cause high background absorbance, its applicability for the protein should first be confirmed. This can be easily accomplished by obtaining the CD spectrum of the protein in a solution with low background absorbance such that the *FH* value predicted using the 230–240 nm slope method can be compared with a conventional full-spectrum algorithm, such as CONTIN, or with the *FH* obtained from the Protein Data Bank If reasonable agreement is found, then the 230–240 nm slope method should be able to be confidently used to predict the *FH* of the protein under conditions that prevent the use of a conventional full-spectrum method. It should also be recognized that the

contribution by β-sheets to spectral features over the range of 230–240 nm can vary for different proteins and their folded states, and its impact on the spectral features at these wavelengths is still not well-understood.[3, 39]

8.5 CHAPTER SUMMARY AND CONCLUSION

In this study we present a new method to analyze CD spectra that provide the capability of determining the helical structure of protein in solution in the presence of chemical additives that strongly adsorb in the 190 to 230 nm range, which otherwise interfere with the ability to determine protein structure using conventional CD analysis algorithms.

We proposed that the slope ('∇') of CD a spectrum over the 230 to 240 nm region should be linearly related to the helix content of the protein in solution. The slope ('*m*') and y-intercept ('*b*') for this relationship were calculated by plotting '∇' vs. the *FH* values determined by the CONTIN program method for CD data obtained for four different proteins in solution with helical content ranging from 0.03 to 0.58. The 230–240 nm slope method was then shown to accurately predict *FH* values for protein solutions with high background absorbance, which prevented the use of the CONTIN algorithm for *FH* determination.

Application of the 230–240 nm slope method to predict *FH* of proteins for the much larger datasets provided in the Protein CD Data Bank showed that the resulting correlation line was not significantly different from the correlation line derived from our much smaller dataset, with the exception of a few outlier examples where the protein's helicity was clearly not well predicted by this method. Given this realization, before using this method to analyze the helicity of a protein in a solution with high background absorbance, it is important to first establish the validity of the method for the designated protein under low-background

conditions where it can be shown to provide close agreement with the helicity predicted by a suitable full-spectrum method or helicity obtained directly from the Protein Data Bank.

Based on these results, we conclude that this new 230–240 nm slope method can be used for the determination of the helical content for proteins in solution when the solution exhibits strong absorbance of wavelengths up to 230 nm, thus prohibiting the use of conventional methods for the determination of protein secondary structure in aqueous solution.

8.6 REFERENCES

1. Li, C. H.; Nguyen, X.; Narhi, L.; Chemmalil, L.; Towers, E.; Muzammil, S.; Gabrielson, J.; Jiang, Y. Applications of circular dichroism (CD) for structural analysis of proteins: qualification of near- and far-UV CD for protein higher order structural analysis. *J. Pharm. Sci.* **2011,** *100* (11), 4642-54.

2. Sreerama, N.; Woody, R. W. Estimation of protein secondary structure from circular dichroism spectra: comparison of CONTIN, SELCON, and CDSSTR methods with an expanded reference set. *Anal. Biochem.* **2000,** *287* (2), 252-60.

3. Greenfield, N. J. Using circular dichroism spectra to estimate protein secondary structure. *Nat Protoc* **2006,** *1* (6), 2876-90.

4. Sreerama, N.; Woody, R. W. Computation and analysis of protein circular dichroism spectra. *Methods Enzymol.* **2004,** *383*, 318-51.

5. Corrêa, D. H. A., Ramos, C.H.I. The use of circular dichroism spectroscopy to study protein folding, form and function. *Afr. J. Biochem. Res.* **2009,** *3* (5), 164-173.

6. Wei, Y.; Thyparambil, A. A.; Latour, R. A. Protein helical structure determination using CD spectroscopy for solutions with strong background absorbance from 190 to 230nm. *Biochim. Biophys. Acta* **2014,** *1844* (12), 2331-2337.

7. Wallace, B. A.; Lees, J. G.; Orry, A. J.; Lobley, A.; Janes, R. W. Analyses of circular dichroism spectra of membrane proteins. *Protein Sci.* **2003,** *12* (4), 875-84.

8. Kelly, S. M.; Price, N. C. The use of circular dichroism in the investigation of protein structure and function. *Curr Protein Pept Sci* **2000,** *1* (4), 349-84.

9. Bohnert, J. L.; Horbett, T. A. Changes in adsorbed fibrinogen and albumin interactions with polymers indicated by decreases in detergent elutability. *J. Colloid Interface Sci.* **1986,** *111* (2), 363-377.

10. Griko, Y.; Sreerama, N.; Osumi-Davis, P.; Woody, R. W.; Woody, A. Y. Thermal and urea-induced unfolding in T7 RNA polymerase: calorimetry, circular dichroism and fluorescence study. *Protein Sci.* **2001,** *10* (4), 845-53.

11. Kelly, S. M.; Jess, T. J.; Price, N. C. How to study proteins by circular dichroism. *Biochim Biophys Acta* **2005,** *10* (2), 119-39.

12. Xia, Z.; Das, P.; Shakhnovich, E. I.; Zhou, R. Collapse of unfolded proteins in a mixture of denaturants. *J. Am. Chem. Soc.* **2012,** *134* (44), 18266-74.

13. DiNitto, J. M.; Kenney, J. M. Noise characterization in circular dichroism spectroscopy. *Appl Spectrosc* **2012,** *66* (2), 180-7.

14. Greenfield, N. J. Using circular dichroism collected as a function of temperature to determine the thermodynamics of protein unfolding and binding interactions. *Nat. Protocols* **2007,** *1* (6), 2527-2535.

15. Greenfield, N. J. Determination of the folding of proteins as a function of denaturants, osmolytes or ligands using circular dichroism. *Nat. Protocols* **2007,** *1* (6), 2733-2741.

16. Greenfield, N. J. Analysis of the kinetics of folding of proteins and peptides using circular dichroism. *Nat. Protocols* **2007,** *1* (6), 2891-2899.

17. Yamamoto, T.; Fukui, N.; Hori, A.; Matsui, Y. Circular dichroism and fluorescence spectroscopy studies of the effect of cyclodextrins on the thermal stability of chicken egg white lysozyme in aqueous solution. *J. Mol. Struct.* **2006,** *782* (1), 60-66.

18. Hawe, A.; Kasper, J. C.; Friess, W.; Jiskoot, W. Structural properties of monoclonal antibody aggregates induced by freeze-thawing and thermal stress. *Eur. J. Pharm. Sci.* **2009,** *38* (2), 79-87.

19. Olzmann, J. A.; Brown, K.; Wilkinson, K. D.; Rees, H. D.; Huai, Q.; Ke, H.; Levey, A. I.; Li, L.; Chin, L. S. Familial Parkinson's disease-associated L166P mutation disrupts DJ-1 protein folding and function. *J. Biol. Chem.* **2004,** *279* (9), 8506-15.

20. Fan, H.; Vitharana, S. N.; Chen, T.; O'Keefe, D.; Middaugh, C. R. Effects of pH and polyanions on the thermal stability of fibroblast growth factor 20. *Mol. Pharm.* **2007,** *4* (2), 232-40.

21. Garzon, M. T.; Lidon-Moya, M. C.; Barrera, F. N.; Prieto, A.; Gomez, J.; Mateu, M. G.; Neira, J. L. The dimerization domain of the HIV-1 capsid protein binds a capsid protein-derived peptide: a biophysical characterization. *Protein Sci.* **2004,** *13* (6), 1512-23.

22. Robic, S.; Guzman-Casado, M.; Sanchez-Ruiz, J. M.; Marqusee, S. Role of residual structure in the unfolded state of a thermophilic protein. *Proc. Natl. Acad. Sci. USA* **2003,** *100* (20), 11345-9.

23. Reed, C. J.; Bushnell, S.; Evilia, C. Circular Dichroism and Fluorescence Spectroscopy of Cysteinyl-tRNA Synthetase from Halobacterium salinarum ssp. NRC-1 Demonstrates that Group I Cations Are Particularly Effective in Providing Structure and Stability to This Halophilic Protein. *PloS one* **2014,** *9* (3), e89452.

24. Wei, Y.; Thyparambil, A. A.; Latour, R. A. Quantification of the influence of protein-protein interactions on adsorbed protein structure and bioactivity. *Colloids and Surfaces B: Biointerfaces* **2013,** *110* (0), 363-371.

25. Sivaraman, B.; Fears, K. P.; Latour, R. A. Investigation of the effects of surface chemistry and solution concentration on the conformation of adsorbed proteins using an improved circular dichroism method. *Langmuir* **2009,** *25* (5), 3050-6.

26. Bhogale, A.; Patel, N.; Sarpotdar, P.; Mariam, J.; Dongre, P. M.; Miotello, A.; Kothari, D. C. Systematic investigation on the interaction of bovine serum albumin with ZnO nanoparticles using fluorescence spectroscopy. *Colloids Surf. B. Biointerfaces* **2013,** *102* (0), 257-64.

27. Koutsopoulos, S.; Patzsch, K.; Bosker, W. T.; Norde, W. Adsorption of trypsin on hydrophilic and hydrophobic surfaces. *Langmuir* **2007,** *23* (4), 2000-6.

28. Sabatino, P.; Casella, L.; Granata, A.; Iafisco, M.; Lesci, I. G.; Monzani, E.; Roveri, N. Synthetic chrysotile nanocrystals as a reference standard to investigate surface-induced serum albumin structural modifications. *J. Colloid Interface Sci.* **2007,** *314* (2), 389-97.

29. Trofimova, D.; de Jongh, H. H. J. Modification of β-Lactoglobulin by Oligofructose: Impact on Protein Adsorption at the Air−Water Interface. *Langmuir* **2004,** *20* (13), 5544-5552.

30. Hu, Y.-J.; Ou-Yang, Y.; Dai, C.-M.; Liu, Y.; Xiao, X.-H. Site-selective binding of human serum albumin by palmatine: spectroscopic approach. *Biomacromolecules* **2009,** *11* (1), 106-112.

31. Vertegel, A. A.; Siegel, R. W.; Dordick, J. S. Silica nanoparticle size influences the structure and enzymatic activity of adsorbed lysozyme. *Langmuir* **2004,** *20* (16), 6800-7.

32. Verma, A.; Simard, J. M.; Rotello, V. M. Effect of ionic strength on the binding of alpha-chymotrypsin to nanoparticle receptors. *Langmuir* **2004,** *20* (10), 4178-81.

33. Clarke, D. T. Circular Dichroism in Protein Folding Studies. In *Current Protocols in Protein Science*; John Wiley & Sons, Inc., 2001.

34. Walters, J.; Milam, S. L.; Clark, A. C. Chapter 1 Practical Approaches to Protein Folding and Assembly: Spectroscopic Strategies in Thermodynamics and Kinetics. In *Methods in Enzymology*, Michael L. Johnson, J. M. H.; Gary, K. A., Eds.; Academic Press, 2009; Vol. Volume 455, pp 1-39.

35. Morrisett, J. D.; David, J. S.; Pownall, H. J.; Gotto, A. M., Jr. Interaction of an apolipoprotein (apoLP-alanine) with phosphatidylcholine. *Biochemistry (Mosc).* **1973,** *12* (7), 1290-9.

36. Duarte, A. M.; Wolfs, C. J.; van Nuland, N. A.; Harrison, M. A.; Findlay, J. B.; van Mierlo, C. P.; Hemminga, M. A. Structure and localization of an essential

transmembrane segment of the proton translocation channel of yeast H+-V-ATPase. *Biochim. Biophys. Acta* **2007,** *1768* (2), 218-27.

37. Fujiwara, Y.; Kurokawa, T.; Takeshita, K.; Kobayashi, M.; Okochi, Y.; Nakagawa, A.; Okamura, Y. The cytoplasmic coiled-coil mediates cooperative gating temperature sensitivity in the voltage-gated H(+) channel Hv1. *Nat Commun* **2012,** *3*, 816.

38. Paci, E.; Karplus, M. Unfolding proteins by external forces and temperature: the importance of topology and energetics. *Proc. Natl. Acad. Sci. USA* **2000,** *97* (12), 6521-6.

39. Whitmore, L.; Wallace, B. A. Protein secondary structure analyses from circular dichroism spectroscopy: methods and reference databases. *Biopolymers* **2008,** *89* (5), 392-400.

40. Whitmore, L.; Wallace, B. A. DICHROWEB, an online server for protein secondary structure analyses from circular dichroism spectroscopic data. *Nucleic Acids Res.* **2004,** *32* (Web Server issue), W668-73.

41. Abdul-Gader, A.; Miles, A. J.; Wallace, B. A. A reference dataset for the analyses of membrane protein secondary structures and transmembrane residues using circular dichroism spectroscopy. *Bioinformatics* **2011,** *27* (12), 1630-1636.

42. Lees, J. G.; Miles, A. J.; Wien, F.; Wallace, B. A. A reference database for circular dichroism spectroscopy covering fold and secondary structure space. *Bioinformatics* **2006,** *22* (16), 1955-62.

43. Whitmore, L.; Woollett, B.; Miles, A. J.; Klose, D. P.; Janes, R. W.; Wallace, B. A. PCDDB: the Protein Circular Dichroism Data Bank, a repository for circular dichroism spectral and metadata. *Nucleic Acids Res.* **2011,** *39* (Database issue), D480-6.

44. Lees, J. G.; Miles, A. J.; Wien, F.; Wallace, B. A. A reference database for circular dichroism spectroscopy covering fold and secondary structure space. *Bioinformatics* **2006,** *22* (16), 1955-1962.

45. Hadi, A. S.; Simonoff, J. S. Procedures for the Identification of Multiple Outliers in Linear Models. *Journal of the American Statistical Association* **1993,** *88* (424), 1264-1272.

CHAPTER NINE

QUANTIFYING THE ROLE OF CHEMICAL EXCIPIENTS ON THE SURFACE COVERAGE, SECONDARY STRUCTURE, AND BIOACTVITY OF PROTEINS PRE-ADSORBED ON A MATERIAL SURFACE

9.1 INTRODUCTION

Non-specific adsorption of proteins is a common phenomenon that is important in any application involving contact of protein solutions with material surfaces.[1-2] This inadvertent adsorption of proteins often renders underlying material surfaces bioactive, and is particularly a concern in biodefense applications,[3-6] where the release of proteins like toxins,[5] in a confined area will result in the contamination of all of the environmental surfaces that the protein comes in contact with. Strategies are therefore needed for the safe and effective decontamination of environmental surfaces — by either denaturing the adsorbed protein in attempts to eliminate its bioactivity or by eluting the adsorbed protein from surface. Such strategies would not only benefit bio-defense applications but also are of relevance in other sectors like biopharmaceutical and medical device industry, where the elution of adsorbed protein, and the structure of retained fraction of proteins on a material surface are a concern in influencing the operational stability, therapeutic efficacy, and quality of the product.[7-12]

Chemical excipients like salts and surfactants are attractive decontamination agents considering its aqueous solubility and interaction with the native structure of protein are fairly well-characterized.[13-16] However, its modes of interaction with an

adsorbed protein are less understood; especially since these proteins tend to undergo conformational shifts, and the affinity and interaction of a chemical excipient with a given protein is also influenced by its conformational state.[13] But, the lack of a direct technique to quantify the structure of adsorbed proteins has generally limited a quantitative understanding on the influence of the adsorbed structure of a protein on the elution process by a chemical excipient.[17-21] As a result, much of the current mechanistic understanding is based on the assumption that the influence of chemical excipients on the adsorbed protein structure would be identical to that in its solution state.[17-21]

Previous studies have demonstrated that the conformational shifts in proteins that are adsorbed on flat surfaces with relatively low surface coverage can be quantified using CD over the full spectral range of wavelengths from 190-240 nm.[22-23] However, most chemical excipients tend to strongly absorb at spectral wavelengths up to 230 nm, which limits the conventional method for quantifying the secondary structural content in proteins.[24-25] But, with the recent development of a method that uses linear slope *('A')* within the 230 to 240 nm region of the CD spectrum, the helical content of adsorbed proteins in the presence of strongly absorbing chemical excipients can be potentially quantified.[24-25] This improvement is of added significance, considering that much of the current data is limited to the influence of chemical excipients on the tertiary structure of adsorbed protein and its bioactive state.[24, 26] Therefore, the objective of current study was to expand the CD methodology to quantify and assess the influence of chemical excipients on the surface coverage, structure, and bioactivity of retained fraction of adsorbed proteins so as to better understand its interaction with the pre-adsorbed proteins.

Towards this purpose, the influence of two types of chemical excipients (surfactants and salts) on adsorbed protein structure and bioactivity were investigated using CD spectroscopy. The proteins, ribonuclease-A (RNase A) and hen egg-white lysozyme (HEWL) were used as toxin simulants,[27] and were adsorbed on silica glass, high density polyethylene, and poly(methyl) methacrylate surfaces. Subsequently, we compared the influence of two types of salt (urea and guanidium hydrochloride) and three types of surfactants (sodium dodecyl sulphate, n-octyl-β-D-glucoside, and 3-[(3-Cholamidopropyl) dimethylammonio]-1-propanesulfonate) on the surface coverage, helix content, and bioactivity of proteins pre-adsorbed from two different bulk solution concentrations.

9.2 EXPERIMENTAL SETUP AND METHODOLOGY

9.2.1 Material Surface Preparation and Characterization

The selected material surfaces include fused silica glass (glass), high density polyethylene (HDPE), and poly (methyl methacrylate) (PMMA). Custom cut glass slides (0.375″(L) × 0.0625″ (W)× 1.625″ (H), Chemglass Life Sciences) were procured and cleaned at 50°C by immersing in piranha solution (7:3 v/v H_2SO_4(EMD Chemicals, SX 1244)/H_2O_2) for at least 30 minutes, followed by basic wash (1:1:5 v/v NH_4OH (BDH Chemicals, BDH3016)/H_2O_2/H_2O), and this procedure was repeated twice. Standard operating procedures were followed for the handling, storage, and disposal of these wash solutions.

HDPE and PMMA surfaces were spin–coated onto the glass slides using dodecalin (0.5% (w/w) at 1500 rpm for 60s) and chloroform solutions (1.5% (w/w) at

1000 rpm for 60s), respectively. All chemicals including the polymers of HDPE (M_w = 125,000 Da, Sigma 181900) and PMMA (M_w = 350,000 Da, Sigma 445746) and dodecalin (Sigma 294772) and chloroform (EMD Chemicals, CX 1054) were used as supplied by the manufacturer. Prior to conducting the adsorption studies, all the substrates were rinsed in absolute ethanol, followed by nanopure water, and then dried under nitrogen gas.

Characterization of material surfaces was performed to determine the static air–water contact angle, surface composition, film thickness, and surface roughness of the substrates. For each surface, the static air–water contact angle was analyzed using a contact–angle goniometer (Krüss, DSA–20E), surface composition was verified via X–ray photoelectron spectroscopy (NESCA/BIO, University of Washington), and average RMS surface roughness was analyzed using atomic force microscopy (Asylum Research, MFP–3D) over an area of 5 × 5 μm. Thickness of the polymer films was characterized using variable angle spectroscopic ellipsometer (Sopra Inc., GES–5).

9.2.2 Protein Adsorption and Equilibration

Proteins used in the study were ribonuclease-A from bovine pancreas (RNase A, 13.7 kDa, 124 residues, Sigma, R5503), and hen egg-white lysozyme (HEWL, 14.1 kDa, 129 residues, Sigma, L6876). Stock solutions (1.00 mg/ml) of each protein were first prepared in 10 mM potassium phosphate buffer (PPB) at pH 7.4 and filtered to remove impurities. PPB was prepared by mixing appropriate amounts of monobasic potassium phosphate (Sigma, P8708) and dibasic potassium phosphate (Sigma, P8508) to a final pH

of 7.4. The final concentration of protein in PPB was verified via absorbance of protein solutions at 230 nm (A_{230}).[28]

The adsorption of proteins on each material surface was carried out from 0.03 mg/ml and 1.00 mg/ml protein solutions in order to vary the surface coverage and structure of the adsorbed protein (see Figs. 5.3-5.9).[22-23, 29-30] Briefly, the experiments were conducted in PPB using protein solutions with concentrations of 0.03 mg/ml and 1.00 mg/ml for a time period of 2 h, following which the material surfaces were gently rinsed under a steady gentle flow (12 ml/min) of PPB for 5 min to remove weakly adsorbed proteins. The surfaces with the adsorbed layer of proteins were then immersed in PPB for 15 h to allow the adsorbed layers to structurally equilibrate on the surface at room temperature (≈ 25°C). The effect of adsorption time and equilibration time in PPB on the surface coverage and structure of the protein were also characterized (see Chapter 5 and appendix C). From these studies, it was determined that the designated time of 2 h for initial adsorption followed by 15 h of relaxation under PPB was sufficient for system equilibration for each of our treatment conditions.

9.2.3. Chemical Treatment of Material Surfaces pre-Adsorbed with Proteins

Solutions of sodium dodecyl sulfate (SDS; $NaC_{12}H_{25}SO_4$; 288 Da, 0.5% (w/v), Sigma, L3771), n-octyl-β-D-glucoside (Octyl; $C_{14}H_{28}O_6$; 292 Da, 30 mM, Sigma, O8001), 3- [(3- Cholamidopropyl) dimethyl ammonio] -1-propane sulfonate (CHAPS, 20 mM, Sigma, C3023), urea ($CO(NH_2)_2$, 60 Da, 8 M, Fisher Scientific, U15500) and chloride salts of guanidinium hydrochloride (GdmHCl; CH_6ClN_3, 95 Da, 6 M, Sigma,

G3272) were prepared in PPB and filtered to remove impurities. No further pH adjustments were made in any of the set-ups.

Proteins in solution (1.00 mg/ml) and material surfaces, pre-adsorbed with proteins from low bulk solution (0.03 mg/ml) and high bulk solution (1.00 mg/ml) conditions, were exposed to solutions of the chemical excipients for 15 h. Following this, the material surfaces were rinsed under a gentle flow (12 ml/min) of fresh solution of the chemical excipients in order to remove weakly adsorbed proteins. The surface coverage of adsorbed protein and its structure were subsequently recorded using CD spectropolarimetry. The results were averaged over three separate runs. A single run involved the analysis of responses from proteins on six different samples of each material surface.[22]

9.2.3.a Estimation of Surface Coverage and Elution Efficiency of Different Chemical Additives. Since solutions with chemical excipients strongly absorb at wavelengths below 230 nm, the concentration of protein in solution and on the surface was determined via the spectroscopic absorbance at 230 nm (A_{230}).[28] The effectiveness of A_{230} in estimating the concentration of proteins, in the presence of strongly absorbing chemical excipients, was verified by estimating the concentration of five different standard solution concentrations (C_{soln}) of each of the proteins (0.20 mg/ml, 0.40 mg/ml, 0.60 mg/ml, 0.80 mg/ml and 1.00 mg/ml) in the presence of each of these chemical excipients. Subsequently, the surface coverage of adsorbed protein (Q_{ads}) at 230 nm with the adsorbed layer immersed in pure buffer solution (i.e., protein only on the surface) was estimated using equation 9.1

$$Q_{ads} = \frac{A_w}{\varepsilon_w} \tag{9.1}$$

where, A_w is the absorbance of the adsorbed layer of protein at wavelength (w) and ε_w (units of cm^2g^{-1} or $(g/ml)^{-1}$ cm^{-1}) is the molar extinction coefficient corresponding to wavelength, w. The elution efficiency (EE, %) of different chemical excipient (D) on a given surface (S) were subsequently estimated by equation 9.2

$$EE(\%) = \frac{(Q_{ads})_S - (Q_{ads})_{DS}}{(Q_{ads})_S} * 100 \tag{9.2}$$

where $(Q_{ads})_S$ is the amount of protein on the surface following the 15 h of equilibration in PPB without the chemical additive and $(Q_{ads})_{DS}$ is the amount of protein on the surface following the 15 h of treatment with the chemical excipients.

9.2.3.b Quantifying the Helix Content in the Adsorbed and Solution Phases of Protein.

The structure of the desorbed fraction of the proteins in each of the solution conditions was determined in a quartz cuvette (Starna Cells) of 0.01 cm path length while the structure of adsorbed proteins was determined in a custom–made cuvette, using the previously established methodology for CD spectropolarimeter (Jasco J-810).[22] Briefly, each CD spectrum, with its associated ellipticity and absorbance values, was obtained over a wavelength range from 220 nm to 300 nm, at a scan rate of 50 nm/min and a response time of 0.25 s. Each spectrum represented an accumulation of 6 scans. In the case of adsorbed proteins, the CD spectra were recorded from 220 nm to 300 nm at a scan rate of 10 nm/min with a response time of 2 s, and a bandwidth of 0.5 nm. The spectra

were averaged from six such accumulations.[22] The background-corrected CD signals were converted to molar ellipticity, $\theta_{\lambda}^{\exp}$, given in deg.cm^2/(dmol)), using equation 9.3.

$$\theta_{\lambda}^{\exp} = \frac{\theta_{\lambda}^{raw} \times M}{1000 \times C_{\text{soln}} \times L}, \qquad (9.3)$$

where $\theta_{\lambda}^{\text{raw}}$ is the background corrected raw CD signal (degrees), L is the path length of the cuvette (mm), C_{soln} is the solution concentration of the protein (mg/ml), M is the mean residue molecular weight of 115 g/mol.

The helix content of proteins (FH) in the solution and adsorbed phase was determined using the 230-240 nm slope method.[24] Prior to application of this technique, the reliability of the slope method was assessed by correlating the structure in solution or thermally unfolding the protein in aqueous solution when predicted by the empirical equation 9.4 against a CONTIN method using the SP43 and SP48 protein reference datasets provided with the CDPro package.

$$\text{FH} = 0.000514 * \nabla + 0.00297 \qquad (9.4)$$

The '∇' parameter that was obtained from the slope of the linear regression analysis of 230 – 240 nm region in the scaled CD spectrum for the adsorbed or solution phase of the protein was used to predict the FH of proteins exposed to the different chemical excipients and in PPB solution at room temperature.

9.2.4 Estimating the Relative Bioactivity of Adsorbed Protein.

A spectrophotometric assay was used to measure the relative bioactivity of proteins in order to assess the impact of structural unfolding. All activity studies were carried out in CD cuvettes containing 10 mM PPB at pH 7.4. Briefly, ribonucleic acid (Baker's yeast, Sigma R6750), was prepared in PPB to a final concentration of 20 mg/ml and exposed to RNase A in solution and following its adsorption on material surface. Enzymatic activity was then measured by monitoring the change in absorbance at 300 nm at pH 7.4 for a time period of 10 min. Similarly, the bioactive substrates for HEWL was prepared in PPB to a final concentration of 60 mg/L *Micrococcus lysodeikticus* (Sigma M3770) and the assays to determine the enzymatic bioactivity were done at pH 7.4 for a time period of 10 min at 450 nm.

The specific activities of both the adsorbed proteins were calculated by normalizing the ΔA_{300} or ΔA_{450} absorbance values by the total amount of protein adsorbed on the surface (Q_{ads}* area of adsorbent surface) or the total amount of protein in solution.[31] The relative bioactivities (%) of adsorbed proteins were determined by normalizing the measured adsorbed-state specific activity to the protein's solution-state specific activity.[31]

9.2.4. Statistical analysis

The results from this study are presented as the mean values ± 95% confidence intervals (C.I.). The statistical significance of differences between mean values for different samples/conditions was evaluated using either the Student's t-test, with values of $p < 0.05$ being considered as statistically significant.

9.3 RESULTS AND DISCUSSION

9.3.1 Surface Characterization

Table 5.1 presents the results analyzed by characterization techniques applied to the surfaces used in this study. All the measured values reported in Table 5.1 fall within the expected range.[32-36]

9.3.2 Effect of Chemical Additives on the Solution Structure of Proteins

Two types of chemical excipients were considered in the current study – salts and surfactants. The surfactants used in the current study differed in the character of their head groups (ionic, non-ionic, and zwitterionic) and were used at concentrations well above their CMCs.[13, 37-39] Similarly, 6 M GdmHCl and 8 M urea salts represented model ionic and non-ionic denaturants, respectively. As previously mentioned, all experiments were done at default pH; i.e., no pH adjustments were made to the solutions of chemical excipients. The native pH of all chemical excipients used in the current study were similar to that of PPB (pH = 7.4), except for 6 M GdmHCl (pH = 6.2) and 8 M urea (pH = 8.0). Since, the strong background absorbance by chemical excipients like 8 M urea, 6 M GdmHCl, and 20 mM CHAPS in our CD cuvettes at wavelengths < 230 nm limits the application of the structural quantification of proteins by CDPro package, the 230-240 nm slope methodology was used to estimate the helix content of protein.[24]

Table 9.1 presents the solution structure of HEWL and RNase A in presence of different excipients using the 230-240 nm slope methodology.[24] All measurements were done at 25°C and no pH adjustments were done to the solution.

Table 9.1 Estimates on helical content (%) within the solution structures of HEWL and RNase-A when exposed to different chemical additives using the 230-240 nm slope method. (Mean ± 95% C.I., N = 3.)

Proteins	PPB (%)	Urea (%)	GdmHCl (%)	SDS (%)	Octyl (%)	CHAPS (%)
HEWL	34 (2)	30 (3)	3 (2)	31 (2)	34 (3)	29 (3)
RNase A	20 (3)	4 (3)	3 (2)	15 (3)	19 (3)	12 (3)

As shown in Table 9.1, the estimates of helical content by 230-240 nm (see Chapter 8) for HEWL and RNase A in PPB were in reasonable agreement with those obtained by conventional algorithms like CDPro package and 222 nm method.[24] But when exposed to chemical excipients, the native structure of RNase A was relatively more sensitive to chemical excipient-induced denaturation than HEWL, with a statistically significant decrease in the average helical content in all of the chemical excipients, except when octyl treated. Both proteins were however, very sensitive to denaturation by 6 M GdmHCl, as evident by the significant loss in the helix content (> 85%) at room temperatures. These results were largely consistent with the estimates obtained by other investigators.[13, 40-41] These presented results also illustrate that the 230-240 nm slope method is an effective quantification tool for tracking the impact of chemical excipients on the helical structure of proteins by CD spectroscopy.

9.3.3 The Decontamination Efficiency of a Chemical Excipient is Strongly Influenced by the Adsorbed Configuration of Protein.

Fig. 9.1 and Fig. 9.2 illustrate the amount of residual proteins (HEWL and RNase A) and the retained helical content on different surfaces (glass, HDPE, and PMMA) following 15 h of exposure to different chemical excipients. Both proteins were adsorbed from 0.03

mg/ml and 1.00 mg/ml solution concentration for 2 h and equilibrated in PPB for 15 h, prior to exposing to different chemical excipients. Because of the strong background absorbance by excipients like 6 M GdmHCl, 8 M urea, and 20 mM CHAPS at wavelengths < 230 nm, the surface coverage of proteins were estimated by absorbance at 230 nm method as opposed to the 205 nm used in our previous studies. The residual helix content of the proteins in different chemical excipients was determined using the 230-240 nm slope method.

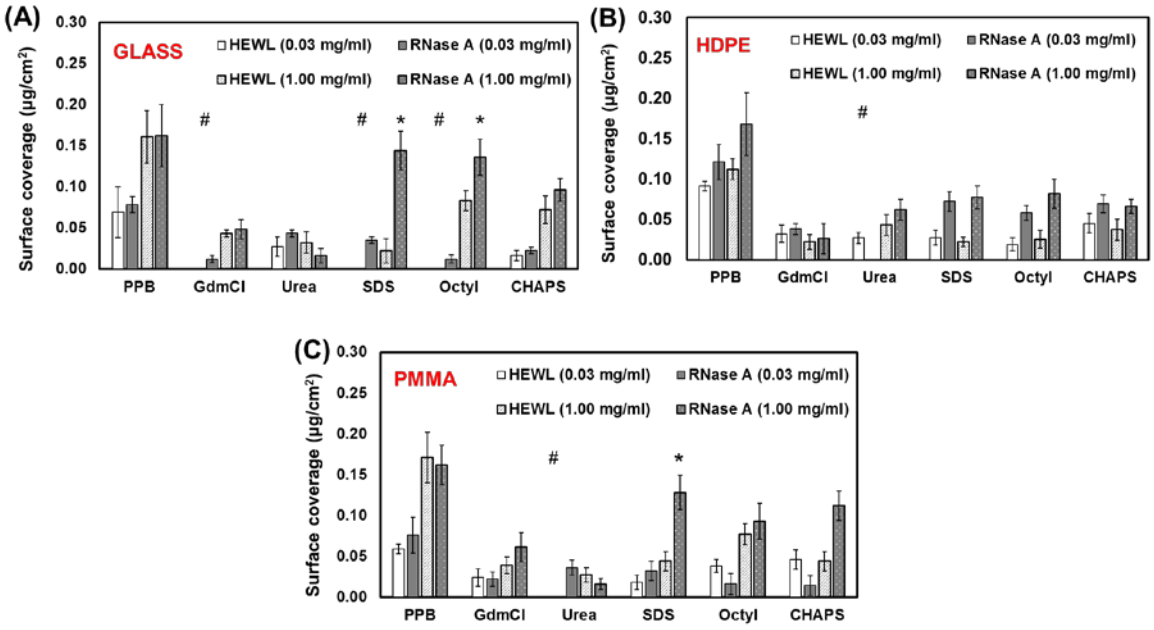

Figure 9.1. Residual surface coverage of HEWL and RNase A on (a) glass, (b) HDPE, and (c) PMMA surfaces following 15 h of exposure in PPB, 8 M urea, 0.5 % SDS, 30 mM octyl, and 20 mM CHAPS (n = 3, mean ± 95% C.I.). The proteins were initially adsorbed for 2 h from 0.03 mg/ml and 1.00 mg/ml bulk solution concentrations, and then equilibrated in PPB for 15 h prior to exposing to the different chemical excipients for an additional 15 h. The theoretical full surface coverage of HEWL for adsorption in 'side–on' and 'end–on' orientations are τ_{side} (0.17 µg/cm^2) and τ_{end} (0.26 µg/cm^2), respectively.[42] Similarly, the theoretical full surface coverage of RNase A for adsorption in 'side–on' and 'end–on' orientations are τ_{side} (0.21 µg/cm^2) and τ_{end} (0.28 µg/cm^2), respectively.[29] '#' refers to the surface coverage < 0.01 µg/cm^2 which were considered the limit of detection for our instrument. '*' refers to surface coverages for a specific chemical excipient treatment which were not significantly different from the corresponding control in PPB.

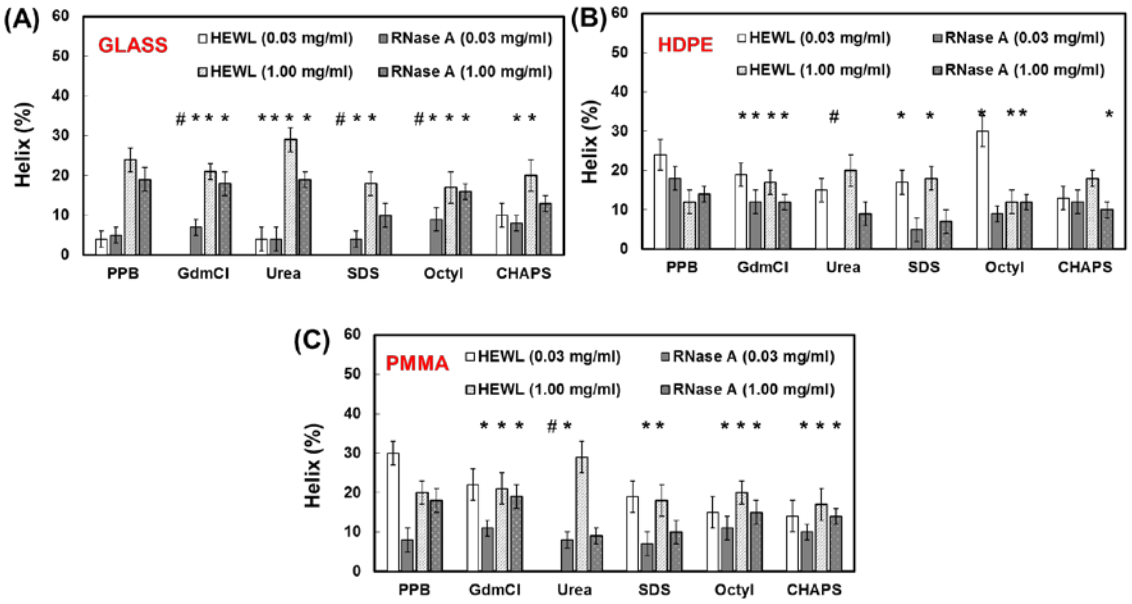

Figure 9.2. Helix content of HEWL and RNase A on (a) glass, (b) HDPE, and (c) PMMA surfaces following 15 h of exposure in PPB, 8 M urea, 0.5 % SDS, 30 mM octyl, and 20 mM CHAPS (n = 3, mean ± 95% C.I.). The proteins were initially adsorbed for 2 h from 0.03 mg/ml and 1.00 mg/ml bulk solution concentrations, and then equilibrated in PPB for 15 h prior to exposing to the different chemical excipients for an additional 15 h. The helix content in the native structure of protein by the 230-240 nm slope methodology for HEWL and RNase A were found to be 34% (± 2%) and 20% (± 2%) respectively. (see chapter 8) '*' refers to helix content in the retained fraction of protein for a specific chemical excipient treatment which were not significantly different from the corresponding control in PPB. '#' refers to the helix content for proteins that could not be determined in our studies for the surface coverage < 0.01 μg/cm^2 because of concerns of the limit of detection for our instrument.

9.3.3.1 Surface Coverage and Helix content of Proteins on Different Material Surfaces post Exposure to PPB. The protein surface coverage estimates obtained using the 230 nm, and the helix content of adsorbed proteins by the 230-240 nm slope method compared reasonably well (≈ 5% average error) with the estimates that were obtained in PPB with our previous studies (see section E.1.). Furthermore, the timeframes (i.e., 2 h adsorption, 15 h relaxation) used in our studies, were selected to represent equilibrated conditions where the amount and structure of the adsorbed protein was found to stabilize

and undergo no further noticeable changes (see Chapter 5 and appendix C).[22-24, 29-30] In addition, control studies were conducted to measure the helix structure of proteins in solution over timeframes of at least 24 h and showed no significant change in either the helix structure during this time, thus supporting that the changes in the protein structure on the materials surfaces were due to interactions of the protein with the surface rather than being simply an aging phenomenon of the protein itself.

When HEWL and RNase A proteins were adsorbed from a 1.00 mg/ml solution concentration for 2 h and followed by 15 h of equilibration under pure PPB (i.e., protein-free PPB solution), the resulting surface coverage of the adsorbed protein on each surface was within 25% of a saturated, close–packed monolayer with side–on protein orientation (Fig 9.1). In contrast, when proteins were adsorbed from a 0.03 mg/ml solution for 2 h and equilibrated, the resulting surface coverage of the proteins was about half of that obtained when it was adsorbed from the 1.00 mg/ml solution. These results show that different degrees of surface coverage for proteins were obtained in our studies by varying the protein-solution concentration from which it is adsorbed. As intended, higher solution concentration resulted in higher surface coverage, which we assume results in a greater degree of protein-protein interaction (PPI) effects on the surface.

As it could be further seen from the data presented in Figs. 9.1 and 9.2, when the surface coverage was low (e.g., 0.08 μg/cm^2, nearly 3x less than the closed-packed side-on arrangement of 0.21 μg/cm^2), in which case the effects of PPI can be expected to be relatively low, the extent of helix unfolding on the glass surface was generally very high (> 75%). However, at high surface coverages (> 0.16 μg/cm^2, close to the close-packed

side-on arrangement), where PPI effects can be expected to be substantially greater, these effects apparently tend to inhibit surface-induced unfolding, and result in much preservation of the native state of the helical content with less than 35% loss. In direct contrast to the stabilizing effect of PPIs on the helical content of adsorbed proteins on the glass surface, it is apparent that PPI on the hydrophobic HDPE surface had a destabilizing effect on the helical structure—adsorption to HDPE induced more than 50% loss in native-state % helicity at higher surface coverages when compared to less than 30 % loss at low surface coverages.

Unlike glass and HDPE surfaces, which tend to strongly interact with the adsorbed proteins, PMMA surfaces, which have relatively moderate hydrophobic and hydrogen-bonding characteristics compared to HDPE and glass surfaces, respectively, showed weaker interactions with proteins. On this surface, the influence of PPI effects on the structure of the proteins tended to depend on the type and composition of the proteins. In case of HEWL and RNase-A, which are similar sized *'hard'* proteins, but differ in the relative composition of hydrophilic to hydrophobic amino acids, the PPI effect had a stabilizing influence on the helix content of the more hydrophilic RNase-A while having a destabilizing influence on the helix content of the more hydrophobic HEWL. The helix shifts in the adsorbed proteins were further corroborated by the mass spectrometric results.[22, 29-30]

9.3.3.2 Elution Efficiency of a Chemical Excipient is Strongly Influenced by the Initial Structure of the Adsorbed Protein. Fig. 9.1 shows the amount of proteins retained on the surface post exposure to different chemical excipients. In general, the

amount of proteins that were retained on the surface significantly varied with the type of surface, and the solution concentration from which the protein were adsorbed. When comparing the residual surface coverage of the protein post exposure to chemical excipients with those that was initially adsorbed amount of protein on each surface in PPB, majority of the systems showed that significant amounts of both the pre-adsorbed proteins (HEWL and RNase A) were desorbed or eluted from glass, HDPE, and PMMA surfaces following exposure to different chemical excipients. However, with the octyl and SDS treatments of RNase A adsorbed from 1.00 mg/ml solution concentration on glass and PMMA surfaces, no significant differences were observed in the initial and final surface coverages.

In many of the earlier studies, the apparent greater resistance to elution by a chemical excipient was often considered to be representative of its higher binding strength, and was directly associated with the higher extent of protein unfolding on the adsorbent surfaces.[17, 19, 43-45] However, this assumption may not be entirely accurate. For instance, similar amounts of proteins, HEWL and RNase A, were initially adsorbed on each surface in PPB. But, post exposure to chemical excipients, the residual amounts of the more hydrophilic RNase A were generally higher on each of the surfaces as opposed to HEWL. While, the lower internal stability of RNase A when compared to HEWL at 25°C (see Fig 5.1), and the stronger influence of these excipients on the native structure of these proteins (Table 9.1) would provide some base for the above assumption, the relatively insignificant difference in the residual helical structure of both these proteins in majority of the systems (Fig. 9.2) as well as the lowered elution (Fig. 9.1) of both these

proteins at higher surface coverages undermines the validity of this assumption. A better explanation for the observed data could be obtained by considering the influence of the initial adsorbed configuration of protein on the elution process of a chemical excipient.

The helix unfolding process in proteins generally results in the severing and exposing of the internal hydrogen bonds that were formed between the peptide-bond functional groups along the polypeptide chain as well as the hydrophobic contacts that were stabilizing the helical structure. As it has been previously reported, the interaction of a chemical excipient with the same type of protein, can vary depending upon the changes in a protein's conformation.[13] The helix unfolding in the protein on the adsorbent surfaces could provide an ideal environment for better solvation of its unfolded segments by a chemical excipient,[13, 39, 46-48] and could in turn promote the higher elutability of the more unfolded fractions of adsorbed proteins. Therefore, quantifying the elution efficiency of a chemical excipient as a function of the loss in its helix content (%) when the proteins are initially adsorbed on the surface, may provide more detailed insights into the role of conformational changes in proteins on the elution efficiency of chemical excipients. The elution efficiency (%) of each chemical excipient on a given surface was estimated based on the relative difference in the surface coverage of protein post- and pre-exposure to different excipients using equation 9.2.

Fig 9.3 and Fig 9.4 present the correlation between the extent of helix unfolded in the adsorbed proteins and the elution efficiency of salts and surfactants respectively. The helix loss in proteins represents the combined influence of the type of surface, type of protein, and effect of surface coverage on the helix content of adsorbed proteins.

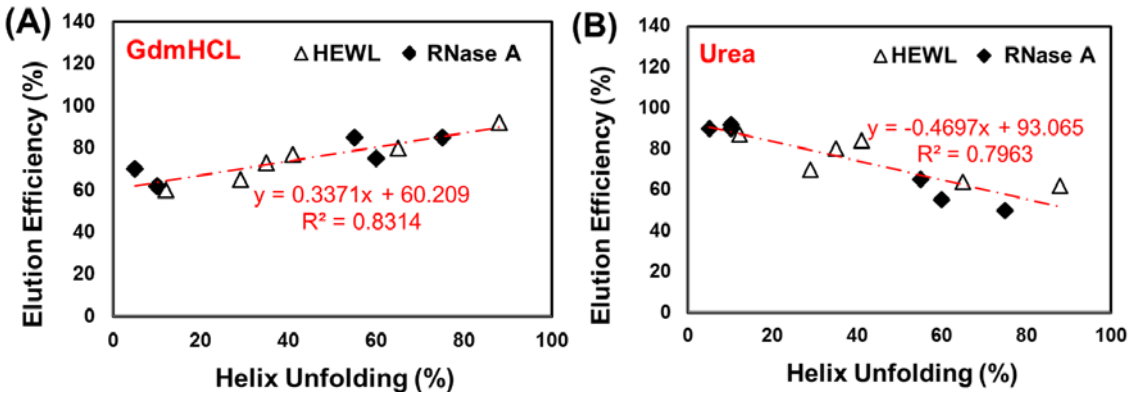

Figure 9.3. Efficiency of (a) 6 M GdmHCl and (b) 8 M urea in eluting pre-adsorbed HEWL and RNase A off the glass, HDPE, and PMMA surfaces following 15 h of treatment, v/s helix unfolding in the protein on different material surfaces, prior to chemical treatment. The data points for both the proteins on each of the surfaces were overlaid for purposes of comparing the effect of helical unfolding in the proteins to its role in influencing the extent of protein elution from a material surface following treatment by a given chemical additive. (Each point represents the mean of three values for each of the material surfaces.). Raw data for the figure is provided in Tables E.1, E.2, E.5, and E.6.

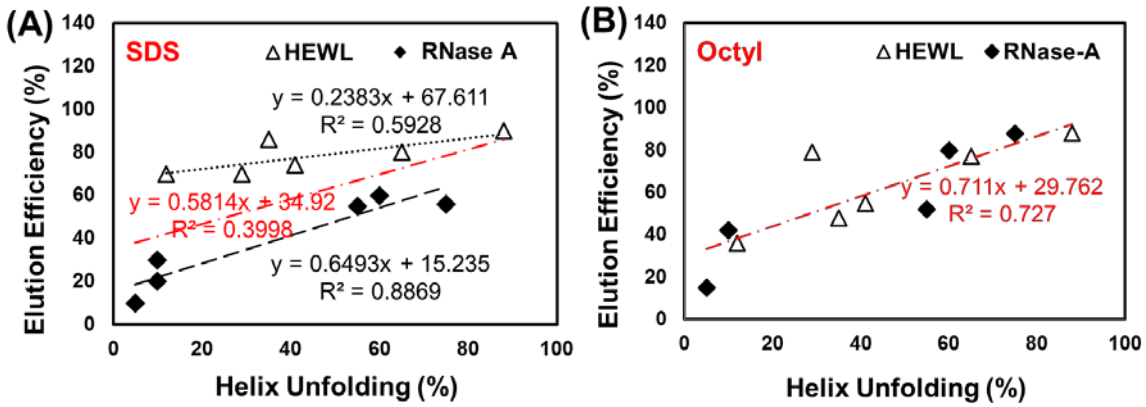

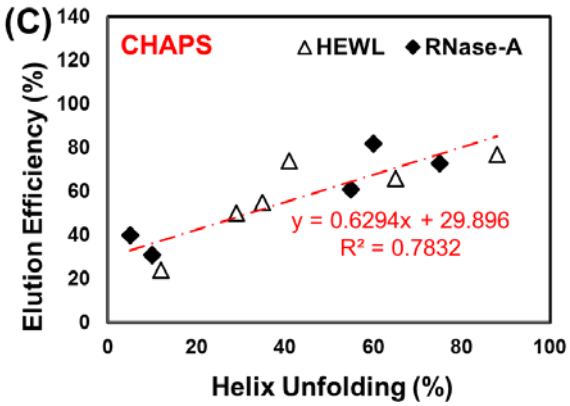

Figure 9.4. Efficiency of (a) SDS, (b) Octyl, and (c) CHAPS in desorbing HEWL and RNase A that were pre-adsorbed on the glass, HDPE, and PMMA surfaces following 15 h of treatment, v/s helix unfolding in the protein on different material surfaces, prior to chemical treatment. The data points for both the proteins on each of the surfaces were overlaid for purposes of comparing the effect of helical unfolding in the proteins to its role in influencing the extent of protein desorption from a material surface following treatment by a given chemical additive. (Each point represents the mean of three values for each of the material surfaces.). Raw data for the figure is provided in Tables E.1, E.2, E.5, and E.6.

As it can be seen from Fig 9.3 and Fig 9.4, the elution efficiency of a chemical additive correlates fairly strongly to the conformational shift in the adsorbed proteins, and would in part explain the dependency of chemical excipients on the surface coverage and the type of surface in the elution process.[17, 19] Additionally, it was also evident that the elution efficiency of a chemical excipient, except for urea, generally increased with the increased unfolding of the helix content in the adsorbed protein. A possible mechanism mediating the solvation of the unfolded protein segments by each of the chemical excipient is explained in the following sub-sections.

9.3.3.2.a Influence of Adsorbed Protein Structure on the Elution Efficiency of Salts. At high concentrations (> 6 M) ionic and non-ionic salts have a strong influence on a protein's native structure. But similar to the observation by other investigators, strong

denaturants like urea (Fig 9.3 a) and GdmHCl (Fig 9.3 b) also showed high elution (> 50%) of the adsorbed proteins in our studies as well.[17, 49] Although Fig 9.1 and Fig 9.2 would indicate that there might be specific role of adsorbent surface and type of protein on the elution process, Figs 9.3a and 9.3b, clearly shows that the elution efficiencies (%) of urea ($R^2 \approx 0.80$), and GdmHCl ($R^2 \approx 0.83$) were more strongly correlated to the helix unfolding in these two adsorbed proteins.

However, these data also indicate that opposing molecular mechanisms may be involved in the elution process of urea and GdmHCl. Though both urea and GdmHCl are polar molecules that denature protein structure, the nature of the unfolding processes induced by these denaturants is considered to be different, especially at high concentrations.[41, 50-53] For example, while GdmHCl is an ionic molecule that masks the electrostatic contributions within proteins, urea is a non-ionic molecule that interferes with the hydrogen bonding in proteins. Similarly there are differences in its interactions with the amino acids and the peptide backbone.[51, 53-56] Guanidinium is generally considered to interact directly with the hydrophobic residues and is known to bind to the bulkier amino acids.[51-53] In contrast, urea is considered to more favorably interact with the polar groups in the protein.[53, 57-58] These differences in interactions may in part explain the higher elutability of the more unfolded proteins segments on the surfaces by GdmHCl than urea.

9.3.3.2.b Influence of Adsorbed Protein Structure on the Elution Efficiency of Surfactants. The surfactant concentration plays a critical role in the elution process.[13, 37-38, 43, 59] In order to reduce the complexity of the concentration isotherms on the elution

process, the concentration of all the detergents used in current study were above their CMC. The typical CMCs at 25°C for SDS, Octyl, and CHAPS excipient in aqueous solution similar to PPB were 10 mM, 20 mM, and 6 mM respectively.[13, 37-39] The surfactant interactions with the adsorbed proteins was expected to be mediated by an interplay of the interaction by micelles, via their hydrophilic functional head groups, and also by the lateral interactions that cause the individual detergent monomers to associate into micelles.[13] From Fig 9.4, it was clearly evident that the elution process is promoted by the increased unfolding of the protein on the surface. But, unlike other surfactants, the elution process of adsorbed proteins by SDS on all of the surfaces was also influenced by the type of protein that was unfolding ($R^2 \approx 0.59$ for HEWL, $R^2 \approx 0.89$ for RNase-A).

SDS, is an anionic detergent, and has been widely studied.[17-19, 60-62] As reported in the literature, the binding isotherm of SDS involves an initial stage of strong binding to the protein via positively charged groups or a hydrophobic pocket followed by a second stage that involves self-association of the surfactants.[48] Both HEWL and RNase A have more of the positively charged amino acid groups than negatively charged groups (pI of HEWL and RNase A or 11.35 and 9.6, respectively) and are thus expected to be positively charged in PPB (pH 7.4).[19] Yet, the elution process of both these proteins by SDS was found to be drastically different (Fig. 9.5a), even at similar extent of unfolding. At relatively low surface coverages when the unfolding tendency in the adsorbed proteins were high, the elution of protein elution by SDS was generally higher (> 70%) as opposed to the maximal elution of 60% at surface coverages near surface saturation, when the unfolding tendencies in the proteins were minimal (Fig 9.2). The extent of

elution in both these cases were directly related to the increased extent of unfolding in these proteins. Although, the dependence on the type of protein on elution process by SDS was certainly not expected, a possible explanation for this behavior could be because of the amino acid composition of these proteins. Among HEWL and RNase A, HEWL is relatively more hydrophobic and has a prominent hydrophobic core as opposed to RNase A. Therefore, it is likely that these sites could be an important site for promoting the self-association of the micelles via the necklace or protein-decorated micelle model.[13, 46]

In contrast to the ionic surfactants which tend to elute the adsorbed protein by directly binding to the protein, non-ionic and zwitterionic surfactants are usually considered to elute proteins by competing for the adsorbent surface as these excipients are generally thought to bind weakly or excluded from the surface of the native protein.[13, 17, 19] Octyl is a non-ionic detergent commonly used to solubilize and preserve the structure of membrane bound proteins, and is roughly similar in size to SDS. CHAPS, however, is relatively bulkier excipient and is zwitterionic in nature with surfactant characteristics intermediate to that of octyl and SDS.

Figs 9.4 (b) and 9.4 (c) for octyl ($R^2 \approx 0.72$) and CHAPS ($R^2 \approx 0.78$) clearly shows that these agents are most efficient in eluting adsorbed proteins as it tend to undergo increased conformational changes on the adsorbent surfaces. Additionally, these responses were independent of the type of surface, and the type of protein, and were thus inconsistent with the general notion that elution process by these agents are entirely driven by displacement mechanism alone. Based on this study, it is likely that the

excipients could also be directly interacting with the unfolded segments of adsorbed proteins, and facilitating the elution process.

9.3.4. The Bioactivity of Residual Proteins are Strongly Influenced by the Residual Structure of the Adsorbed Protein. Although the exposure of pre-adsorbed proteins to chemical excipients resulted in substantial reduction in its initial surface coverages, the shifts in surface coverage were weakly correlated to the residual structure of the adsorbed protein. In majority of the systems (41 of the 60) within the current study (Fig 9.2), the exposure of pre-adsorbed proteins to chemical excipients was not found to induce or significantly affect the helix content of residual proteins. Even when comparing the structural shift in the systems which showed a significant shift in adsorbed structure (i.e, 10 of the HEWL systems and 9 of the RNase A systems), a weak correlation was observed between the residual surface coverage and residual helix content of the adsorbed proteins. This behavior is clearly in stark contrast to the strong correlation observed between the surface coverage and the helix content observed in the adsorbed protein exposed to PPB (see Chapter 5). To further explore the influence of chemical excipients on the structure of adsorbed proteins, the influence of helix unfolding in the residual proteins on its initial adsorbed state bioactivity were assessed.

Fig. 9.5 and Fig. 9.6 represents the correlation between extent of helix unfolding (%) in the residual amounts of adsorbed HEWL and RNase A and its adsorbed state bioactivity (%) on each of our three surfaces post-treatment with each of the chemical excipient. The bioactivity of all chemically treated samples were compared on an equivalent basis (i.e, in PPB, pH 7.4 and room temperature), because of the concerns in

the influence of intrinsic environment of each chemical excipients on the overall bioactivities of the proteins.[63-64] For this purpose, all chemical treated samples were transferred to fresh PPB containing solution for 15 h. None of the samples showed any significant change in the adsorbed protein structure during this duration.

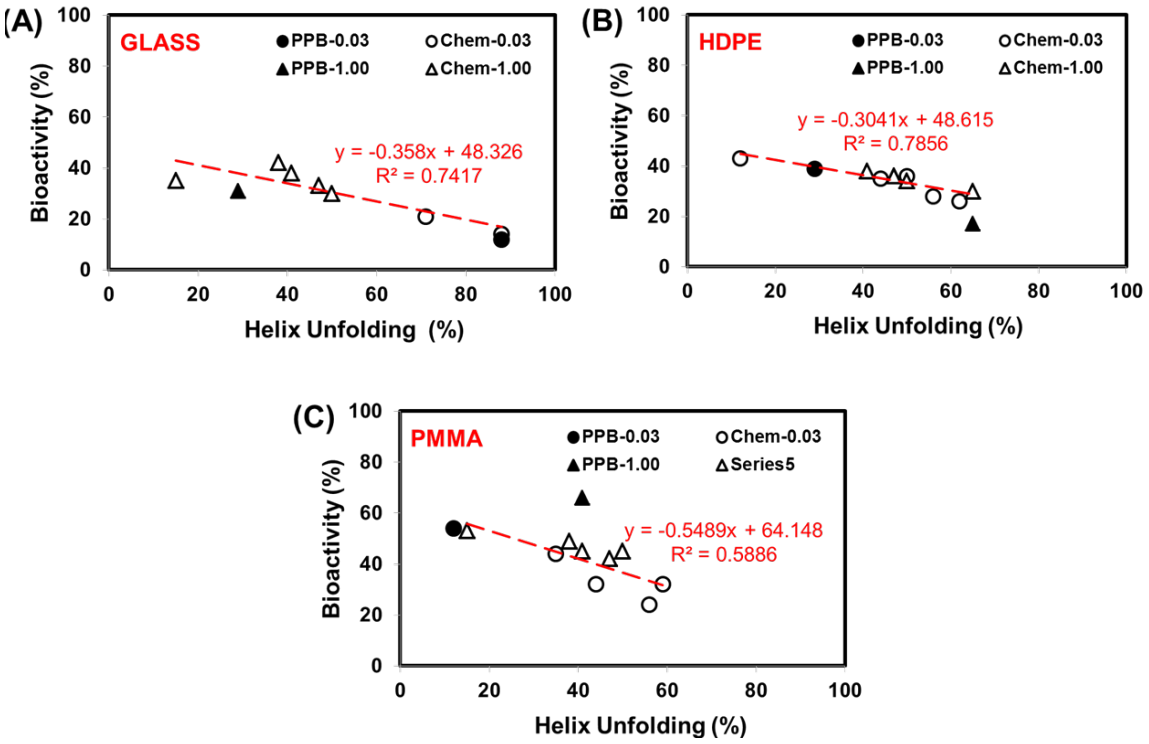

Figure 9.5 Bioactivity of HEWL on (A) glass, (B) HDPE, and (C) PMMA v/s extent of helix unfolding post exposure to different chemical excipients. The helix content of HEWL was estimated using the 230-240 nm slope methodology. The triangle and circle marker represent the bioactivities of HEWL when adsorbed on different surfaces from 0.03 mg/ml and 1.00 mg/ml protein solution concentrations. Similarly, the filled and empty markers represent the bioactivities of HEWL when exposed to PPB and chemical excipients respectively. (n = 3). The linear trendline represents the correlation between the helix content and bioactivities of chemically treated proteins samples. Average 95% C.I. for the estimation of bioactivity of adsorbed HEWL post chemical treatment was 4%. Raw data for the figure is provided in Tables E.7 and E.9.

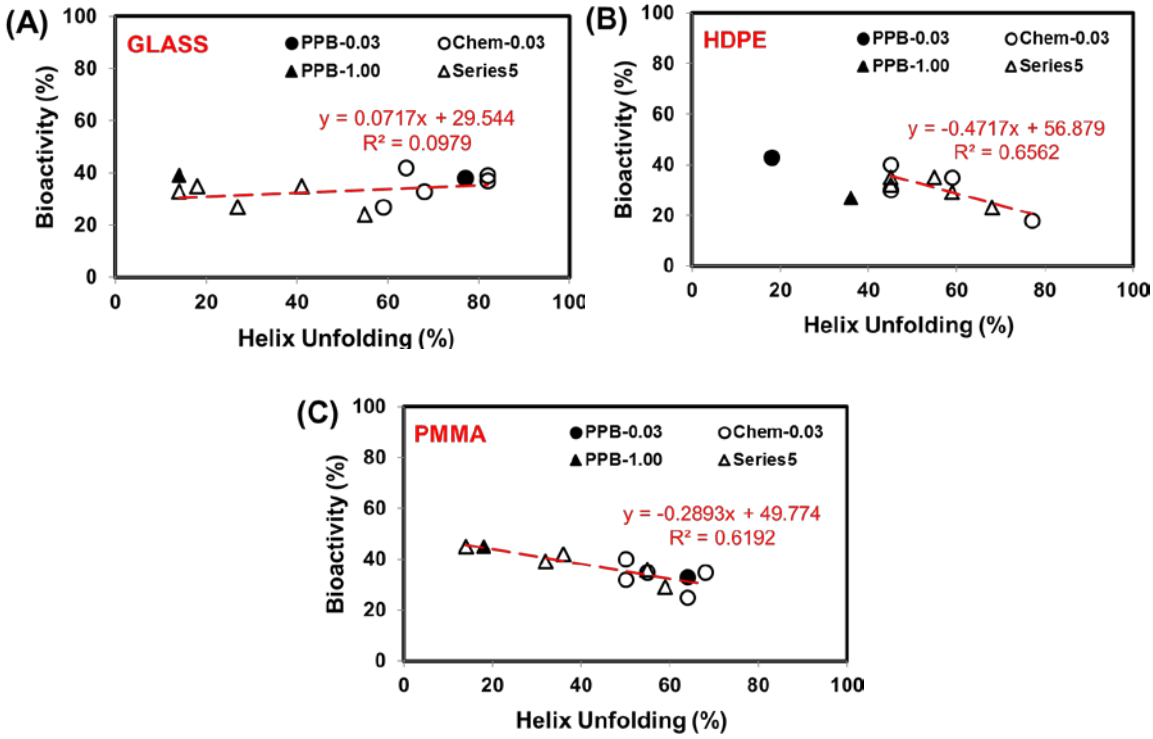

Figure 9.6. Bioactivity of RNase A on (A) glass, (B) HDPE, and (C) PMMA surfaces v/s extent of helix unfolding post exposure to different chemical excipients. The helix content of RNase A was estimated using the 230-240 nm slope methodology. The triangle and circle marker represent the bioactivities of RNase A when adsorbed on different surfaces from 0.03 mg/ml and 1.00 mg/ml protein solution concentrations. Similarly, the filled and empty markers represent the bioactivities of RNase A when exposed to PPB and chemical excipients respectively. (n = 3). The linear trendline represents the correlation between the helix content and bioactivities of chemically treated proteins samples. Average 95% C.I. for the estimation of bioactivity of adsorbed RNase A post chemical treatment was 4%. Raw data for the figure is provided in Tables E.8 and E.10.

Fig 9.5 shows a strong correlation between the extent of helix unfolding and the residual bioactivity of HEWL on the glass ($R^2 \approx 0.74$), HDPE ($R^2 \approx 0.78$), and PMMA surfaces ($R^2 \approx 0.58$). Similarly, Fig 9.6 also showed a strong correlation between the extent of helix unfolding and residual bioactivity of RNase A on HDPE ($R^2 \approx 0.67$) and PMMA ($R^2 \approx 0.61$) surface post exposure to chemical excipients. As evident, most

systems showed a shift in its initial bioactivity, especially when proteins adsorbed from 1.00 mg/ml solution concentration were exposed to chemical excipients. For instance, the chemical treatment of HEWL on PMMA surface (Fig 9.5c) and RNase on HDPE surface (Fig 9.6b) was almost always accompanied by the loss in its initial bioactivity because of the loss in helix structure. But in other systems like HEWL on glass and HDPE surfaces, and RNase A on PMMA surfaces, the chemical treatment resulted in an increase or decrease in its overall residual activity and were directly correlated to change in its residual structure (Fig 9.5a-b, Fig. 9.6c). But in systems like that of RNase A on glass surface, a weak correlation ($R^2 \approx 0.10$) was observed between its structure and activity, despite the protein retaining different helix content.

Taken together, these data confirms that the chemical excipients does have an influence on the structure and thereby, the bioactivity of residual protein. However, the specific effects of chemical excipients on the adsorbed protein structure could not be further assessed in this study, specifically since the influence of chemical excipients on the solution structure of proteins was not an adequate representative of its interaction in the adsorbed state. For example, 8 M urea was found to either increase (Fig 9.2c and 9.3b), decrease (Fig 9.2c and 9.3b), or have no effect (Fig 9.2a) on the overall helix content of adsorbed HEWL, despite having a no significant effect on these proteins when in solution (Table 9.1). Similarly, despite urea being a strong destabilizer of the helix structure of RNase A in solution, these agents had either destabilizing (Fig 9.2b and Fig 9.2c) or no influence (Fig 9.2a and 9.2c) on the helix content of the adsorbed phase of these proteins. A possible cause for the differences in the interaction of chemical

excipients with the adsorbed proteins could be due to the conformational unfolding which it underwent on the surface, and could result in significant differences in the interaction of chemical excipients with the adsorbed and native structures of proteins. This was further evident in the elution process of the adsorbed proteins by a specific chemical excipient. For this reason, it is important to systematically assess the impact of chemical excipients on the adsorbed structure and bioactivity of proteins, as opposed to solely relying on the interaction of chemical excipients with the proteins in solution.

9.4 CHAPTER SUMMARY AND CONCLUSION

The purpose of this study was to assess the impact of adsorbed protein structure on the decontamination efficiency (i.e., the elution efficiency and neutralizing the initial bioactivity) of chemical excipients like salts and surfactants. Towards this purpose, a CD based methodology was used to quantitatively assess the influence of five types of chemical excipient (0.5% SDS, 30 mM Octyl, 20 mM CHAPS, 6 M GdmHCl and 8M urea) on the initial surface coverage, structure, and bioactivity of adsorbed proteins. The surface coverage and structure of proteins were determined in chemical excipients using the absorbance at 230 nm, and the 230-240 nm slope method respectively.

As evident from this study, the chemical treatment of adsorbed protein substantially reduced the initial surface coverage of proteins. The amount of proteins eluted from adsorbent surfaces was strongly correlated to the extent of helix unfolding in adsorbed layer proteins prior to its exposure to chemical excipients. While the elution efficiency of most chemical excipients (GdmHCl, SDS, Octyl, and CHAPS) was found to increase with the increasing extent of structural unfolding, the elutability of adsorbed

protein by urea was found to decrease for similar extent of unfolding. Similarly, unlike other chemical excipients which were strongly influenced by only the extent of protein unfolding, the elution process by an anionic excipient like SDS was also influenced by the type of protein that was unfolding on the adsorbent surface.

Although the elution process removed significant amount of the adsorbed proteins on the surface, there was a very weak correlation between the residual surface coverage and its residual structure, which was in stark contrast to the control conditions in protein-free buffer. Additionally, the residual bioactive state of the chemical treated proteins were different from its initial bioactive state. Based on these results, it was evident that the residual structure and bioactive state of the protein was clearly influenced by the chemical excipients. But, the specific mechanism by which these chemical excipients influence the adsorbed protein structure could not be identified by the current study. However, the results from the current study clearly demonstrated that the interactions of chemical excipient in the solution phase of a protein are not a good predictor of its interaction in the adsorbed phase, and must be individually assessed for an adsorption system. Therefore, with further refinements to the methodologies presented in the current study, the molecular mechanism underlying the interaction of chemical excipients on the structure and thereby, the bioactivity of an adsorbed protein could be better understood, and would eventually aid in the selection, design, and development of more effective decontamination agents for proteins on adsorbent surfaces.

9.5 REFERENCES

1. Latour, R. A. Biomaterials: Protein-Surface Interactions. In *The Encyclopedia of Biomaterials and Bioengineering*, 2 ed.; Bowlin, G. E. W. a. G. L., Ed.; Informa Healthcare, 2008; Vol. 1, pp 270-284.
2. Rabe, M.; Verdes, D.; Seeger, S. Understanding protein adsorption phenomena at solid surfaces. *Adv. Colloid Interface Sci.* **2011,** *162* (1-2), 87-106.
3. Emanuel, P. A.; Chue, C.; Kerr, L.; Cullin, D. Validating the performance of biological detection equipment: the role of the federal government. *Biosecur Bioterror* **2003,** *1* (2), 131-7.
4. Bramwell, V. W.; Eyles, J. E.; Oya Alpar, H. Particulate delivery systems for biodefense subunit vaccines. *Adv Drug Deliv Rev* **2005,** *57* (9), 1247-65.
5. Audi, J.; Belson, M.; Patel, M.; Schier, J.; Osterloh, J. Ricin poisoning: a comprehensive review. *J. Am. Med. Assoc.* **2005,** *294* (18), 2342-51.
6. Herr, A. E. Protein Microarrays for the Detection of Biothreats. Dill, K.; Liu, R. H.; Grodzinski, P., Eds.; Springer New York, 2009, pp 169-190.
7. Zoungrana, T.; Findenegg, G. H.; Norde, W. Structure, Stability, and Activity of Adsorbed Enzymes. *J. Colloid Interface Sci.* **1997,** *190* (2), 437-48.
8. Norde, W.; Giacomelli, C. E. In *Conformational changes in proteins at interfaces: from solution to the interface, and back*, Macromolecular Symposia, 1999; Wiley Online Library, pp 125-136.
9. Schellekens, H.; Jiskoot, W. Erythropoietin-Associated PRCA: Still an Unsolved Mystery. *J. Immunotoxicol.* **2006,** *3* (3), 123-30.
10. Sharma, B. Immunogenicity of therapeutic proteins. Part 1: impact of product handling. *Biotechnol. Adv.* **2007,** *25* (3), 310-7.
11. Sharma, B. Immunogenicity of therapeutic proteins. Part 2: impact of container closures. *Biotechnol. Adv.* **2007,** *25* (3), 318-24.
12. Kerwin, B. A. Polysorbates 20 and 80 used in the formulation of protein biotherapeutics: structure and degradation pathways. *J. Pharm. Sci.* **2008,** *97* (8), 2924-2935.
13. Otzen, D. Protein-surfactant interactions: a tale of many states. *Biochim. Biophys. Acta* **2011,** *1814* (5), 562-91.
14. Zhang, Y.; Cremer, P. S. Chemistry of Hofmeister anions and osmolytes. *Annu. Rev. Phys. Chem.* **2010,** *61*, 63-83.
15. Zhang, Y.; Cremer, P. S. Interactions between macromolecules and ions: The Hofmeister series. *Curr. Opin. Chem. Biol.* **2006,** *10* (6), 658-63.

16. Gurau, M. C.; Lim, S. M.; Castellana, E. T.; Albertorio, F.; Kataoka, S.; Cremer, P. S. On the mechanism of the hofmeister effect. *J. Am. Chem. Soc.* **2004,** *126* (34), 10522-3.

17. Elwing, H.; Gölander, C.-G. Protein and detergent interaction phenomena on solid surfaces with gradients in chemical composition. *Adv. Colloid Interface Sci.* **1990,** *32* (4), 317-339.

18. Elwing, H.; Welin, S.; Askendal, A.; Nilsson, U.; LundstrÖm, I. A wettability gradient method for studies of macromolecular interactions at the liquid/solid interface. *J. Colloid Interface Sci.* **1987,** *119* (1), 203-210.

19. Sigal, G. B.; Mrksich, M.; Whitesides, G. M. Effect of surface wettability on the adsorption of proteins and detergents. *J. Am. Chem. Soc.* **1998,** *120* (14), 3464-3473.

20. Svendsen, I. E.; Lindh, L.; Arnebrant, T. Adsorption behaviour and surfactant elution of cationic salivary proteins at solid/liquid interfaces, studied by in situ ellipsometry. *Colloids Surf. B. Biointerfaces* **2006,** *53* (2), 157-66.

21. Kapp, S. J.; Larsson, I.; Van De Weert, M.; Cardenas, M.; Jorgensen, L. Competitive adsorption of monoclonal antibodies and nonionic surfactants at solid hydrophobic surfaces. *J. Pharm. Sci.* **2015,** *104* (2), 593-601.

22. Thyparambil, A. A.; Wei, Y.; Latour, R. A. Experimental characterization of adsorbed protein orientation, conformation, and bioactivity. *Biointerphases* **2015,** *10* (1), 019002.

23. Wei, Y.; Thyparambil, A. A.; Latour, R. A. Quantification of the influence of protein-protein interactions on adsorbed protein structure and bioactivity. *Colloids Surf. B. Biointerfaces* **2013,** *110* (0), 363-71.

24. Wei, Y.; Thyparambil, A. A.; Latour, R. A. Protein helical structure determination using CD spectroscopy for solutions with strong background absorbance from 190 to 230nm. *Biochim. Biophys. Acta* **2014,** *1844* (12), 2331-2337.

25. Kelly, S. M.; Jess, T. J.; Price, N. C. How to study proteins by circular dichroism. *Biochim. Biophys. Acta* **2005,** *1751* (2), 119-39.

26. Wu, X.; Narsimhan, G. Effect of surface concentration on secondary and tertiary conformational changes of lysozyme adsorbed on silica nanoparticles. *Biochim. Biophys. Acta* **2008,** *1784* (11), 1694-701.

27. Cole, K. D.; Gaigalas, A.; Almeida, J. L. Process Monitoring the Inactivation of Ricin and Model Proteins by Disinfectants Using Fluorescence and Biological Activity. *Biotechnol. Progr.* **2008,** *24* (3), 784-791.

28. Liu, P. F.; Avramova, L. V.; Park, C. Revisiting absorbance at 230nm as a protein unfolding probe. *Anal. Biochem.* **2009,** *389* (2), 165-70.

29. Wei, Y.; Thyparambil, A. A.; Wu, Y.; Latour, R. A. Adsorption-induced changes in ribonuclease A structure and enzymatic activity on solid surfaces. *Langmuir* **2014,** *30* (49), 14849-58.

30. Thyparambil, A. A.; Wei, Y.; Wu, Y.; Latour, R. A. Determination of orientation and adsorption-induced changes in the tertiary structure of proteins on material surfaces by chemical modification and peptide mapping. *Acta Biomater.* **2014,** *10* (6), 2404-14.

31. Wei, Y.; Thyparambil, A. A.; Latour, R. A. Quantification of the influence of protein-protein interactions on adsorbed protein structure and bioactivity. *Colloids and Surfaces B-Biointerfaces* **2013,** *110*, 363-371.

32. Banik, I.; Kim, K. S.; Yun, Y. I.; Kim, D. H.; Ryu, C. M.; Park, C. S.; Sur, G. S.; Park, C. E. A closer look into the behavior of oxygen plasma-treated high-density polyethylene. *Polymer* **2003,** *44* (4), 1163-1170.

33. Oiseth, S. K.; Krozer, A.; Lausmaa, J.; Kasemo, B. Ultraviolet light treatment of thin high-density polyethylene films monitored with a quartz crystal microbalance. *J. Appl. Polym. Sci.* **2004,** *92* (5), 2833-2839.

34. Ton-That, C.; Shard, A. G.; Daley, R.; Bradley, R. H. Effects of Annealing on the Surface Composition and Morphology of PS/PMMA Blend. *Macromolecules* **2000,** *33* (22), 8453-8459.

35. De Geyter, N.; Morent, R.; Van Vlierberghe, S.; Dubruel, P.; Leys, C.; Gengembre, L.; Schacht, E.; Payen, E. Deposition of polymethyl methacrylate on polypropylene substrates using an atmospheric pressure dielectric barrier discharge. *Prog. Org. Coat.* **2009,** *64* (2-3), 230-237.

36. Serra, J.; González, P.; Liste, S.; Serra, C.; Chiussi, S.; León, B.; Pérez-Amor, M.; Ylänen, H. O.; Hupa, M. FTIR and XPS studies of bioactive silica based glasses. *J. Non-Cryst. Solids* **2003,** *332* (1-3), 20-27.

37. Fuguet, E.; Ràfols, C.; Rosés, M.; Bosch, E. Critical micelle concentration of surfactants in aqueous buffered and unbuffered systems. *Anal. Chim. Acta* **2005,** *548* (1–2), 95-100.

38. Chattopadhyay, A.; Harikumar, K. G. Dependence of critical micelle concentration of a zwitterionic detergent on ionic strength: implications in receptor solubilization. *FEBS Lett.* **1996,** *391* (1–2), 199-202.

39. Mukerjee, P.; Chan, C. C. Effects of High Salt Concentrations on the Micellization of Octyl Glucoside: Salting-Out of Monomers and Electrolyte

Effects on the Micelle−Water Interfacial Tension1. *Langmuir* **2002,** *18* (14), 5375-5381.

40. Timasheff, S. N.; Xie, G. Preferential interactions of urea with lysozyme and their linkage to protein denaturation. *Biophys. Chem.* **2003,** *105* (2-3), 421-448.

41. Vanzi, F.; Madan, B.; Sharp, K. Effect of the Protein Denaturants Urea and Guanidinium on Water Structure: A Structural and Thermodynamic Study. *J. Am. Chem. Soc.* **1998,** *120* (41), 10748-10753.

42. Anand, G.; Sharma, S.; Dutta, A. K.; Kumar, S. K.; Belfort, G. Conformational transitions of adsorbed proteins on surfaces of varying polarity. *Langmuir* **2010,** *26* (13), 10803-11.

43. Rapoza, R.; Horbett, T. The effects of concentration and adsorption time on the elutability of adsorbed proteins in surfactant solutions of varying structures and concentrations. *J. Colloid Interface Sci.* **1990,** *136* (2), 480-493.

44. Rapoza, R. J.; Horbett, T. A. Changes in the SDS elutability of fibrinogen adsorbed from plasma to polymers. *J. Biomater. Sci. Polym. Ed.* **1989,** *1* (2), 99-110.

45. Bohnert, J. L.; Horbett, T. A. Changes in adsorbed fibrinogen and albumin interactions with polymers indicated by decreases in detergent elutability. *J. Colloid Interface Sci.* **1986,** *111* (2), 363-377.

46. Otzen, D. E. Protein unfolding in detergents: effect of micelle structure, ionic strength, pH, and temperature. *Biophys. J.* **2002,** *83* (4), 2219-30.

47. Kondyurin, A.; Nosworthy, N. J.; Bilek, M. M. Effect of low molecular weight additives on immobilization strength, activity, and conformation of protein immobilized on PVC and UHMWPE. *Langmuir* **2011,** *27* (10), 6138-48.

48. Lad, M. D.; Ledger, V. M.; Briggs, B.; Green, R. J.; Frazier, R. A. Analysis of the SDS−Lysozyme Binding Isotherm. *Langmuir* **2003,** *19* (12), 5098-5103.

49. Docoslis, A.; Rusinski, L. A.; Giese, R. F.; van Oss, C. J. Kinetics and interaction constants of protein adsorption onto mineral microparticles — measurement of the constants at the onset of hysteresis. *Colloids Surf. B. Biointerfaces* **2001,** *22* (4), 267-283.

50. Sagle, L. B.; Zhang, Y.; Litosh, V. A.; Chen, X.; Cho, Y.; Cremer, P. S. Investigating the hydrogen-bonding model of urea denaturation. *J. Am. Chem. Soc.* **2009,** *131* (26), 9304-10.

51. Camilloni, C.; Rocco, A. G.; Eberini, I.; Gianazza, E.; Broglia, R. A.; Tiana, G. Urea and guanidinium chloride denature protein L in different ways in molecular dynamics simulations. *Biophys. J.* **2008,** *94* (12), 4654-61.

52. Moglich, A.; Krieger, F.; Kiefhaber, T. Molecular basis for the effect of urea and guanidinium chloride on the dynamics of unfolded polypeptide chains. *J. Mol. Biol.* **2005,** *345* (1), 153-62.

53. Hedoux, A.; Krenzlin, S.; Paccou, L.; Guinet, Y.; Flament, M. P.; Siepmann, J. Influence of urea and guanidine hydrochloride on lysozyme stability and thermal denaturation; a correlation between activity, protein dynamics and conformational changes. *PCCP* **2010,** *12* (40), 13189-96.

54. Dempsey, C. E.; Mason, P. E.; Jungwirth, P. Complex ion effects on polypeptide conformational stability: chloride and sulfate salts of guanidinium and tetrapropylammonium. *J. Am. Chem. Soc.* **2011,** *133* (19), 7300-3.

55. Tobias, D. J.; Hemminger, J. C. Chemistry. Getting specific about specific ion effects. *Science* **2008,** *319* (5867), 1197-8.

56. Heyda, J.; Kozisek, M.; Bednarova, L.; Thompson, G.; Konvalinka, J.; Vondrasek, J.; Jungwirth, P. Urea and guanidinium induced denaturation of a Trp-cage miniprotein. *J. Phys. Chem. B* **2011,** *115* (28), 8910-24.

57. Canchi, D. R.; Paschek, D.; Garcia, A. E. Equilibrium study of protein denaturation by urea. *J. Am. Chem. Soc.* **2010,** *132* (7), 2338-44.

58. Panuszko, A.; Bruzdziak, P.; Zielkiewicz, J.; Wyrzykowski, D.; Stangret, J. Effects of urea and trimethylamine-N-oxide on the properties of water and the secondary structure of hen egg white lysozyme. *J. Phys. Chem. B* **2009,** *113* (44), 14797-809.

59. Naidu, K. T.; Prabhu, N. P. Protein-surfactant interaction: sodium dodecyl sulfate-induced unfolding of ribonuclease A. *J. Phys. Chem. B* **2011,** *115* (49), 14760-7.

60. Zdziennicka, A.; Janczuk, B. Effect of anionic surfactant and short-chain alcohol mixtures on adsorption at quartz/water and water/air interfaces and the wettability of quartz. *J. Colloid Interface Sci.* **2011,** *354* (1), 396-404.

61. Anand, G.; Zhang, F.; Linhardt, R. J.; Belfort, G. Protein-associated water and secondary structure effect removal of blood proteins from metallic substrates. *Langmuir* **2011,** *27* (5), 1830-6.

62. Sarkar, D.; Chattoraj, D. K. Kinetics of Desorption of Proteins from the Surface of Protein-Coated Alumina by Various Desorbing Reagents. *J. Colloid Interface Sci.* **1996,** *178* (2), 606-613.

63. Levy-Sakin, M.; Berger, O.; Feibish, N.; Sharon, N.; Schnaider, L.; Shmul, G.; Amir, Y.; Buzhansky, L.; Gazit, E. The Influence of Chemical Chaperones on Enzymatic Activity under Thermal and Chemical Stresses: Common Features

and Variation among Diverse Chemical Families. *PLoS ONE* **2014,** *9* (2), e88541.

64. Subramanian, M.; Sheshadri, B. S.; Venkatappa, M. P. Interaction of Cationic Detergents, Cetyl- and Dodecyl-Trimethylammonium Bromides, with Lysozyme. *J. Biochem.* **1984,** *95* (2), 413-421.

CHAPTER TEN

SUMMARY AND FINAL CONCLUSIONS

The purpose of this body of work was to develop, validate, and apply a complementary set of techniques, (CD, AAL/MS, and adsorbed-state bioactivity assay), for characterizing the influence of adsorbed conditions on the bioactive state of protein. A summary of some of the important findings from this current work are:

A. Improvements in Individual Experimental Techniques

(a) Refinements were made to the existing CD methods with respect to the cuvette design, data acquisition and spectral scaling, and structural quantification.

a) The new cuvette designs were relatively simple, had improved signal-to-noise ratio, better sensitivity, and more importantly had improved operational stability.

b) The data acquisition procedure used in the current studies for CD were optimized for systematic and shot noises. The CD spectra were subsequently scaled according to the amount of proteins in solution and on the adsorbent surface. When the background absorbance from the solution was negligible, absorbance at 205 nm was used for characterizing the amount of proteins. However, in case of strongly absorbing chemical excipient, the absorbance at 230 nm was used to determine the amount of proteins in solution and on adsorbent surfaces.

c) Structural quantification was done using either CDpro package or the 230-240 nm slope method, which was developed in-house. If the spectra could be acquired down to 190 nm, CONTIN and CDSStr provided in the CDPro package were used to

deconvolute and quantify the secondary structural elements in the protein of interest. Towards this purpose SP43 and SP48 were used as the reference databases.

d) However, in the event of strong background absorbance below 230 nm, the previous methods could not be used for structure quantification. Therefore, the 230–240 nm slope method was developed and applied to predict the helical content in proteins when in solution or in an adsorbed state.

(b) The application of the AAL/MS method was extended to multiple amino acid groups within a protein to provide molecular-level information on the factors influencing the solvent exposure of a residue within the adsorbed protein.

a) Multiple amino acid groups were targeted in batch to batch experiments as opposed to modifying the different amino acid groups in a single experiment.

b) Identical reaction conditions were maintained throughout the study in order to avoid any specific influence of the reaction kinetics on the labeling processes. Additionally, caution was also exercised to ensure that these labeling processes would not affect the structure of the proteins in either their solution or adsorbed states.

c) The mass spectra of each of the batch labeling processes were scaled and normalized to the intensity of the internal label, an unmodified peptide fragment within the peptide digest obtained from the proteolytic cleavage.

d) A metrics was developed to correlate the extent of labeling to shifts in the solvent exposure of residues. These shifts in solvent exposure was subsequently correlated to physical changes in the local environment of targeted residues within the adsorbed protein because of conformational unfolding or steric hindrance effects.

(c) The bioactivity assays were refined to be more reflective of the adsorbed configuration of the protein by relative comparison of the specific activities of the adsorbed and solution phase of the proteins. Additionally, precautions were also taken to ensure that identical environmental conditions were maintained in the adsorbed and solution state bioactivity assays to mitigate any concerns of reaction conditions on the bioactivity assays.

B. Synergistic application of CD, AAL/MS, and adsorbed-state spectrophotometric assays provides holistic insight into the role of adsorption conditions on the structure and bioactivity of adsorbed protein

1. Quantitative insights into the individual role of a protein's internal stability, protein-surface interaction, and protein-protein interaction (PPI) to the adsorbed configuration and bioactive state of a protein.

   a) The internal stability of a protein affects the initial footprint of the adsorbed molecule and could subsequently affect the influence of protein proteins

   b) On surfaces like silica glass, which can be expected to exhibit strong hydrogen bond and electrostatic interactions, proteins tend to undergo a higher extent of unfolding at lower surface coverages than at higher surface coverages. The increasing stability provided at higher surface coverages is attributed to an in-plane compressive force provided by PPI effects of neighboring proteins.

   c) On surfaces like HDPE that are strongly hydrophobic, and lack any hydrogen-bondable groups, proteins tend to undergo lower degree of conformational shifts than the silica glass surface. But the increasing surface coverage of the proteins were

found to have either no or a slight destabilizing effect on the structure of adsorbed proteins.

d) On surfaces like PMMA that has only moderate hydrogen bonding and hydrophobic character, the amino acid composition of protein was found to play an important role in influencing the adsorption-induced conformational shift. For proteins like HEWL, the weak interaction with adsorbent surfaces would result in tertiary unfolding, with increasing surface coverages resulting in more prominent destabilization affecting the secondary and tertiary structure. In contrast, more hydrophilic proteins tend to undergo more structural destabilization at lower surface coverages, but are increasingly stabilized at increasing surface coverages.

e) The loss in a protein's activity on different surfaces was shown to be primarily due to adsorption-induced conformational unfolding of the active site. Depending upon the adsorbent surface, the unfolding process lead to an increase or decrease in the solvent exposure of residues.

2. Factors influencing the elution and denaturation of adsorbed protein exposed to chemical excipients.

a) The elution process of adsorbed proteins exposed to chemical excipients was strongly correlated to its extent of unfolding on the adsorbent surface. The elution process of adsorbed proteins by GdmHCl, SDS, octyl, and CHAPS was strongly promoted on surfaces when the adsorbed proteins underwent significant unfolding. However, the elution efficiency of urea tend to decrease as the proteins unfolds more on the

adsorbent surface. It was also observed that except for SDS, the elution process by all other chemical excipient was independent of the type of unfolding protein.

b) Chemical excipients can have influence the structure and bioactivity of the adsorbed proteins. However, the exact mechanism by which these individual chemical excipients would not influence the structure of the protein could not be determined in the current study.

c) The influence of chemical excipients on the structure of protein in its adsorbed and solution phase was not identical. Therefore, the solution-state responses of chemical excipient on the adsorbed phase of the protein are not a good representative of its adsorbed-state response, and must be individually assessed for each adsorption system.

D. Limitations and Future Directions

1. While the techniques presented are certainly complementary in nature and provide a comprehensive set of information on the influence of adsorption conditions on the structure and bioactive response of the proteins, the developed array of techniques does have its limitations. One of the main limitation with these techniques is its limited sensitivity to the type of protein population on the adsorbent surfaces. The responses measured by the techniques developed in this study represents an averaged response and could be meaningfully applied to only a homogenous type of protein system. In this regard, methods like molecular dynamics (MD) simulation are attractive alternatives as it holds potential to probe the role of adsorption condition on a specific population of protein. However, existing MD methods have not yet been validated for

adsorption systems, and must be developed further to be used for these specific types of applications. In this regard, the methodologies and results provided in this study provide much needed data to evaluate and validate these MD methods.

In conclusion, the current set of studies represents a stepping stone towards development of future strategies to control the bioactive state of adsorbed proteins, which would in turn benefit the customized design of surfaces for a broad range of applications in biotechnology and biomedical engineering. Some examples in this regard include the design of substrate surfaces for biosensors to optimally preserve the bioactivity of enzymes that are either adsorbed or tethered to the surface; or, alternatively, the design of filters and decontamination systems for biodefense applications to purposely deactivate adsorbed protein toxins or the protein capsid of virus particles by surface-induced protein unfolding or steric blockage of bioactive sites.

APPENDICES

APPENDIX: A

PROCEDURES AND RAW DATA FOR MEASURING THE SURFACE CHARGE DENSITY OF SILICA SUBSTRATES USING THREE DIFFERENT ANALAYTICAL TECHNIQUES

The supporting information contains (i) procedure for preparing buffers of different pH, (ii) surface charge density measurement using AFM, Electrophoresis Light Scattering (EP) Technique, and Streaming Potential technique, and (iii) quantified data on the surface charge density of silica substrates.

A.1 EXPERIMENTAL SET-UP AND METHODOLOGY

A.1.1. Surface Preparation and Characterization

Silica samples from two different commercial vendors were procured (fused silica glass, Chemglass Life Sciences, USA; and quartz (100), MTI Corporation, USA), with each material being subjected to the same pre-treatment before ζ-potential measurement with each of the three designated methods.[1-5].

A.1.1.1. Surface Preparation.

The surfaces were cleaned by sonicating (Branson Ultrasonic Corporation, USA) in (a) ‘‘piranha’’ [7:3 (v/v) H_2SO_4 (EMD Millipore Chemicals, USA) / H_2O_2 (Ricca Chemicals, USA)], and (b) basic solution [1:1:3 (v/v/v) NH_4OH (Fisher Scientific, USA) / H_2O_2 / H_2O] at 50°C for 1 min. The substrates were subsequently rinsed with copious

amounts of deionized water and stored in deionized water until further use at room temperature. Prior to ζ-potential measurement, the silica surfaces were rinsed with absolute ethanol and nanopure water, following which the samples were dried under a steady stream of nitrogen gas (Airgas National Welders, USA).

A.1.1.2. Surface Characterization.

Surface characterization determined the static air–water contact angle, atomic composition, film thickness, and roughness of the substrate. The air–water contact angles of all samples was analyzed using an optical contact–angle goniometer (DSA25 instrument, Krüss, USA) and the atomic compositions of these substrates were verified via X–ray photoelectron spectroscopy (NESCA/BIO, University of Washington, USA). The average surface roughness was analyzed using atomic force microscopy (AFM) (MFP–3D instrument, Asylum Research, USA) over an area of 5.0 μm × 5.0 μm.

A.1.2. Preparation of the electrolyte solution and estimation of the counter-ion concentration (pC) used in the ζ-potential measurement

10 mM KPB solutions of the desired pH were prepared by mixing appropriate amounts of potassium mono hydrogen phosphate (K_2HPO_4, Sigma-Aldrich, USA) and potassium dihydrogen phosphate (KH_2PO_4, Sigma-Aldrich, USA) (Table A.1). These individual salt solutions when dissolved in water to give twice the concentration of cations ($K_2HPO_4 \rightarrow 2\ K^+$, and $KH_2PO_4 \rightarrow K^+ + H^+$). The contribution by HPO_4^{2-} to form H^+ when associated with water was not significant until a pH of 7.2 (< 5%), and therefore was assumed as 5 % in all the calculations. Using these estimates, the –log of the counter ion concentration (pC) of a 0.01 M solution was found to be 1.69. In the case

of strong electrolyte solutions such as that of NaOH, HCl, and KCl, the pC was equal to its ionic concentration in the solution. Therefore, a 0.001 M NaOH, HCl, or KCl solution would have a pC of 3 while the pC would be 2 for an aqueous solution of a 0.01 M NaOH, HCl, or KCl solution.

Table A.1. Recipe for preparing 10 mM potassium phosphate buffer (KPB). The pKa of $H_2PO_4^-$ in aqueous environment is 6.2 X 10^{-8}

pH	Volume of 1 M K_2HPO_4 (mL)	Volume of 1 M KH_2PO_4 (mL)	pC
4.9	0	10	1.69
5.8	0.85	9.15	1.69
6	1.32	8.68	1.69
6.2	1.92	8.08	1.69
6.4	2.78	7.22	1.69
6.6	3.81	6.19	1.69
6.8	4.97	5.03	1.69
7.0	6.15	3.85	1.69
7.2	7.17	2.83	1.69
7.4	8.02	1.98	1.69
7.6	8.66	1.34	1.69
7.8	9.08	0.92	1.69
8.0	9.4	0.6	1.69
8.5	10	0	1.69

A.1.2.1 Standardization of 0.1 N NaOH and 0.1 N HCl solutions.

The solutions used in the current study were standardized according to established laboratory protocol. For this purpose, HCl and NaOH solutions used in the current study were standardized. The NaOH solution was standardized using 0.065 M potassium hydrogen phthalate (KHP). 0.4 g of KHP was added to 30 ml of deionized water with 2-3 drops of phenolphthalein indicator. The NaOH solution was titrated till the end-point (color fades) and the concentration of NaOH solution was calculated. Similarly, to 25 ml of HCl solution, 2-3

drops of phenolphthalein indicator was initially added, after which standardized NaOH solution was titrated, and final HCl concentration was calculated.

A.1.3 Methodologies for ζ-potential Measurement

Atomic force microscopy (AFM), electrophoresis (EP), and streaming potential (SP) techniques were used to estimate the ζ-potential of each material surface over a range of solution pH in 10 mM potassium phosphate buffer (KPB) solution. Among the techniques used in the current study, the AFM and EP techniques employ charged probes while the SP technique involves the use of mechanical force to create hydrodynamic shear to estimate the ζ-potential of the interfacial system. The pH value of the KPB solution used for comparing the consistency in ζ-potential measurement by the different techniques was varied from 4.9 to 8.5 by mixing appropriate amounts of potassium mono hydrogen phosphate (K_2HPO_4, Sigma-Aldrich, USA) and potassium dihydrogen phosphate (KH_2PO_4, Sigma-Aldrich, USA).

Since KPB (containing different ratios of K_2HPO_4 and KH_2PO_4) is not commonly used as an electrolyte for ζ-potential measurements despite its broad adoption in biological studies, control studies were done to compare the surface charging nature of glass and quartz (100) substrates in more commonly used electrolyte solutions, including 1 mM potassium chloride (KCl), 10 mM potassium chloride (KCl), 10 mM potassium monohydrogen phosphate (K_2HPO_4), and 10 mM potassium dihydrogen phosphate (KH_2PO_4) solutions. Titrations were also done in salt solutions containing varying molar ratios of K_2HPO_4 and KH_2PO_4 with a final molar concentration of 10 mM. The pH of these respective electrolyte solutions was adjusted by adding appropriate amounts of 0.1

M HCl and 0.1 M NaOH solutions previously standardized by titration against 0.065 M potassium hydrogen phthalate. Notwithstanding the type of solution, the addition of titrant will result in a change in the starting concentration of the respective solutions and the effects of these shifts in ionic concentration on ζ-potential measurements were allowed for by normalizing the measured ζ-potential response to the counter-ion concentration ((pC = −log(C), where 'C' is the concentration of counter ions) in each respective solution. The general equation for estimating the pC for an aqueous solution that is titrated in a 0.1 M HCl or 0.1 M NaOH solution is given by equations A.1 and A.2,

$$A_nB_m \leftrightarrow \alpha_A.m.A^+ + \alpha_B.n.B^- \qquad (A.1)$$

$$pC = \log_{10}\left(\frac{\alpha_A.m.c_1.X_1 + n.c_2.X_2}{X_1 + X_2}\right), \qquad (A.2)$$

where, α_A and α_B are the activity coefficients at 23°C for ionic solution A_nB_m, m and n are the stoichiometric coefficients (molar units) associated with the ionic constituents in the salt. The pC estimated for each salt is provided in Table A.2.

The titrant of concentration 'c_2' (0.1 N, activity coefficient of NaOH and HCl was considered equal to 1) and of volume 'X_2' (L) was added to the aqueous solution of initial concentration 'c_1' and volume 'X_1' (L) to adjust the pH of the solution.

Table A.2: Estimation of pC for the solutions used for titrating the glass and quartz (100) substrates at 23°C.

Type of solution		Titrant	Starting concentration (M)	pH range	pC range
1.0 mM salt	KCl	HCl, NaOH	0.001	2.8 – 9.1	2.64 – 3.00
10 mM salts	KCl	HCl, NaOH	0.010	3.1 – 9.6	1.87 – 2.00
	K_2HPO_4	HCl		2.8 – 9.2	1.52 – 1.69
	KH_2PO_4	NaOH		4.8 – 9.6	1.52 – 1.69
	K_2HPO_4, + KH_2PO_4 (KPB)	HCl, NaOH		4.2 – 9.3	1.5 – 1.69
10 mM KPB	K_2HPO_4, + KH_2PO_4	N/A	0.010	4.9 – 8.5	1.69

A single control experiment involved titration of the same substrate in each of the six solutions. Three such control experiments were done in the current study. All the measurements were done on the same batch of flat silica substrates at room temperature (23°C ± 2°C).

A.1.3.1. Atomic Force Microscopy (AFM) Technique

Force measurements on the silica samples were acquired by AFM (MFP-3D instrument, Asylum Research, USA) by following a previously developed methodology.[6] Briefly, high resolution force spectroscopy experiments were performed using gold coated silicon nitride cantilevers (Bruker Nano Inc, USA) that were functionalized with amine terminated and carboxyl terminated self-assembled monolayers (prepared from 1.0 mM $HS(CH_2)_{11}$-NH_2 and $HS(CH_2)_{11}$-COOH solutions (Assemblon, USA), respectively) using an established protocol.[7]

A.1.3.1.a. Preparation of carboxyl and amine-functionalized SAMs.

The bare gold surfaces were purchased from Biacore (SIA Au kit, BR–1004–05, Biacore, Inc., Uppsala, Sweden). Prior to coating, the alkanethiols and gold substrates were cleaned by sonicating (Branson Ultrasonic Corporation, Danbury, CT) in (a) "piranha" (7:3 (v/v) H_2SO_4 (Fisher Scientific, Fair Lawn, NJ, USA) / 35% (w/w) H_2O_2 (Aqua Solutions, Deer Park, TX, USA), and (b) basic solution (1:1:3 (v/v/v) NH_4OH (Fisher Scientific, Fair Lawn, NJ, USA) / H_2O_2 / H_2O) at 50°C for 1 minute. After each stage of the washing process, the gold slides were rinsed in nano–pure water and dried under a steady stream of nitrogen gas (National Welders Supply Co., Charlotte, NC, USA). The cleaned slides were then rinsed with ethanol and incubated in the appropriate alkanethiol solution (1.0 mM in 100% (absolute) ethanol (Pharmco–Aaper, Shelbyville, KY)). However, since amine–terminated alkanethiols have the general tendency to form an upside–down layer or multilayers,[8] the bulk pH was shifted to pH ≈ 12 by adding a few drops of triethylamine solution (Sigma Chemical Co., St. Louis, MO) to the alkanethiol solution to minimize this occurrence. All slides were stored in the respective alkanethiol solution for at least 16 h in the dark. Prior to use, all slides were sonicated in ethanol and water, and dried under a steady stream of nitrogen gas. Control studies were also done with carboxyl terminated SAMs.

A.1.3.1.b. Charge density measurement of AFM tips

Titrations of the tip were done in KPB over the pH range 4-9. All force spectroscopy experiments were performed at room temperature in a fluid cell. The functionalized tip was then brought into contact with the substrates and retracted at a

constant vertical scanning speed of 2 μm/s. In order to convert the deflection signals (volts) to force (Newton), the following settings were applied prior to force measurements: (a) the deflection sensitivity was set within the range of 40~100 nm/volts, (b) the spring constant of the AFM tip was determined by the thermal tune method,[9] (usually in the range of 0.058~0.065 N/m) and (c) an offset deflection correction was enabled. The cantilever tips had a radius of 60 nm. The functionalized tips were brought into contact with the substrates and retracted at a constant vertical scanning speed of 1.0 μm/s. For each of the tip-surface systems for which the approaching force-separation curves were recorded, two different samples from the same material were used, with at least three distinct sites on each substrate being chosen for force measurements. A minimum of ten force-separation curves were recorded at each site. In total, more than 60 force-separation curves were collected to obtain an average value for the charge density of each specific sample at a specific solution pH. Control experiments were also done to determine the exact charge on the amine and carboxyl functionalized tips for a given solution condition (Fig. A.1). [6]

The total force measured by AFM is the effective contribution of the electrostatic interactions, the van der Waal interactions, and the hydrodynamic repulsion.[10-12] By bringing the charged tip into close contact with the surface at 1.0 μm/s and allowing it to equilibrate, the hydrodynamic repulsions were minimized and as a result its contribution to the overall force measurement was ignored.[10, 12] Also, the van der Waals contribution to the force at 10 mM KPB solution was determined to be negligible compared to the strength of the electrostatic interaction.[11-12] Under these conditions, the force sensed by a

probe of known charge density when contacting the substrate was considered to be purely mediated by electrostatic interaction, from which the ζ-potential was obtained from the linearized Poisson-Boltzmann equation by treating the charges on the interacting surfaces as point charges.[6, 10-11] Accordingly, the ζ-potential of the interfacial system was determined from the individual force-distance curves (F(D)) by fitting the linearized Poisson-Boltzmann equation under a constant charge boundary condition as shown in equations 3 and 4, under the assumption that the electrostatic interaction is the only force mediating the interaction between the charged tip and the silica substrate:

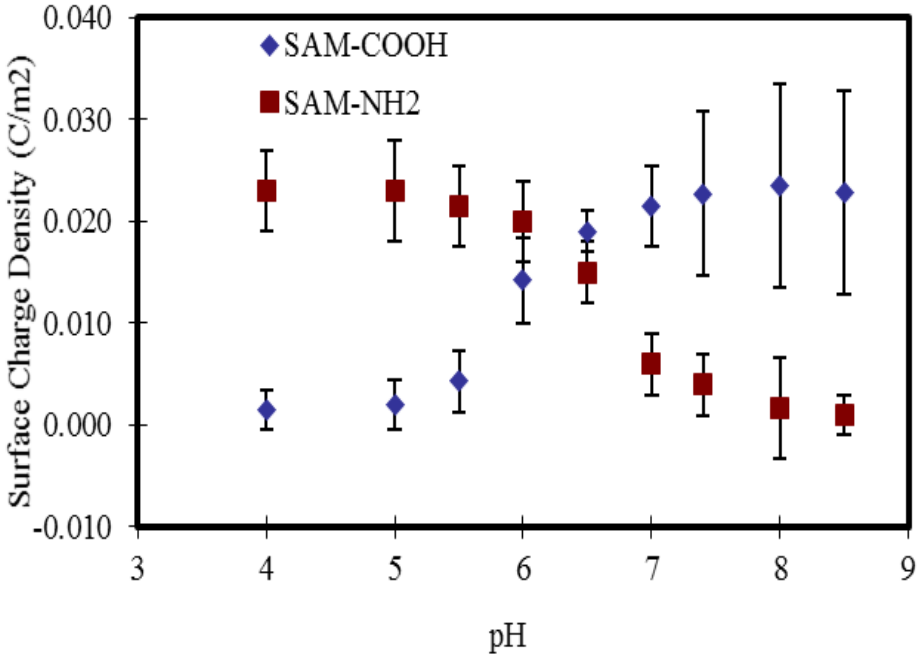

Figure A.1.: The effective surface charge density profile of the amine and carboxyl functionalized tips estimated using the force measured by the AFM on similarly charged substrates. Error bars represent 95% confidence intervals (C.I.). N = 4 for each data point.

$$\zeta_{AFM} = \frac{\sigma_{silica}\lambda_{deb}}{\varepsilon_s} \qquad (A.3)$$

$$\sigma_{silica} = \frac{F(D)\varepsilon_s}{4\pi R_{tip}\sigma_{tip}\lambda_{deb}e^{-D/\lambda_{deb}}} \quad \text{(A.4)}$$

Where, σ_{silica} is the effective charge density on the silica surface at the slip plane, ε_s is the relative permittivity of the aqueous solution, λ_{deb} is the Debye length of the buffer for a given solution condition, R_{tip} is the radius of the AFM tip, σ_{tip} is the effective charge density on the functionalized AFM tip, and D is the distance of the tip from the surface.

A.2.3.2. Electrophoresis Light Scattering (EP) Technique

The EP measurements were obtained using a ZEN1020 surface zeta potential cell accessory for a Zetasizer Nano-ZS instrument (Malvern Instruments, UK) using a previously described technique.[13] Similar to the AFM technique, EP also uses a charged probe (in this case a colloidal tracer) for its measurements. Briefly, the apparent tracer mobility is measured at increasing distances from the surface under an applied electric field within a dip cell. The mono-disperse silica tracer particles (77.4 ± 0.6 nm in diameter, with a pzc at pH 3.55) were custom prepared by the Stöber process, with extensive care taken to ensure any contaminants involved in the preparation process (ammonia and ethanol) were completely removed. Particle size distribution was determined by dynamic light scattering using a Zetasizer Nano-ZS (Malvern Instruments, UK), measuring a Z-average of 77.4 ± 0.6 nm with a polydispersity index in the order of 0.1 in water. Linear regression of tracer zeta potential vs. pH (for the buffer system and pH range used to examine surface charge) suggested the silica particles had a pzc of pH 3.55 (R^2 0.9841) with particle charge varying from -8.1 to -31.3 mV as pH increased.

The silica substrates of interest (7 mm x 4 mm) were mounted on the surface zeta potential dip cell probe and the surface of the substrate aligned to the zero displacement point (closest measurable point to the surface) using forward scattering light from the instrument's laser. The surfaces were then immersed in a suspension of tracer particles in 10 mM KPB. When the tracer particles are near the surface (initial displacement ~125 µm), the mobility of tracer particle is dominated by the electro-osmotic surface flow. Subsequent tracer mobilities were measured further from the surface (125 µm increments) and were considered to be due to the combined influence of the electrophoretic and an incrementally decreasing electro-osmotic influence. For a given solution pH or ionic composition, the mobility of the tracer particles at maximal separation from the surface (500 µm) is considered to be due to the electrophoretic motion of the tracer alone, independent of electro-osmotic effects and was used as the internal control. The silica tracer particles (~ 80 nm) that were used for the mobility measurements were much larger than the estimated Debye-Huckel thickness (< 2 nm) for the KPB solution. Joule heating was minimized though optimal selection of the electric field strength (selected automatically by the instrument depending on conductivity). Under these conditions, the direction and mobility of the tracer under the applied electric field was determined [13] and the ζ-potential of the tracer for the respective solution condition determined using the Smoluchowski equation (equation A.5).

$$\zeta_{EP} = \frac{\eta v_{eo}}{E_x \varepsilon_s} \quad , \qquad \text{(A.5)}$$

where η is the viscosity of the aqueous solution for the corresponding temperature, E_x is the strength of the applied electric field, and ε_s is the relative permittivity of the aqueous solution, under the assumption that the surface conductivity was negligible.[14] The ζ-potential of the particle is a linear function of its displacement from the substrate, and was extrapolated to determine with the tracer ζ-potential the ζ-potential of the surface (v_{eo}) (equation A.6). Similarly, the electrophoretic response was obtained for other solution conditions.

Surface ζ-potential = -intercept + tracer zeta potential (A.6)

A.2.3.3. Streaming Potential (SP) Technique

The measurements using the SP technique were acquired using the adjustable gap cell assembly (SurPASS, Anton Paar GmbH, Austria) using a previously developed technique.[15] Briefly, the streaming potential was measured across the solution which passed through a measuring cell assembly with two opposing silica substrates (2 cm x 1 cm) that were 105 μm apart. Prior to each measurement, samples were first rinsed with the solution, after which flow was induced in the measurement cell by ramping the pressure from 0 to 300 mbar in forward and reverse directions to generate charge separation. For each measurement, two cycles of pressure ramping in the forward and reverse direction were conducted. Prior to streaming potential measurement, it was verified that the change in hydrodynamic pressure as a function of flow was linear and passed through the origin in order to ensure that the asymmetric effect of placing the substrates in the sample holder was negligible.[14, 16-17] The ζ-potentials of substrates using

the SP technique were calculated from the streaming potentials (dU/dP) using the Fairbrother and Mastin equation (equation A.7), (a variant to the Helmholtz-Smoluchowski equation, which accounts for the surface conductance):

$$\zeta_{SP} = \frac{dU}{dP}\frac{\eta R_s \kappa_s}{\varepsilon_s R} \quad , \qquad \text{(A.7)}$$

where η is the viscosity of the aqueous solution, ε_s is the relative permittivity for aqueous solution and R is the direct current (DC) resistance inside the measuring cell. The contribution of the surface conductance was corrected by accounting for the terms κ_s, and R_s, which represent the specific conductivity and resistivity of the aqueous solution, respectively.

A.2.4. Model to determine the σ_0 and surface constants from ζ-potential measurements

Silica substrates are generally considered to acquire charge by an ionization process, the extent of which depends on the alkalinity of the solution.[18-20] At a simplistic level, when a silica surface is exposed to solution conditions, the dissociation equilibria and the equilibrium constants for the silica system can be written as,[18]

$$SiOH_2^+ \leftrightarrow SiOH + H^+ \text{, and} \qquad \text{(A.8)}$$

$$SiOH \leftrightarrow SiO^- (surf) + H^+ \text{ .} \qquad \text{(A.9)}$$

The surface charge of the glass and quartz surfaces per unit area (σ_0) is then given by:

$$\sigma_0 = e([SiOH_2^+] - [SiO^-]) \text{ ,} \qquad \text{(A.10)}$$

where ‘e’ represents the absolute magnitude of the charge of an electron and [$SiOH_2^+$] and [SiO^-] represent areal densities of the designated charged functional groups on the surface, with the total number of surface sites per unit area (N_s) is given by:

$$N_s = [SiOH_2^+] + [SiO^-] + [SiOH] . \qquad (A.11)$$

A.2.4.1. Electro-neutrality condition of the interfacial double layer.

For a charged surface in contact with an aqueous solution of low ionic strength, the GCS model of the interface introduced in Fig. A.1 can be used to estimate the σ_0 of the surface.[18] The GCS model assumes the electrical double layer to be divided into diffuse and bound regions to maintain an electro-neutrality condition of the form:

$$\sigma_0 + \sigma_d = 0, \qquad (A.12)$$

where σ_0 is the charge density of the surface and σ_d is the charge density of the bound region (Stern layer). According to the Stern model, the relation between the σ_d and the potential (ψ_d) is given by the Gouy-Chapman expression:

$$\sigma_d = -\frac{2\varepsilon\varepsilon_0 \kappa k_B T}{ze} \sinh\left(\frac{ze\psi_d}{2k_B T}\right), \qquad (A.13)$$

where ε is the relative dielectric constant of water (ε_{water} 78.54), ε_o is the permittivity of free space (ε_o = 8.85 x 10^{-12} CVm^{-1}), κ is the inverse Debye screening length (m^{-1}), T is the temperature (K), and z is the valence of the counter-ions. Since the location of the slip plane is not precisely known, it is generally assumed that the Stern plane and shear plane

are located within the same plane, (i.e., $\Delta \approx \delta$ (see Figure 1), and thus $\psi_d \approx \zeta$). Using this approximation, equation A.13 may be written as:

$$\sigma_d = -\frac{2\varepsilon\varepsilon_0\kappa k_B T}{ze}\sinh\left(\frac{ze\zeta}{2k_B T}\right) \qquad (A.14)$$

The point of zero charge (pzc) of the interfacial system represents the bulk solution pH at which the net charge on the surface is zero, and therefore it is expected that the ζ-potential = 0. By using equation A.12 and assuming pH >> (pzc), [18]

$$\sigma_o \approx -e[SiO^-] = -\sigma_d = +\frac{2\varepsilon\varepsilon_0\kappa k_B T}{ze}\sinh\left(\frac{ze\zeta}{2k_B T}\right) \qquad (A.15)$$

which, when rearranged for the density of the ionized group $[SiO^-]$, gives:

$$[SiO^-] = -\frac{2\varepsilon\varepsilon_0\kappa k_B T}{ze^2}\sinh\left(\frac{ze\zeta}{2k_B T}\right). \qquad (A.16)$$

Similarly, by assuming the concentration of positively charged groups on the surface is zero (i.e., $[SiOH_2^+] = 0$), an expression for the fraction of the ionized group (*f*) can be expressed as:

$$f = \frac{[SiO^-]}{[SiOH]+[SiO^-]} = -\frac{2\varepsilon\varepsilon_0\kappa k_B T}{ze^2 N_s}\sinh\left(\frac{ze\zeta}{2k_B T}\right) \qquad (A.17)$$

A.2.4.2. Estimation of the surface charge density and point of zero charge (pzc) from the fractional ionization.

The Kiselev–Zhuravlev constant for the silica substrates is considered to be about 4.9 silanol groups/nm^2.[21] Based on this estimate, the density of silanol groups [N_s] is

found to be 20.4 Å^2/site. The σ_0 of the glass and quartz surfaces can then be related to '*f*' (equation A.17), using equation A.18:

$$\sigma_o = \frac{1 \text{ silanol site}}{20.4\ \text{Å}^2} \text{x} \frac{10^{20}\ \text{Å}^2}{\text{m}^2} \text{x} \frac{-1.6\text{x}\ 10^{-19}\ \text{C}}{\text{charged site}} \text{x f} \frac{(\text{charged site})}{(\text{silanol site})}$$

$$= -0.784\ f \text{ (units: Coulombs/m}^2\text{)} \qquad \text{(A.18)}$$

For the current study, the pzc for the interfacial system was obtained from the plot of ζ-potential as a function of bulk solution pH by linearly extrapolating the measured response of the ionization process of the substrate to the x-intercept (i.e., for ζ-potential = 0). To validate the accuracy of the results obtained in the current study, the pzc values, which are considered unique to an oxide system, were compared with those reported by other groups.[18, 22]

A.2.5 Statistical Analysis

The results from the study are presented as the mean values ± 95% confidence intervals (C.I.). The statistical significance of differences between mean values for different samples/conditions was evaluated using either the Student's t-test or a non-parametric sign test with values of $p < 0.05$ (SAS 9.3.1, SAS Inst. Inc., Cary, NC) being considered as statistically significant.

A.2. RESUTS AND DISCUSSION

A.2.1. Solution-induced effects on the ζ-potential.

As previously mentioned, ζ-potential measurements by any technique are obtained within the solution phase of solid-liquid interface and are very sensitive to

variations in solution conditions, such as ion concentration, the type of ions, and solution pH.[14, 19-20, 22-23] Therefore, prior to assessing the effect of different techniques on the ζ-potential measurements, it is important to verify that the ζ-potential measurements obtained from a variety of solution conditions can in fact be used to represent the ionization processes occurring on the glass and quartz (100) substrates at different values of pH. Towards this end, ζ-potential measurements of the glass and quartz (100) surfaces were conducted under three separate solution conditions: 1.0 mM salt (1 mM KCl), 10 mM salts (10 mM KCl, 10 mM K_2HPO_4, 10 mM KH_2PO_4, and 10 mM KPB), and 10 mM KPB solutions (without addition of acidic or basic titrant) using the SP technique and the responses were compared.

Figs A.2A and A.3A show the raw ζ-potential response for glass and quartz (100) substrates, respectively, when acid and base titrated in 1.0 mM salt (1 mM KCl), 10 mM salts (10 mM KCl, 10 mM K_2HPO_4, 10 mM KH_2PO_4, and 10 mM KPB), and 10 mM KPB solutions (without acid or basic titration) using the SP technique. For the same substrate, one complete data set involves measurement of the ζ-potential response in each of the six solutions. Three such data sets were obtained for glass and quartz (100) substrates. The data points presented in Figs A.2A and A.3A represent ζ-potential values using the SP technique and calculated using equation A.6, which include correction for surface conductance.

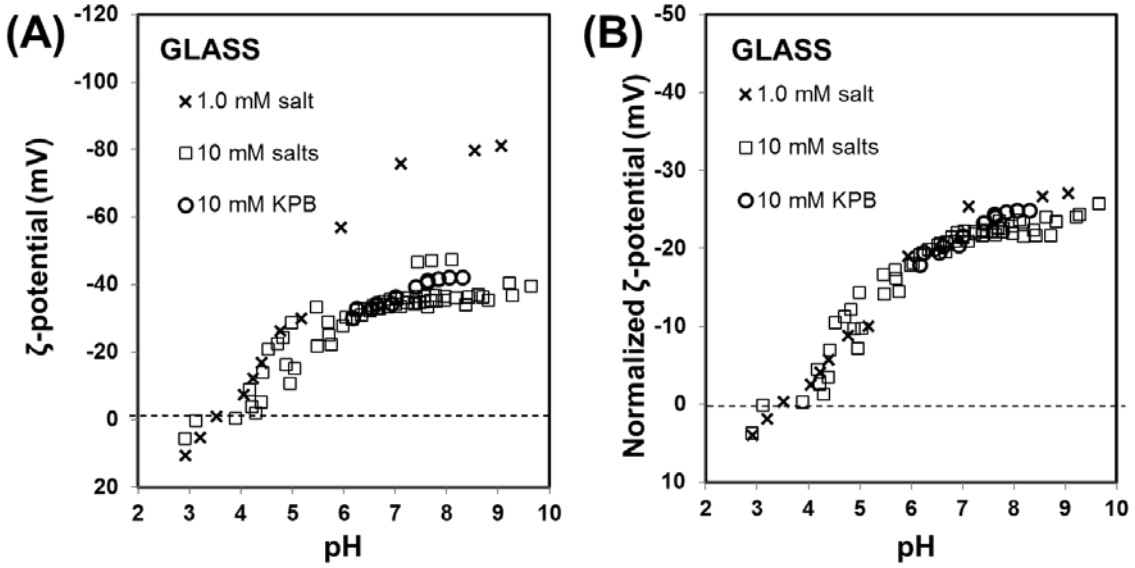

Figure A.2: ζ-potential response (A) of glass substrate when titrated in 1.0 mM salt, 10 mM salts, and 10 mM KPB as a function of pH using the SP technique. The data presented is the complete dataset on one of the three titration runs for each of the solution conditions for the glass surfaces (average 95% C.I. for each of the data point is ± 5.0 mV). The normalized ζ-potential (B) refers to raw ζ-potential values that were normalized to the –log of the counter-ion concentration (pC) of the respective aqueous solutions. The pzc for the glass substrate was found to be 3.3 ± 0.2 mV (mean ± 95% C.I., n = 3).

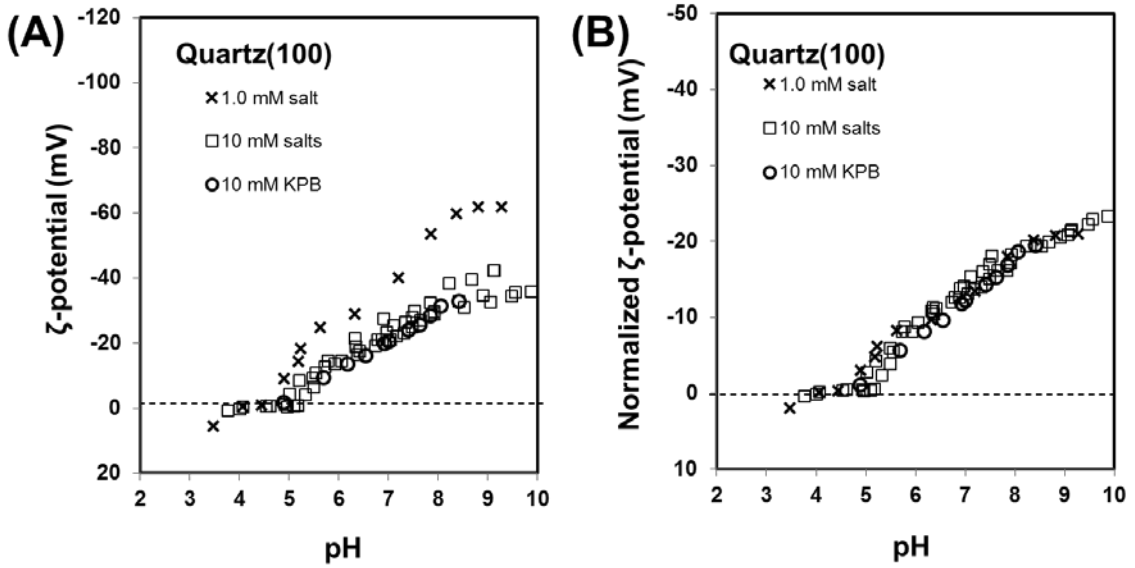

Figure A.3: ζ-potential response (A) of the quartz (100) substrate when titrated in 1.0 mM salt (nominal), 10 mM salts (nominal), and 10 mM KPB solutions as a function of the pH using the SP technique. The data presented is the complete dataset on one of the three titration runs for each of the solution conditions for the quartz (100) surfaces

(average 95% C.I. for each of the data point is ± 4.0 mV). The normalized ζ-potential (B) refers to raw ζ-potential values that were normalized to the –log of the counter-ion concentration (pC) of the respective aqueous solutions. The pzc for the quartz (100) substrate was found to be 4.1 ± 0.2 mV (mean ± 95% C.I., n = 3).

A.2.2. Normalization of ζ-potential values to account for variations in salt composition and concentration.

As clearly shown from Fig. A.2A and A.3A, for a given ionic concentration over the range of pH, the ζ-potential values increased almost linearly (for silica glass: 3.0 < pH < 7.0, for quartz (100): 4.0 < pH < 8.0) and eventually plateaued (for silica glass > 7.0, for quartz (100): pH > 8.0). However, the ζ-potential values were also substantially influenced by the differences in salt composition and concentration at a given pH. It is widely accepted that for a substrate with fixed σ_0, these effects are a result of differences in electrostatic screening and the exponential buildup of counter ions at the charged interface, which influences potential difference across the slip plane.[23]

However, as proposed by Kirby *et al.* for the ionic concentrations used in the current study (0.001 M < ionic concentration < 0.100 M), if the effects of electrolyte strength on the ζ-potential measurements for different pH are accounted for by normalizing these measurements to the –log (counter-ion concentration within the bulk solution), then the solution-induced effect can be effectively eliminated.[23] Accordingly, when the ζ-potential measurements for the substrates were normalized in this way, plots of the normalized ζ-potential vs. pH for the different salt conditions shown in Fig. A.2A and A.3A merged into a single relationship showing a behavior consistent with the ionization process expected for silica substrates.[18, 23] The trends in these data in each of the solution conditions also suggest that ionization in 10 mM KPB was not different from

the ionization of the silica polymorphs in simpler salts of similar concentration. From the trends shown in Figs. A.3B and A.2B, it is evident that variations in ζ-potential measurements for the glass and quartz (100) surfaces, respectively, in the 1.0 mM salt (1 mM KCl), 10 mM salts (10 mM KCl, 10 mM K_2HPO_4, 10 mM KH_2PO_4, and 10 mM KPB), and 10 mM KPB solutions (without addition of acid or basic titration) using the SP technique were due to variations in the composition of the solution over the surface as opposed to differences in the ionization of the substrate surface. Under these conditions, the pzc (mean ± 95% C.I.) estimated for the silica glass and quartz (100) surfaces are 3.3 ± 0.2 and 4.1 ± 0.2, respectively. These estimates are well within the reported values for these silica polymorphs, which range from 2.0 to 5.0.[22]

A.2.2.a Comparison of ζ-potential values from different measurement techniques

The preceding section established that raw ζ-potential measurements are sensitive to solution conditions, but that these effects can be accounted for by normalizing the ζ-potential values by the –log (counter-ion concentration within the bulk solution). The results presented in Figs A.2 and A.3 indicate that the normalized ζ-potential response as a function of pH is reflective of the surface charge density of the substrate rather than being dependent on the composition of the solution, with the normalized ζ-potential values in 0.010 M KPB solution conditions being in close agreement with the normalized response obtained in the simpler salt solutions. With these relationships thus established, ζ-potential values were obtained and compared between the three selected measurement

techniques for silica glass and quartz (100) under 0.010 M KPB solution conditions. Fig. A.4 shows the normalized electro-kinetic response for the glass and quartz (100) surfaces in different solution pH (4.9, 5.6, 6.6, 7.4, and 8.5) measured using the AFM, EP, and SP techniques.

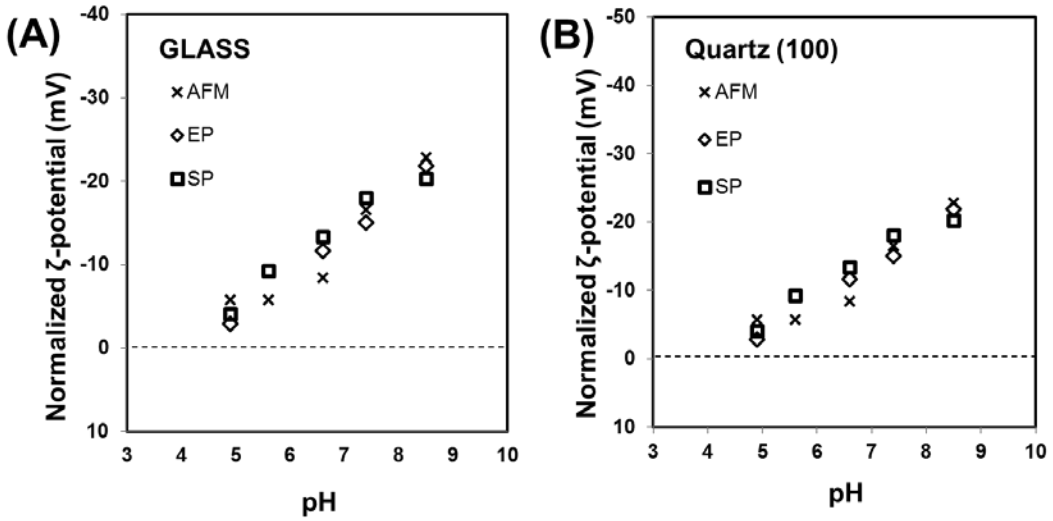

Figure A.4 Normalized ζ-potential values from AFM, EP, and SP measurements on the (A) silica glass and (B) quartz (100) substrates in 10 mM KPB as a function of pH. The data points represents the mean of three measurements for the identical solution conditions by each technique. The averaged 95% C.I. for a glass substrate by AFM, EP, and SP techniques were ± 8 mV, ± 5 mV and ± 5 mV, respectively, while for quartz (100) were ± 9 mV, ± 5 mV and ± 4 mV, respectively.

As clearly evident from Fig. A.4A and A.4B, for the pH range used in the current study for each of the techniques, a linear normalized ζ-potential response for both the substrates (R^2 = 0.95 for glass, R^2 = 0.94 for quartz (100)) over the range of bulk solution pH of 4-9, indicates that the each of these techniques is sensitive to the ionization process occurring on the surface of the substrate of interest. Most importantly, close agreement is shown between the three different methods. Table A.3 provides the pzc values for glass and quartz (100) surfaces for each of these three measurement techniques, with no significant

difference being indicated for the estimated pzc values, thus indicating equivalent reliability for each of these methods for the determination of pzc for our two silica surfaces. Thus, based on the data presented, the ζ-potential values measured for each of the substrates by different techniques were not statistically different from each other.

Table A.3. Estimation of point of zero charge (pzc) using different techniques. The pzc values for glass and quartz (100) substrates were estimated from the ζ-potential values obtained using AFM, EP, and SP techniques in KPB using linear extrapolation of the measurement to zero ζ-potential. For sake of comparison, the pzc obtained from the literature with different solutions using the SP technique for glass and quartz (100) substrates, and the reported pzc values for silica polymorphs are provided.

Substrate	AFM	EP	SP	Different solutions**	Literature values [22, 24]
Fused Glass	4.2	4.33	3.61	3.43 ± 1.45	< 5
Quartz (100)	4.25	4.38	3.72	4.27 ± 0.66	< 5

**indicates 1.0 mM salt, 10 mM salts and 10 mM KPB solutions that were used in Fig A.1;

A.2.3 Reliability of σ_0 estimates from ζ-potential measurements is limited by the interfacial double layer model

With the ζ-potential values shown to be independent of the type of technique used for making these measurements, estimates of σ_0 were obtained in terms of 'f' using equations A.17 and A.18. Based on the GCS model, the σ_0 estimates were between -0.004 C/m^2 and -0.025 C/m^2 for the glass and quartz (100) substrates over the pH range of 4.0 – 9.0, consistent with estimates obtained by other groups using similar models (Table A.4).[11-12, 19, 25-26] The results were also comparable and within the same order of magnitude as other variants of the GCS model that have been used to translate ζ-potential values into σ_0, which additionally account for surface complexation or the hydrated shell

of the ions.[27-28] It should be recognized, however, that since the values of σ_0 rely on assumed conditions at the interface, such as those provided by the GCS model, the underlying assumptions of the model will affect the magnitude of these estimates.

Table A.4. Estimated fraction of ionization *(f)* for the ζ potential measurement obtained by different techniques (AFM, EP, and SP) on the glass (pzc = 4.04, pK_d = 6.48) and (b) quartz (100) (pzc = 4.12, pK_d = 6.51) surface in 10 mM KPB (pH 4.0-9.0). The normalized ζ potential was obtained by dividing the raw ζ potential to the –log (counter ion concentration) of KPB. The counter ion concentration of KPB was ≈ 0.06 M. The average results presented for ζ, and f are the mean values ± 95% confidence intervals (C.I.).

–pH–	Glass		Quartz(100)	
	ζ (mV)	**f (%)**	**ζ (mV)**	**f (%)**
4.9	-6.3 (13)	0.5 (1.0)	-7.2 (7)	0.7 (0.6)
5.6	-14.1 (10)	1.1 (0.8)	-9.1 (3)	0.9 (1.1)
6.6	-22.5 (9)	1.8 (0.8)	-19.3 (13)	1.9 (1.3)
7.4	-30.7 (9)	2.5 (0.8)	-28.6 (9)	2.9 (1.0)
8.5	-40.4 (4)	3.3 (0.4)	-37.8 (3)	3.8 (0.3)

A.3. REFERENCES

1. Snyder, J. A.; Abramyan, T.; Yancey, J. A.; Thyparambil, A. A.; Wei, Y.; Stuart, S. J.; Latour, R. A. Development of a tuned interfacial force field parameter set for the simulation of protein adsorption to silica glass. *Biointerphases* **2012,** *7* (1-4), 56.
2. Thyparambil, A. A.; Wei, Y.; Latour, R. A. Determination of Peptide–Surface Adsorption Free Energy for Material Surfaces Not Conducive to SPR or QCM using AFM. *Langmuir* **2012,** *28* (13), 5687-94.
3. Wei, Y.; Thyparambil, A. A.; Latour, R. A. Peptide–Surface Adsorption Free Energy Comparing Solution Conditions Ranging from Low to Medium Salt Concentrations. *Chemphyschem* **2012,** *13* (17), 3782-85.
4. Wei, Y.; Thyparambil, A. A.; Latour, R. A. Quantification of the influence of protein-protein interactions on adsorbed protein structure and bioactivity. *Colloid Surface B* **2013,** *110* (0), 363-71.

5. Thyparambil, A. A.; Wei, Y.; Wu, Y.; Latour, R. A. Determination of orientation and adsorption-induced changes in the tertiary structure of proteins on material surfaces by chemical modification and peptide mapping. *Acta Biomater* **2014,** *10* (6), 2404-14.

6. Zimmerman, B.; Chow, J.; Abbott, A. G.; Ellison, M. S.; Kennedy, M. S.; Dean, D. Variation of Surface Charge along the Surface of Wool Fibers Assessed by High-Resolution Force Spectroscopy. *J Eng Fiber Fabr* **2011,** *6* (2), 61-66.

7. Wei, Y.; Latour, R. A. Benchmark experimental data set and assessment of adsorption free energy for peptide-surface interactions. *Langmuir* **2009,** *25* (10), 5637-46.

8. Wang, H.; Chen, S.; Li, L.; Jiang, S. Improved Method for the Preparation of Carboxylic Acid and Amine Terminated Self-Assembled Monolayers of Alkanethiolates. *Langmuir* **2005,** *21* (7), 2633-36.

9. Webber, G. B.; Stevens, G.; Grieser, F.; Dagastine, R. R.; Chan, D. Y. C. Variations in properties of atomic force microscope cantilevers fashioned from the same wafer. *Nanotechnology* **2008,** *19* (10).

10. Butt, H. J.; Cappella, B.; Kappl, M. Force measurements with the atomic force microscope: Technique, interpretation and applications. *Surf Sci Rep* **2005,** *59* (1-6), 1-152.

11. Sokolov, I.; Ong, Q. K.; Shodiev, H.; Chechik, N.; James, D.; Oliver, M. AFM study of forces between silica, silicon nitride and polyurethane pads. *J Colloid Interf Sci* **2006,** *300* (2), 475-81.

12. Jing, D.; Bhushan, B. Quantification of surface charge density and its effect on boundary slip. *Langmuir* **2013,** *29* (23), 6953-63.

13. Corbett, J. C. W.; McNeil-Watson, F.; Jack, R. O.; Howarth, M. Measuring surface zeta potential using phase analysis light scattering in a simple dip cell arrangement. *Colloid Surface A* **2012,** *396* (0), 169-76.

14. Delgado, A. V.; González-Caballero, F.; Hunter, R. J.; Koopal, L. K.; Lyklema, J. Measurement and Interpretation of Electrokinetic Phenomena (IUPAC Technical Report). *Pure Appl Chem* **2005,** *77* (10), 1753-805.

15. Ladner, D. A.; Steele, M.; Weir, A.; Hristovski, K.; Westerhoff, P. Functionalized nanoparticle interactions with polymeric membranes. *J Hazard Mater* **2012,** *211*, 288-95.

16. Buksek, H.; Luxbacher, T.; Petrinic, I. Zeta Potential Determination of Polymeric Materials Using Two Differently Designed Measuring Cells of an Electrokinetic Analyzer. *Acta Chim Slov* **2010,** *57* (3), 700-06.

17. Squires, T. M. Electrokinetic flows over inhomogeneously slipping surfaces. *Phys Fluids* **2008,** *20* (9), -.

18. Scales, P. J.; Grieser, F.; Healy, T. W.; White, L. R.; Chan, D. Y. C. Electrokinetics of the silica-solution interface: a flat plate streaming potential study. *Langmuir* **1992,** *8* (3), 965-74.

19. Rimola, A.; Costa, D.; Sodupe, M.; Lambert, J. F.; Ugliengo, P. Silica surface features and their role in the adsorption of biomolecules: computational modeling and experiments. *Chem Rev* **2013,** *113* (6), 4216-313.

20. Sverjensky, D. A. Prediction of surface charge on oxides in salt solutions: Revisions for 1:1 (M+L−) electrolytes. *Geochim Cosmochim Ac* **2005,** *69* (2), 225-57.

21. Zhuravlev, L. T. The surface chemistry of amorphous silica. Zhuravlev model. *Colloid Surface A* **2000,** *173* (1-3), 1-38.

22. Kosmulski, M. pH-dependent surface charging and points of zero charge III. Update. *J Colloid Interf Sci* **2006,** *298* (2), 730-41.

23. Kirby, B. J.; Hasselbrink, E. F., Jr. Zeta potential of microfluidic substrates: 1. Theory, experimental techniques, and effects on separations. *Electrophoresis* **2004,** *25* (2), 187-202.

24. Kosmulski, M. Confirmation of the Differentiating Effect of Small Cations in the Shift of the Isoelectric Point of Oxides at High Ionic Strengths. *Langmuir* **2002,** *18* (3), 785-87.

25. Behrens, S. H.; Grier, D. G. The charge of glass and silica surfaces. *J Chem Phys* **2001,** *115* (14), 6716.

26. Dove, P. M.; Craven, C. M. Surface charge density on silica in alkali and alkaline earth chloride electrolyte solutions. *Geochim Cosmochim Ac* **2005,** *69* (21), 4963-70.

27. Wang, M.; Revil, A. Electrochemical charge of silica surfaces at high ionic strength in narrow channels. *J Colloid Interf Sci* **2010,** *343* (1), 381-86.

28. Leroy, P.; Devau, N.; Revil, A.; Bizi, M. Influence of surface conductivity on the apparent zeta potential of amorphous silica nanoparticles. *J Colloid Interf Sci* **2013,** *410* (0), 81-93.

APPENDIX: B

PROCEDURES AND RAW DATA FOR MEASURING THE SURFACE COVERAGE, SECONDARY STRUCTURE, AND BIOACTVITY OF PROTEINS ADSORBED ON A MATERIAL SURFACE (CHAPTER 5)

This supporting information contains (*i*) adsorption procedure, (*ii*) calibration and instrument performance, (*iii*) effect of adsorption time and equilibration time on the surface coverage of adsorbed proteins, *(iv)* effect of exposure time on the structure of adsorbed proteins, *(v)* estimating solution state bioactivity of the proteins, and *(vi)* raw data of adsorbed proteins responses under varying PPI conditions.

B.1. Adsorption Procedure

The adsorption scheme is shown in Fig B.1. Depending on the type of adsorbent surface, different adsorption scheme were required in order to ensure that protein adsorb only to the substrate of interest and do not randomly adsorb to the exposed surface. For e.g., adsorption scheme depicted in Fig. B.1a was used with glass substrates, but Fig B.1b was used for polymeric substrates like HDPE and PMMA, as the polymer samples were coated on only one side of the glass substrates.

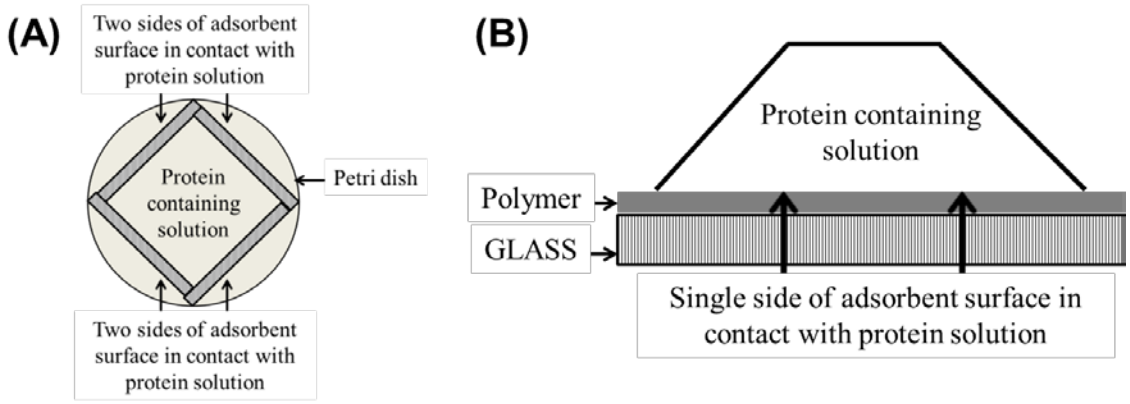

Figure B.1. Schemes used for protein adsorption. (A) Protein adsorbed on both sides of the adsorbent surface and (B) Protein adsorbed on a single side of the adsorbent surface.

B.2. Calibration and Instrument Performance

Prior to structure determination, the performance of the instrument was evaluated using freshly prepared 0.6 mg/ml camphosulfonic acid solution (CSA) using a standard cell with a pathlength of 0.1 cm at room temperature. Under these conditions, the magnitude of the CD signal was calibrated for the wavelengths 192.5 nm and 290.5 nm to −35.992 mdeg and 17.450 mdeg respectively, so that the ratio of the magnitude between these two wavelengths is above 2.05 [1]. Fig. B.2 shows a sample CD spectrum. All CD experiments were done under a steady stream of nitrogen flow (~ 10 liters/minute) with the HT voltage kept below 600 V.

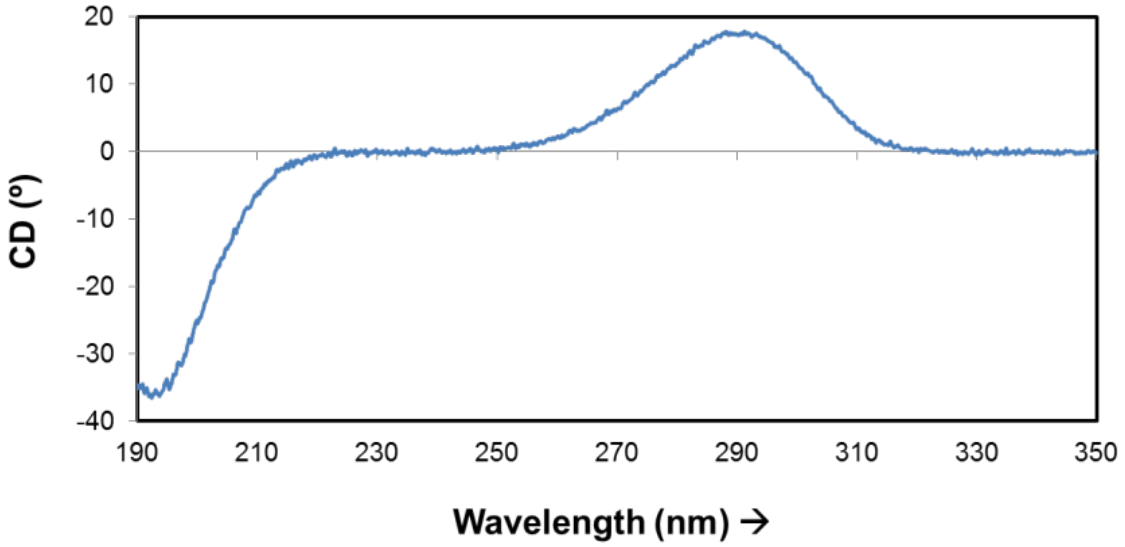

Figure B.2. Raw CD spectra of 0.6 mg/ml camphosulfonic acid solution (CSA) when used in a standard cell of pathlength 0.1 cm.

B.3. Estimating the Solution State Bioactivity of Proteins

The procedure provided here is a general description of the procedure followed for estimating the solution state bioactivity of proteins in our studies using HEWL as an example. HEWL catalyzes the breakdown of cell wall in *Micrococcus lysodeikticus*, which results in the decrease of turbidity in bacterial solution as a function of time. The above bioactivity assay in solution state was carried out in the same cuvette that was used for adsorbed state CD studies. An initial calibration plot for solution state bioactivity for a fixed concentration (60 mg/L) of *Micrococcus lysodeikticus* in PPB (pH 7.4) was obtained for a working range of 0.1 µg – 30 µg of protein (based on the equivalently adsorbed amount of protein on different surfaces). This assay was done by injecting free enzymes into the cuvette containing bare slides of glass, HDPE, and PMMA surfaces and

was monitored over a time period of 10 min at 450 nm (A_{450}). Initially, the microbial solution was added to the bare slides, after which the required amount of protein was injected into the solution. As shown in Fig B.3, the response was linear over this working range for each of the substrates. The solution state specific activities for HEWL for HDPE, PMMA and glass substrates were −0.0028 ΔA_{450} $min^{-1}/\mu g$, −0.0019 ΔA_{450} $min^{-1}/\mu g$ and −0.0014 ΔA_{450} $min^{-1}/\mu g$ respectively.

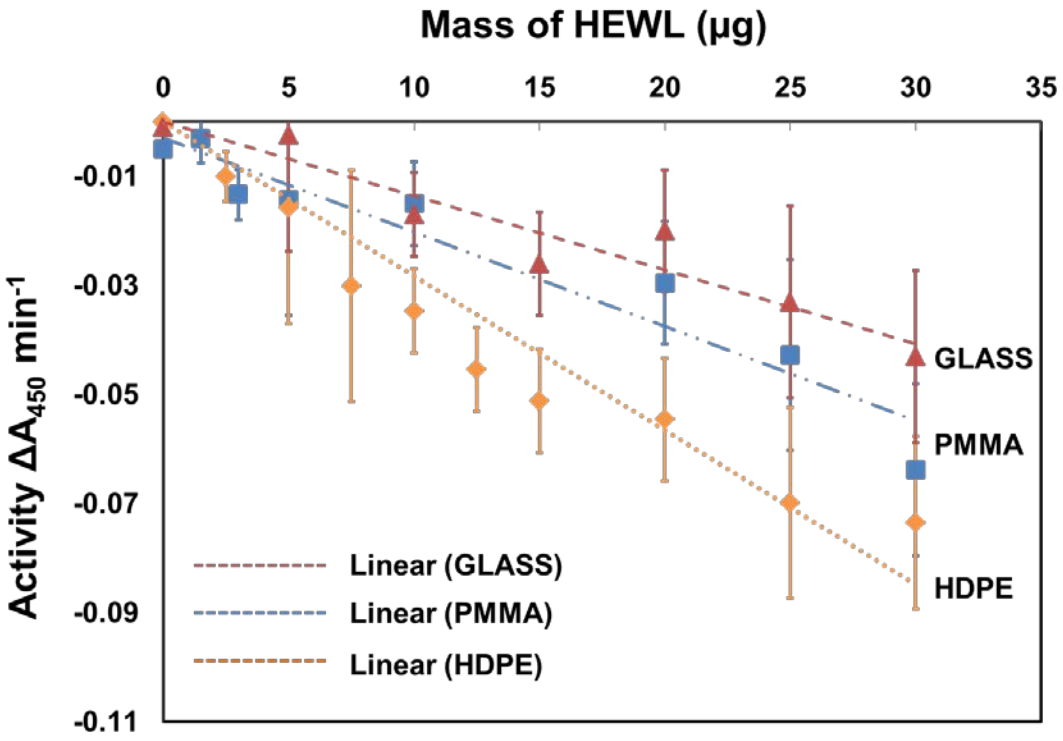

Figure B.3. Solution state bioactivity of HEWL for a substrate concentration of 60 mg/L of *Micrococcus lysodeikticus* dissolved in PPB (pH 7.4) as a function of the mass of enzyme (mg) and its activity (ΔA_{450}/min). (N = 6, error bar presents the mean ± 95% confidence interval, C.I.). The trend lines for each of the surfaces are color coded and indicated in the graph.

B.4. Raw data for Tables 5.1 to 5.8

Table B.1. Raw data on the surface coverage of HEWL on glass, HDPE, and PMMA surfaces when adsorbed from varying bulk solution concentrations as a function of the exposure time. (N = 3, mean ± 95% CI).

HEWL Solution Concentration (mg/ml)		Surface Coverage (μg/cm^2)			
		2nd hour	5th hour	10th hour	17th hour
GLASS	0.03	0.205 ± 0.047	0.076 ± 0.035	0.053 ± 0.029	0.045 ± 0.026
	0.05	0.207 ± 0.043	0.085 ± 0.049	0.062 ± 0.028	0.059 ± 0.019
	0.10	0.213 ± 0.038	0.094 ± 0.027	0.079 ± 0.035	0.072 ± 0.024
	0.20	0.219 ± 0.035	0.124 ± 0.039	0.120 ± 0.032	0.111 ± 0.028
	0.40	0.223 ± 0.023	0.143 ± 0.064	0.135 ± 0.054	0.123 ± 0.042
	0.60	0.230 ± 0.042	0.157 ± 0.093	0.145 ± 0.055	0.145 ± 0.055
	0.80	0.243 ± 0.017	0.155 ± 0.037	0.139 ± 0.032	0.131 ± 0.023
	1.00	0.250 ± 0.023	0.159 ± 0.034	0.138 ± 0.043	0.135 ± 0.026
PMMA	0.03	0.165 ± 0.025	0.065 ± 0.024	0.057 ± 0.018	0.047 ± 0.011
	0.05	0.172 ± 0.055	0.087 ± 0.026	0.075 ± 0.019	0.070 ± 0.017
	0.10	0.175 ± 0.045	0.092 ± 0.018	0.089 ± 0.012	0.088 ± 0.012
	0.20	0.183 ± 0.066	0.132 ± 0.019	0.121 ± 0.034	0.137 ± 0.017
	0.40	0.204 ± 0.054	0.167 ± 0.024	0.166 ± 0.023	0.165 ± 0.023
	0.60	0.232 ± 0.024	0.179 ± 0.028	0.167 ± 0.033	0.165 ± 0.032
	0.80	0.225 ± 0.025	0.159 ± 0.053	0.148 ± 0.045	0.142 ± 0.034
	1.00	0.253 ± 0.064	0.185 ± 0.045	0.173 ± 0.036	0.167 ± 0.032
HDPE	0.03	0.167 ± 0.027	0.068 ± 0.023	0.067 ± 0.022	0.066 ± 0.021
	0.05	0.173 ± 0.019	0.089 ± 0.018	0.088 ± 0.016	0.088 ± 0.016
	0.10	0.187 ± 0.033	0.131 ± 0.024	0.130 ± 0.020	0.129 ± 0.018
	0.20	0.195 ± 0.032	0.126 ± 0.026	0.125 ± 0.017	0.124 ± 0.019
	0.40	0.226 ± 0.028	0.137 ± 0.028	0.133 ± 0.027	0.131 ± 0.024
	0.60	0.243 ± 0.039	0.127 ± 0.030	0.117 ± 0.015	0.116 ± 0.014
	0.80	0.268 ± 0.025	0.104 ± 0.034	0.102 ± 0.032	0.101 ± 0.028
	1.00	0.275 ± 0.015	0.113 ± 0.045	0.099 ± 0.038	0.094 ± 0.036

Table B.2. Raw data on the surface coverage of RNase A on all surfaces when adsorbed from varying bulk solution concentrations as a function of the exposure time. (N = 3, mean ± 95% CI).

RNase A Solution Concentration (mg/ml)		Surface Coverage (μg/cm^2)			
		2nd hour	5th hour	10th hour	17th hour
GLASS	0.03	0.110 ± 0.033	0.09 ± 0.043	0.085 ± 0.030	0.084 ± 0.031
	0.05	0.121 ± 0.028	0.102 ± 0.027	0.093 ± 0.019	0.092 ± 0.017
	0.10	0.138 ± 0.029	0.116 ± 0.008	0.101 ± 0.010	0.099 ± 0.007
	0.20	0.152 ± 0.027	0.119 ± 0.019	0.113 ± 0.008	0.112 ± 0.004
	0.40	0.165 ± 0.012	0.132 ± 0.011	0.123 ± 0.014	0.119 ± 0.016
	0.80	0.222 ± 0.013	0.149 ± 0.015	0.141 ± 0.008	0.136 ± 0.057
	1.00	0.220 ± 0.019	0.165 ± 0.016	0.161 ± 0.009	0.161 ± 0.008
	1.60	0.259 ± 0.025	0.201 ± 0.019	0.188 ± 0.011	0.181 ± 0.012
PMMA	0.03	0.101 ± 0.021	0.092 ± 0.019	0.085 ± 0.018	0.082 ± 0.023
	0.05	0.097 ± 0.022	0.091 ± 0.017	0.088 ± 0.023	0.087 ± 0.021
	0.10	0.122 ± 0.025	0.096 ± 0.019	0.092 ± 0.021	0.091 ± 0.023
	0.20	0.163 ± 0.019	0.110 ± 0.009	0.104 ± 0.014	0.103 ± 0.016
	0.40	0.197 ± 0.018	0.126 ± 0.014	0.121 ± 0.015	0.116 ± 0.013
	0.80	0.231 ± 0.017	0.179 ± 0.016	0.171 ± 0.018	0.157 ± 0.015
	1.00	0.230 ± 0.019	0.164 ± 0.018	0.162 ± 0.022	0.157 ± 0.021
	1.60	0.266 ± 0.021	0.188 ± 0.020	0.181 ± 0.019	0.177 ± 0.018
HDPE	0.03	0.121 ± 0.044	0.110 ± 0.022	0.100 ± 0.025	0.099 ± 0.017
	0.05	0.117 ± 0.008	0.102 ± 0.035	0.099 ± 0.033	0.093 ± 0.035
	0.10	0.149 ± 0.012	0.107 ± 0.009	0.101 ± 0.011	0.098 ± 0.010
	0.20	0.181 ± 0.014	0.124 ± 0.011	0.119 ± 0.009	0.116 ± 0.015
	0.40	0.225 ± 0.012	0.144 ± 0.014	0.137 ± 0.009	0.134 ± 0.005
	0.80	0.303 ± 0.025	0.221 ± 0.007	0.182 ± 0.018	0.176 ± 0.019
	1.00	0.270 ± 0.022	0.185 ± 0.018	0.179 ± 0.020	0.172 ± 0.021
	1.60	0.312 ± 0.024	0.237 ± 0.021	0.219 ± 0.025	0.206 ± 0.023

Table B.3. Raw data on the helical content in HEWL on glass, HDPE, and PMMA surfaces when adsorbed from varying bulk solution concentrations as a function of the exposure time. (N=3, mean ± 95% C.I.).

HEWL Solution Concentration (mg/ml)		**Helix (%)**			
		2nd hour	**5th hour**	**10th hour**	**17th hour**
GLASS	0.03	12 ± 3	6 ± 4	4 ± 3	4 ± 2
	0.05	14 ± 3	6 ± 3	5 ± 4	5 ± 2
	0.10	16 ± 3	8 ± 2	7 ± 4	6 ± 3
	0.20	16 ± 4	10 ± 4	7 ± 3	7 ± 3
	0.40	20 ± 2	11 ± 3	9 ± 4	9 ± 3
	0.60	26 ± 3	18 ± 3	15 ± 4	15 ± 4
	0.80	30 ± 3	22 ± 4	20 ± 3	20 ± 3
	1.00	30 ± 2	24 ± 3	22 ± 5	22 ± 4
PMMA	0.03	30 ± 3	38 ± 4	39 ± 3	39 ± 3
	0.05	30 ± 2	36 ± 4	37 ± 3	38 ± 3
	0.10	30 ± 2	35 ± 4	36 ± 4	36 ± 4
	0.20	27 ± 2	32 ± 4	33 ± 3	33 ± 3
	0.40	26 ± 4	31 ± 4	32 ± 4	32 ± 4
	0.60	24 ± 4	26 ± 3	26 ± 3	26 ± 3
	0.80	24 ± 3	23 ± 3	23 ± 3	23 ± 3
	1.00	24 ± 3	22 ± 3	22 ± 4	22 ± 4
HDPE	0.03	20 ± 8	22 ± 5	22 ± 3	22 ± 3
	0.05	20 ± 5	21 ± 4	21 ± 3	21 ± 3
	0.10	20 ± 6	20 ± 5	20 ± 4	20 ± 4
	0.20	20 ± 6	17 ± 6	17 ± 6	17 ± 4
	0.40	19 ± 5	16 ± 5	16 ± 5	16 ± 4
	0.60	19 ± 5	15 ± 6	15 ± 6	15 ± 4
	0.80	16 ± 3	14 ± 3	14 ± 2	14 ± 2
	1.00	16 ± 4	12 ± 5	12 ± 3	12 ± 3

Table B.4. Raw data on the helical content in RNase A on on glass, HDPE, and PMMA surfaces when adsorbed from varying bulk solution concentrations as a function of the exposure time. (N=3, mean ± 95% C.I.).

HEWL Solution Concentration (mg/ml)		**Helix (%)**			
		2nd hour	**5th hour**	**10th hour**	**17th hour**
GLASS	0.03	5 ± 2	4 ± 2	3 ± 2	3 ± 2
	0.05	6 ± 2	4 ± 3	3 ± 2	3 ± 2
	0.10	11 ± 3	9 ± 4	8 ± 3	7 ± 3
	0.20	13 ± 3	8 ± 2	7 ± 2	6 ± 2
	0.40	15 ± 3	10 ± 3	9 ± 2	9 ± 2
	0.80	20 ± 3	15 ± 3	15 ± 2	14 ± 3
	1.00	20 ± 4	18 ± 4	17 ± 3	17 ± 2
	1.60	22 ± 5	20 ± 4	20 ± 4	19 ± 2
PMMA	0.03	10 ± 3	10 ± 3	9 ± 3	9 ± 2
	0.05	8 ± 2	10 ± 3	11 ± 3	11 ± 2
	0.10	11 ± 3	11 ± 3	12 ± 4	12 ± 2
	0.20	13 ± 4	12 ± 3	13 ± 3	13 ± 2
	0.40	16 ± 3	13 ± 4	13 ± 4	13 ± 3
	0.80	15 ± 4	18 ± 3	19 ± 4	19 ± 2
	1.00	16 ± 3	17 ± 3	18 ± 3	19 ± 2
	1.60	16 ± 4	19 ± 3	20 ± 3	21 ± 3
HDPE	0.03	15 ± 5	16 ± 3	16 ± 2	16 ± 2
	0.05	15 ± 2	17 ± 2	17 ± 5	18 ± 4
	0.10	11 ± 5	16 ± 4	17 ± 3	16 ± 2
	0.20	10 ± 5	15 ± 3	16 ± 4	16 ± 3
	0.40	11 ± 4	12 ± 3	12 ± 3	12 ± 2
	0.80	12 ± 3	11 ± 4	11 ± 3	10 ± 3
	1.00	11 ± 4	12 ± 4	12 ± 4	12 ± 3
	1.60	10 ± 3	10 ± 4	9 ± 4	9 ± 3

Table B.5. Adsorbed responses of HEWL on glass, HDPE, and PMMA surfaces when adsorbed from varying bulk solution concentrations for 2 h and equilibrated in protein free buffer for extended time periods of 15 h. (N = 3, mean ± 95% C.I.).

HEWL Solution Concentration (mg/ml)		**Surface Coverage (μg/cm^2)**	**Helical Content (%)**	**Bioactivity (%)**
GLASS	0.03	0.045 ± 0.026	4 ± 2	12 ± 5
	0.05	0.059 ± 0.019	5 ± 2	13 ± 5
	0.10	0.072 ± 0.024	6 ± 3	16 ± 9
	0.20	0.111 ± 0.028	7 ± 3	18 ± 3
	0.40	0.123 ± 0.042	9 ± 3	22 ± 13
	0.60	0.145 ± 0.055	15 ± 4	23 ± 10
	0.80	0.131 ± 0.023	20 ± 3	28 ± 15
	1.00	0.135 ± 0.026	22 ± 4	31 ± 14
PMMA	0.03	0.047 ± 0.011	39 ± 3	54 ± 22
	0.05	0.070 ± 0.017	38 ± 3	41 ± 9
	0.10	0.088 ± 0.012	36 ± 4	29 ± 8
	0.20	0.137 ± 0.017	33 ± 3	20 ± 10
	0.40	0.165 ± 0.023	32 ± 4	28 ± 10
	0.60	0.165 ± 0.032	26 ± 3	38 ± 11
	0.80	0.142 ± 0.034	23 ± 3	53 ± 10
	1.00	0.167 ± 0.032	22 ± 4	66 ± 9
HDPE	0.03	0.066 ± 0.021	22 ± 3	39 ± 9
	0.05	0.088 ± 0.016	21 ± 3	36 ± 4
	0.10	0.129 ± 0.018	20 ± 4	35 ± 10
	0.20	0.124 ± 0.019	17 ± 4	30 ± 9
	0.40	0.131 ± 0.024	16 ± 4	28 ± 5
	0.60	0.116 ± 0.014	15 ± 4	25 ± 5
	0.80	0.101 ± 0.028	14 ± 2	22 ± 8
	1.00	0.094 ± 0.036	12 ± 3	17 ± 8

Table B.6. Adsorbed responses of RNase A on glass, HDPE, and PMMA surfaces when adsorbed from varying bulk solution concentrations for 2 h and equilibrated in protein free buffer for extended time periods of 15 h. (N = 3, mean ± 95% C.I.).

RNase A Solution Concentration (mg/ml)		**Surface Coverage (μg/cm^2)**	**Helical Content (%)**	**Bioactivity (%)**
GLASS	0.03	0.084 ± 0.020	3 ± 2	41 ± 9
	0.05	0.088 ± 0.193	3 ± 1	39 ± 4
	0.10	0.122 ± 0.028	6 ± 1	36 ± 4
	0.20	0.102 ± 0.029	6 ± 2	38 ± 7
	0.40	0.106 ± 0.038	9 ± 2	41 ± 4
	0.80	0.135 ±0.033	15 ± 3	38 ± 5
	1.00	0.161 ± 0.013	17 ± 3	39 ± 16
	1.60	0.166 ± 0.008	22 ± 3	20 ± 4
PMMA	0.03	0.082 ±0.024	9 ± 2	28 ± 5
	0.05	0.082 ±0.019	11 ± 2	35 ± 3
	0.10	0.103 ±0.030	13 ± 2	31 ± 7
	0.20	0.096 ±0.032	13 ± 2	28 ± 5
	0.40	0.112 ±0.041	13 ± 2	35 ± 5
	0.80	0.158 ±0.045	19 ± 2	38 ± 5
	1.00	0.157 ±0.011	19 ± 2	45 ± 10
	1.60	0.181 ±0.009	22 ± 4	45 ± 7
HDPE	0.03	0.099 ±0.022	16 ± 2	42 ± 6
	0.05	0.104 ±0.019	17 ± 3	43 ± 10
	0.10	0.098 ±0.056	15 ± 2	39 ± 6
	0.20	0.118 ±0.037	16 ± 3	37 ± 3
	0.40	0.146 ±0.038	12 ± 3	30 ± 6
	0.80	0.178 ±0.025	13 ± 3	31 ± 7
	1.00	0.171 ±0.018	12 ± 3	32 ± 10
	1.60	0.245 ±0.010	11 ± 3	33 ± 9

B.5 Additional verification of surface saturation and irreversibility of the adsorbed protein layer

Previous studies had confirmed that small proteins like HEWL and RNase A are considered to saturate the surface within 2 h of exposure to protein solution. [2-3] In order to verify that these adsorption time of 2 h do indeed provide the sufficient time to saturate the adsorbent surfaces, the surface coverage of adsorbed proteins for the bulk protein solution concentrations of 0.05 mg/ml, 0.60 mg/ml and 1.00 mg/ml were compared on glass, HDPE and PMMA surfaces post 2 h and 24 h of protein adsorption. Only HEWL was used in the current study. For each of the adsorption time used in this study, proteins were equilibrated for 24 h in protein-free buffer, before the check by CD. Table B.7 compares the surface coverages using the peptide absorbance at 205 nm.

Table B.7. The effect of varying adsorption time on the surface coverage of the HEWL layers on different surfaces when adsorbed from 0.05 mg/mL, 0.6 mg/ml and 1.0 mg/mL bulk solution concentrations for 2 h and 24 h of protein adsorption followed by equilibration in pure buffer for 24 h. (N = 3, mean ± 95% C.I.).

HEWL Solution Concentration (mg/ml)		**Surface Coverage after 2 h (μg/cm^2)**	**Surface Coverage after 24 h (μg/cm^2)**
GLASS	0.05	0.059 ± 0.019	0.057 ± 0.019
	0.60	0.145 ± 0.055	0.143 ± 0.059
	1.00	0.135 ± 0.026	0.129 ± 0.032
PMMA	0.05	0.047 ± 0.011	0.046 ± 0.014
	0.60	0.165 ± 0.032	0.157 ± 0.033
	1.00	0.167 ± 0.032	0.155 ± 0.042
HDPE	0.05	0.066 ± 0.021	0.065 ± 0.022
	0.60	0.116 ± 0.014	0.114 ± 0.018
	1.00	0.094 ± 0.036	0.090 ± 0.040

Statistical comparison using Student's t-test at the 95% confidence level (α =0.05) showed no significant differences between the means of the surface densities of protein adsorbed on each of the surfaces for the adsorption time of 2 h and 24 h, thereby, confirming that the surfaces are saturated within 2 h of exposure to protein solution. Subsequently, the irreversibility of HEWL adsorbed on glass, HDPE and PMMA surfaces when adsorbed from varying bulk solution concentrations were investigated. Post adsorption, the retained fraction of protein after 15 h of exposure to protein-free buffer represents effectively irreversibly adsorbed protein, the amount of protein on the adsorbent surface were estimated using the peptide absorbance at 205 nm for extended equilibration time period of 24 h, 48 h and 72 h., and summarized in Table B.8. Fresh buffer was added after each 24 h of equilibration.

Table B.8. Adsorbed amount of HEWL on all surfaces when adsorbed from 0.05 mg/mL, 0.60 mg/ml and 1.00 mg/mL bulk solution concentrations for 2 h and equilibrated in protein free buffer for extended time periods of 24 h, 48 h and 72 h. (N = 3, mean ± 95% C.I.).

HEWL Solution Concentration (mg/ml)		**Surface Coverage (μg/cm^2)**		
		24 h	**48 h**	**72 h**
GLASS	0.05	0.057 ± 0.019	0.057 ± 0.012	0.057 ± 0.012
	0.60	0.143 ± 0.059	0.143 ± 0.053	0.142 ± 0.050
	1.00	0.129 ± 0.032	0.128 ± 0.033	0.127 ± 0.041
PMMA	0.05	0.046 ± 0.014	0.043 ± 0.015	0.042 ± 0.010
	0.60	0.157 ± 0.033	0.155 ± 0.044	0.152 ± 0.054
	1.00	0.155 ± 0.042	0.154 ± 0.057	0.153 ± 0.065

HDPE	0.05	0.065 ± 0.022	0.065 ± 0.025	0.063 ± 0.023
	0.60	0.114 ± 0.018	0.110 ± 0.019	0.109 ± 0.025
	1.00	0.090 ± 0.040	0.089 ± 0.043	0.089 ± 0.043

Statistical comparison using Student's t-test at the 95% confidence level (α =0.05) showed no significant differences between the means of the amount of protein retained on each of the surfaces following 24 h and 48 h of equilibration in pure buffer thereby, validating that the amount of protein on the surface after equilibration is effectively irreversibly adsorbed relative to the timeframe of the present study.

B.6 REFERENCES

1. Kelly, S. M.; Jess, T. J.; Price, N. C. How to study proteins by circular dichroism. *Biochimica Et Biophysica Acta-Proteins and Proteomics* **2005,** *1751* (2), 119-39.
2. Wertz, C. F.; Santore, M. M. Adsorption and Reorientation Kinetics of Lysozyme on Hydrophobic Surfaces. *Langmuir* **2002,** *18* (4), 1190-99.
3. van der Veen, M.; Stuart, M. C.; Norde, W. Spreading of proteins and its effect on adsorption and desorption kinetics. *Colloids Surf B Biointerfaces* **2007,** *54* (2), 136-42.

APPENDIX: C

PROCEDURES AND RAW DATA FOR MEASURING THE SOLVENT EXPOSURE SHIFT IN AMINO ACIDS OF PROTEINS THAT WERE ADSORBED ON MATERIAL SURFACE USING THE AAL/MS METHOD

The supporting information contains (i) target residue distribution in in HEWL and RNase A, (ii) labeling agents for modification of target amino acids, (ii) effect of trypsin treatment on the surface coverage of adsorbed proteins, (iii) sample mass spectra for different modifications, and (iv) effect of internal labels on the estimated extent of modification.

C.1. Target residue distribution in HEWL and RNase A.

A total of 32 residues were targeted within HEWL by side-chain modification of Arg, Lys, Trp, Asp, and Glu amino acid groups. The distribution of these groups within the three dimensional structure of HEWL is shown in Fig C.1.

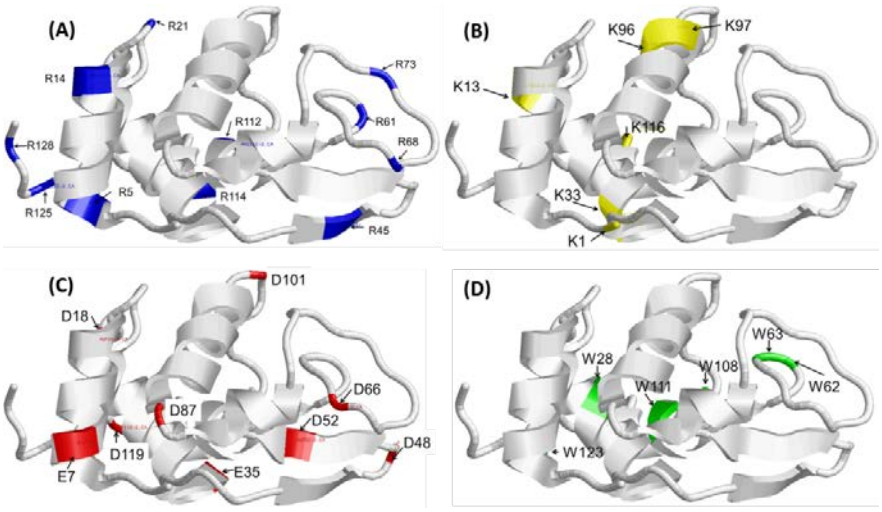

Figure C.1. The residue distribution within HEWL for (A) arginine residues (R), (B) lysine residues (K), (C) aspartic and glutamic acid residues (D, E), and (D) tryptophan

residues (W). Each of the targeted residues are represented by the single letter amino acid code and its primary sequence position

Similarly, a total of 34 residues were targeted within RNase A by side-chain modification of the Arg, Lys, Tyr, His, Asp, and Glu amino acid groups. The distribution of these groups within the three dimensional structure of RNase A is shown in Fig C.2.

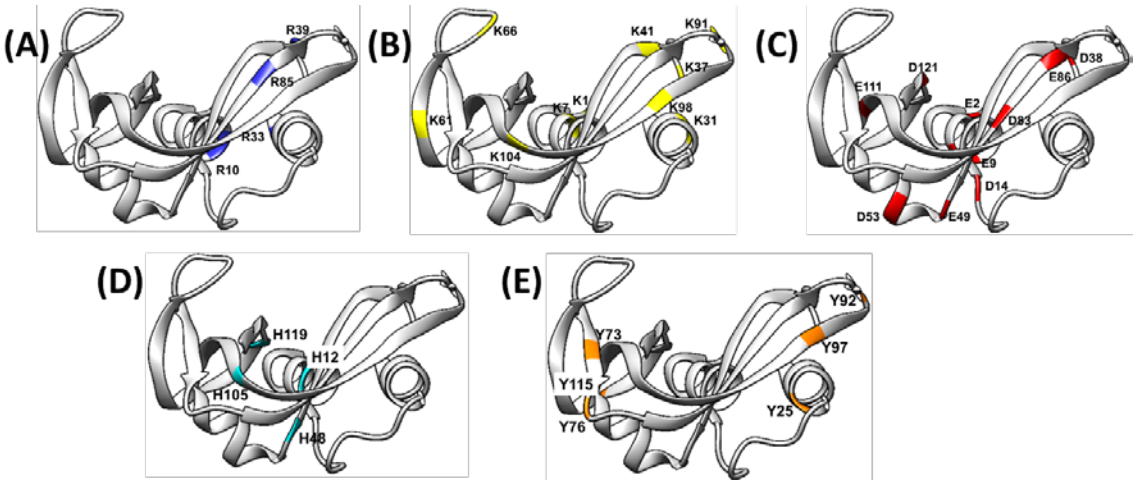

Figure C.2. The residue distribution within RNase A for (A) arginine residues (R), (B) lysine residues (K), (C) aspartic and glutamic acid residues (D, E), (D) histidine residues (H), and (E) tyrosine residues (Y). Each of the targeted residues are represented by the single letter amino acid code and its primary sequence position

C.2. Labeling Agents and Conditions for Modification of Target Amino Acids.

All the target residues within the protein were labeled under a common reaction condition to facilitate direct comparison of the labeling profiles. In the current studies, irrespective of the type of modification process, reaction between the labeling agent and its target amino acid were carried out at 5x the overall molar concentration of reacting amino acids in the dark at 25°C for 3 hours in PPB. The solution pH was maintained at 7.4 by adding required amounts of monobasic potassium phosphate (Sigma, P8708) or dibasic potassium phosphate (Sigma, P8508).

C.2.a Arg modification

Arg accounts for 11 of the 129 residues in the native structure of HEWL (Fig. C.1.A), and 4 of the 124 residues in the native structure of RNase A (Fig C.2.A). Arg modification was carried out in a two-stage reaction process in which the primary reacting agent, 2, 3-butanedione (Sigma, B85307) reacts with the side-chain of solvent-accessible Arg residues, after which the secondary reacting agent, 3-acetamidophenylboronic acid (Sigma, 566012) was added in 1:2 molar ratio to form an aryl complex with an expected mass increase of 172.069 Da per modified Arg residue.[1]

C.2.b Lys modification

While Lys accounts for 6 of the 129 residues in the helix-rich domain of native HEWL (Fig C.1.B), these residues account for 10 of the 124 residues (Fig. C.2.B) within the native structure of RNase A. The acylation of Lys in proteins using acetic anhydride (Sigma, 320102) is a single-stage reaction process with the resulting product showing an expected mass increase of 43.018 Da per modified Lys residue.[2]

C.2.c Asp and Glu modification:

Asp and Glu residues account for 9 of the 129 residues within the native structure of HEWL (Fig. C.1.C) and 10 of the 124 residues in the native structure of RNase A (Fig. C.2.C). The COO^- modification was carried out in a two-stage reaction process in which the primary reacting agent, 1-ethyl-3-[3-dimethylaminopropyl] carbodiimide hydrochloride (Sigma, E6383) reacts with solvent accessible COO^- functional groups of Asp and Glu following which the secondary reacting agent, N-hydroxysuccinimide

(Sigma, 130672) was added in 1:4 molar ratio to form an amide cross-link with an expected mass increase of 97.016 Da per modified Asp and Glu residue.[3]

C.2.d Trp modification:

This side-modification was applied only to HEWL in our studies. Trp accounts for 6 of the 129 residues and is localized in the plane containing the bioactive site in the native structure of HEWL (Fig. C.1.D). This type of modification was done using dimethyl (2-hydroxy-5-nitrobenzyl) sulfonium bromide (Sigma, D6388) in a single-stage process with the resulting product showing an expected mass increase of 152.035 Da per modified Trp residue.[4] It is better to do this reaction within water initially after which the product could be re-suspended in PPB by dialysis.

C.2.e His modification:

This side-modification was applied only to RNase A in our studies. His accounts for 4 of the 124 residues within the native structure of RNase A (Fig C.2.D). The His modification of RNase A was carried out using Diethyl pyrocarbonate in a single stage reaction in which the primary reacting agent was added in 1:2 molar ratio to form a product with a mass increase of 146.14 Da. [5]

C.2.f Tyr modification:

This side-modification was applied only to RNase A in our studies. Tyr accounts for 6 of the 124 residues in the native structure of RNase A (Fig C.2.E). The reaction of RNase-A with tetranitromethane was carried out in a single stage process by reacting in 1:4 ratio. The nitration process results in product with a mass increase of 44.99 Da. [5]

The effect of these individual chemical modification on the structure of HEWL (Fig. 6.3 and Table 6.3) and RNase-A were verified using CD spectroscopy in both the native (Fig C.3) and adsorbed (Table C.1) state of the protein.

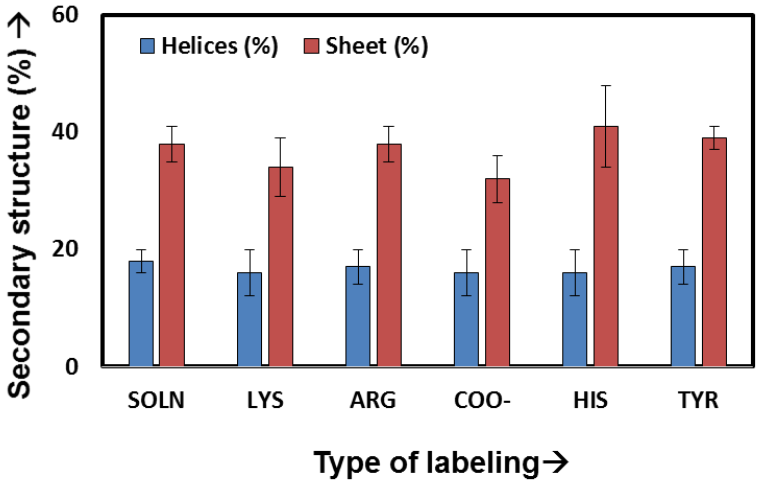

Figure C.3. The effect of chemical labeling on the secondary structure of native RNase A (N = 3, error bar represents the mean ± 95% C.I.). Soln refers to the solution state of the RNase A when none of the amino acids were labeled. LYS refers to lysine labeling, ARG – arginine labeling, COO^-– carboxyl labeling, HIS – histidine labeling**,** TYR – tyrosine labeling.

Table C.1. Helical content (%) within the adsorbed RNase-A before and after chemical labeling (N =3, error bar presents the mean ± 95% C.I.).

RNase A Solution Concentration (mg/ml)		**Unlabeled (%)**	**Lys (%)**	**Arg (%)**	**COO^- (%)**	**His (%)**	**Tyr (%)**
GLASS	0.03	5 ± 2	6 ± 3	4 ± 3	6 ± 2	6 ± 3	4 ± 2
	1.00	19 ± 4	17 ± 4	16 ± 4	18 ± 5	19 ± 4	18 ± 5
HDPE	0.03	18 ± 2	16 ± 4	17 ± 4	16 ± 4	17 ± 3	17 ± 4
	1.00	9 ± 2	10 ± 3	8 ± 3	10 ± 2	9 ± 2	9 ± 2
PMMA	0.03	8 ± 2	10 ± 4	9 ± 3	8 ± 2	10 ± 4	9 ± 3
	1.00	18 ± 3	19 ± 4	18 ± 4	18 ± 3	20 ± 5	20 ± 4

C.3 Sample Preparation for Mass Spectrometry

As a pre-requisite to analyze the mass shift in target residues of a protein by MS, proteolytic digestion of the modified and unmodified protein in solution and in its

adsorbed state was necessary. Proteolytic digestion of the proteins of interest was done using sequence-grade porcine trypsin (Promega) which was diluted in 10 mM hydrochloric acid.

C.3.a Solution state modification and digestion of HEWL and RNase A.

The chemical modification of HEWL (5 mg/mL) and RNase A (5mg/ml) was done to identify the extent of solvent exposure for the targeted residues in a protein's native state. Following the modification, solution samples were dialyzed against PPB (10 kDa cut-off) for 6 hours to remove the unbound labeling agents. Unmodified HEWL samples (5 mg/mL) under identical conditions were used as a negative control. Protease digestion of HEWL in solution was performed according to previously reported methods.[4]

Briefly, 4.0 μL of each protein solution was added to 100 μL of 1.0 mM ammonium bicarbonate. To reduce the disulfide bonds in HEWL, 3.0 μL of 45 mM dithiothreitol (DTT) was added, and the sample was incubated at 37°C for 20 min. After the samples were cooled to room temperature, the reduced cysteines were alkylated by adding 4.0 μL of 100 mM iodoacetamide (IAA). The reaction was allowed to proceed in the dark for 20 min. The excess reagents were removed by lyophilizing to completion in SpeedVac (Savant Instruments Inc.) for 1h. HEWL samples were then digested by trypsin, at a protease-to-substrate ratio of 1:50 (w/w) using 0.04 μg/μL protease solutions in their respective buffers at 37°C for 18 h. Following incubation, 1.5 μL of 0.1% (v/v) trifluoroacetic acid was added to stop the digestion. The solutions containing the peptide fragments were collected after digestion, lyophilized, and processed for MS.

C.3.b Adsorbed state modification and digestion of HEWL and RNase A s.

Identical reaction conditions that were used to determine the extent of solvent exposure for the targeted amino acids in the solution state were also used for the adsorbed protein. Following the labeling process, excess reagents were removed by rinsing the surfaces with pure buffer after which the adsorbent surfaces were dried under a steady stream of nitrogen. The surface coverage of HEWL and RNase A on each adsorbent surface were determined using a variable angle spectroscopic ellipsometer. Subsequently, the surfaces with the adsorbed proteins of interest were initially placed in a digestion box filled with solution 1 (0.2 M NH_4HCO_3 in 50% acetonitrile (v/v), pH 7.8) following which the adsorbed protein layers were reduced (45 mM DTT) and alkylated (100 mM IAA) prior to being tryptic digested (0.04µg/mL) overnight in a temperature-controlled chamber. Digested protein samples were recovered and excess reagents were removed by lyophilizing overnight. Samples were then reconstituted in 50 µl injection solution (50% acetonitrile, 0.1% formic acid), for data acquisition and analysis as described in C.3.c.

The residual amount of proteins on the surfaces were subsequently determined using a variable angle spectroscopic ellipsomete. For this purpose, after digesting the samples, the adsorbent surfaces were rinsed in running buffer and then dried under nitrogen gas to be analyzed using ellipsometry according to de Feijter's equation (c.1).[6]

$$\text{Surface coverage } (\mu g/cm^2) = 0.1 * d_f * (n_f - n_b) / (dn/dc) \qquad \text{(c.1)}$$

In equation (c.1) above, d_f describes the film thickness (in nm), n_f describes the refractive index of the adsorbed protein film, n_b describes the refractive index of the

buffer, and dn/dc refers to the increment of refractive index of protein solution versus protein solution concentration and is considered to be constant for any protein. The following parametric values, n_f =1.42, n_b = 1.33 and dn/dc = 0.188 ml/g were used, to measure the thickness of the protein layers before and after tryptic digestion. Table C.2 and Table C.3 represents the amount of residual protein on each of the surface before and after tryptic digestion of HEWL and RNase A respectively.

Table C.2. Surface coverage of HEWL on different surfaces for different conditions before and after trypsin treatment (N = 3, error bar presents the mean ± 95% confidence interval, C.I.). NA refers to very weak signal when the estimated thickness of the protein film is below 0.1 nm.

HEWL Solution Concentration (mg/ml)		**Surface coverage before trypsin treatment (µg/cm^2)**	**Surface coverage after trypsin treatment (µg/cm^2)**
GLASS	0.03	0.045 ± 0.026	NA
	1.00	0.135 ± 0.026	0.010 ± 0.002
HDPE	0.03	0.066 ± 0.021	NA
	1.00	0.094 ± 0.036	NA
PMMA	0.03	0.047 ± 0.011	NA
	1.00	0.167 ± 0.032	0.011 ± 0.03

Table C.3. Surface coverage of RNase A on different surfaces for different conditions before and after trypsin treatment (N = 3, error bar presents the mean ± 95% confidence interval, C.I.).

RNase A Solution Concentration (mg/ml)		**Surface coverage before trypsin treatment (µg/cm^2)**	**Surface coverage after trypsin treatment (µg/cm^2)**
GLASS	0.03	0.08 ± 0.01	0.021 ± 0.008
	1.00	0.16 ± 0.03	0.033 ± 0.007
HDPE	0.03	0.10 ± 0.01	0.015 + 0.005
	1.00	0.17 ± 0.03	0.034 ± 0.006
PMMA	0.03	0.08 ± 0.02	0.014 ± 0.007
	1.00	0.16 ± 0.03	0.043 ± 0.005

The proteins/peptide fragments remaining on the adsorbent surface could be either from the proteins of interest or the trypsin that was used to digest the protein. However, as it can be seen from the table, since only about 10 % of the initially adsorbed amount of protein was found to be on the adsorbent surface. It was assumed that almost all of the target proteins has been recovered from the adsorbent surface.

C.3.c Procedure for Mass Spectrometry

Trypsin-digested peptides obtained in C.3.b were analyzed using an Ultra Performance Liquid Chromatography System (UPLC, Waters) coupled with a quadrupole time-of-flight mass spectrometer (Q-TOF MS, Waters) with electrospray ionization in both ESI^+-MS and ESI^+-MS/MS (SetMass without fragmentation) mode operated by Masslynx software (V4.1). Each sample in methanol was directly injected into the C18 column (Waters) with a 150 μL/min flow rate of mobile phase, consisting of solution A (95% H_2O, 5% acetonitrile, 0.1% formic acid) and solution B (95% acetonitrile, 5% H_2O, 0.1% formic acid) in a 15 min gradient starting at 95% of solution A to 30% of solution A for 10 min and back to 95% of solution A for 12 min. The ion source voltages were set at 3 KV, the sampling cone at 37 V, and the extraction cone at 3 V. In both modes, the source and desolvation temperatures were maintained at 120°C and 225°C, respectively, with the desolvation gas flow at 200 L/h.

The Q-TOF MS scanning was done from 50 m/z to 1000 m/z at 1 s with a 0.1-s inter-scan delay using extended dynamic range acquisition with centroid data format. For real-time mass calibration, direct infusion of sodium formate solution (10% formic acid/0.1 M sodium hydroxide/acetonitrile at a ratio of 1:1:8) at 1 s/10 s to the ion source

at 2 µl/min was used. Tryptic peptides were acquired from 200 to 2000 m/z, then mass was calibrated against lockmass manually, and then deconvoluted to single charge by MaxEnt 3. The resulting peptide list was copied into GPMAW (ver. 8.20) and searched against known protein sequences to identify potential modifications at 0.1% precision with maximum number of modifications per peptide set at 2 and Check-Fit enabled for trypsin. The intensities obtained from mass matching were subsequently used in quantifying the extent of solvent exposure for the targeted residues in each of the protein of interest. The mass spectra for different surfaces for different modifications for each of the different adsorption conditions were obtained with signal to-noise ratios good enough to resolve the respective peptides. For each of the surfaces, multiple elutions of the adsorbent surface were carried out to ensure that almost all of the peptide containing the target residue was recovered from the tryptic digest.

In the current study, all the peptides with the target residue of interest were recovered for which the mass shift was estimated at 0.1% precision. Sample spectra of HEWL modified with different labeling agents on the HDPE surface when adsorbed at 0.03 mg/ml are shown in Fig C.4

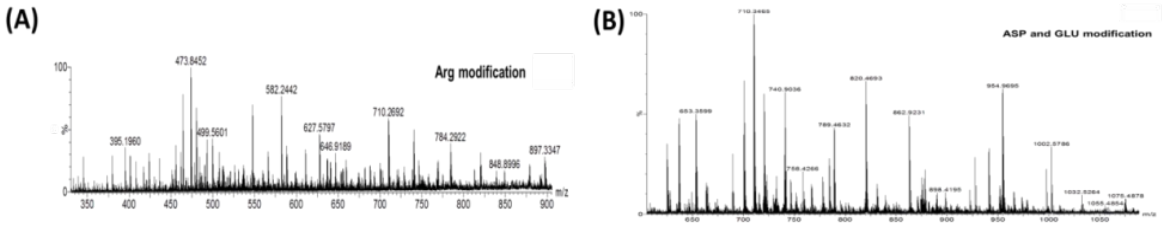

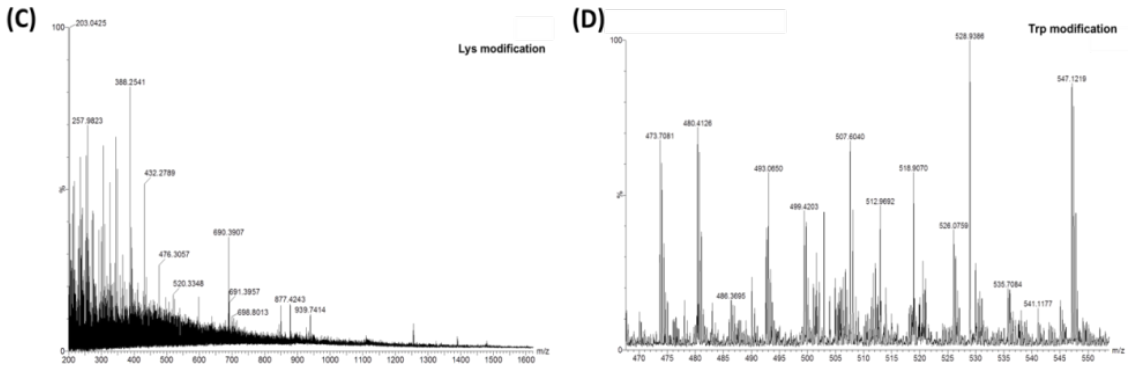

Figure C.4. Sample MS spectra for HEWL adsorbed from 0.03 mg/ml that has been modified on the HDPE surface with different chemical labeling agents. (A) Arg modification, (B) Asp and Glu acid modification, (C) Lys modification, and (D) Trp modification.

C.3.d Effect of Internal Labels on the Estimated Extent of Modification.

Sample-to-sample variation in the ionization process even within unmodified peptides is typically high, and would be further compounded when the target peptides are modified by different chemical labels.[7-8] A very straight-forward approach to dealing with this problem is to normalize the intensity of peptide of interest to an internal standard, which is usually another peptide that does not contain a modifiable residue.[7] Such a strategy has been reported to minimize ionization efficiency concerns and can provide semi-quantitative measurements of the extent of modification.[7]

In the current study, the intensity of peptide without the target residue of interest and generated as a byproduct of tryptic digestion, was used as the internal control. The absolute extent of modification of target amino acids in proteins were then quantified from the normalized spectral intensities acquired for the individual modification process. Table C.4 and Table C.5 provides the detailed listing of the internal reference standards used in the current study for different side-chain modifications done on HEWL and RNase A

Table C.4 Internal controls used in the current study to directly compare the labeling profile of multiple amino acids in HEWL were targeted via different batch experiments

Target residue	Internal control	Start ID	End ID	Mass (Da)	Possible variants
Arg	CELAAAMK	6	13	835	1-13, 1-14, 1-21, 2-13, 2-14, 2-21, 6-14, 6-21
Lys, Asp & Glu	TPGSR	69	73	517	34-73, 46-73, 62-73, 34-96, 46-96, 62-96, 68-96
Trp	CELAAAMK	6	13	835	1-13, 1-14, 1-21, 2-13, 2-14, 2-21, 6-14, 6-21
	TPGSR	69	73	517	34-73, 46-73, 62-73, 34-96, 46-96, 62-96, 68-96

Table C.5 Internal controls used in the current study to directly compare the labeling profile of multiple amino acids in RNase A were targeted via different batch experiments.

Target residue	Internal control	Start ID	End ID
Arg, Asp & Glu	TTQANK	98	103
Lys, Tyr, His	FER	8	10

As could be seen from Table C.4., two different internal controls were used for generating the baseline reference, while either one of these controls were used for generating the baseline reference for Trp modification, in order to minimize any variability in the ionization efficiency due to the modification process. The effect of using two different controls on the I_{soln} for Trp modification was explored as shown in Table C. 6.

Table C.6. Comparison of the I_{soln} for Trp modification for different internal controls, CELAAAMK and TPGSR (N = 3, error bar presents the mean ± 95% confidence interval, C.I.) NA refers to when the peptide containing the residue of interest shows $I_{soln} \leq 0.10$, for which a ceiling value of 0.10 was manually set.

Residue #	I_{soln} -CELAAAMK	I_{soln} -TPGSR
28	NA	NA
62	0.53 ± 0.10	0.56 ± 0.05

63	0.53 ± 0.10	0.56 ± 0.05
108	0.19 ± 0.05	0.14 ± 0.05
111	0.19 ± 0.06	0.14 ± 0.06
123	0.18 ± 0.07	0.19 ± 0.07

The use of two different controls did not significantly affect the absolute extent of modification, as evident from the quantification of Trp modification (Table C.4), from which it was inferred that the type of internal controls used for scaling the MS spectra do not significantly influence the final magnitude of I_{soln}. However, it is essential to establish that the labeling agents do not have a significant effect on the CD structure of native and adsorbed protein structures, as demonstrated for HEWL in section 6.3.2.1a and in section Fig C.3. for RNase A.

C.3.d.1 Role of Internal Labels in Estimating the Extent of Modification.

Although all of the reagents used in current study are well-characterized, and are expected to be highly specific to the targeted amino acid with minimal cross-reactions, possible side-reactions were assessed using mass spectrometry based on the signal-to-noise ratio of the spectra when a threshold was applied to investigate possible side-reactions. Since minimal to no side-reactions were observed, the internal controls was considered to be relatively less affected by the labeling agents, and therefore their ion abundances within a given spectra was considered to ideally serve as the baseline to scale intensities of peptide segments undergoing modification. Nevertheless, Table C.7.shows the possible side reactions that could occur when different labeling agents were applied for a wide range of conditions.

Table C.7. The labeling reagent used in the current study, along with the target amino acid and side-reaction to quantify the adsorption-induced structural changes in protein by AAL/MS technique.

Labeling reagent	Target amino acid	Side-reaction [1, 7, 9-11]
Acetic anhydride	Lysine	Histidine, Tyrosine, Cysteine
Dimethyl(2-hydroxy-5-nitrobenzyl) sulfonium bromide	Tryptophan	None
1-ethyl-3-[3-dimethylamino pro-pyl] carbodiimide hydrochloride + N-hydroxysuccinimide (EDC/NHS)	Aspartic acid and Glutamic acid	Primary amines
2, 3-butanedione + 3-acetamido phenylboronic acid	Arginine	None
Diethylpyrocarbonate	Histidine	Lysine
Tetranitromethane	Tyrosine	None at pH < 8

In the event of such cross-reaction, the results of the current study could be impacted if the internal controls are affected. In case of HEWL and RNase A, the internal controls used for lysine modification (TPGSR and FER) lacks amino acids, histidine, cysteine, and tyrosine, thus avoiding the complication of non-specific labeling by acetic anhydride modification. Similarly, potential side effects due to side-chain modification that could result in possible variants to internal controls (CELAAAMK, TPGSR, TTQANK and FER) and ionization efficiency corrections were considered. (Table C.4 and Table C.5)

C.4. Raw data for Fig 6.4 and Fig 6.5

Table C.8. Estimate on the profile for the residues within the adsorbed protein that were targeted in the current study using either CELAAAMK or TPGSR or both as the internal control. For each of the surface, tryptic digests of the protein were pooled from four different samples.

Residue #	I_{soln}	Concentration (mg/ml)	Glass	HDPE	PMMA
1	0.40 ± 0.11	0.03	-0.60	0.36	-0.60
		1.00	0.19	0.40	0.40
5	0.36 ± 0.02	0.03	0.40	0.37	0.31
		1.00	-0.55	-0.55	-0.55
7	0.50 ± 0.15	0.03	0.19	0.11	0.19
		1.00	0.17	0.04	-0.03
13	0.47 ± 0.06	0.03	0.32	-0.01	0.32
		1.00	0.15	0.32	0.32
14	0.30 ± 0.02	0.03	0.49	0.46	0.46
		1.00	-0.48	-0.48	-0.48
18	0.26 ± 0.14	0.03	0.44	0.42	0.43
		1.00	0.51	0.33	-0.41
21	0.43 ± 0.18	0.03	0.37	0.32	0.37
		1.00	-0.63	-0.13	-0.63
28	NA	0.03	0.98	0.99	0.24
		1.00	0.80	0.99	0.98
33	0.55 ± 0.09	0.03	-0.60	-0.49	0.23
		1.00	-0.05	0.22	0.26
35	NA	0.03	0.43	0.52	0.98
		1.00	0.34	-0.02	-0.02
45	0.60 ± 0.06	0.03	0.22	0.22	0.22

		1.00	-0.35	-0.20	-0.02
48	0.31 ± 0.10	0.03	0.12	-0.07	-0.49
		1.00	0.31	0.34	-0.49
52	NA	0.03	0.56	0.38	-0.05
		1.00	0.32	0.78	-0.05
61	0.20 ± 0.09	0.03	0.71	0.67	-0.29
		1.00	0.42	0.10	0.47
62	0.53 ± 0.10	0.03	-0.12	0.28	-0.12
		1.00	-0.05	0.17	0.28
63	0.53 ± 0.10	0.03	-0.12	0.28	-0.12
		1.00	-0.05	0.17	0.28
66	0.25 ± 0.07	0.03	0.45	0.60	-0.04
		1.00	0.57	0.60	-0.40
68	0.60 ± 0.17	0.03	0.22	0.21	0.17
		1.00	0.22	0.22	-0.17
73	0.59 ± 0.10	0.03	0.10	0.10	0.10
		1.00	-0.23	-0.21	-0.36
87	0.49 ± 0.10	0.03	-0.35	-0.68	-0.42
		1.00	0.26	-0.57	0.32
96	0.24 ± 0.07	0.03	0.62	0.54	0.58
		1.00	0.33	0.35	-0.38
97	0.56 ± 0.09	0.03	0.25	0.0	0.20
		1.00	0.02	-0.02	0.11
101	0.35 ± 0.18	0.03	0.54	-0.34	0.41
		1.00	0.10	-0.10	0.27
108	0.19 ± 0.05	0.03	0.22	0.75	0.73

		1.00	0.63	0.73	0.11
111	0.19 ± 0.06	0.03	0.22	0.73	0.73
		1.00	0.63	0.73	0.11
112	0.50 ± 0.04	0.03	-0.70	0.19	0.19
		1.00	0.22	-0.19	0.0
114	0.41 ± 0.10	0.03	-0.61	-0.15	-0.33
		1.00	0.38	0.12	0.31
116	0.54 ± 0.20	0.03	0.27	-0.06	0.17
		1.00	0.13	0.27	-0.73
119	0.42 ± 0.14	0.03	0.30	0.28	0.21
		1.00	-0.41	-0.63	-0.63
123	0.19 ± 0.07	0.03	0.62	0.41	0.74
		1.00	0.74	0.73	0.43
125	0.78 ± 0.11	0.03	-0.89	-0.13	-0.23
		1.00	0.11	-0.44	0.02
128	0.78 ± 0.21	0.03	-0.89	-0.11	-0.20
		1.00	0.11	-0.44	0.06

C.5. Raw data for Fig 7.2 - Fig 7.4

Table C.9. Estimation of the profile values for the residues within the adsorbed protein that were targeted in the current study using either TTQANK and FER or both as the internal control. For each of the surface, tryptic digests of the protein were pooled from four different samples.

Residue #	I_{soln}	Concentration (mg/ml)	Glass	HDPE	PMMA
1	1	0.03	-1	-0.10	-0.10
		1.00	-0.301	-1	-1
2	0.339	0.03	0.169	0.47	0.47
		1.00	0.169	0.47	0.345
7	0.54	0.03	-0.334	0.210	0.188
		1.00	-0.210	-0.732	-0.732
9	0.447	0.03	-0.127	0.094	0.049
		1.00	-0.252	0.299	0.119
10	0.359	0.03	-0.555	0.445	0.093
		1.00	0.32	0.32	0.445
12	0.1	0.03	0.673	0.523	0.673
		1.00	0.845	0.523	0.699
14	0.1	0.03	0.61	0.75	0.523
		1.00	0.398	0.954	0.813
25	0.1	0.03	0.731	0.578	0.632
		1.00	0.778	0.319	0
31	0.608	0.03	-0.562	0.158	0.137
		1.00	0.102	-0.784	-0.784
33	0.268	0.03	0.095	0.467	0.133
		1.00	0.309	0.309	-0.428

37	0.506	0.03 1.00	-0.102 0.12	0.12 -0.482	0.216 -0.248
38	0.943	0.03 1.00	-0.385 -0.276	-0.099 -0.196	-0.151 -0.19
39	0.724	0.03 1.00	-0.86 -0.115	-0.559 -0.115	-0.258 -0.337
41	0.283	0.03 1.00	0.247 0.109	-0.452 0.004	0.247 -0.151
48	0.1	0.03 1.00	0.786 0.523	0.808 0.824	0.786 0.699
49	0.279	0.03 1.00	0.102 0.333	-0.446 0.291	0.253 0.121
53	0.623	0.03 1.00	-0.247 -0.016	-0.794 -0.058	-0.096 -0.162
61	0.569	0.03 1.00	-0.056 -0.194	-0.755 -0.755	-0.056 -0.357
66	0.706	0.03 1.00	0.151 -0.451	-0.849 -0.849	-0.15 -0.849
73	0.156	0.03 1.00	0.682 0.108	-0.193 0.409	0.409 0.029
76	0.593	0.03 1.00	0.102 -0.472	-0.773 -0.171	-0.171 -0.551
83	0.2	0.03 1.00	0.155 0.331	0.699 0.363	0.699 0.444
85	0.597	0.03 1.00	-0.776 -0.01	-0.077 -0.01	0.048 -0.776

86	0.291	0.03 1.00	0.235 0.013	0.536 0.156	0.536 0.332
91	0.891	0.03 1.00	0.05 -0.126	-0.95 -0.95	-0.251 -0.251
92	0.465	0.03 1.00	0.333 0.156	-0.145 0.032	-0.667 -0.145
97	0.1	0.03 1.00	1 0.824	0.523 0.699	0 0.523
98	0.738	0.03 1.00	-0.169 0.132	-0.868 -0.868	-0.169 0.007
104	0.447	0.03 1.00	0.35 -0.65	-0.65 -0.65	0.35 0.049
105	0.324	0.03 1.00	0.188 -0.511	0.489 -0.511	0.188 -0.511
111	0.569	0.03 1.00	-0.755 0.245	0.245 -0.01	-0.755 -0.153
115	0.1	0.03 1.00	0 0.398	0 1	0 0
119	0.487	0.03 1.00	0.011 -0.688	0.312 -0.688	0.011 -0.688
121	0.1	0.03 1.00	0 1	1 0.745	0 0.602

REFERENCES

1. Leitner, A.; Amon, S.; Rizzi, A.; Lindner, W. Use of the arginine-specific butane dione/phenylboronic acid tag for analysis of peptides and protein digests using matrix-assisted laser desorption/ionization mass spectrometry. *Rapid Communications in Mass Spectrometry* **2007,** *21* (7), 1321-30.

2. Suckau, D.; Mak, M.; Przybylski, M. Protein Surface Topology-Probing by Selective Chemical Modification and Mass-Spectrometric Peptide-Mapping. *P Natl Acad Sci USA* **1992,** *89* (12), 5630-34.

3. Rappsilber, J. The beginning of a beautiful friendship: cross-linking/mass spectrometry and modelling of proteins and multi-protein complexes. *J Struct Biol* **2011,** *173* (3), 530-40.

4. Fears, K. P.; Sivaraman, B.; Powell, G. L.; Wu, Y.; Latour, R. A. Probing the Conformation and Orientation of Adsorbed Enzymes Using Side-Chain Modification. *Langmuir* **2009,** *25* (16), 9319-27.

5. Fears, K. P.; Sivaraman, B.; Powell, G. L.; Wu, Y.; Latour, R. A. Probing the conformation and orientation of adsorbed enzymes using side-chain modification. *Langmuir* **2009,** *25* (16), 9319-27.

6. De Feijter, J. A.; Benjamins, J.; Veer, F. A. Ellipsometry as a tool to study the adsorption behavior of synthetic and biopolymers at the air–water interface. *Biopolymers* **1978,** *17* (7), 1759-72.

7. Mendoza, V. L.; Vachet, R. W. Probing protein structure by amino acid-specific covalent labeling and mass spectrometry. *Mass Spectrom Rev* **2009,** *28* (5), 785-815.

8. Duncan, M. W.; Aebersold, R.; Caprioli, R. M. The pros and cons of peptide-centric proteomics. *Nat Biotechnol* **2010,** *28* (7), 659-64.

9. Lundblad, R. L. The Modification of Amino Groups. In *Chemical Reagents for Protein Modification, Third Edition*; CRC Press, 2004.

10. Lundblad, R. L. The Modification of Carboxyl Groups. In *Chemical Reagents for Protein Modification, Third Edition*; CRC Press, 2004.

11. Lundblad, R. L. The Chemical Modification of Tryptophan. In *Chemical Reagents for Protein Modification, Third Edition*; CRC Press, 2004.

APPENDIX: D

PROTOCOL AND RAW DATA FOR THE 230-240 NM SLOPE METHOD TO DETERMINE THE HELIX CONTENT IN PROTEINS

This supporting information contains the (1) protocol for determining the fractional helical (FH) content using the 230-240 nm slope method and (2) raw data for Figs 8.3 – 8.6 in Chapter 8.

D.1. Protocol for determining the fractional helical (FH) content using the 230-240 nm slope method

For conditions involving high background absorbance, the protein structure cannot be estimated by the conventional method and as a result 230-240 nm slope method would be useful if the background absorbance is negligible at wavelengths greater than 230 nm. The protocol for determining these are described as follows.

D.1.a Preliminary Test.

(1) Before applying this 230-240 nm slope method to analyze the structure of a given protein, in cases where chemical agents are present that cause high background absorbance, the reliability of this slope method should first be tested against a conventional analysis method (e.g., CONTIN) or against Protein Data Bank values, with the protein in a solution without strong background absorbance to verify that the method can be used for that protein.

D.1.b. General Protocol to obtain the 'm' and 'b' parameters for estimating the FH using the 230-240 nm Slope Method for a specific algorithm and specific reference database.

(2) Acquire the CD spectra for the protein of interest in dilute salt conditions that are not strongly absorbing, over the spectra range of 190 nm to 300 nm using the scan settings that are appropriate for each specific application.

(3) Scale the CD spectra to account for the CD pathlength, mean residue weight, and protein concentration.

(4) Estimate the '∇' parameter from the slope of the linear regression analysis done on the CD curve obtained between 230 – 240 nm.

(5) Select an appropriate reference database and algorithm to estimate the *FH* for the protein. Ensure that the algorithm and reference databases are compatible. Generally, reference databases that are optimized for the spectral scan range are preferred.

(6) Develop a calibration curve to provide a wide range of *FH* either by temperature denaturation or from databases containing circular dichroism (CD) data of resolved protein structures such as protein CD Databank (PCDDB).

(7) Make a plot of the FH versus '∇'. Do a linear regression to obtain the '*m*' and '*b*' parameters that are specific to the reference database and deconvolution algorithm.

D.1.c General Protocol for estimating the FH using the 230-240 nm Slope Method for conditions involving high absorption at wavelengths < 230 nm after the determination of the ‘m’ and ‘b’ parameters

(8) Acquire the CD spectra for the protein of interest in high absorptive conditions over the spectra range of 230 nm to 300 nm using the scan settings that are appropriate for each specific application.

(9) Scale the CD spectra to account for the CD pathlength, mean residue weight, and protein concentration.

(10) Estimate the ‘∇’ parameter from the slope of the linear regression analysis done on the CD curve that was obtained between 230 – 240 nm.

(11) Use the formula $FH = m*\nabla + b$, to quantify the helical content in the protein, which will be specific to the algorithm and reference databases that were used for ‘m’ and ‘b’ determination. For the CONTIN algorithm and reference database of SP43 or SP48, this relation has been determined in our study to be: $FH = 0.000514*\nabla + 0.00297$.

D.1. Raw data for Figures 8.3 to 8.7

Table D.1. The fractional helicity (*FH*) of a protein in solution was determined using two different algorithms—the CONTIN program method and the 222 nm method. The corresponding empirical parameter '∇' values from proposed 230-240 nm slope method were also provided. The structure of each protein in D.I. water (0.01 mg/ml) was determined in a quartz cuvette (Starna Cells) of 1.0 cm path length using a standardized methodology for CD spectropolarimeter (Jasco J-810) over a range of temperatures to induce various degrees of protein unfolding.

Temperature (°C)	**Empirical parameter '∇' (deg.cm^2/(dmol)/nm)**	**CD at 222 nm (*FH*)**	**CONTIN procedure (*FH*)**
Lysozyme from chicken egg white (HEWL)			
5	617	0.34	0.37
15	571	0.34	0.35
25	557	0.32	0.33
35	530	0.31	0.32
45	485	0.29	0.30
55	408	0.27	0.26
65	302	0.21	0.16
75	161	0.16	0.04
85	93	0.13	0.03
Ribonuclease A from bovine pancreas (RNase A)			
5	352	0.25	0.19
15	340	0.24	0.18
25	329	0.23	0.17
35	273	0.20	0.15
45	265	0.20	0.16
55	202	0.18	0.11
65	155	0.15	0.06
75	109	0.13	0.05
85	95	0.11	0.04
Albumin from human serum			
10	1168	0.59	0.58
20	1121	0.57	0.58
30	1077	0.55	0.57
40	1005	0.53	0.57
50	872	0.47	0.40
60	766	0.42	0.37
70	590	0.35	0.33
80	345	0.23	0.20

Fibrinogen from human plasma			
5	724	0.40	0.29
25	684	0.35	0.31
45	560	0.31	0.23
65	352	0.23	0.18
85	81	0.10	0.04

Table D.2. Raw data for *FH* values calculated from 222 nm method versus the 230-240 nm slope method for four different proteins in the presence of 4 M and 8 M urea at room temperature (Fig. 8.6). The urea solutions were prepared in deionized water, and the pH was adjusted to pH 5.5 with 0.1 N HCl to induce protein unfolding. (N=3 with average 95% confidence interval = 0.03)

Proteins	**CD at 222 nm (*FH*)**		**230-240 nm slope method (*FH*)**	
	Urea (8M)	**Urea (4M)**	**Urea (8M)**	**Urea (4M)**
HEWL	0.32	0.19	0.27	0.21
RNase A	0.08	0.20	0.04	0.18
Albumin	0.09	0.60	0.08	0.55
Fibrinogen	0.29	0.33	0.25	0.36

Table D.3. Raw data for helical structure contents (α-helix + $3_{,10}$ helix) derived from the X-ray structures and the 230-240 nm slope (molar ellipticity/nm) from the CD spectra of proteins in the SP175 and MP 180 reference subsets. Outliers shown in Fig 8.7 are marked in red, which were identified as points that have unusually large (or small) residuals (i.e., residuals ≥ 3 or ≤ -3).

Slope	**Helix**	**Protein**	**Standardized Residuals**
936	0.458	Aldolase	-0.01
545	0.310	Alkaline phosphatase	0.07
843	0.277	Alpha amylase	-1.13
600	0.383	Beta amylase	0.47
282	0.142	Beta lactoglobulin	-0.41

1415	0.760	c-Phycocyanin	0.84
1278	0.568	Calmodulin	-0.23
611	0.382	Carboxypeptidase A1	0.43
734	0.332	Catalase	-0.35
1170	0.611	Citrate synthase	0.45
786	0.480	Cytochrome C	0.64
311	0.073	Beta-B2 crystallin	-1.04
1101	0.457	3-dehydroquinate dehydratase	-0.54
718	0.438	3-dehydroquinate dehydratase	0.53
448	0.289	Deoxyribonuclease-1	0.22
135	0.128	Ferredoxin	-0.05
1208	0.495	Glutamate dehydrogenase I	-0.58
886	0.486	Glycogen phosphorylase-b	0.37
936	0.449	Haloalkane dehalogenase	-0.08
1302	0.768	Hemoglobin	1.26
1639	0.720	Human serum albumin	-0.19
651	0.579	Insulin	1.84
346	0.318	Lactoferrin	0.77
384	0.043	Lectin (lentil)	-1.50
1340	0.610	Leptin	-0.10
777	0.403	Lysozyme	0.07
1498	0.739	Myoglobin	0.41
1706	0.782	Myoglobin	0.09
778	0.355	Nitrogen metabolite repression regulator	-0.31
706	0.291	Ovalbumin	-0.58
575	0.292	Ovotransferrin	-0.16
478	0.041	Lectin (pea)	-1.82
636	0.13	Pectate lyase C	-1.62

676	0.500	Peroxidase C1	1.14
805	0.357	Phosphoglucomutase 1	-0.38
783	0.345	Phosphoglycerate kinase	-0.41
1049	0.496	Phospholipase A2	-0.07
686	0.352	Phenylethanolamine N-methyltransferase	-0.04
815	0.385	Pyruvate kinase	-0.20
426	0.325	Rhodanese	0.57
144	0.043	Superoxide dismutase [Cu-Zn]	-0.74
825	0.446	Triose phosphate isomerase	0.25
326	0.250	Ubiquitin	0.30
523	0.116	Alpha chymotrypsin	-1.37
484	0.207	Aprotinin	-0.54
215	0.117	Ceruloplasmin	-0.39
354	0.038	Concanavalin A	-1.45
368	0.341	Glucose oxidase	0.88
472	0.259	Papain	-0.09
63	0.148	Pepsinogen	0.33
301	0.209	Ribonuclease, pancreatic	0.06
-69	0.046	Alpha bungarotoxin	-0.05
196	0.134	Alpha chymotrypsinogen	-0.20
178	0.139	Beta galactosidase	-0.10
157	0.158	Carbonic anhydrase II	0.11
252	0.120	Gamma-s-crystallin C terminus	-0.48
270	0	Jacalin	-1.48
213	0.170	Monellin	0.03
-129	0.106	Thaumatin I	0.61
-8	0.177	Carbonic anhydrase I	0.79
110	0.092	Gamma-B crystallin	-0.25

139	0.090	Gamma-D crystallin	-0.36
-92	0.064	Gamma-E-crystallin	0.17
146	0.081	Gamma-D crystallin	-0.45
-1.99	0.096	Elastase	0.13
33	0.072	Immunoglobulin G	-0.17
-5	0.017	Trypsin inhibitor A	-0.47
1012	0.625	Ammonia channel	1.06
801	0.507	Acriflavine resistance protein B	0.80
1317	0.697	Bacteriorhodopsin	0.65
568	0.055	Vitamin B12 transporter BtuB	-1.99
836	0.570	Vitamin B12 import system permease protein BtuC	1.18
1469	0.644	ClC-ec1	-0.24
1214	0.529	cytochrome bc1	-0.33
752	0.570	cytochrome C oxidase	1.45
146	0.055	Ferrienterobactin receptor	-0.66
340	0.046	Ferrichrome-iron receptor	-1.34
985	0.534	Voltage-gated potassium channel	0.43
455	0.274	inwardly rectifying k+ channel	0.08
1612	0.676	Lactose permease	-0.45
1391	0.730	Na(+):neurotransmitter symporter (Snf (nss) family)	0.68
1062	0.723	Light harvesting protein	1.66
1236	0.528	Large-conductance mechanosensitive channel	-0.41
548	0.075	NalP	-1.77
56	0.014	Outer membrane protein G	-0.69
261	0.016	Outer membrane protein OPCA	-1.33
144	0.134	TraF protein	-0.03
860	0.482	Reaction centre protein	0.42
917	0.482	Photosynthetic reaction centre	0.24

861	0.600	Rhodopsin (dark)	1.34
1078	0.572	Preprotein translocase subunit secY	0.43
906	0.458	Sarcoplasmic/endoplasmic reticulum calcium ATPase 1	0.09
1043	0.553	Succinate dehydrogenase	0.40
337	0.068	Sucrose porin	-1.16
396	0.260	outer membrane lipoprotein Wza	0.15
-430	0.071	Avidin	1.29
663	0.167	Rubredoxin	-1.42
-582	0.063	Streptavidin	1.71
1463	0.292	Subtilisin Carlsberg	-2.98
827	0.807	Sensory rhodopsin-2	3.07
88	0.658	Rhomboid protease glpG	4.24

APPENDIX E:

RAW DATA FOR THE ROLE OF CHEMICAL EXCIPIENTS ON THE SURFACE COVERAGE, SECONDARY STRUCTURE, AND BIOACTVITY OF PROTEINS PRE-ADSORBED ON A MATERIAL SURFACE

This supporting information contains data which (*i*) validate the methods for quantifying the surface coverage and helix content of proteins, (*ii*) Raw data for the desorbed amount, residual surface coverage, structure, and bioactivity of HEWL and RNase A adsorption systems post exposure to different chemical excipients, and (iii) CD method for determining the internal stability of protein in different chemical excipients.

E.1. Methods for quantifying the surface coverage and helix content of protein

Since, the background absorbance due to some of the additives like 6 M GdmHCl, 8 M urea, and 20 mM CHAPS were substantial at wavelengths < 230 nm, the use of absorbance at 195 nm or 205 nm for estimating the surface coverage of proteins was prohibitive with our custom cuvette for our adsorbed proteins. Instead, the surface coverage of proteins was estimated using absorbance at 230 nm (A_{230}) as peptide absorbance are high at this wavelength region. Similarly, the helix content in adsorbed proteins was estimated using the 230-240 nm slope method, instead of the CDPro package that was typically used in our previous studies. The estimates on surface coverage and secondary structure of adsorbed HEWL and RNase A determined by these newly applied methodologies were compared with the standard methods in Table E.1 and Table E.2.

Table E.1. Surface coverage (μg/cm^2) and helix content (%) of HEWL that was adsorbed from two different protein solution concentrations (0.03 and 1.00 mg/mL) on (a) glass, (b) HDPE, and (c) PMMA (N = 3; average ± 95% C.I. values). The degree of unfolding (%) in the adsorbed HEWL was estimated by relative comparison of the average helical content in the adsorbed and solution phase (34 ± 2 %) of the protein using the 230-240 nm slope methodology. The theoretical full surface coverage of HEWL for adsorption in 'side–on' and 'end–on' orientations are τ_{side} (0.17 μg/cm^2) and τ_{end} (0.26 μg/cm^2), respectively.

Surface	Soln. conc. (mg/mL)	Surf coverage (μg/cm^2) 205 nm	Surf coverage (μg/cm^2)- 230 nm	Helices (%) CDpro	Helices (%) 230-240 nm	Unfolded Fraction (%)
Glass	0.03	0.07 ± 0.03	0.06 ± 0.02	4 ± 2	4 ± 2	88
	1.00	0.16 ± 0.03	0.18 ± 0.03	22 ± 4	22 ± 4	35
HDPE	0.03	0.09 ± 0.02	0.11 ± 0.03	22 ± 3	24 ± 2	29
	1.00	0.11 ± 0.04	0.10 ± 0.03	12 ± 3	12 ± 2	65
PMMA	0.03	0.06 ± 0.01	0.08 ± 0.02	39 ± 3	30 ± 2	12
	1.00	0.17 ± 0.03	0.19 ± 0.03	22 ± 4	20 ± 3	41

Table E.2. Surface coverage (μg/cm^2) and helix content (%) of RNase A that was adsorbed from two different protein solution concentrations (0.03 and 1.00 mg/mL) on (a) glass, (b) HDPE, and (c) PMMA (N = 3; average ± 95% C.I. values). The degree of unfolding (%) in the adsorbed RNase A was estimated by relative comparison of the average helical content in the adsorbed and solution phase (20 ± 3%) of the protein using the 230-240 nm slope methodology. The theoretical full surface coverage of RNase A for adsorption in 'side–on' and 'end–on' orientations are τ_{side} (0.21 μg/cm^2) and τ_{end} (0.28 μg/cm^2), respectively.

Surface	Soln. conc. (mg/mL)	Surf coverage (μg/cm^2) 205 nm	Surf coverage (μg/cm^2)- 230 nm	Helices (%) CDpro	Helices (%) 230-240 nm	Unfolded Fraction (%)
Glass	0.03	0.08 ± 0.01	0.06 ± 0.01	5 ± 2	5 ± 2	75
	1.00	0.16 ± 0.03	0.17 ± 0.03	20 ± 4	19 ± 4	5
HDPE	0.03	0.10 ± 0.01	0.12 ± 0.01	18 ± 3	18 ± 2	10
	1.00	0.17 ± 0.03	0.15 ± 0.03	9 ± 2	9 ± 2	55
PMMA	0.03	0.10 ± 0.02	0.07 ± 0.02	8 ± 2	8 ± 2	60
	1.00	0.16 ± 0.03	0.18 ± 0.03	19 ± 4	18 ± 3	10

E.1.1 Effectiveness of A_{230} in estimating the surface coverage of proteins

As previously mentioned, the surface coverage of proteins was estimated using the A_{230} method. These estimates (Table E.1 and Table E.2) compared reasonably well (≈ 5% average error) with the surface coverage obtained using the A_{205} method used in our previous studies. Additionally, the chemical excipients used in our current study were not found to significantly interfere with the estimates of the protein solution concentration that were obtained using the A_{230} method. Based on these observations, the A_{230} method was used for estimating the surface coverage of proteins on different surfaces when exposed to different chemical additives.

E.1.2 Effectiveness of 230-240 nm Slope Method in estimating the Helix Content of Adsorbed Proteins

The helix content in adsorbed proteins that were predicted by the 230-240 nm method were in general agreement with those predicted by the conventional analysis tools provided with the CDPro package (CONTIN/LL and CDSSTR), except for the helix content predicted for HEWL on PMMA surface, when these proteins were adsorbed from 0.03 mg/ml solution concentration (30% error). This deviation is due to the inherent disadvantage of the universal correlation that is provided in equation 9.4, which tends to slightly under predict the higher helix contents in protein. Additionally, such variations in the predicted helix content are common even with standard tools like CONTIN/LL and CDSSTR. Therefore, by considering the overall accuracy in the prediction of the helix content in proteins that are exposed to chemical excipients, and the overall conservation of the trends observed with the adsorption-induced helical shifts in the proteins, the 230-

240 nm slope method was considered to be sufficiently accurate for quantifying the helix content in adsorbed proteins that were exposed to chemical excipients; especially given the fact that alternative methods are not available for this analysis.

E.2. Raw data for the Surface coverage, Helix content, and Bioactivity of Adsorbed Proteins post Exposure to Different Chemical Excipients

The residual surface coverage (Table E.3 and Table E.4), elution efficiency of different chemical excipients (Table E.5 and Table E.6), residual helix content of the proteins (Table E.7 and Table E.8), residual bioactivity of the proteins (Table E.9 and Table E.10) are presented in the subsequent sections/

E.2.a Residual Surface Coverages of Proteins post exposure to Chemical Excipients

Table E.3. Residual surface coverage of HEWL on glass, HDPE, and PMMA surfaces following its 15 h of exposure to different chemical excipients. HEWL were pre-adsorbed from 0.03 mg/ml and 1.00 mg/ml solution concentration (n = 3, mean ± 95% CI). τ_{side} (0.17 μg/cm^2) and τ_{end} (0.26 μg/cm^2) refers to the theoretical full surface coverage of HEWL for adsorption in 'side-on' and 'end-on' orientations, respectively. Surface coverage < 0.01 μg/cm^2 represents the limit of detection of the instrument.

Surface	Bulk conc. (mg/mL)	PPB (μg/cm^2)	GdmHCl (μg/cm^2)	Urea (μg/cm^2)	SDS (μg/cm^2)	Octyl (μg/cm^2)	CHAPS (μg/cm^2)
Glass	0.03	0.069 (0.031)	< 0.01	0.027 (0.012)	< 0.01	< 0.01	0.016 (0.006)
	1.00	0.161 (0.032)	0.043 (0.004)	0.032 (0.013)	0.022 (0.015)	0.083 (0.012)	0.072 (0.017)
HDPE	0.03	0.091 (0.006)	0.032 (0.011)	0.027 (0.007)	0.027 (0.009)	0.019 (0.008)	0.045 (0.012)
	1.00	0.112 (0.013)	0.022 (0.009)	0.043 (0.013)	0.022 (0.006)	0.025 (0.011)	0.037 (0.013)
PMMA	0.03	0.059 (0.012)	0.024 (0.009)	< 0.01	0.018 (0.008)	0.038 (0.012)	0.046 (0.015)
	1.00	0.171 (0.031)	0.039 (0.010)	0.027 (0.009)	0.044 (0.012)	0.077 (0.013)	0.044 (0.012)

Table E.4. Residual surface coverage of RNase A on glass, HDPE, and PMMA surfaces following its 15 h of exposure to different chemical excipients. RNase A were pre-adsorbed from 0.03 mg/ml and 1.00 mg/ml solution concentration (n = 3, mean ± 95% CI). τ_{side} (0.21 μg/cm^2) and τ_{end} (0.28 μg/cm^2) refers to the theoretical full surface coverage of RNase-A for adsorption in 'side-on' and 'end-on' orientations, respectively. Surface coverage < 0.01 μg/cm^2 represents the limit of detection of the instrument.

Surface	Bulk conc. (mg/mL)	PPB (μg/cm^2)	GdmHCl (μg/cm^2)	Urea (μg/cm^2)	SDS (μg/cm^2)	Octyl (μg/cm^2)	CHAPS (μg/cm^2)
Glass	0.03	0.078 (0.019)	0.012 (0.008)	0.043 (0.012)	0.035 (0.007)	0.012 (0.005)	0.022 (0.008)
	1.00	0.162 (0.038)	0.048 (0.012)	0.016 (0.009)	0.144 (0.024)	0.136 (0.022)	0.096 (0.014)
HDPE	0.03	0.121 (0.022)	0.038 (0.007)	< 0.01	0.072 (0.012)	0.058 (0.009)	0.069 (0.011)
	1.00	0.168 (0.039)	0.026 (0.019)	0.062 (0.013)	0.077 (0.014)	0.082 (0.018)	0.066 (0.009)
PMMA	0.03	0.076 (0.022)	0.022 (0.009)	0.036 (0.009)	0.032 (0.009)	0.016 (0.006)	0.014 (0.007)
	1.00	0.162 (0.024)	0.061 (0.018)	0.016 (0.007)	0.128 (0.021)	0.093 (0.022)	0.112 (0.018)

E.2.b Elution Efficiency of Different Chemical Excipients

Table E.5. Elution efficiency of different chemical excipients in removing HEWL from glass, HDPE, and PMMA surfaces following its pre-adsorption from 0.03 mg/ml and 1.00 mg/ml solution conditions (n = 3, mean ± 95% CI).

Surface	Bulk conc. (mg/mL)	SDS (%)	Octyl (%)	CHAPS (%)	GdmHCl (%)	Urea (%)
Glass	0.03	90 ± 6	89 ± 5	77 ± 12	91 ± 7	61 ± 10
	1.00	56 ± 12	88 ± 8	77 ± 13	85 ± 12	50 ± 15
HDPE	0.03	70 ± 10	79 ± 13	50 ± 9	69 ± 4	70 ± 10
	1.00	30 ± 8	42 ± 9	31 ± 8	62 ± 12	92 ± 5
PMMA	0.03	70 ± 12	37 ± 11	23 ± 7	60 ± 8	87 ± 4
	1.00	60 ± 8	80 ± 9	83 ± 9	75 ± 9	55 ± 9

Table E.6. Elution efficiency of different chemical excipients in removing RNAse A from glass, HDPE, and PMMA surfaces following its pre-adsorption from 0.03 mg/ml and 1.00 mg/ml solution conditions (n = 3, mean ± 95% CI).

Surface	Bulk conc. (mg/mL)	SDS (%)	Octyl (%)	CHAPS (%)	GdmHCl (%)	Urea (%)
Glass	0.03	86 ± 8	48 ± 10	55 ± 11	73 ± 7	80 ± 8
	1.00	10 ± 7	15 ± 8	40 ± 8	70 ± 10	90 ± 7
HDPE	0.03	80 ± 10	77 ± 9	66 ± 8	80 ± 7	64 ± 6
	1.00	55 ± 11	52 ± 9	61 ± 8	85 ± 6	65 ± 9
PMMA	0.03	74 ± 7	55 ± 6	74 ± 9	77 ± 7	84 ± 5
	1.00	20 ± 6	42 ± 13	31 ± 8	62 ± 9	90 ± 5

E.2.c Residual Structure of Proteins post exposure to Chemical Excipients

Table E.7. Helical content (%) in the residual amount of HEWL on glass, HDPE, and PMMA surfaces post 15 h exposure to chemical excipients. HEWL was adsorbed from 0.03 mg/ml and 1.00 mg/ml solution conditions (n = 3, mean ± 95% CI). The helix content in the native structure of protein by the 230-240 nm slope methodology was found to 34% (± 2%). N.A. refers to the inability in quantifying the helical content because of the limit of detection for CD.

Surface	Bulk conc. (mg/mL)	PPB	GdmHCl (%)	Urea (%)	SDS (%)	Octyl (%)	CHAPS (%)
Glass	0.03	4 (2)	NA	4 (3)	NA	NA	10 (3)
	1.00	24 (3)	21 (2)	29 (3)	18 (3)	17 (4)	20 (4)
HDPE	0.03	24 (4)	19 (3)	15 (3)	17 (3)	30 (4)	13 (3)
	1.00	12 (3)	17 (3)	20 (4)	18 (3)	12 (3)	18 (2)
PMMA	0.03	30 (3)	22 (4)	NA	19 (4)	15 (4)	14 (4)
	1.00	20 (3)	21 (4)	29 (4)	18 (4)	20 (3)	17 (4)

Table E.8. Helical content (%) in the residual amount of RNase A on glass, HDPE, and PMMA surfaces post 15 h exposure to chemical excipients. RNase A was adsorbed from 0.03 mg/ml and 1.00 mg/ml solution conditions (n = 3, mean ± 95% CI). The helix content in the native structure of protein by the 230-240 nm slope methodology was found to 20% (± 2%). N.A. refers to the inability in quantifying the helical content because of the limit of detection for CD.

Surface	Bulk conc. (mg/mL)	PPB	GdmHCl (%)	Urea (%)	SDS (%)	Octyl (%)	CHAPS (%)
Glass	0.03	5 (2)	7 (2)	4(3)	4 (2)	9 (3)	8 (2)
	1.00	19 (3)	18 (3)	19 (2)	10 (3)	16 (2)	13 (2)
HDPE	0.03	18 (3)	12 (3)	NA	5 (3)	9 (2)	12 (3)
	1.00	14 (2)	12 (2)	9 (3)	7 (3)	12 (2)	10 (2)
PMMA	0.03	8 (3)	11 (2)	8 (2)	7 (3)	11 (3)	10 (2)
	1.00	18 (3)	19 (3)	9 (2)	10 (3)	15 (3)	14 (2)

E.2.d Residual Bioactivity of Proteins post exposure to Chemical Excipients

Table E.9. Residual Bioactivity (%) of adsorbed HEWL on glass, HDPE, and PMMA surfaces post 15 h exposure to chemical excipients. HEWL was adsorbed from 0.03 mg/ml and 1.00 mg/ml solution conditions (n = 3, mean ± 95% CI). N.A. refers to the inability in quantifying the bioactivity of the protein.

Surface	Bulk conc. (mg/mL)	PPB	GdmHCl (%)	Urea (%)	SDS (%)	Octyl (%)	CHAPS (%)
Glass	0.03	12 (6)	NA	12 (4)	NA	NA	21 (8)
	1.00	31 (7)	42 (6)	35 (6)	33 (4)	30 (8)	38 (9)
HDPE	0.03	39 (6)	35 (5)	28 (7)	36 (10)	43 (9)	26 (7)
	1.00	17 (8)	34 (5)	38 (5)	36 (6)	30 (8)	36 (9)
PMMA	0.03	54 (9)	44 (6)	NA	32 (6)	24 (8)	32 (6)
	1.00	66 (7)	49 (5)	53 (5)	42 (8)	45 (10)	45 (7)

Table E.10. Residual Bioactivity (%) of adsorbed RNase A on glass, HDPE, and PMMA surfaces post 15 h exposure to chemical excipients. RNase A was adsorbed from 0.03 mg/ml and 1.00 mg/ml solution conditions (n = 3, mean ± 95% CI). N.A. refers to the inability in quantifying the bioactivity of the protein.

Surface	Bulk conc. (mg/mL)	PPB	GdmHCl (%)	Urea (%)	SDS (%)	Octyl (%)	CHAPS (%)
Glass	0.03	38 (8)	33 (5)	39 (5)	37 (6)	27 (4)	42 (8)
	1.00	39 (9)	35 (4)	33 (3)	24 (7)	27 (8)	35 (8)
HDPE	0.03	43 (6)	30 (6)	NA	18 (5)	35 (7)	40 (12)
	1.00	27 (5)	35 (5)	29 (4)	23 (7)	32 (10)	35 (11)
PMMA	0.03	33 (5)	40 (5)	25 (8)	35 (7)	32 (5)	35 (9)
	1.00	45 (9)	45 (8)	29 (7)	36 (8)	39 (10)	42 (6)

E.3. CD method for Temperature Unfolding of Protein in different Chemical Excipients

The '∇' parameter obtained in equation 9.3 was also used to assess the influence of excipients on the internal stability of HEWL and RNase A, by monitoring the influence of these chemical excipients on the T_m of the protein. As CD technique characterizes the ensemble average of the native protein structures, T_m of the protein in solution corresponds to 50% of the proteins existing in denatured state, which in our studies was represented as 50% unfolding in the secondary structure. Such scale normalization permits equivalent comparisons of the influence of chemical excipient on the helix content in a given protein, which in turn provides insight into the role of these excipients on a protein's structural stability. The fraction of denatured protein (f_d) in each chemical excipient were obtained by using equation.E.1,

$$f_d = \frac{\nabla_{obs} - \nabla_n}{\nabla_d - \nabla_n} \qquad \text{(E.1)}$$

Where, ∇_{obs} is the 230-240 nm slope at each temperature step increase for each chemical excipient, ∇_n is the 230-240 nm slope for the native state of HEWL (∇_n = 700)and RNase A (∇_n = 400), and ∇_d is 230-240 nm slope for the fully denatured state of the protein and was set equal to 0 for both the proteins.

Temperature control within the CD instrument was done using Peltier temperature control device that was integrated within our instrument. The data was acquired at a bandwidth of 0.5 nm, response time of 4 s at a heating rate of 0.5°C/min and equilibrated 3 times. Data was recorded after every 1°C rise in temperature over 220 nm to 300 nm.

Fig. E.1 presents the thermal stability of both proteins in 8 M urea, 0.5% (w/v) SDS, 30 mM Octyl, and 20 mM CHAPS. The fraction of unfolded protein (f_d) was monitored using the 230-240 nm slope methodology described in equation E.1.

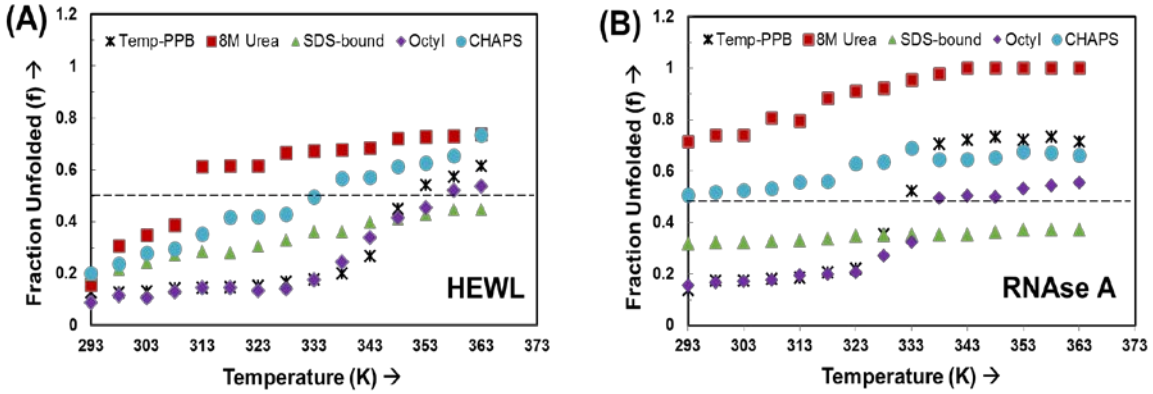

Figure E.1. Thermal unfolding of helix content in (a) HEWL and (b) RNase A in PPB, 8 M urea, 0.5% (w/v) SDS, 30 mM octyl, and 20 mM CHAPS using the 230-240 nm slope method. The data points for both the proteins in each of the excipients were overlaid for the purpose of comparing the effect of helical unfolding in the proteins by a given chemical additive using equation 9.5. The black dotted line indicate the 50% unfolding in the protein's helical structure.

From Fig. E.1, it was evident that 8 M urea and 20 mM CHAPS accelerates while octyl slightly decelerated the process of thermal unfolding of helix structure in both the proteins, suggesting that 8 M urea and 20 mM CHAPS have a destabilizing influence on the overall structure of protein while octyl has a slight stabilizing influence on the helical structures of the protein. The influence of SDS compared with the unfolding behavior of the protein in PPB was mixed, however, with SDS generally destabilizing the structure of the proteins at room temperature, but then exhibiting a stabilizing influence on the helical structure of the protein as temperature was increased. These results thus clearly illustrate that the influence of the interaction of a chemical excipient with a protein can greatly vary depending upon its conformational state, as observed by other investigators.[1-8] Additionally,

the results presented clearly show that the 230-240 nm slope method is an effective quantification tool for tracking the impact of chemical additives on the helical structure of proteins by CD spectroscopy.

E.4 REFERENCES

1. Moriyama, Y.; Kawasaka, Y.; Takeda, K. Protective effect of small amounts of sodium dodecyl sulfate on the helical structure of bovine serum albumin in thermal denaturation. *J. Colloid Interface Sci.* **2003,** *257* (1), 41-6.
2. Moriyama, Y.; Kondo, N.; Takeda, K. Secondary structural changes of homologous proteins, lysozyme and alpha-lactalbumin, in thermal denaturation up to 130 degrees C and sodium dodecyl sulfate (SDS) effects on these changes: comparison of thermal stabilities of SDS-induced helical structures in these proteins. *Langmuir* **2012,** *28* (47), 16268-73.
3. Naidu, K. T.; Prabhu, N. P. Protein-surfactant interaction: sodium dodecyl sulfate-induced unfolding of ribonuclease A. *J. Phys. Chem. B* **2011,** *115* (49), 14760-7.
4. Kumar, E. K.; Prabhu, N. P. Differential effects of ionic and non-ionic surfactants on lysozyme fibrillation. *PCCP* **2014,** *16* (43), 24076-88.
5. Lad, M. D.; Ledger, V. M.; Briggs, B.; Green, R. J.; Frazier, R. A. Analysis of the SDS−Lysozyme Binding Isotherm. *Langmuir* **2003,** *19* (12), 5098-5103.
6. Otzen, D. Protein-surfactant interactions: a tale of many states. *Biochim. Biophys. Acta* **2011,** *1814* (5), 562-91.
7. Otzen, D. E. Protein unfolding in detergents: effect of micelle structure, ionic strength, pH, and temperature. *Biophys. J.* **2002,** *83* (4), 2219-30.
8. Hedoux, A.; Krenzlin, S.; Paccou, L.; Guinet, Y.; Flament, M. P.; Siepmann, J. Influence of urea and guanidine hydrochloride on lysozyme stability and thermal denaturation; a correlation between activity, protein dynamics and conformational changes. *PCCP* **2010,** *12* (40), 13189-96.